GENETIC AND FUNCTIONAL ANALYSIS OF THE PROTEOLYTIC CLEAVAGE AT THE JUNCTION OF THE NS1 AND NS2A PROTEINS OF MURRAY VALLEY ENCEPHALITIS VIRUS

Siti Nor Khadijah Addis

Australian National University

A thesis submitted for the degree of
Doctor of Philosophy of
The Australian National University

Nov 2011

Dedicated to my parents Addis Addi & Rokiah Ali
&
To my husband Ahmad Faisal Mohamad Ayob

Statement

The work described in this thesis was performed by the author under the supervision of Assoc. Prof. Dr. Mario Lobigs, Dr. Jayaram Bettadapura and Dr. Eva Lee at The John Curtin School of Medical Research, Canberra, Australia. These studies were completed between Feb 2007 and July 2011 to fulfill requirements for the degree of Doctor of Philosophy in The Australian National University, Canberra, Australia. This thesis does not contain any material that has been accepted for the award of any other degree at this or any other University. To the best of my knowledge, this thesis does not contain any material that has been published previously, except where due reference is made in the text. The research described in this thesis is my own original work unless otherwise stated in the text.

Siti Nor Khadijah Addis
The John Curtin School of Medical Research
The Australian National University
Canberra, Australia
28th Nov 2011

Acknowledgements

I would like to thank all the wonderful people who have made this work possible and have made significant contributions to my PhD research.

First and foremost, I would like to express my deepest gratitude to my supervisor, Associate Professor Dr. Mario Lobigs for his invaluable guidance, discussions, encouragement, support, trust and constructive criticism throughout my PhD journey. Thanks for your patience and for shedding light on the importance of the results we have obtained. I would also like to dedicate my special thanks to my co-supervisors, Dr. Jayaram Bettadapura & Dr. Eva Lee for their kind assistance, helpful guidance and useful advices all throughout the studies.

My particular appreciation also goes to Megan Pavy and Paivi Lobigs for being good friends and mentor especially in helping up with important technical issues during my PhD studies and making difficult task seemed more relaxing than what it meant to be.

Not to forget, my colleagues in Molecular Virology Lab and the John Curtin School of Medical Research (former and present) especially to Max Larena, Leah Leang, Saila Ismail, Carolina Silva, & Miheer Sabale. Thanks for making our lab and office lively with your stories, jokes, heaps of laugh and contributed such an enjoyable, colourful and encouraging atmosphere. Thanks for being such a great company during so many morning teas and lunches, even chats at the corridor! For Max, thanks for interesting discussions about science, life in general and for being a good, helpful & encouraging colleague. To all my Malaysian friends in Canberra especially to Nurul Wahida Othman, Norefrina Shafinaz Md Nor & Suriati Paiman, thank you for being there with words of encouragement.

I would like to express my hearties appreciation to my loving husband and my best friend, Ahmad Faisal Mohamad Ayob, for his love, care, support and understanding during the years of the research. Thank you for being such a good listener, for all your valuable advice, for your warmth and endurance, for everything I could ever ask for (including computer technical advice!). I cannot thank you enough and I look forward to our next journey together.

My acknowledgements are incomplete without thanking my family. My sincere thanks goes to my parents, Addis Addi & Rokiah Ali and my family for their unconditional love, prayers, moral support and confidence in me, which inspired me to keep going even through the worst times. *Terima kasih Mak & Ayah.*

I wish to acknowledge my sponsorship sources: The Ministry of Higher Education, Malaysia and Universiti Malaysia Terengganu (UMT). Finally, I would like to say 'Alhamdulillah' as my stay in Canberra has been an exciting, amusing, constructive and memorable journey.

Pulau Pandan jauh ke tengah
Gunung Daik bercabang tiga
Hancur badan dikandung tanah
Budi yang baik dikenang juga

Abstract

Flaviviruses are a group of positive-strand RNA viruses of global significance. The flavivirus RNA genome encodes a single open reading frame that is directly translated into a single polyprotein and cleaved by host and virally encoded proteases prior to protein maturation. Hence, the proteolytic cleavage events play a central role in the process of viral gene expression in flaviviruses. Despite the importance of these events, the mechanism of proteolytic cleavage leading to the generation of the two non-structural proteins, NS1 and NS2A is poorly defined.

Sequence comparisons among the flaviviruses and experimental work on Dengue virus (DENV) NS1-NS2A cleavage revealed an octapeptide sequence motif at the C-terminus of NS1 predicted to allow recognition by a protease for the cleavage of the NS1 and NS2A proteins. Of the eight-residue recognition sequence, positions P1, P3, P5, P7 and P8 (with respect to N-terminus of NS2A protein) are highly conserved and substitutions in these positions influenced DENV NS1-NS2A cleavage efficiency. However, the role of this recognition sequence in NS1 and NS2A production of other flaviviruses has not been experimentally addressed to date. It is also unclear whether insight gained from subgenomic expression experiments carried out in DENV is applicable to other flaviviruses. In this thesis, investigations were carried out *in vitro* and *in vivo* to assess the role of the octapeptide motif, in the efficiency of cleavage at the Murray Valley encephalitis virus (MVEV) NS1-NS2A junction. Expression cassettes encoding NS1 and NS2A genes were engineered and used for the site-directed mutagenesis of residues in the octapeptide motif. Analysis from the mutagenesis studies showed that cleavage efficiency is influenced by mutations at conserved and non-conserved residues in the octapeptides of MVEV, putatively recognized by a host protease, although overall mutations at the conserved octapeptide residues impacted more on cleavage efficiency than mutations at the non-conserved positions.

Subsequently, four mutations in the octapeptide sequence (P2-Gly, P3-Gly, P8-Ala and P7,8-Ala) were introduced into an MVEV full-length infectious clone to

investigate the impact of the substitutions during virus infection. Analysis from this study demonstrates for the first time that the efficiency of NS1-NS2A cleavage tightly controls viral RNA replication, growth in mammalian and insect cells, and virulence in mice. Despite poor conservation of amino acid at the position P2 in the octapeptide sequence, a Gln to Gly substitution at this position dramatically reduced virus replication, as demonstrated by small plaque morphology, poor RNA replication, impaired protein processing and attenuation of virulence in IFN-α-receptor knock-out mice relative to the wild-type virus. On the contrary, non-conservative changes at highly conserved residue P3 (Val→Ala) and P8 (Leu→Ala), only slightly reduced NS1-NS2A cleavage efficiency relative to wild-type and did not markedly affect virus replication. These results clearly implicate a direct association of NS1-NS2A processing with viral replication, and suggest a vital role for the octapeptide motif in modulating NS1-NS2A proteolytic cleavage.

Finally, multiple growth passages of the two NS1-NS2A cleavage defective mutants, rP2-Gly and rP7,8-Ala in cell culture and mice had generated variants with revertant phenotypes. Interestingly, sequencing of the viral genome revealed that the variants had a second-site mutation in E protein in addition to the P2-Gly and rP7,8-Ala mutation at the NS1-NS2A junction. Introduction of compensatory mutation in codon 65 of E (V65A) together with the P2-Gly mutation restored the virus growth in cell culture. This result illustrates for the first time that growth deficiency of MVEV NS1-NS2A cleavage site mutants could be substantially repaired by compensatory mutations in E protein, suggesting an as-yet-unidentified role of the structural protein in NS1-NS2A cleavage or down-stream replication events. This proposition is further supported by the isolation of a putative E-NS1 polypeptide in rP2-Gly variant (containing the V65A change in E) infected cells, showing an interaction of E with NS1.

Table of Contents

CHAPTER 3

CHAPTER 4

CHAPTER 5

Abbreviations

°C	Degrees Celsius
Å	Angstrom(s)
%	Percent
μCi	Micro-curie
μF	Micro-Faraday(s)
μg	Micro-gram(s)
μl	Micro-litre(s)
Ab	Antibody
Ala (A)	Alanine
anchC	Anchored Capsid protein
APS	Ammonium persulphate
Arbovirus	Arthropod borne virus
Arg (R)	Arginine
Asn (N)	Asparagine
Asp (D)	Aspartic acid
ATP	Adenosine Triphosphate
BHK	Baby hamster kidney
bp	Base pair(s)
BSA	Bovine serum albumin
C	Capsid protein
C6/36	*Aedes albopictus* salivary gland cells
cDNA	Complementary DNA
CM	Convoluted membranes
CMV	Cytomegalovirus
CNS	Central nervous system
CO_2	Carbon dioxide
CPE	Cytopathic effect
CS	Cyclization sequence
CS1	Complementary sequence 1

Cys (C)	Cysteine
DENV	Dengue virus
DMSO	Dimethyl sulfoxide
DNA	Deoxynucleic acid
dATP	Deoxyadenosine triphosphate
dCTP	Deoxycytidine triphosphate
DEAE	Diethylaminoethyl cellulose
dGTP	Deoxyguanosine triphosphate
dNTP	Deoxynucleotide triphosphate
dsRNA	Double-stranded RNA
dTTP	Deoxythymidine triphosphate
DTE	Dithioerythritol
DTT	Dithiothretol
E	Envelope protein
EDTA	Ethylene Diamine Tetra Acetic acid
EF-1α	Elongation factor 1α
Endo H	Endoglycosidase H
ER	Endoplasmic reticulum
FACS	Fluorescence-activated cell sorter
FCS	Foetal calf serum
FITC	Fluorescence isothiocyanate
g	Gram(s)
g	Gravitational speed
Glu (E)	Glutamic acid
Gln (Q)	Glutamine
Gly (G)	Glycine
GPI	Glycosylphosphotidylinositol
GRP	Glucose receptor protein
h	Hour(s)
HA	Hemagglutinin
HBSS	Hanks' balanced salt solution
HCl	Hydrochloric acid (hydrogen chloride)
HCV	Hepatitis C virus

HEPES	4-(2-hydroxyethyl)-1-piperazineethanesulfonic acid
His (H)	Histidine
HSP	Heat shock protein
IC	Intermediate compartment
IF	Immunofluorescence
IFN	Interferon
IFN-α-$R^{-/-}$	Interferon-alpha receptor knockout
Ig	Immunoglobulin
Ile (I)	Isoleucine
i.p	Intraperitoneal
JEV	Japanese encephalitis virus
kb	Kilo-base(s)
kDa	Kilo-dalton(s)
KUN	Kunjin virus
l	Litre(s)
LAMR	Laminin receptor
LB	Luria-Bertani media
Leu (L)	Leucine
LGTV	Langat virus
Lys (K)	Lysine
M	Membrane protein
M	Molar
mAb	Monoclonal antibody
MEM	Minimum essential medium
Met (M)	Methionine
mg	Milli-gram(s)
$MgCl_2$	Magnesium chloride
$MgSO_4$	Magnesium sulphate
min	Minute(s)
ml	Milli-litre(s)
mm	Milli-metre(s)
mM	Milli-molar
MOI	Multiplicity of infection

MVEV	Murray Valley encephalitis virus
MTase	Methyl transferase
NaCl	Sodium chloride
NCR	Non-coding region
ng	Nanogram(s)
$NaHCO_3$	Sodium hydrogen carbonate
NaOH	Sodium hydroxide
NEB	New England Biolabs
NLS	Nuclear localization sequence
NS	Non-structural protein
nt	nucleotide
NTPase	Nucleoside triphosphatase
OD	Optical density
ORF	Open reading frame
p.i	post infection
PAGE	Polyacrylamide gel electrophoresis
PBS	Phosphate-buffered saline
PC	Paracrystalline arrays
PCR	Polymerase chain reaction
PEG	Polyethylene glycol
PFU	Plaque forming unit
Phe (F)	Phenylalanine
PNGase F	peptide-N4-(N-acetyl-beta-glucosaminyl)-asparagine amidase
pmol	Pico-mole(s)
prM	pre-Membrane protein
PSL	Photostimulated luminescence
PSN	Penicillin-streptomycin
PTPB	Polypyrimidine-binding protein
Pro (P)	Proline
qRT-PCR	Quantitative reverse transcription polymerase chain reaction
RC	Replication complex
RdRp	RNA-dependent RNA-polymerase
RER	Rough endoplasmic reticulum

RF	Replicative form
RI	Replicative intermediate
RIPA	Radio-immunoprecipitation buffer
RNA	Ribonucleic acid
rpm	Revolutions per minute
RT-PCR	Reverse transcriptase polymerase chain reaction
RTPase	RNA triphosphatase
S.E	Standard error
SAM	S-Adenosyl-L-Methionine
sec	second(s)
SDS	Sodium dodecyl sulphate
SEM	Standard error of mean
Ser (S)	Serine
sfRNA	small flavivirus RNA
SL	Stem-loop
SLEV	St. Louis encephalitis virus
ssRNA	single-stranded RNA
STAT	Signal transducers and activators of transcription protein
TAE	Tris-Acetic acid-EDTA Buffer
TBEV	Tick-Borne Encephalitis virus
TEMED	Tetramethylethylenediamine
TGN	Trans Golgi network
Thr (T)	Threonine
Trp (W)	Tryptophan
tRNA	transfer ribonucleic acid
Tyr (Y)	Tyrosine
UPR	Unfolded protein response
UTR	Untranslated region
U	Unit
UV	Ultra violet
V	Volt(s)
V1	Variant 1
V2	Variant 2

Val (V)	Valine
VP	Vesicle packet
WNV	West Nile virus
wt	wild-type
w/v	weight per volume
XRN1	Exoribonuclease 1 protein
YFV	Yellow fever virus

List of Figures

CHAPTER 5

Selection and characterization of the MVEV NS1-NS2A cleavage site variants with enhanced virus growth

CHAPTER 6

Confirmation of complementation of a deleterious mutation at the NS1-NS2A cleavage site by a single amino acid change in E protein

List of Tables

CHAPTER 4

MVEV variants with mutation in the octapeptide at the NS1-NS2A junction

CHAPTER 5

Selection and characterization of the MVEV NS1-NS2A cleavage site variants with enhanced virus growth

CHAPTER 6

Confirmation of complementation of a deleterious mutation at the NS1-NS2A cleavage site by a single amino acid change in E protein

Conferences attended and Award

Conferences attended:

1. Australasian Virology Group meeting (4th AVG); Brisbane, Australia (2007)
   - Poster presentation
2. The Australian Society for Medical Research, Young Investigator Forum; Canberra, Australia (2009)
   - Oral presentation
3. First International conference on Translational Medicine; Canberra, Australia (2010)
   - Poster presentation
4. International Congress of Virology, International Union of Microbiological Societies (IUMS); Sapporo, Japan (2011)
   - Oral presentation

Award:

1. Malaysian Ministry of Higher Education postgraduate sponsorship (2007-2011)

2. The Best Oral Presentation award
   The Australian Society for Medical Research, Young Investigator Forum; Canberra, Australia (2009)

CHAPTER 1

Literature review

1.1 Literature review

1.1.1 Flaviviruses

The flaviviruses have been one of the great challenges confronting public health for many centuries. Flaviviruses are of great concern as a group of pathogens at the forefront of emerging and re-emerging infectious diseases. They affect all segments of society and have become increasingly important human and veterinary pathogens, contributing to severe morbidity and mortality worldwide.

The *Flaviviridae* (from the Latin *flavus*, or 'yellow') were initially classified into the *Togaviridae* family, but later established as a separate virus family due to their distinct genome organization. Current classification identifies 3 genera of the family, namely *Flavivirus*, *Pestivirus* (from the Latin *pestis*, plague) and *Hepacivirus* (from the Greek *hepar*, *hepatos*, liver) (Heinz et al., 2000; Knipe, 2001; Lindenbach, 2001; Westaway et al., 1985).

Flaviviruses in general are arthropod-borne viruses (arboviruses) with a very diverse host range, including arthropods (mosquito and tick) as obligatory vectors for transmission to their vertebrate hosts that can range from reptiles to primates (Gaunt et al., 2001; Weaver and Reisen, 2010; Zhang et al., 2008). Most flaviviruses are spread through the sylvatic transmission between the invertebrate vector and an enzoonotic amplifying vertebrate reservoir (water birds) (Gubler, 2007). Flavivivirus infection in human and domestic animals, such as horses are generally thought to be incidental during this cycle as dead-end hosts (Hollidge et al., 2010). However, for some important flaviviruses like Dengue virus (DENV) and Yellow fever virus (YFV), man is often the major host. In spite of this, some flaviviruses have neither known vector nor vertebrate host associated with its infection.

The flaviviruses are by far the most common and widely distributed of the *Flaviviridae*, accounting for the majority of infections worldwide (Hurrelbrink et al., 1999; Lindenbach, 2001; Mackenzie et al., 2004; Solomon, 2004; Solomon et al., 2000) (Fig 1.1). The genus consists of more than 70 members, 40 of which have

been associated with human illness (Hurrelbrink et al., 1999; Lindenbach, 2001). Among all identified viruses grouped in the genus Flavivirus, 40 are mosquito-borne, 16 are tick-borne while 18 with no known vector (Heinz et al., 2000). The clinical manifestations of flavivirus infections range from mild (fever and malaise) to severe (fatal encephalitis, hepatitis and hemorrhagic fever). Some of the diseases caused by flaviviruses such as yellow fever, dengue hemorrhagic fever and dengue shock syndrome and Japanese encephalitis are of global concern (Gardner and Ryman, 2010; Misra and Kalita, 2010; Weaver and Reisen, 2010). Several flaviviruses are also recognized as important veterinary pathogens, including West Nile virus (WNV) that causes encephalitis in horses, and Japanese encephalitis virus (JEV) that causes encephalitis in horses as well as stillbirth in domestic pigs (Lindenbach, 2001).

Current treatment against flavivirus infection is still lacking effective antiviral drugs and the only treatment for flavivirus infections that currently exist is supportive care. Attempts to control mosquito spread are being investigated and critical in the prevention of future outbreaks. Recently, a strategy in controlling the spread of mosquito using an innovative biological approach has been put forward. The naturally occurring bacterial agent, known as *Wolbachia pipientis* has been shown to halve the mosquito lifespan. The infection of life-shortening *Wolbachia* strains into the mosquito may reduced the mosquito age and thus reducing the transmission of mosquito-borne pathogens such as DENV (McMeniman et al., 2009). Moreover, vaccines development and antiviral therapies are also of great importance and remain a high priority for the World Health Organisation (Leyssen et al., 2000). Currently, vaccines against YFV, JEV and Tick-borne encephalitis virus (TBEV) are available commercially (Pugachev et al., 2003). However, the development of a vaccine against DENV is complicated by the presence of several serotypes.

1.1.2 Murray Valley encephalitis virus

Murray Valley encephalitis virus (MVEV) is a member of the genus *Flavivirus* within the *Flaviviridae* family. Like other flaviviruses, such as YFV, WNV, JEV, Kunjin virus (KUN), DENV and TBEV, MVEV causes clinically significant disease in

humans (reviewed in Knipe, 2001). MVEV was first isolated in Victoria in the summer of 1950-1951. The disease caused by this virus was previously called Australian X disease (or Australian encephalitis) and later was given its name Murray Valley encephalitis as this was the area from which most cases was reported (Mackenzie and Broom, 1995). Although uncommon and most MVEV infection in humans remain asymptomatic, 1:1000 of infected person could develop a range of symptoms (fever, headache, drowsiness, nausea, neck stiffness, lethargy, seizures, tremors and unconsciousness), which could be potentially fatal, and patients who survive often experience long-term neurological sequelae (Mackenzie and Broom, 1995). MVE is endemic in Australia and Papua New Guinea and causes annually encephalitic disease in human in northern Australia (Lobigs et al., 1986; Mackenzie and Broom, 1995). MVEV has been responsible for occasional disease outbreak, particularly in the Murray Valley region of Southeastern Australia and the Kimberly region of north Western Australia (Mackenzie and Broom, 1995; Mackenzie et al., 1994; Mackenzie et al., 1993).

The number of new cases of MVEV infection is recently increasing. The disease has recently re-emerged in several areas in Western and Southern Australia. At least two fatalities have been reported in recent months in 2011, including travellers who contracted the disease after visiting the Northern Territory (McLean et al., 2011; Robertson, 2011). The threat of an outbreak of MVEV in Australia is growing, underscoring the need for a specific antiviral treatment or vaccines to prevent MVEV infection.

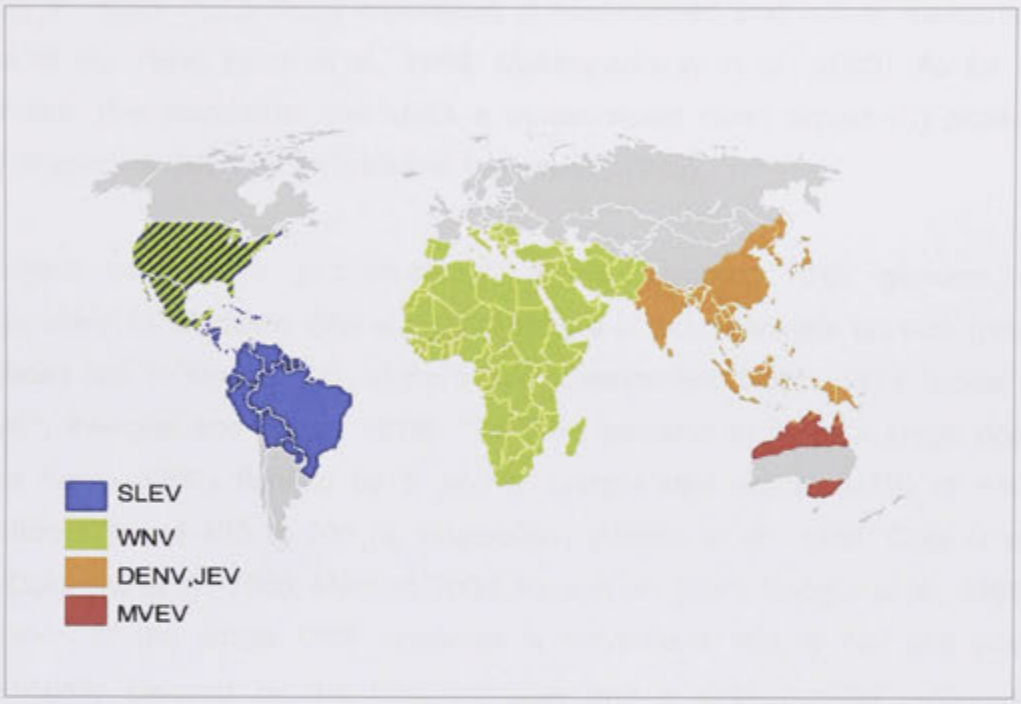

Fig. 1.1 The approximate global distribution and spread of medically important flaviviruses.

The map was adapted from a map of the distribution of major neurotropic flaviviruses, St. Louis encephalitis virus (SLEV), West Nile virus (WNV), Japanese encephalitis virus (JEV) and Murray Valley encephalitis virus (MVEV), but altered to reflect the Dengue virus (DENV) endemic areas in Asia and Australia (Mackenzie et al., 2004; Solomon, 2004; Solomon et al., 2000).

1.2 Flavivirus structure

1.2.1 Virion and genome structure

Flaviviruses are small, enveloped viruses with approximately 500 Å in diameter with icosahedral symmetry (Mukhopadhyay et al., 2003; Murphy et al., 1968; Nishimura et al., 1968). The structural elements of the virus consist of membrane (M) and envelope (E) proteins embedded in host-derived lipid bilayer membrane (Kitano et al., 1974; Kuhn et al., 2002; Mukhopadhyay et al., 2003). As for all flaviviruses, this membrane surrounds a nucleocapsid core; capsid (C) protein, bound to genomic RNA (Khromykh and Westaway, 1996).

The virion contains a positive-sense, single stranded RNA genome of approximately 11 kilobases (kb) in length, lacks a 3' polyadenylate tail with type I methylated cap, $m^7GpppAmpN_1$ at the 5' end (Cleaves and Dubin, 1979; Stollar et al., 1967; Wengler and Gross, 1978). The RNA genome encodes a single open reading frame (ORF) flanked by 5' and 3' untranslated region (UTR) of ~100 nucleotide (nt) and 400 to 700 nt, respectively (Castle et al., 1986; Coia et al., 1988; Dalgarno et al., 1986; Markoff, 2003; Rice et al., 1985; Speight et al., 1988). Translation of the single ORF produces a polyprotein that is co- and post-translationally cleaved by the host protease and a viral-encoded proteinase producing at least 10 discrete proteins in the order NH_2-C-prM/M-E-NS1-NS2A-NS2B-NS3-NS4A-NS4B-NS5-COOH' (Castle et al., 1986; Castle et al., 1985; Coia et al., 1988; Dalgarno et al., 1986; Rice et al., 1985; Speight et al., 1988; Wengler et al., 1985). The polyprotein is organized with the structural proteins (C, prM/M and E) at the NH_2-terminal end and the non-structural proteins at the COOH-terminal end (NS1, NS2A, NS2B, NS3, NS4A, NS4B and NS5) (Fig. 1.2).

Fig. 1.2 Flavivirus genome organization.

The positive-sense RNA genome is translated into a single polyprotein containing structural (C,prM,E) and non-structural proteins (NS1, NS2A, NS3, NS4A, NS4B and NS5).

1.2.2 The flavivirus structural proteins

1.2.2.1 Capsid (C) protein

The ~14 kDa C protein is a highly basic protein, having approximately 21% of conserved Lys and Arg amino acid content (Khromykh and Westaway, 1996). The N- and C- terminal regions of C protein (residue 1-32 and 82-105 in WNV) are highly basic, and flanking a central hydrophobic region (Khromykh et al., 1998a; Khromykh and Westaway, 1996). During translation of the polyprotein in the cytoplasm, the structural proteins are translocated and anchored in the endoplasmic reticulum (ER) by various signal sequences and membrane anchor domains. The C-terminal hydrophobic residues of nascent C (or anchored C; anch C) serve as a signal sequence for ER translocation of prM immediately downstream (Nowak et al., 1989; Stocks and Lobigs, 1995). This hydrophobic anchor region is cleaved by the viral NS2B/NS3 protease to generate a mature 105 residues form of C protein that remains free in the cytosol (Lobigs, 1993; Stocks and Lobigs, 1995).

The nucleocapsid (NC) complex consists of multiple copies of C protein together with the viral RNA genome and localized within the electron-dense core of the particle. The positively charged region at the N- and C- terminal ends are suggested to bind to both the 5' and 3' UTR of the flavivirus genomic RNA to form the NC (Khromykh et al., 1998b; Khromykh and Westaway, 1996). Mature C protein exists as a dimer that is organized into tetramers, with each monomer folded into four alpha helices (Dokland et al., 2004; Jones et al., 2003; Ma et al., 2004). The internal hydrophobic residues of C protein facilitate the interaction between mature C and the lipid membrane of the ER to initiate budding of the

immature virus particles (Markoff et al., 1997). Deletion of this region attenuates the virus, possibly due to defective virus assembly, suggesting an important role of this protein during assembly of virion components (Kofler et al., 2002).

In addition to its role in NC formation and virion assembly, C protein has also been shown to localize in the nucleus (Bulich and Aaskov, 1992; Wang et al., 2002; Westaway et al., 1997a) and residues 85-101 of KUN C protein encodes a conserved nuclear localization signal (NLS) (Westaway et al., 1997a). The purpose of C protein localization in these subcellular locations is yet to be elucidated. The gene sequence of C protein also encodes the 5' cyclization sequence (CS) and this will be discussed in detail in section 1.2.3.6.

1.2.2.2 Pre-membrane/Membrane (prM/M) protein

The flavivirus prM (22 kDa) protein is the glycoprotein precursor of M (8kDa) protein. prM protein is mostly found on immature, non-infectious particles and to a lesser extent on secreted infectious particles (Randolph et al., 1990; Zhang et al., 2003; Zhang et al., 2007). The prM protein is translocated into the ER by the C-terminal hydrophobic domain of the C protein. Sequential proteolytic cleavage of C and prM has been previously reported, wherein the signal peptidase cleavage of prM remains inefficient until the cleavage of C has taken place (Stocks and Lobigs, 1998). Coordinated cleavage serves to delay structural protein processing and virus production until viral serine protease levels are sufficiently high late in infection (Lindenbach, 2007). Preservation of this sequential cleavage is critically important for flavivirus replication, while uncoupling this cleavage coordination was detrimental for virus growth (Lee et al., 2000; Lobigs et al., 2010).

The prM protein contains two transmembrane-spanning domains. The first transmembrane domain of prM anchors the prM protein to the membrane and involved in heterodimerization between prM and E (Lin and Wu, 2005; Wengler and Wengler, 1989). The conserved His at residue 99 in this region is important for the formation of prM/E heterodimer (Lin and Wu, 2005; Op De Beeck et al., 2004). The second transmembrane domain of prM functions as the signal sequence for host signal peptidase cleavage at the prM-E protein junction (Markoff et al., 1994).

The prM proteins act as a shield during exocytosis of immature virion through the acidic compartments in the secretory pathway. The fusion peptide of E protein is covered by prM thereby preventing E from undergoing acid-catalyzed rearrangement, causing premature fusion of nascent virus particles (Guirakhoo et al., 1992; Heinz et al., 1994). At the final stage of maturation, the N-terminal prM segment is cleaved off by furin (Stadler et al., 1997) in an acidic compartment in the trans-Golgi network to yield unglycosylated M protein which remains part of the mature virion together with the E protein (Castle et al., 1985; Guirakhoo et al., 1992; Heinz et al., 1994; Wengler and Wengler, 1989).

1.2.2.3 Envelope (E) protein

The E protein (~50 kDa) is the dominant protein present on the surface of the mature virion (Kuhn et al., 2002; Mukhopadhyay et al., 2003). Flavivirus E protein is a type I integral membrane protein with a C-terminal membrane anchor and an ectodomain. The E proteins of DENV, TBEV and WNV have been crystallized and the 3D structures were elucidated by X-ray crystallography (Modis et al., 2003; Nybakken et al., 2006; Rey et al., 1995). The crystal structure of the E protein reveals that the ectodomain is largely folded into β-sheets containing three distinctive domains: domain I (central domain), domain II (fusion or dimerization domain) and domain III (immunoglobulin [Ig] -structure-like domain) (Nybakken et al., 2006) (Fig.1.3). The structure of the protein is stabilized by the presence of six disulphide bridges generated by 12 highly conserved Cys residues (Nowak and Wengler, 1987; Roehrig et al., 1990).

Domain I (residue 1-51, 137-189 and 285-302 of TBEV) is comprised of 120 amino acid residues and folded into an eight-strand β-barrel (Rey et al., 1995). Domain I is the central domain linking domain II and domain III (Rey et al., 1995). Domain I and domain II are linked by two large loops between residues 53-132 and 194-280 in DENV or 52-136 and 190-284 in TBEV that branch out from domain I in an extended finger-like manner (Modis et al., 2003; Rey et al., 1995). The residue near or at position 154 in domain I contains the conserved N-linked glycosylation site (Mandl et al., 1988). The effect of the glycan on flavivirus assembly, secretion,

virulence and growth has been widely studied and in some cases the gain or loss of glycosylation site exhibited contradictory results (Chambers et al., 1998; Halevy et al., 1994; Hanna et al., 2005; Kawano et al., 1993; Lee et al., 2010; Rey et al., 1995).

Domain II (52-136 and 190-284 in TBEV) is responsible for generating the majority of contacts with its neighboring dimer during E protein dimerization (Rey et al., 1995). The domain contains a putative fusion peptide loop with a conserved glycine-rich, hydrophobic sequence located at the distal end of the domain (residue 98 to 110 in WNV) (Nybakken et al., 2006). The amino acid sequence at the fusion peptide contains the proposed GLFG motif found in fusion peptides of other enveloped viruses (Guirakhoo et al., 1992). The hinge region between the domain I and II provides flexibility of the protein allowing conformational changes during fusion (Zhang et al., 2004).

Domain III (303-395 in TBEV) is an Ig-like domain and folded into a ten-stranded β-barrel (Rey et al., 1995). Domain III of the E protein in the mosquito-borne flaviviruses contains the putative receptor binding site motif (RGD motif) that possibly allows the contact between E protein and the prospective cellular receptor (Lobigs et al., 1990; Nybakken et al., 2006; Rey et al., 1995; Zhang et al., 2004). Relative to domain I and II, domain III is perpendicular to the surface of the virus and the tip of the domain is projected slightly away from other part of the E dimer (Bhardwaj et al., 2001; Rey et al., 1995; Zhang et al., 2004).

Studies utilizing forward and reverse genetics approaches highlighted the significant role of E protein in two major tasks during infection: receptor-binding and membrane fusion during entry, which in turn, determined the flavivirus neuroinvasiveness and neurovirulence. Mutations in domain I, especially on the glycosylation motif, have been associated with a decrease or increase in neurovirulence (Beasley et al., 2005; Chambers et al., 1998; Halevy et al., 1994; Kawano et al., 1993; Lee et al., 2010), affecting growth in cell culture and impairment on virus production (Hanna et al., 2005; Mondotte et al., 2007; Scherret et al., 2001). In addition, mutation in the fusion peptide of domain II was shown to

cause an increase or decrease in virulence (Cecilia and Gould, 1991; Hanna et al., 2005; Monath et al., 2002; Sumiyoshi et al., 1995) and mutations in domain III are associated with alteration in neuroinvasiveness (Lee and Lobigs, 2000, 2002; Lobigs et al., 1990), and modulate virus binding and entry into host cells (Hung et al., 2004; Liu et al., 2004; Modis et al., 2004; Vlaycheva et al., 2004).

Fig. 1.3 Soluble ectodomain of TBEV E protein.

(A) Linearized of the polypeptide of the E protein ectodomain. **(B)** Monomeric pre-fusion arrangement of E protein found in mature TBEV. The three domains in E protein are shown as DI (shaded in pink), DII (shaded in blue) and DIII (shaded in brown). Fusion loop (FL) is in light blue and transmembrane domain (TM) in shaded brown. The TBEV monomer is coloured as in panel A. The figure was created using Cn3D with PBD file 1SVB (TBEV) (Rey et al., 1995).

1.2.3 The flavivirus non-structural proteins

1.2.3.1 NS1

The NS1 protein is a glycoprotein with an approximate size of 40 to 46 kDa (Chambers et al., 1990; Mason, 1989; Zhao et al., 1987). NS1 exists predominantly as a heat-labile homodimer that can be detected within infected cells, expressed on the cell surface and secreted in the extracellular medium (Chambers et al., 1990; Mason, 1989; Winkler et al., 1989; Winkler et al., 1988; Zhao et al., 1987). The NS1 protein dimerization is important for virus replication as mutation at Pro250 to Leu, which prevents NS1 dimerization, resulted in marked decrease in RNA replication in early infection (Hall et al., 1999). Soluble NS1 binds back to the plasma membrane of uninfected cells through interactions with sulfated glycosaminoglycans (Avirutnan et al., 2007). Although NS1 lacks a transmembrane domain, NS1 is directly transported and expressed on the surface of infected cells. The mechanism of NS1 cell surface expression is currently unclear although some NS1 interactions through an atypical glycosyl-phosphotidylinositol anchor (GPI) or lipid raft have been demonstrated (Jacobs et al., 2000; Noisakran et al., 2008; Noisakran et al., 2007). A short sequence immediately C-terminal to the signal sequence cleavage site has been shown to function in regulating NS1 localization to the plasma membrane or secreted to the extracellular milieu (Youn et al., 2010).

While no precise function has been ascribed to NS1, a role in RNA replication is emerging. NS1 appears to co-sediment in sucrose gradients with heavy membrane fractions containing RNA-dependent RNA polymerase (RdRp) activity from KUN-infected cells (Chu and Westaway, 1992). NS1 has been implicated to play a role in RNA replication as demonstrated by the co-localization of NS1 with the viral double-stranded RNA (dsRNA) replicative form (RF) (Lindenbach and Rice, 1997; Mackenzie et al., 1996; Muylaert et al., 1996; Muylaert et al., 1997). The NS1 dimers also have been shown to co-localize with NS2A, NS3, and NS4A proteins in the vesicle packet containing the viral replication complex (RC) (Lindenbach and Rice, 1997; Mackenzie et al., 1996; Muylaert et al., 1996; Muylaert et al., 1997). In addition, mutations on first or both N-linked glycosylation sites of NS1 markedly impaired viral RNA replication and virus growth in cell culture and decreased viral neurovirulence *in vivo* (Muylaert et al., 1996). Studies in YFV have shown that a

virus genome bearing a large deletion (YFVΔSK) in the NS1 gene is severely defective in viral replication (Lindenbach and Rice, 1999). They also revealed that a genetic interaction occurs between NS1 and NS4A for compensating the deletion in NS1.

The NS1 protein is also known to elicit protective immune responses upon infection, although anti-NS1 antibodies (Ab) do not function in virus neutralization (Hall et al., 1996). However, passive transfer of monoclonal antibodies (mAb) against YFV NS1 protected monkey against YF encephalitis (Schlesinger et al., 1985). Remarkably, active immunization with YFV NS1 also protected monkey against classical YFV infection (Schlesinger et al., 1986). Recent work suggests that NS1 exhibits an immunomodulatory function and attenuates the classical and alternative pathway of complement activation (Avirutnan et al., 2011; Chung et al., 2006; Krishna et al., 2009).

1.2.3.1.1 NS1'

Mason (1989) demonstrated the presence of two different cleavage products of NS1 in JEV-infected cells. One of the NS1 proteins has an estimated molecular mass of 42 kDa, similar to the protein observed in cells infected with other flaviviruses. The second NS1 protein which is known as NS1' has an estimated molecular mass of 47 kDa. This finding has been corroborated in cells infected with MVEV (Blitvich et al., 1995; Blitvich et al., 1999; Clark et al., 2007) and KUN (Mackenzie et al., 1998). The molecular weight variation between NS1 and NS1' was initially thought due to a C-terminal extension in the protein generated from an alternative cleavage sites within NS2A (Blitvich et al., 1999; Mason, 1989). However, recent studies by computational analysis supported by experimental evidence have shown that the NS1' is a product of ribosomal frameshifting (Firth and Atkins, 2009; Melian et al., 2010). Ribosomal frameshifting occurs at a canonical frameshift-stimulating motif containing a slippery heptanucleotide and a 3' adjacent pseudoknot near the beginning of NS2A gene (Brierley et al., 1992; Firth and Atkins, 2009; Wang et al., 1993). It was shown that mutations that disrupt the pseudoknot structure, A30P NS2A and A30A' NS2A (with silent Ala mutation at residue 30), or contains silent mutation in the slippery heptanucleotide abolished

the production of NS1' (Melian et al., 2010). Virulence analysis of mice infected with A30P NS2A mutant virus exhibited significant reduction in neuroinvasiveness, indicating putative role of NS1' in viral pathogenicity (Melian et al., 2010).

1.2.3.2 NS2A and NS2B

NS2A is small hydrophobic protein (about 22 kDa) (Chambers et al., 1998; Coia et al., 1988; Rice et al., 1985). Two forms of NS2A are found in YFV infected cells: full-length NS2A (224 amino acid), which is the product of cleavage at the NS1/NS2A and NS2A/NS2B sites, and NS2Aα, which is a C-terminally truncated form of 190 amino acids resulting from partial cleavage by viral the NS2B-3 protease at the sequence QK↓T within NS2A (Nestorowicz et al., 1994). Mutations at the NS2Aα cleavage site resulted in defect in infectious virus production, despite apparently normal levels of RNA amplification and viral protein synthesis (Kummerer and Rice, 2002). The NS2A defect, however, could be complemented in *trans* by providing NS1-NS2A or NS2-2Aα. Furthermore, a mutation of QK↓T to SK↓T could be compensated by amino acid substitutions in the NS3 helicase domain, which restored infectious virus production. This suggested an interaction of NS2A and NS3 during virion assembly or release.

A series of studies with KUN virus have shown that NS2A together with NS3 and NS5, co-localize with double stranded RNA and interact with the 3' untranslated region of the RNA. This process presumably occurs at the RC in the induced membranes of vesicle packets (VP), implying a role of NS2A during viral replication (Liu et al., 2003; Mackenzie et al., 1998).

The NS2A protein has been demonstrated to be a major inhibitor of interferon (IFN)-β promoter-driven transcription. A single amino acid substitution in Ala30Pro in NS2A abolished inhibition of the IFN response and attenuates the virulence of KUNV in mice (Liu et al., 2006). Immunization of mice with the NS2A (Ala30Pro) mutant virus resulted in induction of an Ab response that confer complete protection against a lethal dose of the highly virulent New York 99 strain of WNV. These findings demonstrate that the targeted disabling of a viral mechanism of

evading the IFN response (i.e. inhibition of NS2A function) can be applied to the development of live attenuated flavivirus vaccine candidates (Liu et al., 2006).

The ~14.5 kDa NS2B protein is a membrane-associated, hydrophobic protein that functions as cofactor for the viral protease, NS3 (Chambers et al., 1993; Falgout et al., 1993). This protein forms complexes with NS3 protease domain via a conserved hydrophilic region on NS2B facilitating a correct folding of NS3 for its catalytic activity (Chambers et al., 1993; Falgout et al., 1993; Leung et al., 2001). The hydrophobic, non-polar residues of NS2B are essential for co-translational insertion of the NS2B-NS3 precursor into the site of translation on the membrane (Brinkworth et al., 1999; Chambers et al., 2005; Clum et al., 1997). The NS2B co-factor can be supplied in *trans* although the proteolytic activity of NS3 is required in *cis* (Wu et al., 2003). Recent studies with NS2B have also suggested a role of NS2B in inhibition of IFN α/β signaling (Liu et al., 2005).

1.2.3.3 NS3

The NS3 protein (~70 kDa) is a multidomain protein with several functions required for polyprotein processing and RNA replication. While the N-terminal portion of NS3 is involved in co-translational processing of the polyprotein due to protease activity, the C-terminal portion is involved in RNA replication due to helicase, RNA triphosphatase (RTPase) and RNA-stimulated nucleoside triphosphatase (NTPase) activity (Chambers et al., 1991; Chambers et al., 1993; Cui et al., 1998; Li et al., 1999; Wengler, 1991, 1993).

The protease activity of NS3 is strongly dependent on the association of a 40 amino acid hydrophilic domain of NS2B required as a cofactor. Genetic interaction between the proteins resulted in the formation of a NS2B/NS3 heterodimeric complex (Falgout et al., 1993). NS2B/NS3 is a viral serine protease that cleaves at several sites in the polyprotein: at the junction between NS2A-NS2B, NS2B-NS3, NS3-NS4A and NS4B-NS5 (Arias et al., 1993; Chambers et al., 1991; Falgout et al., 1991), internal sites in NS2A (Jan et al., 1995), NS4A (Preugschat and Strauss, 1991) and removal of prM signal sequence from C (Amberg et al., 1994; Lobigs, 1993; Sato et al., 1993; Stocks and Lobigs, 1998) . The protease function of NS3 is

restricted to the N-terminal third region of NS3 (residues 1-160 in WNV and 1-160 in DENV2) (Arias et al., 1993; Leung et al., 2001; Li et al., 1999; Preugschat et al., 1990). Sequence and structural comparative analysis of flavi- and pestivirus suggested a significant sequence homology of this one-third region of NS3 with cellular trypsin family protease, comprising a His, Asp and Ser catalytic triad (His51, Asp75 and Ser135 in WNV) (Bazan and Fletterick, 1989; Chambers et al., 1991; Gorbalenya et al., 1989a; Wengler, 1991). Mutation in the catalytic triad prevents the proteolytic activity and mutations within the conserved region in NS3 significantly diminished the protease activity (Chambers et al., 1991; Valle and Falgout, 1998; Wengler, 1991). Inhibition of NS3 protease activity significantly reduced virus replication and thus the NS2B/NS3 region is currently a hotspot target for antiviral therapy (Chappell et al., 2008).

In addition to its protease activity, NS3 also encodes for three other enzymatic activities required for RNA replication. The C-terminal two-third portion of NS3 encodes for RNA helicase activity, which facilitates the initiation of single stranded RNA (ssRNA) replication by unwinding the RNA secondary structure in the 3' UTR (Gorbalenya et al., 1989b; Li et al., 1999; Matusan et al., 2001; Takegami et al., 1995; Utama et al., 2000; Wengler, 1991). The function of NS3 as RNA-stimulated nucleoside triphosphatase (NTPase) utilizes the energy released due to ATP hydrolysis to unwind the base-paired regions of the RI to allow synthesis of nascent strands (Kuo et al., 1996; Li et al., 1999; Warrener et al., 1993; Wengler, 1991). The enzymatic activity of NS3 as RNA triphosphatase activity (RTPase) was proposed to function in dephosphorylating the 5' end of viral genome RNA prior to cap addition by the NS5 encoded guanyltransferase and methyltransferase (MTase) (Bartelma and Padmanabhan, 2002; Issur et al., 2009; Wengler, 1993). Studies with DENV showed that the helicase and protease functional domains are overlapped with each other although the function of all three is distinctly dissociated (Borowski et al., 2002; Li et al., 1999; Warrener et al., 1993; Wengler, 1991). The NS3 function as helicase utilizes energy from NTPase hydrolysis to unwind the base-paired regions of RNA allowing the synthesis of new strands. However, the NTPase activity was not directly coupled to the helicase unwinding reaction (Borowski et al., 2001).

Interaction between NS3 and the viral polymerase, NS5, for RNA replication has also been demonstrated. *In vitro* NTPase activity of recombinant DENV NS3 was stimulated by the addition of recombinant NS5, suggesting the regulation of NTPase activities by the interaction of two proteins (Brinton, 2002; Cui et al., 1998). In addition to its enzymatic function, the necessities of NS3 for flavivirus assembly have also been observed (Khromykh et al., 2000; Kummerer and Rice, 2002; Liu et al., 2002; Patkar and Kuhn, 2008; Pijlman et al., 2006). Mutation in YF NS2A that blocks the assembly could be rescued by compensatory mutation in NS3 helicase region, implicating involvement of the NS3 helicase in flavivirus assembly (Kummerer and Rice, 2002).

1.2.3.4 NS4A and NS4B

Flavivirus NS4A is a small hydrophobic (~16kDa) and membrane- associated protein, which consists of four transmembrane domains and a cytosolic N-terminal region (Speight et al., 1988). Immunofluorescence (IF) studies showed the cytosolic region of NS4A co-localized with dsRNA and associated with the virally induced ER membranes later in infection (Mackenzie et al., 1998). Direct interaction between NS4A and NS1 is shown to be important for viral RNA synthesis (Lindenbach and Rice, 1999), suggesting that NS4A is part of the components of the replication complex. Association between NS4A and host cell polypyrimidine-binding protein (PTPB) has been recently reported and this PTPB-NS4A interaction influenced DENV production by modulating negative strand RNA synthesis (Jiang et al., 2009). Recently another function of NS4A in mediating flavivirus-induced protection against apoptosis via NS4A-mediated upregulation of autophagy signaling has been reported (Liu et al., 2005; McLean et al., 2011; Munoz-Jordan et al., 2005). Analogous with NS4B, studies have also suggested a role of these proteins in modulation of immune response by blocking IFN α/β signaling (Liu et al., 2005; Munoz-Jordan et al., 2005). The NS4A together with NS4B has been shown to inhibit Jak-STAT signaling in response to IFN-α by inducing the unfolded protein response (UPR) (Ambrose and Mackenzie, 2011; Westaway et al., 1997b).

NS4B is a small, hydrophobic and membrane associated protein of ~29 kDa. NS4B has been observed to localize with dsRNA in the perinuclear region and was also found to be actively translocated to the nucleus of infected cells late in infection (Westaway et al., 1997a). Although little is known about the function of this protein, a role for this protein in RNA replication has been suggested (Westaway et al., 1997a). The ability of NS4B to suppress the IFN response via inhibition of the phosphorylation of STAT1 has been reported, indicating the ability of this protein to modulate host immune responses (Liu et al., 2005; Munoz-Jordan et al., 2005).

1.2.3.5 NS5

The flavivirus NS5 is the largest (~100 kDa; 900 amino acid) and most conserved proteins across the genus flavivirus (Koonin, 1991, 1993; Lindenbach, 2007). This multifunctional protein contains both MTase and RdRP activities that are required for capping and synthesis of the RNA genome (Koonin, 1991, 1993). The N-terminal portion of NS5 has been shown to exhibit significant homology to S-adenosyl-L-methionine (SAM)-dependent methyltransferase domain (Koonin, 1993) and the C-terminal regions contains significant homology with RdRP of other positive-strand RNA viruses (Bruenn, 2003; Koonin, 1991; Poch et al., 1989; Rice et al., 1985). The NS5 is usually found associated with membrane-bound RC, where it typically co-localized with dsRNA and other non-structural protein components. NS5 is also found in the nucleus for YFV, DEV and JEV infected cells where it potentially interacts with host factors (Buckley et al., 1992; Edward and Takegami, 1993; Kapoor et al., 1995). Sequence alignment of NS5 also led to the identification of NLS, which lies between the MTase and RdRP domains (Brooks et al., 2002). The functional role of nuclear localization of NS5 is unclear. NS3 has also been shown to bind to the same region of NLS, suggesting the translocation of NS5 requires an interaction with NS3 (Johansson et al., 2001).

The flavivirus RNA structure contains a type I cap structure ($m^7GpppAmpN_1$) and the N-terminal region of NS5 has been associated with SAM dependent MTase activity and involved in the mRNA capping process (Ingrosso et al., 1989; Koonin, 1993). NS5 as the viral MTase is involved in transferring a methyl group from the cofactor SAM onto the N7 atom on the cap guanine and onto the ribose 2'-OH

group of the ribose moiety of the first RNA nucleotide (Bollati et al., 2010; Ray et al., 2006; Zhou et al., 2007). Sequence analysis of NS5 identified conserved RdRP GDD active site (amino acid residue 665-667 in WNV) (Kamer and Argos, 1984; Khromykh et al., 1998a; Poch et al., 1989). The crystal structure of the carboxyl-terminal portion of the NS5 showed the classical palm, thumb and finger subdomains characteristic of right-hand structure of RdRP (Koonin, 1993; Malet et al., 2007; Rice et al., 1985).

Recent studies on NS5 also suggest that NS5 is involved in viral pathogenicity by regulating host immune response. NS5 protein from JEV and Langat virus (LGTV) exhibited an inhibition of JAK-STAT signaling (Best et al., 2005; Lin et al., 2006), by preventing STAT1 phosphorylation and nuclear translocation.

1.2.3.6 Untranslated regions (UTRs)

The highly structured 5' and 3' UTRs of the flavivirus genome are variable in length (96-100 and 350-700 nt, respectively) depending on the flavivirus (reviewed in Lindenbach, 2007). Sequences at the 5' and 3' UTR are not well conserved among the flaviviruses; however a common RNA secondary structure of the 5' UTR and 3' terminal region (~350 nt) of the 3' UTR has been described (Brinton et al., 1986; Proutski et al., 1997; Rauscher et al., 1997; Wallner et al., 1995).

The 5' UTR serves an important role during the translation of the genome and virus replication. The 5' UTR has been proposed to function as the promoter for the polymerase recognition and activity, and contains CS upstream of the translation start AUG codon (Alvarez et al., 2008; Filomatori et al., 2006; Yu et al., 2008; Zhang et al., 2008). The 5' CS, which is located at 10 base pairs (bp) upstream of the C proteins gene, found to form base-pair with the complementary sequence 1 (CS1) at 3' UTR. Mutation and deletions in the 5' and 3' CS impaired RNA synthesis without significantly altering translation of the input RNA, indicating that the process of genome cyclization during RNA replication is independent of RNA translation (Alvarez et al., 2008; Cahour et al., 1995; Filomatori et al., 2006; Yu et al., 2008; Zhang et al., 2008). Interestingly, base pairing between 5' and 3' CS can

be substituted with foreign nt of the sequences and is sufficient to rescue viral RNA replication, as long as the complementarity of the sequenced is maintained. These experiments clearly indicate that the complementarity rather than nucleotide sequence *per se* is essential for RNA synthesis (Alvarez et al., 2005; Alvarez et al., 2008; Khromykh et al., 2001; Lo et al., 2003; You and Padmanabhan, 1999).

The organization of 3 'UTR is greatly different between mosquito- and tick-borne viruses; however, similar pattern of conserved sequences and structures have been found among flaviviruses (Markoff, 2003). The 62 nt downstream of the 3' CS formed the 3' step-loop (SL) structure (Brinton et al., 1986) and region in the SL is essential for virus- and host-specific function (Elghonemy et al., 2005; Tilgner et al., 2005; Yu and Markoff, 2005; Zeng et al., 1998). Analysis in DENV has shown that this structure binds to cellular proteins, phosphorylation elongation factor 1α (EF-1α) and La protein (a nuclear protein that is involved in protein transport from cytoplasm to the nucleus) (Blackwell and Brinton, 1995; De Nova-Ocampo et al., 2002). In addition to the above functions, the SL together with pseudoknots at the 3' UTR of flaviviruses is important for the production of a small, noncoding subgenomic RNA fragment, termed small flavivirus RNA (sfRNA) (Pijlman et al., 2008). The sfRNA is a product of incomplete degradation of the genomic RNA by the cellular 5'-3' exoribonuclease 1 (XRN1) and this structure is essential for efficient viral replication, cytopathogenicity and pathogenicity (Funk et al., 2010; Pijlman et al., 2008).

1.3 Flavivirus life cycle

1.3.1 Virus attachment and entry

The first step in the flavivirus life cycle is the attachment of the virus particle to the host cell at the entry point via interaction between the viral surface glycoprotein and cellular receptors (Ng and Lau, 1988). Flaviviruses are thought to enter the host cells via receptor-mediated endocytosis. Virion attachment to cellular receptors triggers the formation of clathrin-coated pits, which engulf the virus particles and subsequently transport them into the endosomal compartment for viral fusion and release of the genome into the cytoplasm (Chu and Ng, 2004).

A broad range of host cell surface molecules has been recently shown to have high affinity for flaviviruses, depending on the nature of target cells. The negatively charged heparan sulfate, which is expressed on many different vertebrate cell types, has been demonstrated to bind with positively charged residues present on the surface of flavivirus E protein (Chen et al., 1999; Chu and Ng, 2004; Gollins and Porterfield, 1985; Hilgard and Stockert, 2000; Lee et al., 2004; Lee and Lobigs, 2000; Lee et al., 2006). A number of other cell surface receptors have been reported to be involved in flavivirus attachment and entry including Heat Shock Proteins (HSP) 70 and HSP90, Glucose Receptor Protein 78 (GRP78), lipopolysaccharide binding CD14-associated molecules, $\alpha_V\beta_3$ and laminin receptor (LAMR1) (Cabrera-Hernandez et al., 2007; Chen et al., 1999; Chu and Ng, 2004; Jindadamrongwech et al., 2004; Kontny et al., 1988; Thepparit and Smith, 2004). The dendritic cell-specific intercellular adhesion molecule 3-grabbing non-integrin (DC-SIGN) and a related lectin, DC-SIGNR were also demonstrated to assist DENV and WNV, respectively, in attachment to dendritic cells to allow infection (Davis et al., 2006; Navarro-Sanchez et al., 2003; Tassaneetrithep et al., 2003). $\alpha_V\beta_3$ integrin was found to be the main receptor for JEV and WNV, but not for DENV (Chu and Ng, 2004).

Following receptor-mediated endocytosis, the cell membrane forms clathrin-coated pits, which become endosomes within the cell containing the virus (Chu and Ng, 2004; Gollins and Porterfield, 1985; Heinz et al., 1994). This is followed by virus

trafficking along the endosomal and lysosomal endocytic pathway where the viral E protein undergoes conformational changes to allow fusion of the endosomal membrane with the E protein in a pH-dependant manner (Allison et al., 2001; Chu and Ng, 2004). The ectodomain of the E protein that exists as a homodimer in its native form (pre-fusion) rearrange in the disassembly process to monomers before reassembly into homotrimers (post-fusion) after exposure to a low pH (pH 6.5 or less) environment (Allison et al., 1995; Heinz et al., 1994). Following rearrangement into homotrimers, the fusion peptide in domain II of the E protein is exposed, with subsequent release of the RNA-containing nucleocapsid into the cytoplasm in close proximity to the ER membrane (Chu and Ng, 2004).

1.3.2 RNA translation and polyprotein processing

Upon entry into the host cytoplasm, the viral RNA genome is transferred to the ER membrane for translation. Flavivirus translation occurs in viral induced structures, convoluted membranes (CM) and paracrystalline arrays (PC) (Mackenzie and Westaway, 2001; Westaway et al., 1997b). The stop-transfer sequences and signal sequences in the polyprotein determines the cytoplasmic and luminal position of the proteins. This results in prM, E and NS1 remaining in the ER and C with the rest of the nonstructural proteins in the cytoplasm or spanning the membrane (Speight et al., 1988). Flavivirus translation is cap-dependent and is stimulated by an interaction of the specialized cap structure with the 3' SL (Holden and Harris, 2004).

Processing of viral polyproteins and post-translational cleavage events play a central role in the gene expression of positive-strand RNA viruses. Analysis of amino acid sequences at the cleavage site indicates that flaviviruses utilize several different strategies for co- and post-translational cleavage of their polyproteins. At least three different proteases are involved: signal peptidase, viral-encoded protease (NS2B/NS3) and the cellular protease, furin. The enzyme responsible for cleavage at the C terminus of the NS1 resulting in NS1 and NS2A is unknown (Fig. 1.4).

Signal peptidase (or signalase) is known to cleave at the C-prM, prM-E, E-NS1 and NS4A-NS4B junctions in the flavivirus polyprotein (Cahour et al., 1992; Chambers et al., 1989; Markoff, 1989; Speight et al., 1988) on the luminal side of the ER. This host protease requires signal peptides, which typically contains three distinct regions: a positively charged N-terminal region (n-region), a central hydrophobic core (h-region) and a polar C-terminal region (c-region). The cleavage by the signal peptidase occurs at close proximity of the cleavage site to the membrane in which the n- and h-regions facilitates binding to the surface and interior of the ER membranes, respectively, and the c-region involved in defining the cleavage site (von Heijne, 1984, 1985). The polar c-region typically follows the -1, -3 rule with respect to the cleavage site, which ascertains cleavage of the signal peptide by signal peptidase. According to this rule (i) the -1 position does not contain amino acid residues with bulky aromatic side chain (Phe, His, Tyr, Trp) and is occupied by amino acids with small or hydrophobic side chains (Ala, Gly, Ser, Cys, Thr or Gln) (ii) the -3 position must not contain charged (Asp, Glu, Lys, Arg), or large polar (Gln, Asn) residues and (iii) Pro must not be present between -3 to +1 (von Heijne, 1983, 1984).

The viral trypsin-like serine protease composed of NS3 plus the NS2B cofactor cleaves after a dibasic amino acid residue, such as Lys-Arg or Arg-Arg at the -1 and -2 positions and a small side chain amino acid (Gly, Ser, Ala, Thr) at +1 (Cahour et al., 1992; Chambers et al., 1989; Falgout et al., 1991; Speight et al., 1988). This enzyme mediates cleavages at the NS2A-NS2B, NS2B-NS3, NS3-NS4A and NS4-NS5 junctions. The virus serine-protease is also responsible for mediating cleavage at the cytoplasmic side of the signal peptide to generate mature C protein (Lobigs, 1993), where the signalase cleavage of prM remains inefficient until the cleavage of C protein has taken place (Stocks and Lobigs, 1995, 1998). Similarly, a cleavage within the NS4A protein (referred to as "4A/2K" site) by the virus protease is required prior to signalase cleavage of 2K/4B (Lin et al., 1993).

Cleavage of prM to produce mature M occurs at a late step in virion maturation. This cleavage is mediated by the host enzyme, furin, shortly before virus release

and occurs at a characteristic motif containing multiple positively charged residues (Stadler et al., 1997).

1.4.2.1 Polyprotein cleavage at NS1-NS2A cleavage site

The knowledge on the processing and cleavage of flavivirus NS1-NS2A polyprotein has remained elusive for over than a decade. The mechanism(s) underlying the cleavage of NS1-NS2A is not clearly defined. In DENV virus, polyprotein processing at the NS1-NS2A junction has been previously shown to occur in the lumen of the ER (Falgout and Markoff, 1995). This event requires translocation of NS1 into the ER, following the removal of a hydrophobic NH_2- terminal signal peptide (Falgout et al., 1989). The same study has also shown that the NS1-NS2A cleavage was impaired subsequent to the deletion of the N-terminal signal sequence, suggesting an obligatory entry of NS1 into the ER lumen. The presence of almost 70% of the NH_2 –terminal of NS2A downstream the NS1-NS2A cleavage site is also indispensable for cleavage, even though the actual requirement of this region for the cleavage is greatly speculative (Falgout et al., 1989; Leblois and Young, 1995). Some studies suggest that cleavage of NS1-NS2A may be autocatalytic, however this hypothesis requires further investigation (Falgout and Markoff, 1995).

Key evidences from in-*vitro* transcription/translation, site-directed mutagenesis and analysis of the amino acid sequence at the NS1-NS2A cleavage site has led to the proposal that an unknown ER-resident host protease, most likely signal peptidase, is responsible for polyprotein cleavage at the NS1-NS2A junction (Falgout and Markoff, 1995). Few studies conducted in DENV have shown that flavivirus NS1-NS2A cleavage requires a long cleavage recognition sequence (L/MVXSXVXA), comprising of eight amino acids at the C-terminal of NS1 (Hori and Lai, 1990). This octapeptide motif is the minimal sequence requirement in the NS1 protein for cleavage at the NS1-NS2A junction, given that deletion of all other NS1 sequence except the NH_2- terminal signal peptide will still allow proteolytic processing to occur (Falgout et al., 1989; Falgout and Markoff, 1995). The NS1-NS2A cleavage site conforms with the -1,-3 rule for signal peptidase processing; however it lacks a

preceding stretch of hydrophobic amino acids characteristics of cleavable signal peptides.

Site-directed mutagenesis at the octapeptide motif revealed the importance of conservation of amino acid at P1, P3, P5, P7 and P8 positions, as mutation at these residues led to non-cleavable substrates (Pethel et al., 1992). This octapeptide recognition sequence is relatively long and unique, as its unusual length and pattern has never been described in any signal peptidase substrate studies. Interestingly, there is striking amino acid conservation at residue P1, P3, P5, P7 and P8 with very minor variability of the amino acid at P8. On the contrary, the amino acid at P2, P4 and P6 are highly variable and mutations in these residues are mostly tolerated (Hori and Lai, 1990; Pethel et al., 1992). Besides the exquisite requirements of the NS1 octapeptide motif and ~2/3 of NS2A region during NS1-NS2A proteolytic processing, no further direct investigations on the mechanism of NS1-NS2A cleavage have been published.

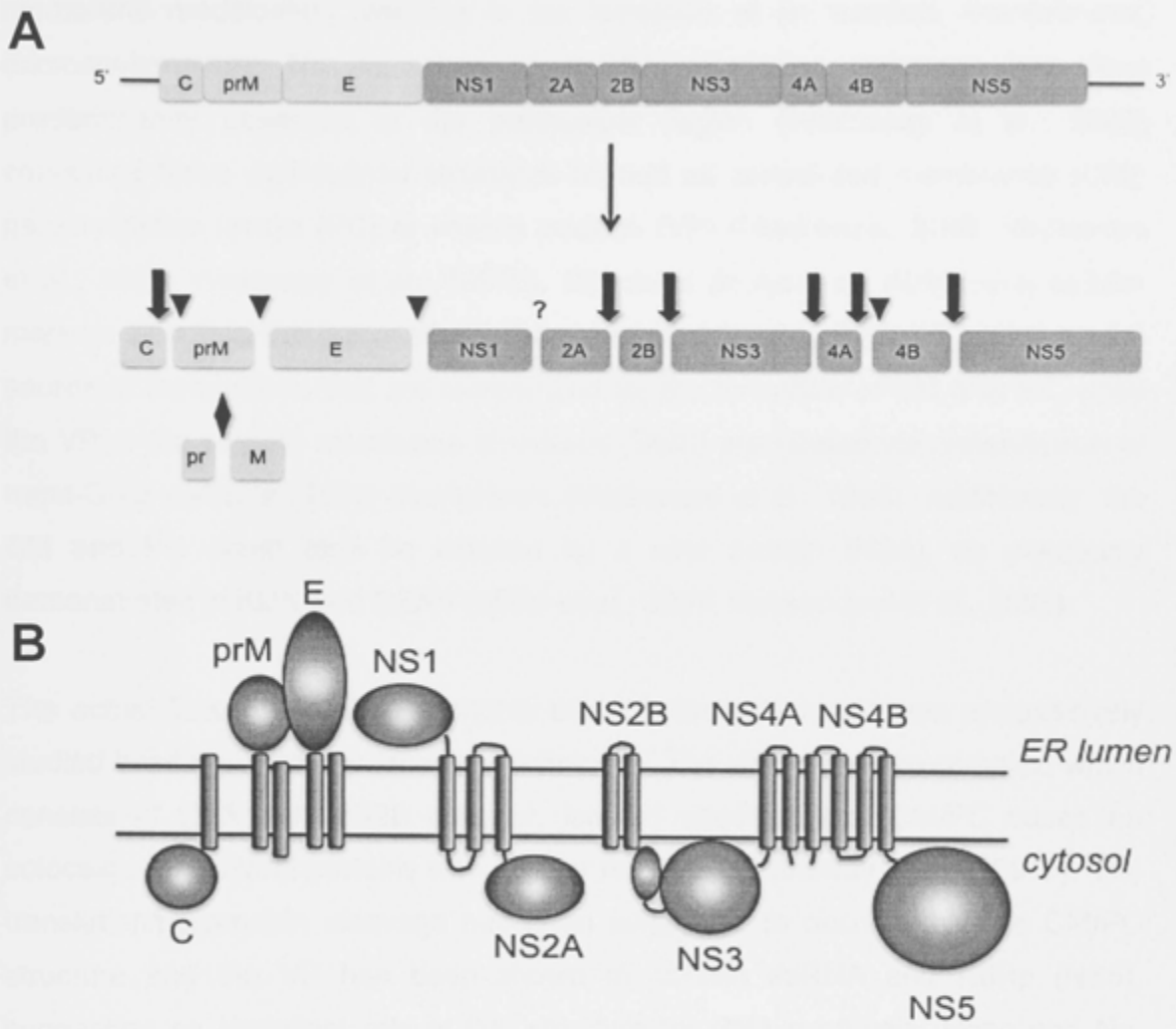

Fig. 1.4 Schematic representations of flavivirus polyprotein organization and translated protein products.

(A) The positive sense RNA genome is translated into a long, single polyprotein, which is cleaved co- and post-translationally by host signalase (arrow head), NS2B/NS3 virus-encoded protease (solid arrow), furin (♦) or an unidentified protease (?). The genome is not drawn to scale. **(B)** The putative membrane topology of flavivirus polyprotein cleavage products with respect to the ER membrane is shown. The protein drawings are approximately to scale where the areas are proportional to the number of amino acid and arranged in order from left to right of their appearance in the polyprotein. This figure is adapted from Lindenbach (2007).

1.4.3 Cellular membrane organization for flavivirus replication

The RNA replication process of flaviviruses is associated with significant membrane modification resulting in the formation of an isolated, membranous, microenvironment. The formation of distinct membrane structures has been predominantly observed in the perinuclear region (Westaway et al., 2002) containing three well-defined structures termed as convoluted membranes (CM), paracrystalline arrays (PC) or vesicle packets (VP) (Mackenzie, 2005; Mackenzie et al., 1996; Westaway et al., 1997b). Structural analysis on KUN using cellular markers identified the intermediate compartment (IC) and rough ER (RER) as the source of membranes that are reorganized for the formation of CM and PC, while the VP or the smooth membrane structures (SMS) are formed via redistribution of trans-Golgi network (TGN) membranes (Mackenzie et al., 1999). Additionally, the CM and PC could also be induced by a viral protein (NS4), as previously demonstrated in KUN and DENV (Miller et al., 2007; Roosendaal et al., 2006).

The actual functions and components of each structure have been progressively studied based on immuno-labelling techniques. The virus protease complex, which consists of NS3 with NS2B cofactor, located specifically at CM/PC based on colocalization of viral proteins with cellular markers (Westaway et al., 1997b). The translation/polyprotein cleavage has been suggested to occur within the CM/PC structure and the VP has been shown to contain dsRNA and RdRp (NS5), suggesting an important role of this structure for RNA synthesis (Hong and Ng, 1987; Mackenzie et al., 1996; Mackenzie et al., 2007; Mackenzie et al., 1998; Ng, 1987; Westaway et al., 1999). The proliferation of virus-induced membranes has also been shown to provide a protective environment for WNV replication components from the IFN-induced antiviral MxA protein, where the dsRNA replication intermediate (RI) did not trigger host defences (Hoenen et al., 2007). In addition, this microenvironment also provides a stable and confined surface area for the viral polymerase and the replication complex (RC) to congregate and function (Mackenzie, 2005).

1.4.4 RNA replication

Three major forms of flavivirus RNA have been identified in the replication cycle: positive sense genomic viral RNA, double-stranded replicative form (RF) and partially double-stranded species denoted as the RI. The RI contains heterogenous ssRNA and dsRNA, where the recently synthesized positive strand RNA is displaced by nascent strands undergoing elongation (Chu and Westaway, 1985; Cleaves et al., 1981; Grun and Brinton, 1986; Stollar et al., 1967). Flavivirus RNA replication is asymmetric, wherein positive strand RNA synthesis is in 10- to 100-fold excess over negative strands (Cleaves et al., 1981; Muylaert et al., 1996). Replication begins with the synthesis of genome-length minus strand, which serves as a template for the synthesis of additional positive strand RNA. These positive strands serve the purpose of translation of polyprotein, packaging into new virion or production of more RNA.

The site of flavivirus RNA replication is intimately linked to the viral protein replicative complex and ultimately wrapped around by highly structured membrane, VP (Chu and Westaway, 1992). Several virus components, namely NS1, NS2A, NS3, NS4A, NS5, dsRNA and RF have been identified to be localized to RC, which is anchored to the membrane by hydrophilic extension of NS4A in association with luminal NS1 (Chu and Westaway, 1992; Lindenbach and Rice, 1999; Mackenzie et al., 1998; Westaway et al., 1997b). Cyclization of RNA, which is promoted by CS in the C coding region and the 3' UTR structure, is essential for RNA replication (Bredenbeek et al., 2003; Corver et al., 2003; Khromykh et al., 2001). The genome cyclization initiates transcription of complementary negative strand RNA, preventing replication of truncated RNAs and ensuring transcription and translation from happening simultaneously (Corver et al., 2003; Hahn et al., 1987). During the replication process, the complementary RNA strand base-pair to form the dsRNA RF, which is subsequently used as template to synthesize nascent positive RNA (Chu and Westaway, 1985). Synthesis of nascent positive RNA is involved in recycling of both RC and RF, suggesting continuous protein synthesis is not required (Chu and Westaway, 1985; Westaway et al., 1999).

1.4.5 Virion assembly and budding

Flavivirus assembly is believed to occur in association with intracellular membranes, within compartment of the ER membrane. The prM and E proteins have been shown to localized to the ER and virions have been commonly observed within the lumen of the ER (Mackenzie and Westaway, 2001). Immature virions acquire their envelope by budding through the membrane of the ER. The membranes are modified with viral glycoproteins and envelop the nucleic acid-containing core particle or nucleocapsid, while the prM and E protein remain associated as heterodimer on the surface of the virion (Khromykh et al., 1998b; Khromykh and Westaway, 1996; Kiermayr et al., 2004).

The immature virion is rendered in its non-fusogenic stage by the presence of the pr segment, which prevents pH-induced fusion from occurring within the secretory pathway (Heinz et al., 1994; Lorenz et al., 2003; Mackenzie and Westaway, 2001). Immature virion is transported through the TGN where the pr segment is cleaved from the surface of the virion by the host protease furin prior to virus release (Guirakhoo et al., 1992; Mackenzie and Westaway, 2001; Nowak et al., 1989). Although mature virus containing M protein is abundantly released from cells, intracellular M-containing virion has not been detected, suggesting that prM cleavage occurs just before release of mature virions. Inhibition of prM cleavage does not severely impact on virus release, although major structural alteration in prM or modulation in furin cleavage could affect in the production of infectious virus (Stadler et al., 1997; Wengler and Wengler, 1989).

Although the processes of virus encapsidation and release are not completely understood, emerging molecular links between virus and host determinants have been found. As previously mentioned in section 1.2.3.2 and 1.2.3.3, NS2A and NS3 are involved in the assembly process, independent of their role in RNA replication and proteolytic cleavage. Recent studies with WNV indicate that Src family kinase c-Yes is involved in the egress of virion to post-ER compartment (Hirsch et al., 2005). Inhibition of c-Yes kinase demonstrates alternative pathways by which the virus can exit the cells different from the previously described exocytosis pathway.

1.4 Thesis outline

1.4.1 Rationale for the studies

Cleavage at the NS1-NS2A junction is vital for flavivirus infectivity. The host enzyme(s) which catalyses this cleavage is unknown. The protease is probably highly conserved, given that it is needed for flavivirus growth in insects and vertebrates (Falgout and Markoff, 1995; Leblois and Young, 1995). The length of the cleavage recognition sequence (8 amino acids) is relatively unusual in that it does not conform to the usual signal sequence (von Heijne 1984). Furthermore, the protease involved in NS1-NS2A cleavage is the last enzyme involved in flavivirus polyprotein processing, which remains to be identified. If this is a host enzyme and the enzyme is not crucial for cellular metabolism, inhibition of its proteolytic function could constitute an effective treatment against flavivirus infection. Understanding of the substrate specificity of the enzyme that catalyses the NS1-NS2A cleavage may allow new antiviral intervention using specific inhibitors that interrupts the viral proteolytic processing. Elucidation of the rules that govern NS1-NS2A cleavage is also important for the understanding of flaviviruses biology, in particular with respect to the control of flavivirus replication, assembly, and pathogenesis.

Thus, this thesis presents a collection of work that describes the events of NS1-NS2A processing of an encephalitis flavivirus, MVEV. Forward and reverse genetic approaches have been used to elucidate the mechanism of NS1-NS2A processing. The underlying molecular interaction between flavivirus proteins during NS1-NS2A polyprotein processing is demonstrated. The utilization of reverse genetic approach sheds a new light on the important role of amino acids at the NS1-NS2A cleavage site on virus replication.

1.4.2 Organization of the thesis

In the Literature Review Chapter (Chapter 1), a general review of the *Flaviviridae* family, flavivirus genome organization, proteins functions and virus life cycle is described. Following the Literature review, the thesis has been divided into six chapters and organized as follows:

In Chapter 2, all research materials and methods used to conduct the study are elaborated. This includes details of reagents used followed by explanation and rationale for each stage of the experimental work.

The Results chapters are divided into four chapters, from Chapter 3 to Chapter 6.

In Chapter 3, I have described the requirements for proteolytic cleavage at the MVEV NS1-NS2A junction as demonstrated by site-directed mutagenesis. The mammalian cells were transfected with DNA construct encoding the MVEV NS1-NS2A proteins tagged at the C-terminus with a hemagglutinin (HA) epitope tag. The recovery of NS1-NS2A proteins by immunoprecipitation was facilitated by the use of anti-NS1 (4G4) and anti-HA mAbs. This study elucidates the role of amino acids in the octapeptide motif in MVEV NS1-NS2A cleavage and provides a comparison with published studies carried out with DENV.

Chapter 4: Despite the analysis of NS1-NS2A cleavage in a eukaryotic expression system, modulation of NS1-NS2A processing during live virus infection has not been fully defined. Studies in this chapter were designed to describe the effect of amino acid mutations at NS1-NS2A cleavage site on viral replication using the MVEV full-length infectious clone. Analysis was focussed on four selected MVEV NS1 mutants in terms of virus viability, polyprotein processing, RNA replication and protein expression. The impact of these mutations on virus pathogenicity was assessed in mice.

Chapter 5: In this chapter, detailed analysis was carried out on the MVEV variants that exhibited enhanced growth properties (Chapter 4). One hypothesis to explain the increase of virus growth is due to the presence of compensatory mutations resulting in amino acid reversions either in the octapeptide motif or in another part of the viral genome. Sequencing of the entire coding region of MVEV variant genome showed compensatory mutations in the structural protein, E.

Chapter 6: To further confirm the role of mutations in E structural protein for compensating NS1-NS2A cleavage, two MVEV infectious clones containing mutation in E protein with the presence or absence of mutation in NS1 protein were constructed. Preliminary growth analysis of these infectious clone derived-variants is presented in this chapter.

Finally in Chapter 7, the summary and outcomes of the thesis are presented. The key findings from this study are highlighted and accompanied with some potential path for further research.

CHAPTER 2

Materials and Methods

2.1 Cell culture

African green monkey kidney cells (Vero and COS-7) and baby hamster kidney (BHK-21) cells were cultured in Eagle's minimum essential medium (MEM; Gibco) supplemented with 5% heat-inactivated foetal calf serum (FCS), 0.1 mM non-essential amino acids (Gibco) and 100 U/ml penicillin-streptomycin (PSN; Gibco), and were grown in a 5% humidified 37°C CO_2 incubator. *Aedes albopictus* (C6/36) cells were maintained at 28 °C in MEM containing 10% FCS, 0.1 mM non-essential amino acids and 100 U/ml PSN.

2.2 Eukaryotic expression plasmid

2.2.1 Construction of pRc.NS1-NS2A.HA expression construct and mutant derivatives

MVEV sequences used for this study were derived from MVE strain 1-51 (Dalgarno et al., 1986; Lee et al., 1990). The plasmid pRc/CMV.NS1-NS2A.HA, was provided by Dr. Jayaram Bettadapura (JCSMR, ANU). In this expression construct, the entire MVEV NS1 and NS2A gene sequence are cloned into pRc/CMV (Invitrogen) (Fig. 2.1A) using the *Hin*dIII/*Xba*I sites. The NS1 protein gene sequence is preceded by its authentic signal sequence and the NS2A protein is fused with the influenza HA epitope tag, which allows recovery of NS2A by immunoprecipitation with a mAb produced by the 12CA5 hybridoma (Fig. 2.1B) (Wilson et al., 1984).

2.2.2 Overview of site-directed mutagenesis method

Site-directed mutagenesis was achieved by the fusion polymerase chain reaction (PCR) following the method described by (Ho et al., 1989). As schematically shown in Fig. 2.2, this method involves the synthesis of two PCR products that overlap at the octapeptide sequence motif at the C-terminus of NS1. For each mutation, forward and reverse mutagenesis primers are required, where both are complementary to each other and contain the altered codon(s). In addition, upstream and downstream primers are required for amplification of the two fragments. These primers were designed such that two unique restriction sites were contained in the amplified region for subsequent cloning of the DNA fragment containing the mutation into the expression plasmid.

In the first round of PCR, two sets of reaction were prepared containing: (1) upstream primer and reverse mutagenesis primer and (2) forward mutagenesis primer and downstream primer. The two PCR products were subsequently separated by agarose gel electrophoresis and the DNA bands were excised and extracted using the Wizard® SV Gel and PCR Clean-Up System (Promega) (section 2.2.5). In the second PCR (fusion PCR), the two isolated PCR fragments were then used as templates, together with the upstream and downstream primers. The oligonucleotides used for site-directed mutagenesis are listed in Table 2.3 and Table 2.4.

2.2.3 PCR protocol

To generate mutants containing various changes at the NS1-NS2A junction, plasmid pRc/CMV.NS1-NS2A.HA was used as template in the first round of mutagenesis PCR. The PCR mixture contained 10 ng of pRc/CMV.NS1-NS2A.HA DNA, 0.25 μl of iProof™ High-Fidelity DNA Polymerase (2 units/μl) (Bio-Rad), 0.8 mM dNTPs (Invitrogen), 1x iProof™ HF buffer, 10 pmol mutagenesis primer and 10 pmol flanking primer (NS1 #3 or Vector #1; Table 2.4) plus nuclease-free water in a final volume of 25 μl. The PCR reaction was performed as shown in Table 2.1.

The PCR products were resolved by 0.8% agarose (Amresco) gel electrophoresis and DNA bands with the sizes of ~460 and ~850 bp were excised and gel extracted. These products were subsequently used as templates in the fusion PCR reaction: 10 ng of each of the two PCR products, 0.25 μl of iProof™ High-Fidelity DNA Polymerase (2 units/μl), 0.8 mM dNTPs, 1x iProof™ HF buffer, 10 pmol upstream primer (NS1 #3) and 10 pmol downstream primer (Vec #1) in a total volume of 25 μl, followed by PCR amplification in an iCycler Thermal Cycler (Bio-Rad) using the conditions given in Table 2.1. The fusion PCR product of ~1250 bp in size was gel-purified and stored at -20 °C.

2.2.4 Cloning of mutant pRc/CMV.NS1-NS2A.HA expression cassettes

Construction of mutant derivatives from plasmid pRc/CMV.NS1-NS2A.HA was by double digestion of fusion PCR products and wild-type (wt) plasmid with restriction enzymes *Ppu*MI and *Xba*I (Fermentas), according to the manufacturer's recommendation. The restricted vector band (~6413 bp) and the PCR fragments were gel-purified as described in section 2.2.5. The vector DNA was dephosphorylated by incubation with 1 U of shrimp alkaline phosphatase (Roche) in a buffer containing 0.5 M Tris-HCl and 50 mM $MgCl_2$ (pH 8.5) for 30 min at 37 °C, followed by inactivation of the enzyme by incubation at 65°C for 15 min.

For ligation of *Ppu*MI/*Xba*I-cut vector DNA and PCR products, 20 ng of insert DNA and 60 ng of vector DNA were incubated with 1 U of T4 DNA ligase (Roche) in a buffer containing 66 mM Tris-HCl, 5 mM $MgCl_2$, 1 mM dithioerythritol (DTE) and 1 mM ATP at pH 7.5, in a final volume of 20 μl overnight at 16°C. The ligation mix was subsequently transformed into *Escherichia coli* MC1061.1 competent cells (section 2.2.7). The amino acid sequences encoded by the pRc/CMV.NS1.NS2A.HA mutant expression cassettes are listed in the Table 2.2.

2.2.5 Agarose gel electrophoresis and DNA extraction from agarose gels

Flat bed agarose gels of 0.8% (w/v) (Amresco) were prepared with TAE buffer (40mM Tris-acetate, 1 mM ethylenediaminetetraacetic acid [EDTA]), which contained ethidium bromide at a final concentration of 0.5 μg/ml. DNA samples were loaded into wells on the gel following suspension in 6x agarose loading buffer (0.25% bromophenol blue, 0.25% xylene cyanol FF and 40% [w/v] sucrose in water). Electrophoresis was carried out at 90 to 100 V in TAE buffer until the bromophenol blue (faster-migrating dye) had migrated as far as 2/3 the length of the gel.

The DNA band of interest was excised using a scalpel for collection in a 1.5 ml tube. The extraction and purification of DNA from agarose gels was performed by using the Wizard® SV Gel Purification kit (Promega), as directed by the manufacturer's instruction.

2.2.6 Preparation of *Escherichia coli* competent cells

Bacterial cells competent for transformation were prepared from cultures grown overnight at 37°C. *Escherichia coli* strain MC1061.1 and JM110 were grown on 1.5% Luria-Bertani (LB) plates without antibiotic. A single, well-isolated bacterial colony was selected and subsequently scraped into antibiotic-free LB broth and incubated with shaking at 37°C overnight. Bacterial cells from the overnight culture were in LB broth diluted such that the OD_{600} of the culture was about 0.1, and were then incubated with vigorous shaking at 37°C until the OD_{600} of the culture was around 0.5. Subsequently, the culture was diluted 1 in 100 (in 100 ml volume) and growth was allowed to continue until the OD_{600} again reached 0.35 to 0.4. The cells were collected by centrifugation for 10 min at 1800 x *g* in sterile 50 ml Falcon tubes, and were suspended in one-tenth of the culture volume using ice-cold TSS buffer (0.2 g/ml polyethylene glycol [PEG] 8000 [Sigma], 5% dimethyl sulfoxide [DMSO] and 20 mM $MgSO_4$ in LB). The cells were incubated on ice for 10 min and were aliquoted into Eppendorf tubes, which had been chilled on ice, and the aliquots were stored at -70°C.

2.2.7 Transformation of *Escherichia coli*

Transformation of plasmid DNA into competent bacterial cells was performed by the heat-shock method. When required for transformation, a 100 µl aliquot of competent cells was thawed on ice and plasmid DNA or ligation reaction mixtures (in a volume of less than 5 µl) were added. The cells were incubated on ice for 30 min, heat-shocked at 42°C in a water bath for 30 to 40 seconds, placed on ice for 2 min, before being diluted with 400 µl of LB broth and incubation at 37°C for 1 h. The transformed bacterial cells were then spread on a 1.5% LB agar plate containing 100 µg of ampicillin (Amresco) per ml and incubated overnight at 37°C.

2.2.8 Plasmid DNA isolation from small and medium scale bacterial cultures

Small scale preparations of plasmid DNA (mini-preps) with 1 – 20 µg of plasmid DNA yield were performed by selecting well isolated single bacterial colonies to inoculate 10 ml LB broth containing ampicillin (100 µg/ml). The cultures were grown overnight at 37°C in an incubator with shaker. Bacterial cells were pelleted

by centrifugation for 5 min at 5,000 rpm and 4°C in a Beckman SS34 rotor. Following removal of the growth medium, the bacterial cell pellet was processed using the Wizard® *Plus* SV Minipreps DNA Purification System (Promega) according to the manufacturer's protocol.

Medium scale preparations of plasmid DNA (midi-preps) with DNA yields of up to 100 μg were performed by using the QIAGEN® Plasmid Midi Kit (QIAGEN). Single colonies of bacteria were used to inoculate 2 ml of LB broth containing ampicillin (100 μg/ml) and grown with shaking for at least 6-8 h at 37°C. One hundred μl of these cultures were transferred into a flask containing 50 to 100 ml of LB broth plus antibiotic and were grown with vigorous shaking at 37°C for overnight. Bacteria from the overnight cultures were pelleted by centrifugation for 15 min at 6,000 rpm at 4°C (SLA1500 rotor in a Sorvall RC 6 plus centrifuge). The plasmid DNA was extracted from the bacterial pellets using the kit and following the manufacturer's protocol.

A

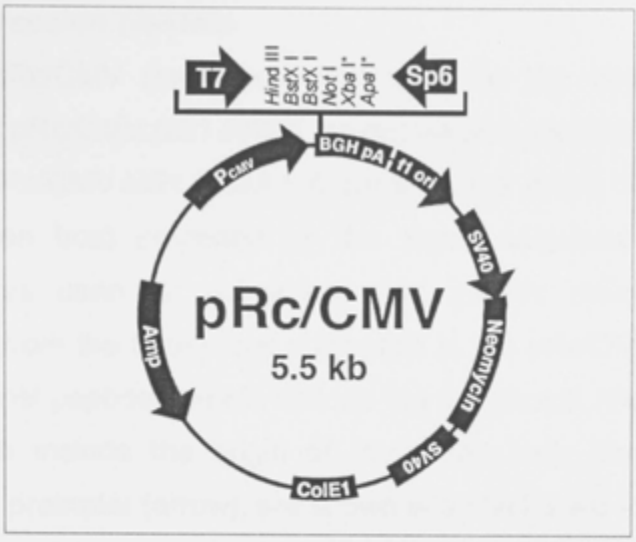
T7
Hind III
BstX I
BstX I
Not I
Xba I*
Apa I*
Sp6
BGH pA
f1 ori
SV40
Neomycin
SV40
ColE1
Amp
Pcmv
pRc/CMV
5.5 kb

B

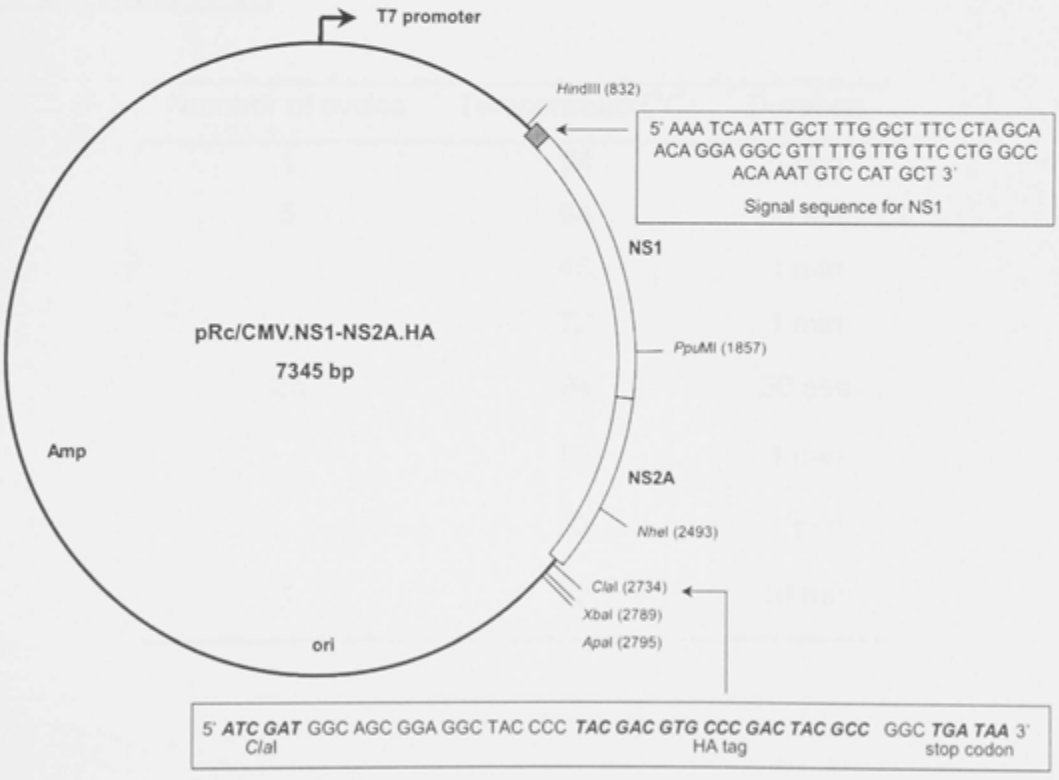
T7 promoter
HindIII (832)
5' AAA TCA ATT GCT TTG GCT TTC CTA GCA
ACA GGA GGC GTT TTG TTG TTC CTG GCC
ACA AAT GTC CAT GCT 3'
Signal sequence for NS1
NS1
pRc/CMV.NS1-NS2A.HA
7345 bp
PpuMI (1857)
Amp
NS2A
NheI (2493)
ClaI (2734)
XbaI (2789)
ApaI (2795)
ori
5' ATC GAT GGC AGC GGA GGC TAC CCC TAC GAC GTG CCC GAC TAC GCC GGC TGA TAA 3'
ClaI
HA tag
stop codon

Fig. 2.1. Schematic diagram of pRc/CMV vector plasmid and pRc/CMV.NS1-NS2A.HA expression plasmid

(A) Plasmid pRc/CMV (Invitrogen) was used as the vector backbone for the construction of pRc/CMV.NS1-NS2A.HA expression plasmid.

(B) Plasmid pRc/CMV.NS1-NS2A.HA contains the entire MVEV NS1 and NS2A sequence (open box) preceded by the signal sequence of NS1 (grey box). Restriction sites used for subcloning and genetic manipulations are shown (numbering is from the 5'-terminal nucleotide in the pRc/CMV vector). Sequences of the NS1 signal peptide and HA epitope tag are shown. Vector sequences in this plasmid, which include the origin of replication (ori), ampicillin resistant gene (Amp), and T7 promoter (arrow), are shown in a black solid line.

Table 2.1. Fusion PCR

Number of cycles	Temperature (°C)	Duration
1	94	5 min
5	94	30 sec
	45	1 min
	72	1 min
25	94	30 sec
	52	1 min
	72	1 min
1	72	10 min

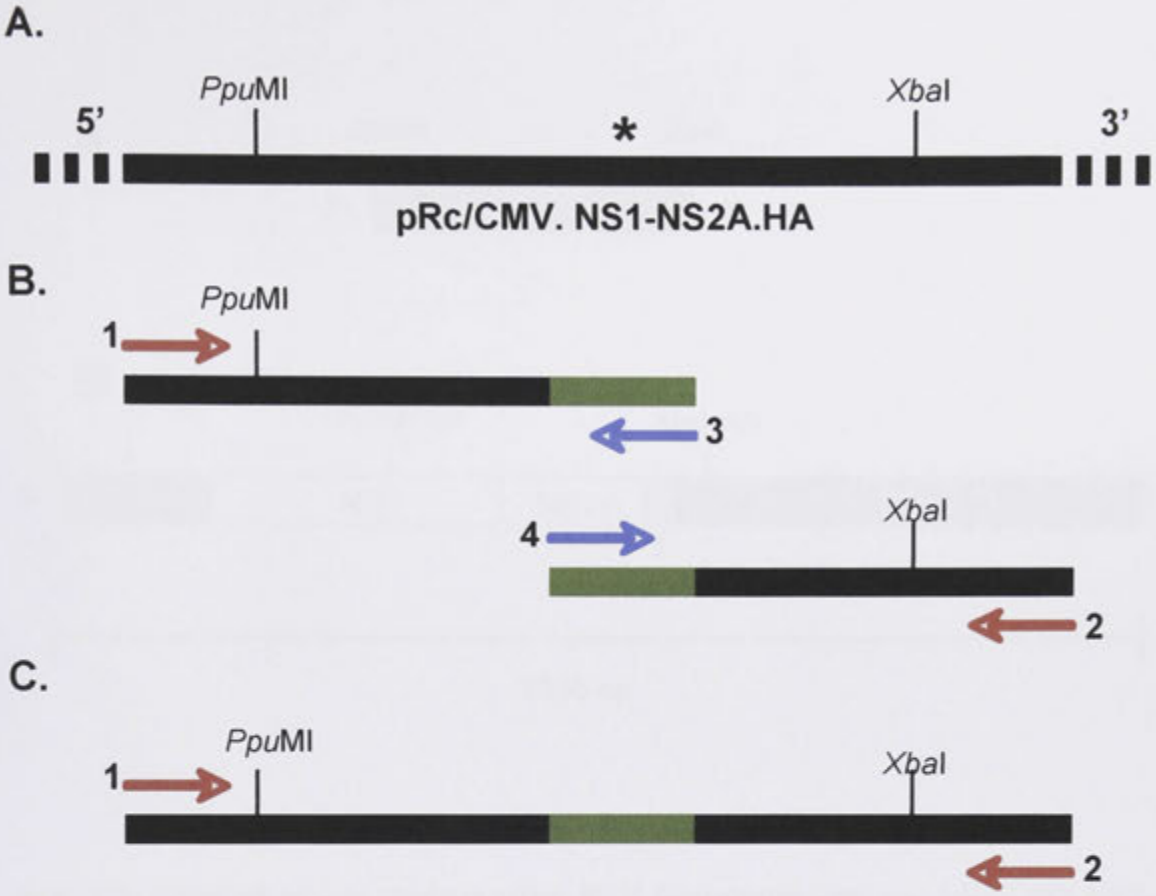

Fig. 2.2. Site-directed mutagenesis using fusion PCR.

(A) To generate a nucleotide mutation at (*), the pRc/CMV.NS1-NS2A.HA vector was used as the template for the first PCR. The unique restriction sites, *Ppu*MI and *Xba*I, in this vector are shown and were used for exchange of mutated PCR fragments with the corresponding region in the wt plasmid. **(B)** The mutagenesis primers (arrow 3 and 4) were used to generate the first PCR product harbouring a specific mutation at (*). Arrow 1 and 2 designate the upstream and downstream primers, respectively **(C)** Both fragments from the first PCR were used as templates for the fusion PCR by utilizing the upstream and downstream primers (arrow 1 and 2). The final product from the fusion PCR contained the specific mutation and was flanked by the *Ppu*MI and *Xba*I restriction sites.

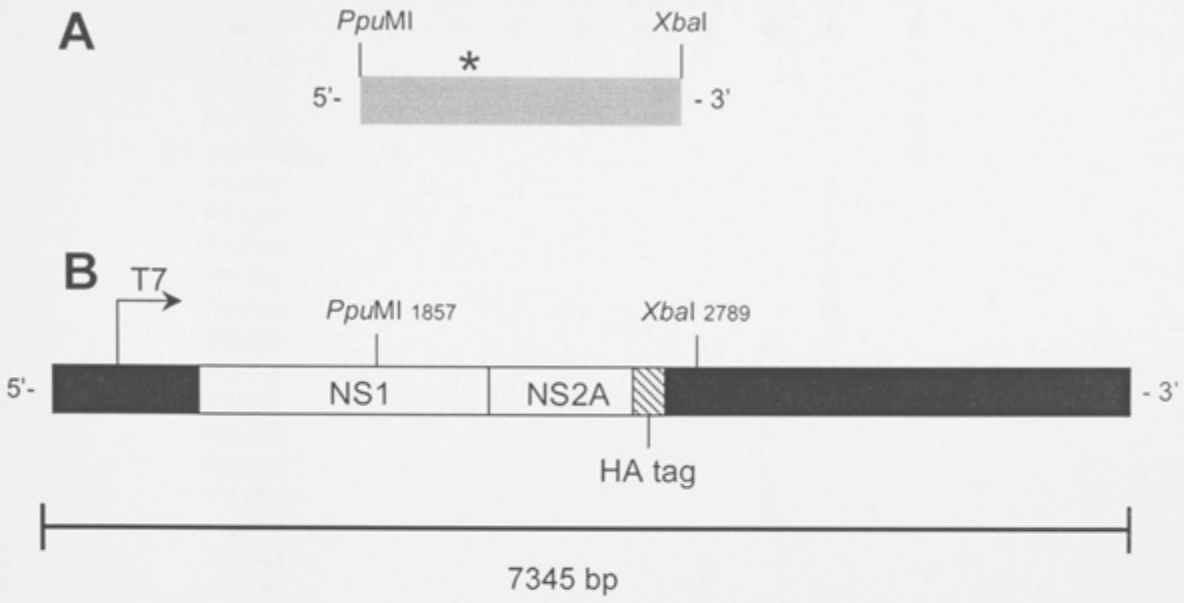

Fig. 2.3. Cloning of the mutagenized PCR fragments into the pRc/CMV.NS1-NS2A.HA vector.

A 932 bp DNA fragment containing a specific mutation (denoted as *) was double digested with *Ppu*MI and *Xba*I **(A)** and subcloned into the corresponding sites in the pRc/CMV.NS1-NS2A.HA vector **(B)**, generating a mutant plasmid of 7345 bp in length. The region corresponding to the NS1-NS2A genes is indicated by white box, and the HA tag is designated by diagonal lines. Vector sequences in this plasmid, including the T7 promoter region, are shown in black. This diagram is not drawn to scale.

Table 2.2. Mutations introduced into the octapeptide sequence motif

Construct	Amino acid sequence at the NS1-NS2A junction								
	P8	P7	P6	P5	P4	P3	P2	P1	P1'
wt	L	V	K	S	R	V	Q	A	F
P1' Phe	.	.	.	.	.	.	.	.	Y
P1' Val	.	.	.	.	.	.	.	.	V
P1' Gly	.	.	.	.	.	.	.	.	G
P1' Gly+P8 Ile	I	.	.	.	.	.	.	.	G
P1-Ser	.	.	.	.	.	.	.	S	.
P1-Leu	.	.	.	.	.	.	.	L	.
P1-Phe	.	.	.	.	.	.	.	F	.
P1-Arg	.	.	.	.	.	.	.	R	.
P1-Asp	.	.	.	.	.	.	.	D	.
P2-Ala	.	.	.	.	.	.	A	.	.
P2-Tyr	.	.	.	.	.	.	Y	.	.
P2-Gly	.	.	.	.	.	.	G	.	.
P2-Asp	.	.	.	.	.	.	D	.	.
P2-Leu	.	.	.	.	.	.	L	.	.
P2-Pro	.	.	.	.	.	.	P	.	.
P2-Arg	.	.	.	.	.	.	R	.	.
P3-Ala	.	.	.	.	.	A	.	.	.
P3-Leu	.	.	.	.	.	L	.	.	.
P3-Gly	.	.	.	.	.	G	.	.	.
P3-Lys	.	.	.	.	.	K	.	.	.
P3-Asp	.	.	.	.	.	D	.	.	.
P3-Phe	.	.	.	.	.	F	.	.	.
P4-Glu	.	.	.	.	E	.	.	.	.
P4-Gly	.	.	.	.	G	.	.	.	.
P4-Leu	.	.	.	.	L	.	.	.	.
P4-Trp	.	.	.	.	W	.	.	.	.
P5-Ala	.	.	.	A	.	.	.	.	.
P5-Arg	.	.	.	R	.	.	.	.	.
P5-Leu	.	.	.	L	.	.	.	.	.
P5-Glu	.	.	.	E	.	.	.	.	.
P5-Pro	.	.	.	P	.	.	.	.	.
P7-Ala	.	A	.	.	.	.	.	.	.
P7-Gly	.	G	.	.	.	.	.	.	.
P7-Arg	.	R	.	.	.	.	.	.	.
P8-Ala	A	.	.	.	.	.	.	.	.
P8-Glu	E	.	.	.	.	.	.	.	.
P8-Lys	K	.	.	.	.	.	.	.	.
P2,3-Ala	.	.	.	.	.	A	A	.	.
P3,8-Ala	A	.	.	.	.	A	.	.	.
P7,8-Ala	A	A	.	.	.	.	.	.	.
P5,6,7,8-Ala	A	A	A	A	.	.	.	.	.

The amino acid sequence at the MVEV NS1-NS2A cleavage junction (P8 to P1') is shown. Substitutions introduced into this region and designation of mutant constructs are given below. Residues which are unchanged relative to wt are denoted as dots.

Table 2.3. Oligonucleotides used for mutagenesis

Oligo name	Type	Sequence 5'-3'	Target region*
P1' Tyr (+)	forward	GTTCAAGCATACAATGGAGATATGATT	$NS1^{1048}$ - $NS2A^{18}$
P1' Tyr (-)	reverse	ATCTCCATTGTATGCTTGAACCCTTGA	$NS1^{1042}$ - $NS2A^{12}$
P1' Val (+)	forward	GTTCAAGCAGTGAATGGAGATATGATT	$NS1^{1048}$ - $NS2A^{18}$
P1' Val (-)	reverse	ATCTCCATTCACTGCTTGAACCCTTGA	$NS1^{1042}$ - $NS2A^{12}$
P1' Gly (+)	forward	GTTCAAGCAGGAAATGGAGATATGATT	$NS1^{1048}$ - $NS2A^{18}$
P1' Gly (-)	reverse	ATCTCCATTTCCTGCTTGAACCCTTGA	$NS1^{1042}$ - $NS2A^{12}$
P1-Ser (+)	forward	AGGGTTCAATCCTTTAATGGAGATATG	$NS1^{1045}$ - $NS2A^{15}$
P1-Ser (-)	reverse	TCCATTAAAGGATTGAACCCTTGATTT	$NS1^{1039}$ - $NS2A^{9}$
P1-Leu (+)	forward	AGGGTTCAATTGTTTAATGGAGATATG	$NS1^{1045}$ - $NS2A^{15}$
P1-Leu (-)	reverse	TCCATTAAACAATTGAACCCTTGATTT	$NS1^{1039}$ - $NS2A^{9}$
P1-Phe (+)	forward	AGGGTTCAATTCTTTAATGGAGATATG	$NS1^{1045}$ - $NS2A^{15}$
P1-Phe (-)	reverse	TCCATTAAAGAATTGAACCCTTGATTT	$NS1^{1039}$ - $NS2A^{9}$
P1-Arg (+)	forward	AGGGTTCAAAGATTTAATGGAGATATG	$NS1^{1045}$ - $NS2A^{15}$
P1-Arg (-)	reverse	TCCATTAAATCTTTGAACCCTTGATTT	$NS1^{1039}$ - $NS2A^{9}$
P1-Asp (+)	forward	AGGGTTCAAGACTTTAATGGAGATATG	$NS1^{1045}$ - $NS2A^{15}$
P1-Asp (-)	reverse	TCCATTAAAGTCTTGAACCCTTGATTT	$NS1^{1039}$ - $NS2A^{9}$
P2-Ala (+)	forward	TCAAGGGTTGCTGCATTTAATGGAGAT	$NS1^{1042}$ - $NS2A^{21}$
P2-Ala (-)	reverse	ATTAAATGCAGCAACCCTTGATTTAAC	$NS1^{1036}$ - $NS2A^{6}$
P2-Tyr (+)	forward	CAAGGGTTTACGCATTTAATGGAGAT	$NS1^{1042}$ - $NS2A^{21}$
P2-Tyr (-)	reverse	ATTAAATGCGTAAACCCTTGATTTAAC	$NS1^{1036}$ - $NS2A^{6}$
P2-Gly (+)	forward	CAAGGGTTGGAGCATTTAATGGAGAT	$NS1^{1042}$ - $NS2A^{21}$
P2-Gly (-)	reverse	ATTAAATGCTCCAACCCTTGATTTAAC	$NS1^{1036}$ - $NS2A^{6}$
P2-Asp (+)	forward	CAAGGGTTGACGCATTTAATGGAGAT	$NS1^{1042}$ - $NS2A^{21}$
P2-Asp (-)	reverse	ATTAAATGCGTCAACCCTTGATTTAAC	$NS1^{1036}$ - $NS2A^{6}$
P2-Leu (+)	forward	CAAGGGTTTTGGCATTTAATGGAGAT	$NS1^{1042}$ - $NS2A^{21}$
P2-Leu (-)	reverse	ATTAAATGCCAAAACCCTTGATTTAAC	$NS1^{1036}$ - $NS2A^{6}$
P2-Pro (+)	forward	CAAGGGTTCCTGCATTTAATGGAGAT	$NS1^{1042}$ - $NS2A^{21}$
P2-Pro (-)	reverse	ATTAAATGCAGGAACCCTTGATTTAAC	$NS1^{1036}$ - $NS2A^{6}$
P2-Arg (+)	forward	CAAGGGTTAGAGCATTTAATGGAGAT	$NS1^{1042}$ - $NS2A^{21}$
P2-Arg (-)	reverse	ATTAAATGCTCTAACCCTTGATTTAAC	$NS1^{1036}$ - $NS2A^{6}$
P3-Ala (+)	forward	AAATCAAGGGCTCAAGCATTTAATGGA	$NS1^{1039}$ - $NS2A^{9}$
P3-Ala (-)	reverse	AAATGCTTGAGCCCTTGATTTAACTAG	$NS1^{1033}$ - $NS2A^{3}$
P3-Leu (+)	forward	AAATCAAGGTTGCAAGCATTTAATGGA	$NS1^{1039}$ - $NS2A^{9}$
P3-Leu (-)	reverse	AAATGCTTGCAACCTTGATTTAACTAG	$NS1^{1033}$ - $NS2A^{3}$
P3-Gly (+)	forward	AAATCAAGGGGACAAGCATTTAATGGA	$NS1^{1039}$ - $NS2A^{9}$
P3-Gly (-)	reverse	AAATGCTTGTCCCCTTGATTTAACTAG	$NS1^{1033}$ - $NS2A^{3}$
P3-Lys(+)	forward	AAATCAAGGAAACAAGCATTTAATGGA	$NS1^{1039}$ - $NS2A^{9}$
P3-Lys (-)	reverse	AAATGCTTGTTTCCTTGATTTAACTAG	$NS1^{1033}$ - $NS2A^{3}$
P3-Asp (+)	forward	AAATCAAGGGACCAAGCATTTAATGGA	$NS1^{1039}$ - $NS2A^{9}$
P3-Asp (-)	reverse	AAATGCTTGGTCCCTTGATTTAACTAG	$NS1^{1033}$ - $NS2A^{3}$
P3-Phe (+)	forward	AAATCAAGGTTCCAAGCATTTAATGGA	$NS1^{1039}$ - $NS2A^{9}$
P3-Phe (-)	reverse	AAATGCTTGGAACCTTGATTTAACTAG	$NS1^{1033}$ - $NS2A^{3}$
P4-Glu (+)	forward	GTTAAATCAGAGGTTCAAGCATTTAAT	$NS1^{1036}$ - $NS2A^{6}$
P4-Glu (-)	reverse	TGCTTGAACCTCTGATTTAACTAGAGT	$NS1^{1030\text{-}1056}$
P4-Gly (+)	forward	GTTAAATCAGGGGTTCAAGCATTTAAT	$NS1^{1036}$ - $NS2A^{6}$
P4-Gly (-)	reverse	TGCTTGAACCCCTGATTTAACTAGAGT	$NS1^{1030\text{-}1056}$

P4-Leu (+)	forward	GTTAAATCATTGGTTCAAGCATTTAAT	$NS1^{1036}$ - $NS2A^{6}$
P4-Leu (-)	reverse	TGCTTGAACAACTGATTTAACTAGAGT	$NS1^{1030-1056}$
P4-Trp (+)	forward	GTTAAATCATGGGTTCAAGCATTTAAT	$NS1^{1036}$ - $NS2A^{6}$
P4-Trp (-)	reverse	TGCTTGAACCCATGATTTAACTAGAGT	$NS1^{1030-1056}$
P5-Ala (+)	forward	CTAGTTAAAGCTAGGGTTCAAGCATTT	$NS1^{1033}$ - $NS2A^{3}$
P5-Ala (-)	reverse	TTGAACCCTAGCTTTAACTAGAGTGGA	$NS1^{1027-1053}$
P5-Arg (+)	forward	CTAGTTAAAAGAAGGGTTCAAGCATTT	$NS1^{1033}$ - $NS2A^{3}$
P5-Arg (-)	reverse	TTGAACCCTTCTTTTAACTAGAGTGGA	$NS1^{1027-1053}$
P5-Leu (+)	forward	CTAGTTAAATTGAGGGTTCAAGCATTT	$NS1^{1033}$ - $NS2A^{3}$
P5-Leu (-)	reverse	TTGAACCCTCAATTTAACTAGAGTGGA	$NS1^{1027-1053}$
P5-Glu (+)	forward	CTAGTTAAAGAAAGGGTTCAAGCATTT	$NS1^{1033}$ - $NS2A^{3}$
P5-Glu (-)	reverse	TTGAACCCTTTCTTTAACTAGAGTGGA	$NS1^{1027-1053}$
P5-Pro (+)	forward	CTAGTTAAACCTAGGGTTCAAGCATTT	$NS1^{1033}$ - $NS2A^{3}$
P5-Pro (-)	reverse	TTGAACCCTAGGTTTAACTAGAGTGGA	$NS1^{1027-1053}$
P7-Ala (+)	forward	TCCACTCTAGCTAAATCAAGGGTTCAA	$NS1^{1027-1053}$
P7-Ala (-)	reverse	CCTTGATTTAGCTAGAGTGGACTCATC	$NS1^{1021-1047}$
P7-Gly (+)	forward	TCCACTCTAGGAAAATCAAGGGTTCAA	$NS1^{1027-1053}$
P7-Gly (-)	reverse	CCTTGATTTTCCTAGAGTGGACTCATC	$NS1^{1021-1047}$
P7-Arg (+)	forward	TCCACTCTAAGAAAATCAAGGGTTCAA	$NS1^{1027-1053}$
P7-Arg (-)	reverse	CCTTGATTTTCTTAGAGTGGACTCATC	$NS1^{1021-1047}$
P8-Ala (+)	forward	GAGTCCACTGCTGTTAAATCAAGGGTTC	$NS1^{1023-1051}$
P8-Ala (-)	reverse	TGATTTAACAGCAGTGGACTCATCATGC	$NS1^{1017-1044}$
P8-Glu (+)	forward	GAGTCCACTGAGGTTAAATCAAGGGTTC	$NS1^{1023-1051}$
P8-Glu (-)	reverse	TGATTTAACCTCAGTGGACTCATCATGC	$NS1^{1017-1044}$
P8-Lys (+)	forward	GAGTCCACTAAAGTTAAATCAAGGGTTC	$NS1^{1023-1051}$
P8-Lys (-)	reverse	TGATTTAACTTTAGTGGACTCATCATGC	$NS1^{1017-1044}$
P3,8-Ala (-)	reverse	AAATGCTTGAGCCCTTGATTTAACAGC	$NS1^{1039}$ - $NS2A^{9}$
P7,8-Ala(+)	forward	GAGTCCACTGCTGCTAAATCAAGGGTTCAAG	$NS1^{1024-1054}$
P7,8-Ala (-)	reverse	TGATTTAGCAGCAGTGGACTCATCATGCTTC	$NS1^{1014-1044}$
P5,6,7,8-Ala(+)	forward	ACTGCTGCTGCTGCTAGGGTTCAAGCATTT	$NS1^{1030}$ - $NS2A^{3}$
P5,6,7,8-Ala(+)	reverse	TTGAACCCTAGCAGCAGCAGCAGTGGACTC	$NS1^{1024-1053}$

The sequences and orientation of primers used for mutagenesis PCR are given, together with the region in the target MVE strain 1-51 (Dalgarno et al., 1986; Lee et al., 1990) sequence to which they were designed to anneal. Nucleotides that mismatch with the target DNA are underlined.

* Numbering is from the 5' end of the target gene.

Table 2.4. Oligonucleotides used for PCR and sequencing

Oligo name	Type	Sequence (5'-3')	Target region*
5' UTR #1	forward	GATCATTGATTAACGCGGTTTGAACAGTTTTT	5' UTR$^{44-75}$
C #1	forward	GGAACACTGATTGATGTGGTGAAC	C$^{265-288}$
E #1	reverse	TGTGATCTGCCCGCTTCGTG	E$^{246-265}$
E #2	forward	ACGAAACACTTTCTAGTGCATCG	E$^{622-644}$
E #3	reverse	TGGTGCAAAGCTCCTTCC	E$^{774-791}$
E #4	forward	GTTTAAGTGTGCTGCTCGAAAAC	E$^{818-840}$
E #5	forward	CAAGCAGATCAATCACCACTGGC	E$^{1170-1192}$
E #6	reverse	AGAGGGTTCTAAATGCTCCTCC	E$^{1339-1360}$
NS1 #1	reverse	CACACTTGAGCTCCCTCCT	NS1$^{28-46}$
NS1 #2	forward	CAAGCAACTGGCTAAAGTGG	NS1$^{117-136}$
NS1 #3	forward	ACTGGATTGAGAGTGGACTCAATG	NS1$^{599-622}$
NS1 #4	forward	TTGATAATCCCAGTGACTC	NS1$^{721-739}$
NS2A #1	reverse	GAAGGCCTAACTGAAAAG	NS2A$^{23-40}$
NS2A #2	forward	ACTGGATTGAGAGTGGACTCAATG	NS2A$^{154-174}$
NS2A #3	reverse	TATGTGTCAAGGTGAAGCATTCTC	NS2A$^{486-509}$
NS3 #1	forward	GGAACTTCAGGATCCCCAATAGTCAATAGC	NS3$^{397-426}$
NS3 #2	reverse	GCTATTGACTATTGGGGATCCTGAAGTTCC	NS3$^{397-426}$
NS3 #3	reverse	AGGGGTGGCCGTCATAAA	NS3$^{940-958}$
NS3 #4	reverse	CAGCACTGGCACTAGTGA	NS3$^{1349-1366}$
NS3 #5	forward	GTGTATTCAGACCACCAGTC	NS3$^{1801-1820}$
NS4A #1	reverse	CTGCAAAATGCTCTGGCATCCG	NS4A$^{31-52}$
NS4B #1	forward	GCAACAATACTGGTAACCCTC	NS4B$^{349-359}$
NS4B #2	reverse	CCAGCTCTGGAACATCTGTCGCGA	NS4B$^{473-496}$
NS4B #3	forward	GCGGGAGCTTCAATAGCCTGG	NS4B$^{715-735}$
NS5 #1	forward	GACTGGCTAAGCCGTGGTCC	NS5$^{507-526}$
NS5 #2	forward	CTGAAGGAGGAGTATGCAGCC	NS5$^{856-876}$
NS5 #3	forward	TGGGAAATGGTGGATGAGGAAAGG	NS5$^{1301-1323}$
NS5 #4	reverse	AACTCCAAGAATCTGGCTCCCA	NS5$^{1142-1163}$
Vector #1	reverse	CTGATCAGCGAGCTCTAGCATTTAAGGTGA	Vector $^{2803-2831}$ (a)
Vector #2	reverse	AGGTGACACTATAGAATAGGGCCC	Vector $^{2785-2808}$ (b)

(a) Oligonucleotide anneals in the pRc/CMV.HA vector DNA at 25 residues downstream from the *Xba*I site (see Fig. 2.1 and 2.3)

(b) Oligonucleotide anneals in the pRc/CMV.HA vector DNA at 7 residues downstream from the *Xba*I site (see Fig. 2.1 and 2.3)

* Numbering from 5' end of the target gene.

2.2.9 Construction of truncated NS2A constructs

To facilitate the construction of two NS1-NS2A expression plasmids with C-terminal truncations corresponding to 40% and 14% of NS2A (pRc/CMV.NS1-NS2A[60%] and pRc/CMV.NS1-NS2A[86%], respectively), *Cla*I sites were introduce in the NS2A. A single *Cla*I site is present in the wt pRc/CMV.NS1-NS2A.vector (Fig. 2.1), and the additional sites introduced allowed restriction enzyme digestion in the NS2A gene at codons corresponding to amino acid 137 or 196 of NS2A. The *Cla*I sites were introduced by site-directed mutagenesis using mutagenesis primers P137 (+) and P137 (-) or P196 (+) and P96 (-) (Table 2.5).

To produce the intermediate vectors, a 938-bp *Ppu*MI-*Apa*I fragment from pRc/CMV.NS1-NS2A.HA was exchanged with that obtained from fusion PCR following digestion with the same enzymes. Plasmid pRc/CMV.NS1-NS2A(60%) and pRc/CMV.NS1-NS2A(86%) were constructed by digesting the intermediate vector with *Cla*I, religation and transformation into JM110 cells. The candidate bacterial colonies were subcultured overnight prior to small scale plasmid DNA isolation and the plasmid DNA was subjected to sequence analysis.

Table 2.5. Oligonucleotides used for introduction of *Cla*I sites into pRc/CMV.NS1-NS2A.HA

Oligo name	Type	5' to 3' sequence	Target region*
P137(+)	forward	ACAGCTTGGATCGATTTGCGAGCAATGGCTTTT	$NS2A^{400-432}$
P137 (-)	reverse	TGCTCGCAAATCGATCCAAGCTGTAGCAGCTGA	$NS2A^{391-423}$
P196 (+)	forward	AAGAAAGGAATCGATTTAATTGGTCTAGCCCTG	$NS2A^{577-609}$
P196 (-)	reverse	ACCAATTAAATCGATTCCTTTCTTTTTCTCCAC	$NS2A^{590-622}$

Oligonucleotides incorporating *Cla*I site in NS2A sequence is underlined.

* Numbering is determined from the 5' end of the target gene.

2.3 Sequence verification and analysis

2.3.1 Eukaryotic expression plasmid DNA

Nucleotide sequences of pRc/CMV.NS1-NS2A.HA and its mutant derivatives were verified by automated nucleotide sequencing using an AB 3730 DNA Analyzer (Applied Biosystems). Cycle sequencing was performed by using BigDye® Terminator Cycle Sequencing Ready Reaction Kit (Applied Biosystems) according to the manufacturer's recommendation. 150-300 ng of plasmid DNA was mixed with 1 μl of BigDye®, 5 pmol of sequencing primer (NS1 #4; Table 2.4), 5x sequencing buffer and water to a final volume of 20 μl. The cycle sequencing was run according to the conditions given in Table 2.6.

Table 2.6. PCR condition for cycle sequencing

Number of cycle	Temperature (°C)	Duration
1	94	5 min
30	96	10 sec
	50	5 sec
	60	4 min

Following the PCR, DNA was precipitated with 2 μl of 125 mM EDTA, 2 μl 3M sodium acetate and 55 μl of absolute ethanol and the mixture was incubated at room temperature for 15 min. The DNA was pelleted by centrifugation at 14,000 x *g* for 15 min, washed twice with 1 ml of 70% ethanol and air-dried. The DNA pellet was submitted to the Biomolecular Resource Facility, JCSMR, ANU for automated nucleotides sequencing. Sequence analysis was performed by using Sequencher® version 4.8 (Gene Codes).

2.3.2 MVEV full-length infectious clone (pMVEV) derived plasmids

Sequencing of pMVEV and its derivatives was performed by first generating PCR fragments of region in the MVEV structural and non-structural protein genes. The PCR reaction mix was prepared by using 12.5 μl EconoTaq® PLUS 2x Master Mix (Lucigen) (containing 0.1 units/ml of EconoTaq DNA polymerase, reaction buffer (pH 9.0), 400 μM dATP, 400 μM dGTP, 400 μM dCTP, 400 μM dTTP, 3 mM $MgCl_2$, and a proprietary PCR enhancer/stabilizer), 1 μl of each 20 pmol upstream and downstream primers, 1 μl of full-length infectious clone plasmid DNA (50-100 ng/μl) and nuclease-free water to a final volume of 25 μl. The PCR reaction was performed in an iCycler Thermal Cycler (Bio-Rad) according to the condition given in Table 2.7.

Table 2.7. PCR condition for EconoTaq®

Number of cycle	Temperature (°C)	Duration
1	95	2 min
30	95	30 sec
	50	1 min
	72	2 min
1	72	10 min

Following amplification, the PCR products were gel-purified by electroporesis on an 0.8% agarose gel, excised and processed DNA bands using and the Wizard® SV Gel and PCR Clean-Up System (Promega). PCR products with the size range of 500 to 1000 bp (30 to 100 ng DNA) were used as the template for cycle sequencing as described in section 2.3.1.

2.3.3 Total infected cell RNA

2.3.3.1 RNA extraction from infected cells

To detect mutations in MVEV variants, subconfluent Vero cell monolayers were infected with virus until signs of cytopathic effects (CPE) were apparent. Cell monolayers (~1 x 10^6 cells) were carefully washed with ice-cold phosphate-buffered saline (PBS) and 750 μl of TRI reagent® (Molecular Research Centre) was added to lyse the cells, lysates were stored at -70°C or directly used for RNA extraction. Two hundred μl of chloroform (Sigma) was added to the cell lysates, the mixture was vortexed vigorously for 10-20 sec prior to centrifugation at 10,000 x *g* for 15 min at 4°C in an Eppendorf microfuge and the aqueous phase was collected. An equal volume of isopropanol (Sigma) was added to the aqueous phase and the mixture was incubated for at least 30 min on ice. The RNA was then pelleted by centrifugation at 10,000 x *g* for 15 min at 4°C in an Eppendorf microfuge, washed twice with 0.5 ml of 75% ice-cold ethanol made up in RNAse-free water, air dried and resuspended in 20 μl of RNAse-free water and stored at -70°C.

2.3.3.2 Reverse transcription and amplification of viral structural or non-structural protein genes and sequence analysis of amplified products

Expand Reverse Transcriptase (Roche) was used for cDNA synthesis from RNA extracted from infected cells. For reverse transcription, reactions containing 1.5 μl of RNA sample, 1x RT buffer (provided with the Expand Reverse Transcriptase), 10 mM dithiothreitol (DTT), 1 mM dNTPs, 20 U RNaseOUT™ Ribonuclease Inhibitor (Invitrogen), 25 pmol random hexamer mix, and 25 U Expand Reverse Transcriptase enzyme were prepared in a final volume of 10 μl. The reaction mixture was rested at room temperature for 5 min, incubated at 37°C for 10 min, followed by 1 h incubation at 42°C.

One to 2 μl of cDNA mixture was used for PCR amplification using EconoTaq® PLUS 2x Master Mix Kit as described in section 2.3.2 and in Table 2.7. Gel-purified PCR products were subjected to cycle sequencing as described in section 2.3.1.

2.4 Transfection in COS-7 cells

Transfection of eukaryotic expression plasmid DNA into COS-7 cells was performed by the diethylaminoethyl cellulose (DEAE)-dextran method, as described (Lobigs, 1992). Subconfluent COS-7 cell monolayers grown in 60 mm plastic Petri dishes were incubated for 4 h at 37°C with 1.5 ml transfection medium (serum-free MEM containing 250 μg DEAE-dextran [Sigma] per ml) and ~5 μg of plasmid DNA. Subsequently, the transfection medium was removed by aspiration and the cells were shocked by the addition of 2 ml Hanks' balanced salt solution (HBSS) containing 10% DMSO and 0.1% glucose for 1.5 min at room temperature. The medium was aspirated and the monolayers were washed twice with serum-free MEM. Four ml of MEM supplemented with 5% FCS was added and cells were incubated for 2 days at 37°C in a humidified 5% CO_2 incubator.

2.5 Metabolic labeling

Metabolic labeling of proteins was performed on transfected, infected or uninfected control cell monolayers grown in 35 mm or 60 mm diameter dishes. The cell monolayers were washed twice with PBS prior to starvation for 1 h in 1 ml or 2 ml of methionine- and cysteine-free MEM, respectively. Following removal of medium, cells were metabolically labeled for 0.5 to 3 h with 0.5 ml or 1 ml of the above medium containing 100 μCi of Trans ^{35}S-label (ICN) per ml. For chases, the cell monolayers were washed twice with warmed PBS, growth medium was added, and the cells were incubated for 1 h or as described in figure legends.

Subsequent to the labelling interval, dishes of labelled cells were placed on ice and cells were washed once with ice-cold PBS. The monolayers were lysed by incubation on ice for 30 min with 0.5 ml or 1 ml of radio-immunoprecipitation assay (RIPA) buffer (50 m Tris-HCl, pH 7.4, 0.15 M NaCl, 1% NP-40, 1% sodium deoxycholate, 0.1% SDS, 0.2 mM EDTA) containing a mammalian protease inhibitor cocktail (Biosciences) according to supplier's specification. The cells were scraped from the dishes followed by nuclei removal by centrifugation for 10 min at 14,000 x *g* in an Eppendorf microfuge in the cold room and the lysates were pre-cleared by incubation with protein A-Sepharose CL-4B (GE Healthcare; 30 μl of a

5% [w/v] suspension in RIPA buffer) for 2 to 3 h at 4°C. Beads were removed by centrifugation at 6,000 x *g* for 2 min at 4°C followed by immunoprecipitation.

2.6 Immunoprecipitation of ^{35}S-labelled MVEV proteins

Immunoprecipitation was performed by overnight incubation of cell lysates at 4°C with 2 μl of anti-HA epitope tag Ab (12CA5) (1.5 mg/ml), 60 μl of NS1 protein-specific monoclonal antibody (mAb) 4G4 (Clark et al., 2007) or 60 μl of E protein-specific mAb, 8E7 (Hall et al., 1990). The immune complexes were collected by the addition of protein A-Sepharose CL-4B (60 μl of 5% [w/v] suspension) and incubated at 4°C on a rotating wheel for another 3 h. The beads were then collected by centrifugation at 6000 x *g* for 1 min in an Eppendorf centrifuge and washed twice with 1 ml of ice-cold buffer A (0.2% NP-40, 10mM Tris-HCl [pH 7.5], 150mM NaCl, 2mM EDTA), twice with 1 ml of ice-cold buffer B (0.2% NP-40, 10mM Tris-HCl [pH 7.5], 500mM NaCl, 2mM EDTA), and once with 1 ml of ice-cold PBS. Unless subjected to sodium dodecyl sulfate polyacrylamide gel electrophoresis (SDS-PAGE) on the same day, the beads were frozen at -20°C until use.

2.7 Endoglycosidase H digestion

For endoglycosidase H (endo H) treatment of immunoprecipitated proteins, bound immune complexes were eluted from the protein A-Sepharose beads by heating to 95°C for 5 min in 30 μl of denaturing buffer containing 1% SDS, 10mM Tris-HCl buffer (pH 6.8) and 5% β-mercaptoethanol. The beads were removed by centrifugation and half of the supernatant was digested with an equal volume of digestion buffer containing 50 mM sodium citrate (pH 5.5) and 1 U of endo H (Roche) for 16 h at 37°C. The other half of the supernatants received the same treatment in the absence of the enzyme.

2.8 SDS polyacrylamide gel electrophoresis (SDS-PAGE) and phosphorimaging

Separation of proteins by discontinuous SDS-PAGE was based on the method of Leammli (Laemmli, 1970). The beads used for collection of immunoprecipitated protein products were suspended in 60 μl of SDS sample buffer (2% SDS, 100mM Tris-HCl [pH8.8], 10% glycerol, 2.5 mM EDTA, 0.01% bromophenol blue) containing 5% β-mercaptoethanol and were heated at 95°C for 5 min. Samples were applied to a 20 cm x 20 cm polyacrylamide gel consisting of a 5% acrylamide stacking gel (5% Acrylamide-Bis [Amersco], 0.1 M Tris-HCl [pH6.8], 0.1% SDS, 0.05% tetramethylethylenediamine [TEMED; Sigma] and 0.07% ammonium persulphate [APS]) and a 12.5% resolving gel (12.5% Acrylamide-Bis, 0.4 M Tris-HCl [pH8.8], 0.1% SDS, 0.05% TEMED, and 0.05% APS), unless otherwise specified in the figure legends. Electrophoresis was performed in SDS running buffer (0.6% [w/v] Tris base, 2.88% [w/v] glycine and 1% SDS) at a constant voltage of 45 V until the bromophenol blue marker was within 1 cm of the bottom of the gel. A carbon-14 (^{14}C) radiolabeled marker protein mix (GE Healthcare) was used for estimation of the molecular sizes of the sample proteins.

Following electrophoresis, the gels were fixed by incubation for 30 min in 200 ml of 20% acetic acid, thoroughly rinsed in distilled water and dried on Whatman 3M paper using a gel dryer. Dried gels were placed in contact with a Photo-Imager screen (Fuji Film) for 3 to 4 days before the screen was scanned using a Fuji Film FLA/LAS or Typhoon FLA 9000 instrument (Biomolecular Resource Facility, JCSMR). Image analysis for protein band quantitation was performed using the Multi Gauge version 2.0 program (Fuji Film).

2.9 *In vitro* transcription of infectious RNA from full-length MVEV cDNA clones

Approximately 5 μg of pMVEV infectious cDNA clone was linearized by digestion with *Nsi*I (NEB) as described (Lobigs et al., 2010). Following 2 h digestion, the DNA was treated with 1 U of T4 DNA polymerase (Roche) in the presence of 1 μl of 10 mM dNTPs mix for 10 min at 37°C to fill in the overhangs. The DNA was phenol extracted by adding 100 μl of buffer-saturated phenol (Ambion, Inc.) to the DNA after adjusted the volume to 100 μl with distilled water, vigorous vortexing for 30 sec and centrifugation at 14 000 x *g* for 1 min in an Eppendorf microfuge. The aqueous phase (top phase) containing the DNA was mixed with 500 μl of water-saturated ether and centrifuged at 14 000 x *g* for 1 min. The ether (top) phase was aspirated, the ether-extraction step repeated twice and the DNA was precipitated on ice with 220 μl of absolute ethanol and 10 μl of 3 M sodium acetate (pH 5.2) for 30 min prior to centrifugation (14,000 x *g* for 15 min in the cold-room) to pellet the DNA. The DNA pellet was washed twice with ice-cold 70% ethanol, air-dried at room temperature and suspended in 10 μl of nuclease-free water.

Transcription of genome-length RNA from linearized plasmid DNA was carried out as described (Lee and Lobigs, 2000). Reaction mix containing 1x SP6 buffer (40 mM Tris-HCl [pH 7.5], 6 mM $MgCl_2$, 4 mM spermidine, 10 mM dithiothreitol [DTT], 1 mM RNA cap structure analogue m^7G[5']ppp[5']G (Epicentre), 1 mg of bovine serum albumin (BSA) per ml, 1 mM of each ATP, UTP and CTP, 25 U RNaseOUT™ Ribonuclease Inhibitor (Invitrogen), 1 U T7 RNA polymerase (Epicentre) and ~0.1 μg linear cDNA was incubated for 5 min at 37°C. One μl of 25 mM GTP was then added and the incubation continued for 90 min at 37°C. Two μl of the reaction product was used for diagnostic agarose gel electrophoresis and the rest was frozen in aliquots at -70°C.

The *in vitro*-transcribed RNA product was run for 15 min at 90 V on a 0.8% agarose gel containing 0.5 μg of ethidium bromide per ml. Prior to electrophoresis, the apparatus was thoroughly cleaned using RNaseZap® (Ambion, Inc.) to ensure

RNAse-free conditions. Yield of genome length RNA was estimated by visual inspection of gels on an UV light transilluminator.

2.10 Transfection of RNA transcripts into BHK cells

The RNA transcribed *in vitro* was transfected into BHK cells by electroporation as previously described (Lee and Lobigs, 2000). BHK cells were washed twice in PBS and suspended in serum-free MEM at 1.2 x 10^7 cells/ml. Cells (1 x 10^7) were mixed with *in vitro* RNA transcripts in an electroporation chamber (0.4-cm gap; GibcoBRL) and were subjected to two consecutive pulses at 250 V, 800 μF, and the low-Ohm setting using the Cell-Porator electroporation system I (GibcoBRL). The transfected cells were rested at room temperature for 5 min, suspended in 25 ml of growth medium and transferred to culture dishes for incubation at 37°C. Culture medium was harvested after 3 days for virus titration by plaque assay and frozen in aliquots at -70°C.

2.11 Virus characterization

2.11.1 Virus stocks

The MVEV prototype strain, MVE-1-51 (French, 1952), was used. To produce a working stock, subconfluent Vero cells in a 175 cm^2 tissue culture flask (Thermo Scientific) were infected at a multiplicity of infection (MOI) of ~1 with virus diluted to 2 ml in HBSS containing 0.2% BSA and 20 mM 4-(2-hydroxyethyl)-1-piperazineethanesulfonic acid (HEPES), (pH 8.0) (HBSS-BSA). The virus was adsorbed at 37°C for 1 h, growth medium was added, followed by incubation for 72 h or when CPE was evident. The culture medium was clarified by centrifugation at 960 x *g* for 5 min and 1 M HEPES (pH 8.0) was added to give a final concentration of 20 mM. Virus stocks were aliquoted and stored at -70°C.

2.11.2 Determination of virus titre

Virus was titrated by plaque formation on 80% confluent monolayers of Vero cells (3 x 10^5 cells/well) in six-well plastic tissue culture plates (Thermo Scientific) as described (Licon Luna et al., 2002). Samples to be assayed were serially diluted in HBSS-BSA diluent on ice and monolayers were infected in duplicate with 100 μl

aliquots of the diluted virus sample. Virus adsorption was for 1 h at 37°C in an atmosphere of 5% CO_2 with occasional shaking. An agar overlay medium (M199 medium [Gibco], 1% Bacto-agar [Oxoid], 2% FCS, 100 U/ml of PSN) was added to the monolayer (4 ml per well), and the cells were incubated for 72 to 96 h at 37°C. The monolayers were stained by the addition of 1 ml of 0.02% neutral red (BDH Chemicals) in HBSS and plaques were counted 10 to 16 h later following removal of the stain and the overlay. Virus titer was calculated as plaque forming unit (PFU) per 1 ml.

2.11.3 Plaque purification

Plaques were purified according to Lee et al., (2000). Infected Vero cell monolayers under an overlay agar were stained with 0.02 % neutral red for 10 to 16 h for plaque visualization. Single, well-isolated plaques were collected by aspirating the agar overlay with a sterile Pasteur pipette and suspension of the agar plug in 100 µl HBSS-BSA. Plaque picks were stored at -70°C.

2.11.4 Viral growth analysis

To measure virus release from infected mammalian cells, Vero cell monolayers in 6-well plastic tissue culture plate seeded with 3 x 10^5 cells/well were infected at a MOI of 0.1. After a 1 h incubation at 37°C, the inoculum was removed, the monolayers were washed twice with prewarmed PBS to remove unbound viruses, 3 ml of growth medium was added and the incubation at 37°C continued. A growth analysis was generated by harvesting and replenishing 100 µl of the culture supernatants at 2, 16, 24, 40, 48 and 64 h post-infection (p.i). Aliquots were stored at -70°C following additions of HEPES (pH 8.0) to a 10 mM final concentration. Virus content was determined by plaque assay on Vero cells.

For determination of viral growth in mosquito C6/36 cells, the monolayers were seeded in 6-well plastic tissue culture plate at 1 x 10^6 cells/well and were infected at MOI of 0.1 on the following day. Following 1 h virus adsorption at 28 °C, the monolayers were washed twice with PBS followed by addition of 4 ml growth medium and the incubation was continued at 28°C. The culture supernatants were

collected at 2, 24, 48, 48, 72 and 98 h p.i, supplemented with HEPES (pH 8.0) to a 10 mM final concentration, stored at -70°C and titres were determined by plaque assay on Vero cells.

2.11.5 Flow cytometry for measuring virus infection of Vero and C6/36 cells

The infectivity of viruses in Vero and C6/36 cells was measured by using a fluorescence-activated cell sorter (FACS)-based assay, as described previously (Lee et al., 2010). To determine the virus infectivity in Vero cells, cell monolayers were harvested with trypsin (Gibco), thoroughly washed with PBS and cells were pelleted by centrifugation at 960 x *g* for 5 min. The cell pellets were fixed and permeabilized by incubation with ice-cold 75% ethanol at 4°C for at least 30 min. Fixed cells were pelleted by centrifugation prior to 1 h staining with 200 µl of the NS1 protein-specific mAb, 4G4, diluted in growth medium (1:200 dilution of a hybridoma culture fluid). Cells were washed twice with growth medium and then incubated with 200 µl of fluorescence isothiocyanate (FITC)-coupled anti- mouse immunoglobulin (Ig) G (Dako laboratories) (diluted 1:200 in growth medium) and incubated at 4°C for 30 min. The cells were washed once with growth medium and once with PBS, resuspended in 200 µl of 2% para-formaldehyde (w/v) made up in PBS and analysed using a FACScan (BD Biosciences) equipment and Cell Quest Pro software (Becton Dickinson) (Microscopy and Cytometry Resource Facility, JCSMR, ANU).

Analysis of virus infectivity in C6/36 cells was performed as follows: C6/36 cells were harvested and fixed with 200 µl of 2% para-formaldehyde made up in PBS for 30 min on ice, followed by permeabilization in 200 µl of 0.5% saponin (made up in PBS) for 10 min at room temperature. Cells were washed once with PBS and were collected by centrifugation (960 x *g*, 5 min) and stained with anti-NS1 mAb, 4G4, and FITC-conjugated anti-mouse Ig as described above.

2.11.6 Specific infectivity of viruses for mammalian cells

Vero cells monolayers were seeded at 3 x 10^5 cells per well in 6-well plastic tissue culture plate and infected with virus at MOI of 0.1. Cell culture medium was

removed at 48 or 72 h p.i, and the cell monolayers were washed twice with PBS, followed by addition of 3 ml of growth medium and further incubation at 37°C. Virus release harvest were collected after 2 h incubation and centrifuged at 960 x *g* for 5 min to remove cell debris. Virus content in the 2-h release stock was titrated by Vero cells plaque assay and the amount of RNA copies in the same stock was determined by real-time quantitative reverse transcription PCR (qRT-PCR). Specific infectivity values were calculated as the ratio of viral RNA copies per PFU.

2.12 Virus-specific RNA synthesis

2.12.1 Kinetics of RNA synthesis *in vitro*

Vero cells (3 x 10^5 cells) in a 6-well tissue culture plate were infected with virus at MOI of 1. After 1 h of virus adsorption, the monolayers were washes twice with PBS and 3 ml of growth medium was added, followed by incubation at 37°C. Cell monolayers were harvested at 2, 12, 18, 24 and 48 h p.i. The monolayers were washed twice with PBS and the RNA was extracted by using TRI reagent® (described in section 2.3.3.1) and resuspended in 20 μl of nuclease-free water. Intracellular viral genome copy numbers were determined real-time qRT-PCR.

2.12.2 RNA isolation from culture supernatant

Culture medium (50 μl) from virus infected cells was treated with 20 μg/ml RNAse A (Sigma) for 30 min at 37°C to remove free viral RNA. For RNA extraction, 500 μl of TRI reagent® containing 10 μg of yeast tRNA (Sigma), 1 μl of pellet paint (Novagen) and 50 μl of chloroform were added, incubated on ice for 5 min and subsequently processed according to the procedure described in section 2.3.3.1. The RNA was subsequently resuspended in 20 μl of nuclease-free water and stored at -70°C.

2.12.3 Genome copy number quantitation by real-time qRT-PCR

Intracellular viral RNA copies or virion-associated genome content in culture supernatants were measured by real-time qRT-PCR. Reverse-transcription and real-time PCR were performed following the previously described method (Lee and Lobigs, 2008). cDNA was generated by RT using Expand Reverse Transcriptase

(Roche). The RT-step was performed in a 10 μl reaction mixture containing 2 μl of sample RNA or serially diluted MVEV RNA standards, 10 mM dNTPs, 5 pmole downstream primer (NS5 #4), 10 mM DTT, 10 U RNaseOUT™ Ribonuclease Inhibitor (Invitrogen), 25 U of Expand Reverse Transcriptase and the manufacturer's recommended buffer conditions. The reaction mixture was incubated at 43.5°C for 90 min, followed by addition of 40 μl of nuclease-free water and stored at -20°C.

MVEV RNA standards were provided as *in vitro*-transcribed RNA generated from plasmid pMVEV-rep (MVEV full-length cDNA clone lacking most of C, prM and E proteins from residue 28 in C protein to residue 480 in E protein) as described (Lobigs et al., 2010). The RNA standards were suspended in nuclease-free water at 10^9 RNA copies/μl (as quantitated by spectrophotometry) and serial dilutions were performed to yield standards of 10^7, 10^6, 10^5 and 10^4 RNA copies/μl.

Quantitative PCR (qPCR) was performed as previously described (Lee et al., 2010) using 10 μl of IQSybr qPCR mixture (Bio-Rad), 2 pmole per primer for upstream primer (NS5 #3) and downstream primer (NS5 #4) and 3 μl of RT mixture and nuclease-free water was added to 20 μl. The qPCR reaction was performed using a Bio-Rad iCycler under cycling conditions as tabulated in Table 2.9.

The virion RNA content was determined by extrapolation from the standard curves generated within each experiment and each RNA sample was analysed in duplicate. The estimation for intracellular viral RNA copies obtained from real-time qPCR was presented as viral RNA copies per monolayer of infected cells (for example 1×10^5 RNA copies obtained from real-time qPCR = 1×10^6 RNA copies per monolayer of infected cells). The number of virion-associated RNA copies obtained from qPCR from the infected culture supernatant was presented as viral RNA copies per 1 ml of the infected culture supernatant (for example 1×10^5 RNA copies obtained from real time qRT-PCR = 2×10^7 RNA copies/ml).

Table 2.8. Oligonucleotides used for RT and qPCR

Oligo name	Type	Sequence 5'-3'	Target region*
NS5 #3	forward	TGGAAATGGTGGATGAGGAAAGG	$NS5^{1186-1207}$
NS5 #4	reverse	AACTCCAAGAATCTGGCTCCCA	$NS5^{1142-1163}$

* numbering from 5' end of NS5 gene

Table 2.9. PCR condition for real time qRT-PCR

Number of cycle	Temperature (°C)	Duration
1	50	2 min
1	95	3 min
40	95	30 sec
	63	30 sec
	72	30 sec
47	72	30 sec

2.13 Viral protein synthesis

2.13.1 Western blot

Vero cells were seeded in 60 mm plastic tissue culture dishes at a concentration of 5 x 10^5 cells per dish and grown for 16 h prior to infection. Cells were infected with virus at MOI of 1, followed by incubation at 37°C for 72 h before cells were trypsinized, washed and pelleted by centrifugation (960 x *g*, 5 min). The cells pellet was treated with 500 µl of RIPA buffer supplemented with mammalian protease inhibitor cocktail (Biosciences) according to the supplier's specification, incubated for 30 min on ice, subjected to centrifugation at 14,000 x *g* at 4°C for 10 min to remove nuclei and cell debris, and supernatant were collected and stored at -20°C.

For analysis, the cell lysate were denatured in 500 µl of SDS sample buffer containing 5% β-mercaptoethanol, heated at 95°C for 5 min and 10 µl of samples were subjected to SDS-PAGE in 12% precast NUView Tris-Glycine iGels (NuSep) at 100 V for 1.5 h in a Bio Rad Mini PROTEAN II electrophoresis system. The

proteins were subsequently transferred onto Immobilon-P (Millipore) membranes and the membranes were saturated with 5% skim milk in Buffer A (10 mM Tris-HCl containing 0.15 M NaCl) for overnight at 4°C. Membranes were briefly washed with wash buffer (Buffer A containing 0.05% NP40) and subsequently stained with 100 µl of anti-NS1 protein mAb (4G4) or 100 µl of anti-E protein mAb (8E7) hybridoma culture fluid diluted in 1:100 in Buffer B (0.25% BSA, 0.1% Tween-20, 10 mM Tris-HCl, 0.15 M NaCl) for 1 h with constant rocking at 4°C. The membranes were washed three times in wash buffer, incubated for 1 h with horse-radish peroxidase-conjugated anti-mouse Ig (DAKO laboratories) diluted 1:200 in Buffer B, further washed three times as described above and developed with ECL Plus™ Western Blotting Reagents (GE Healthcare) according to the manufacturer's protocol. The chemiluminescence signal was detected by exposure to X-Ray film (Fuji Film) or using ImageQuant LAS4000 equipment (GE Healthcare) (Biomolecular Resource facility, JCSMR). All images were processed with Multi Gauge version 2.0 program (Fuji Film) and Microsoft Office Picture Manager software.

2.13.2 Indirect immunofluorescence staining

Vero cells were seeded on cover slips in 24-well plates at a concentration of 2.5 x 10^4 cells per well 16 h prior to infection. Cell monolayers were infected with virus at a MOI of 0.5 or 5 as described in figure legends, and incubated for 24, 48 or 72 h in a 37°C incubator.

For fixation, cells were washed once with PBS and fixed with 4% para-formaldehyde (w/v) made up in PBS for 10 min at room temperature. Thereafter, cells were stored at 4°C in PBS for 2-3 days or used directly. Cell were then treated with 0.1% Triton-X100 in PBS for 5 min to allow membrane permeabilization and washed 3 times with PBS prior to incubation for 5 min with blocking solution (5% FCS diluted in PBS). The cells were washed 3 times with PBS followed by primary and secondary antibody staining.

All primary and secondary antibodies were diluted to the desired concentration with antibody diluent (PBS with 5% BSA). Staining with primary antibody was achieved by incubation with a 1:100 dilution of anti-NS1 mAb (4G4) or 1:100 dilution of E

protein- specific mAb (8E7) hybridoma culture fluids for 1 h in a humidified container at 4°C. Cells were washed thoroughly with PBS (3 changes), followed by incubation with FITC-IgG (1:200 in antibody diluent) under the same condition described for primary staining. After washing with PBS, cells were mounted on glass slides with Vectashield mounting solution (Vector Laboratories) and were viewed with an Olympus fluorescence microscope (Microscopy and Cytometry Resource Facility, JCSMR, ANU). All images were processed with Microsoft Office Picture Manager software.

2.14 Animal experiments

2.14.1 Virulence in mice

All animal experiments were conducted in the animal handling facility operated by the Animal Services Division, ANU Bioscience Services at the John Curtin School of Medical Research according to approved standards for the care and use of laboratory animals. Six-week-old IFN-alpha receptor knockout (IFN-α-$R^{-/-}$) mice (Muller et al., 1994) were inoculated intraperitoneally (i.p) with 1000 PFU of virus prepared in 200 μl of HBSS-BSA. Mice were closely monitored over a period of 28 days for the onset of disease and euthanized when the first sign of encephalitis (hunching, ruffles fur and lethargy, eye closure and/or hind leg flaccid paralysis) were apparent.

2.14.2 Determination of viremia levels

Blood was collected by tail bleeding at day 2 p.i and was kept on ice for 10 min. Blood was clotted by centrifugation (6000 x *g* for 10 min), serum (~50 μl) was collected and stored at -70°C. Virus content in serum was determined by plaque titration on Vero cells.

CHAPTER 3

Mutational and biochemical analysis of the proteolytic cleavage at the Murray Valley encephalitis virus NS1-NS2A junction

3.1 Introduction

Flavivirus gene expression involves the translation of a single ORF to produce a polyprotein, which is co- and post-translationally cleaved into the mature viral proteins by the host enzyme, signal peptidase, and the virally encoded NS2B-protease. While the proteases responsible for cleavages between most of the flavivirus structural and non-structural proteins are known, the enzyme that catalyses NS1-NS2A cleavage remains elusive. Knowledge on the proteolytic processing at the flavivirus NS1-NS2A polyprotein junction has not progressed since the early work conducted on DENV (Falgout and Markoff, 1995; Hori and Lai, 1990; Pethel et al., 1992). Furthermore, it is unclear if the findings in the DENV studies, also apply to other members of the flavivirus genus.

It has been proposed that an ER resident protease, plausibly signal peptidase, executes the flavivirus NS1-NS2A cleavage (Falgout and Markoff, 1995). However, NS1-NS2A cleavage requires an unusually long cleavage recognition sequence, which comprises eight amino acids at the C-terminal of NS1 (Hori and Lai, 1990) and does not include a stretch of hydrophobic residues (8-12 amino acids) characteristic of a cleavable signal peptide. The octapeptide motif is the minimal sequence requirement in NS1 for cleavage at the NS1-NS2A junction, given that deletion of all other NS1 sequence, except the N-terminal signal peptide, allowed proteolytic processing to occur (Falgout et al., 1989; Falgout and Markoff, 1995). In contrast, the presence of the NH_2-terminal ~70% of the NS2A protein downstream of the octapeptide sequence is essential for cleavage and cannot be substituted with an unrelated polypeptide of comparable hydrophobicity (Falgout and Markoff, 1995).

A sequence comparison of the NS1-NS2A cleavage site of a large number of flaviviruses including all antigenic subgroups is shown in Figure 3.1. Interestingly, there is striking amino acid conservation at residues P1, P3, P5, P7 and P8 with only minor variability at P8 (Leu or Met). In contrast, the amino acids at P2, P4 and P6 are highly variable, which altogether creates an interesting pattern of variant and invariant residues from P1 through to P8. Side-directed mutagenesis revealed

the importance of conservation of amino acids at P1, P3, P5, P7 and P8 as conservative or non-conservative substitutions at these residues led in almost all instances to a non-cleavable substrates, except for a Ser→Pro change at P5 (Pethel et al., 1992). On the other hand, conservative or non-conservative changes were mostly tolerated at positions P2, P4 and P6.

In this chapter, I investigate the amino acid sequence requirements in the octapeptide of MVEV that dictate cleavage efficiency at the NS1-NS2A junction. Through transient expression in mammalian cell culture of NS1 and NS2A proteins in combination with side-directed mutagenesis, I have examined the effect of amino acid substitutions in the octapeptide motif on NS1-NS2A cleavage. Constructs encoding truncated NS2A were also made, in order to investigate the requirement of NS2A in MVEV NS1-NS2A cleavage. I establish for the first time that the remarkably conserved residues in the flavivirus octapeptide motif can be replaced with different amino acids without markedly reducing cleavage efficiency of NS1 and NS2A.

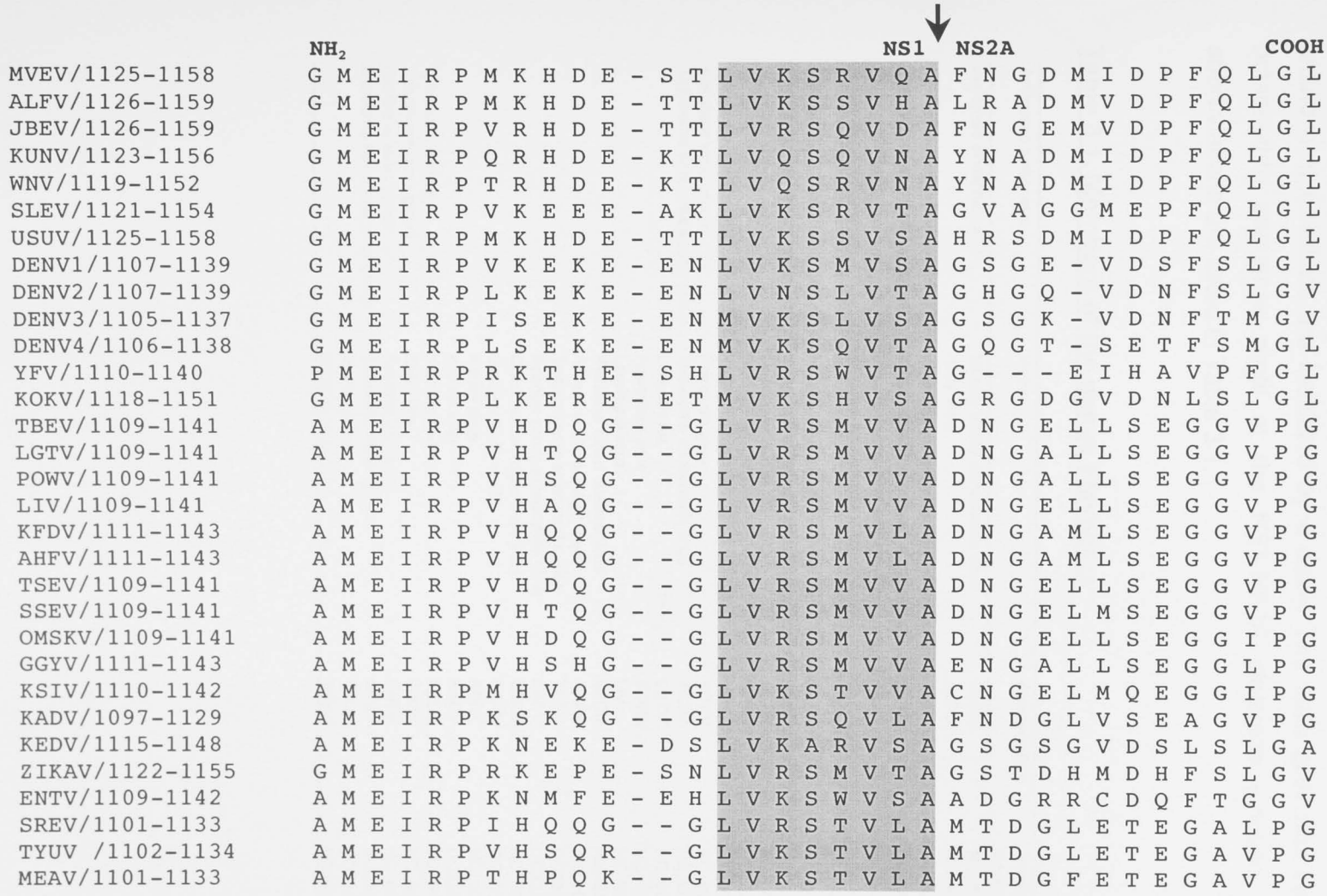

Fig. 3.1. Comparison of NS1-NS2A cleavage site sequences among flaviviruses.

Amino acid sequence alignment at the C-terminal of NS1 and the N-terminal of NS2A of MVEV with other closely and distantly related members of the flaviviruses was modified from Flavitrack (Danecek and Schein, 2010; Misra and Schein, 2007). The arrow shows the NS1-NS2A cleavage site. Numbers of the first and last amino acids included in the alignment are shown next to the virus abbreviation and amino acid deletions are indicated by a dash. The solid grey box indicates the octapeptide sequence motif at the NS1-NS2A cleavage junction. The virus abbreviations are listed in Table 3.1.

Table 3.1. Members of the genus Flavivirus

Antigenic subgroup	Virus	Abbreviation	GenBank Accession no
Japanese encephalitis	Murray Valley encephalitis virus	MVEV	NC_000943
	Alfuy virus	ALFV	AY898809
	Japanese encephalitis virus	JBEV	NC_001437
	Kunjin virus	KUNV	D00246
	West Nile virus (strain 956)	WNV	NC_001563
	St. Louis encephalitis virus	SLEV	NC_007580
	Usutu virus	USUV	NC_006551
Dengue	Dengue virus type 1	DENV1	NC_001477
	Dengue virus type 2	DENV2	NC_001474
	Dengue virus type 3	DENV3	NC_001475
	Dengue virus type 4	DENV4	NC_002640
Yellow fever virus group	Yellow fever virus	YFV	NC_002031
Kokobera virus group	Kokobera virus	KOKV	NC_009029
Tick-borne encephaltis virus group	Tick-borne encephalitis virus	TBEV	NC_001672
	Langat virus	LGTV	NC_003690
	Powassan virus	POWV	NC_003687
	Louping ill virus	LIV	NC_001809
	Kyasanur forest disease virus	KFDV	HM055369
	Alkhurma hemorrhagic fever virus	AHFV	NC_004355
	Turkish sheep encephalitis virus	TSEV	DQ235151
	Spanish sheep encephalitis virus	SSEV	DQ235152
	Omsk hemorrhagic fever virus	OMSKV	NC_005062
	Gadgets Gully virus	GGYV	DQ235145
	Karshi virus	KSIV	NC_006947
	Kadam virus	KADV	DQ235146
Unclassified virus	Kedougou virus	KEDV	NC_012533
Spondweni virus group	Zika virus	ZIKAV	NC_012532
Rio Bravo virus group	Entebbe bat virus	ENTV	NC_008718
Seaborne tick-borne virus group	Saumarez Reef virus	SREV	DQ235150
	Tyuleniy virus	TYUV	DQ235148
	Meaban virus	MEAV	DQ235144

3.2 Results

3.2.1 Generation of a NS1-NS2A expression cassette for the analysis of the NS1-NS2A proteolytic cleavage

The MVEV NS1-NS2A expression cassette was engineered to encode the entire NS1 and NS2A proteins and gene expression was controlled by T7 promoter-driven transcription (see Materials and Methods). In this cassette, the NS1 protein is preceded by the authentic NH_2-terminal signal sequence to allow translocation of NS1 into the lumen of the ER. In addition, due to the absence of antibodies to MVEV NS2A protein, a short immunoreactive HA epitope tag was introduced at the COOH-terminus of NS2A to allow recovery of NS2A by immunoprecipitation. The presence of the HA tag did not affect NS1-NS2A cleavage.

The proteins expressed from the NS1-NS2A constructs were detected following immunoprecipitation and separation by SDS-PAGE. They correspond to NS2A and the uncleaved NS1-NS2A precursors based on their electrophoretic mobility and reactivity with the HA-tag Ab. NS1-NS2A precursor bands were detected as a doublet with approximate sizes of 64 and 66 kDa. Analysis of N-linked glycosylation by endo H digestion showed sensitivity of the doublet to the deglycosylation treatment (Fig. 3.14) suggesting that these protein bands represent glycosylation variants of the NS1-NS2A polyprotein. MVEV NS1 protein has 3 Asp-linked carbohydrate acceptor motif, while NS2A is not glycosylated. Accordingly, inclusion of both bands for quantitation of NS1-NS2A cleavage estimates is required.

NS1-NS2A cleavage efficiency was calculated after normalising for the number of Met and Cys residues in uncleaved NS1-NS2A (30) and NS2A (14). The percentage cleavage efficiency was determined as the radioactivity (expressed as photostimulated luminescence, PSL) in the NS2A band divided by the sum of that in NS2A and the NS1-NS2A precursor bands using the formula:

$$\left[\frac{NS2A}{NS2A+\left(NS1-NS2A_{precursor}\right)}\right]\times 100$$

All transfections of mutant constructs were conducted with a wt NS1-NS2A plasmid as a positive control. The mean cleavage efficiency of wt NS1-NS2A calculated from more than 3 independent experiments was 88% ± 1. The percentage of cleavage for each mutant construct was calculated from the results of at least three independent experiments.

3.2.2 Mutational analysis of the octapeptide sequence at the NS1-NS2A junction of MVEV

The effect of mutations at the five conserved positions, P1, P3, P5, P7 and P8 and three variable positions at P1', P2 and P4 on NS1-NS2A cleavage was explored.

3.2.2.1 Amino acid substitutions at P1'

Studies conducted on DENV have shown that the P1 and P1' positions flanking the cleavage site at the NS1-NS2A junction are highly sensitive to mutations, possibly due to the functional importance of these amino acids in forming the scissile bond at the cleavage site (Pethel et al., 1992). However, sequence comparison among the flaviviruses indicates that the first amino acid down-stream of the NS1-NS2A cleavage site (P1') is not conserved although it is identical among the four DENV (Fig. 3.1). To explore the role of this residue, the P1' Phe was changed to one of three different amino acids: Tyr, Val or Gly (Fig. 3.2). Substitution of Phe with a second aromatic residue (Tyr), or the non-conservative changes to Gly or Val did not markedly impact on cleavage efficiency of NS1 and NS2A (84%, 86% and 80%, respectively) (Table 3.2), indicating that amino acid side chain variability is tolerated at this position. A serendipitous change at P8 in the octapeptide (Leu→Ile) in a mutant construct harbouring the P1' Gly substitution also had no marked effect on cleavage efficiency (Fig 3.2). These findings are in a sharp contrast to substitutions of DENV P1' Gly to Glu, Arg, Val or Trp, where the NS1-NS2A cleavage percentages were relatively poor (19%, 7%, 7% and 48%, respectively) (Pethel et al., 1992).

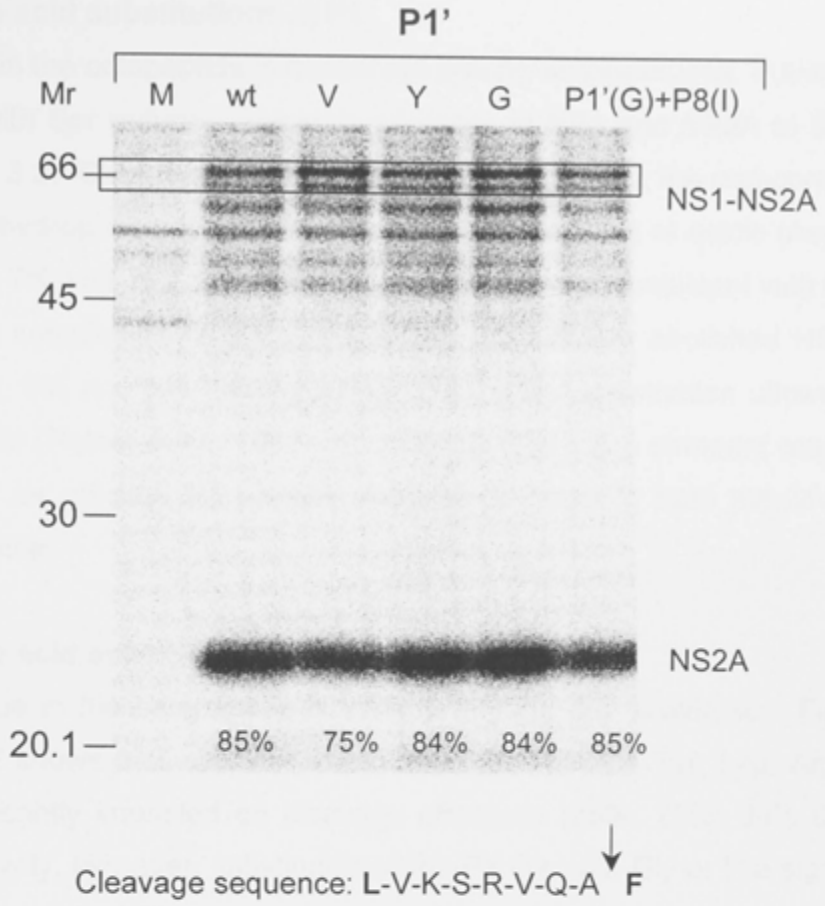

Fig. 3.2. Effect of mutations at position P1' of the octapeptide sequence motif on NS1-NS2A cleavage.

COS-7 cells were transfected with plasmid DNA of wt or mutant constructs encoding single mutations at P1' or left untransfected (M). At 48 h post transfection, the cells were metabolically labelled for 30 min and subsequently chased for 30 min. Immunoprecipitation was with an anti-HA Ab and proteins were subjected to SDS-PAGE (12.5% acrylamide). Bands correspond to cleaved NS2A protein and uncleaved NS1-NS2A precursors (shown in box) are indicated on the right, and the positions of the ^{14}C-labeled marker proteins (in kDa) are given on the left. Percentage of NS1-NS2A cleavage is shown under each lane. Nomenclature for each construct is given by the amino acid at that position that is shown at the top of each lane. For the construct designated as P1'(G),P8(I), the mutant is designated by first referring to position in the octapeptide, with amino acid at that position given in brackets. Cleavage sequence at the NS1-NS2A junction is shown at the bottom with amino acid in bold letter indicating the position for substitution.

3.2.2.2 Amino acid substitutions at P1

Alanine at P1 in the octapeptide is conserved among all flaviviruses. Substitution of this residue with Ser reduced cleavage efficiency of NS1 and NS2A to 53% (Fig. 3.3 and Table 3.2). Cleavage was severely inhibited following the non-conservative changes to a hydrophobic (Leu), aromatic (Phe), large (Arg) or acidic (Asp) amino acid (6%, 7%, 7% and 10%, respectively). These data are consistent with those for DENV, where substitution of Ala at P1 to Leu, Phe or Arg abolished NS1-NS2A cleavage (4%, 0% and 5%, respectively), while a Ser substitution allowed some cleavage (10%) (Pethel et al., 1992). Accordingly, there is a stringent requirement for Ala at P1 for efficient NS1-NS2A cleavage to occur in both the MVEV and DENV polyprotein.

3.2.2.3 Amino acid substitutions at P2

The P2 residue in the octapeptide is variable among the flaviviruses. Figure 3.4 and Table 3.2 shows that substitution of Gln at P2 with Ala, Tyr, Leu, Arg or Asp did not significantly impacted on cleavage efficiency (88%, 79%, 89% 87% and 89%, respectively. However, substitution of the P2 Gln with Gly or Pro significantly reduced cleavage to 37% and 11%, respectively. Both Gly and Pro have poor helix-forming propensities, where Gly tends to disrupt the α-helical structure in a polypeptide (Pace and Scholtz, 1998) and Pro introduces kinks or breaks a helix (Richardson, 1981). This may prevent accessibility of the cleavage site at the NS1-NS2A junction to the protease.

An additional band with a mass of about 23.5 kDa (NS2A*) was observed for construct with Gly or Pro substitutions at P2. The identity of this protein band has not been further investigated, although it appears to arise due to cleavage upstream of the NS1-NS2A cleavage site when authentic NS1-NS2A cleavage is inefficient. A band with faster electrophoretic mobility (~18kDa) was also observed in Fig 3.4 to 3.10. This protein band is most likely a degradation product of NS2A, since it is recovered by immunoprecipitation with the anti-HA mAb, but not found when NS2A is mostly absent.

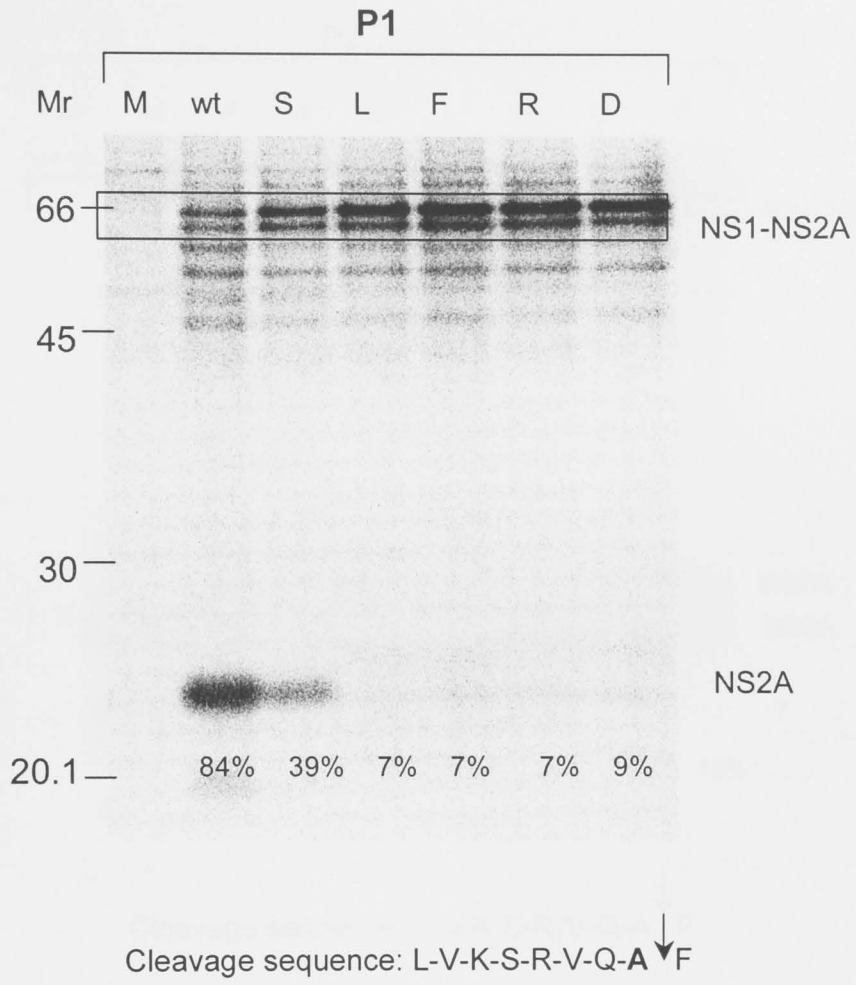

Fig. 3.3. Effect of mutations at position P1 of the octapeptide sequence motif on NS1-NS2A cleavage.

Proteins precipitated with an anti-HA Ab from cells mock transfected (M) or transfected with plasmid DNA of wt or mutants with single mutations at P1 were subjected to SDS-PAGE (12.5 % acrylamide). Nomenclature for each construct is given by the amino acid at that position that is shown at the top of each lane. Bands correspond to cleaved NS2A protein and uncleaved NS1-NS2A precursors (shown in box) are indicated on the right, and the positions of the ^{14}C-labeled marker proteins (in kDa) are given on the left. Cleavage percentage is shown at the bottom of each lane. Cleavage sequence at the NS1-NS2A junction is shown at the bottom with amino acid in bold letter indicating the position for substitution.

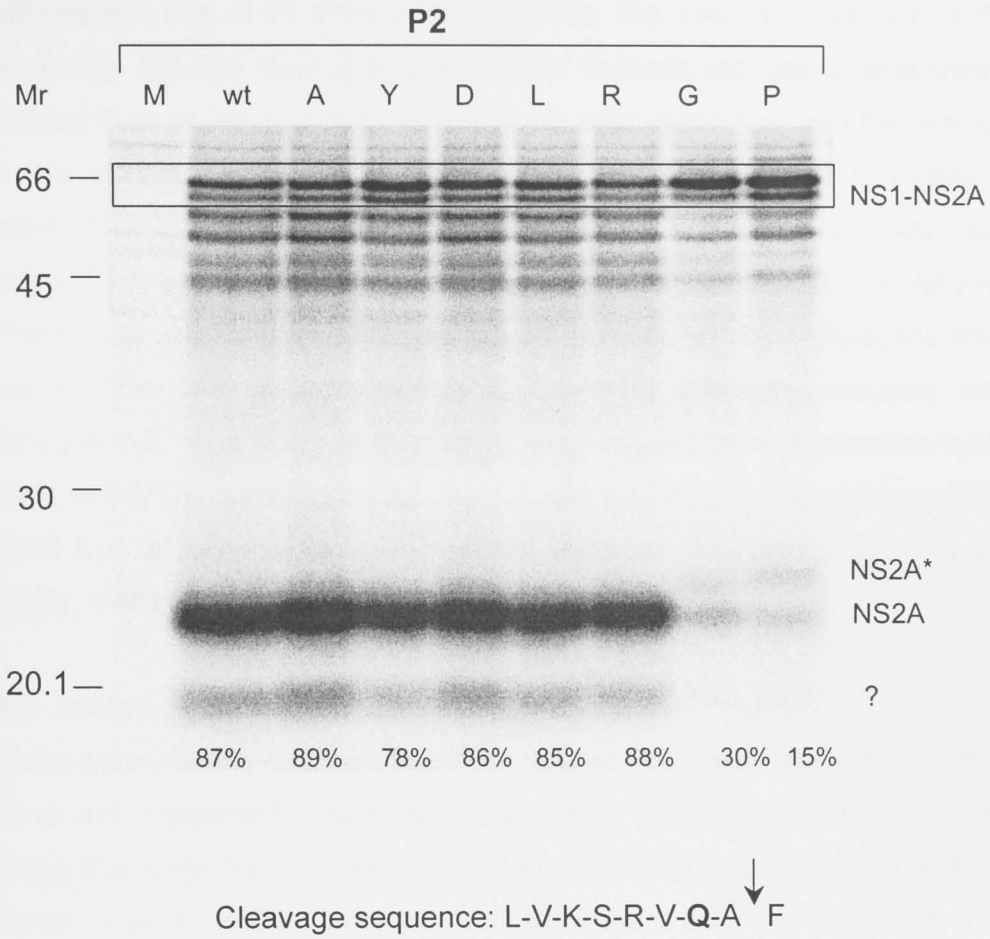

Fig. 3.4. Effect of mutations at position P2 of the octapeptide sequence motif on NS1-NS2A cleavage.

Proteins precipitated with an anti-HA Ab from cells mock transfected (M) or transfected with plasmid DNA of wt or mutants with single mutations at P2 were subjected to SDS-PAGE (12.5 % acrylamide). Nomenclature for each construct is given by the amino acid at that position that is shown at the top of each lane. Bands correspond to uncleaved NS1-NS2A precursors (shown in box), cleaved NS2A protein, NS2A* and an unknown band (?) are indicated on the right, and the positions of the ^{14}C-labeled marker proteins (in kDa) are given on the left. Cleavage percentage is shown at the bottom of each lane. Cleavage sequence at the NS1-NS2A junction is shown at the bottom with amino acid in bold letter indicating the position for substitution.

3.2.2.4 Amino acid substitutions at P3

The amino acid, Val, at P3, which is invariant among all flaviviruses, was substituted with one of six different amino acids: Ala, Leu, Gly, Lys, Asp or Phe. As shown in Fig. 3.5, the cleavage phenotype of mutants with amino acid substitution to charged (Lys or Asp) or bulky hydrophobic side chain (Leu or Phe) amino acids produced predominantly the uncleaved NS1-NS2A precursor. Surprisingly, the substitution of P3 Val with small, aliphatic amino acids, Gly and Ala, was well tolerated (83 % and 88% cleavage, respectively). This shows, for the first time, that the completely conserved residue at the P3 position of the octapeptide motif can be replaced with a different amino acid without markedly reducing cleavage efficiency of NS1 and NS2A in this subgenomic recombinant expression system. In contrast to MVEV, substitution of Gly for Val and non-conservative substitution, Leu and Lys, at the P3 residue in DENV were not tolerated (10%, 4% and 1% cleavage, respectively) (Pethel et al., 1992).

3.2.2.5 Amino acid substitutions at P4

Four non-conservative changes (Glu, Gly, Leu or Trp) were introduced at P4 (Arg), which is not conserved among the flaviviruses. The changes had no effect on cleavage efficiency (Fig. 3.6 and Table 3.2), indicating that the nature of the amino acid side chain at position P4 does not play a major role in maintaining the NS1-NS2A junction in a cleavable conformation.

3.2.2.6 Amino acid substitutions at P5

The amino acids, Ala, Arg, Leu, Glu, and Pro were chosen to replace Ser at the conserved residue P5. While introduction of the basic amino acid Arg at P5 almost completely abolished cleavage (13%), the introduction of an acidic (Glu) or hydrophobic (Leu) amino acid resulted in partial cleavage (57% and 53%, respectively) (Fig. 3.7 and Table 3.2). In the DENV octapeptide, the introduction of Pro at P5 resulted in rare enhancement of cleavage at the NS1-NS2A junction (Pethel et al., 1992). This effect was not noted for MVEV, where Pro at P5 resulted in only partial (67%) cleavage. Similar to our observation for the P3 residue, the introduction of Ala at P5 in the MVEV octapeptide did not markedly affect cleavage efficiency relative to wt.

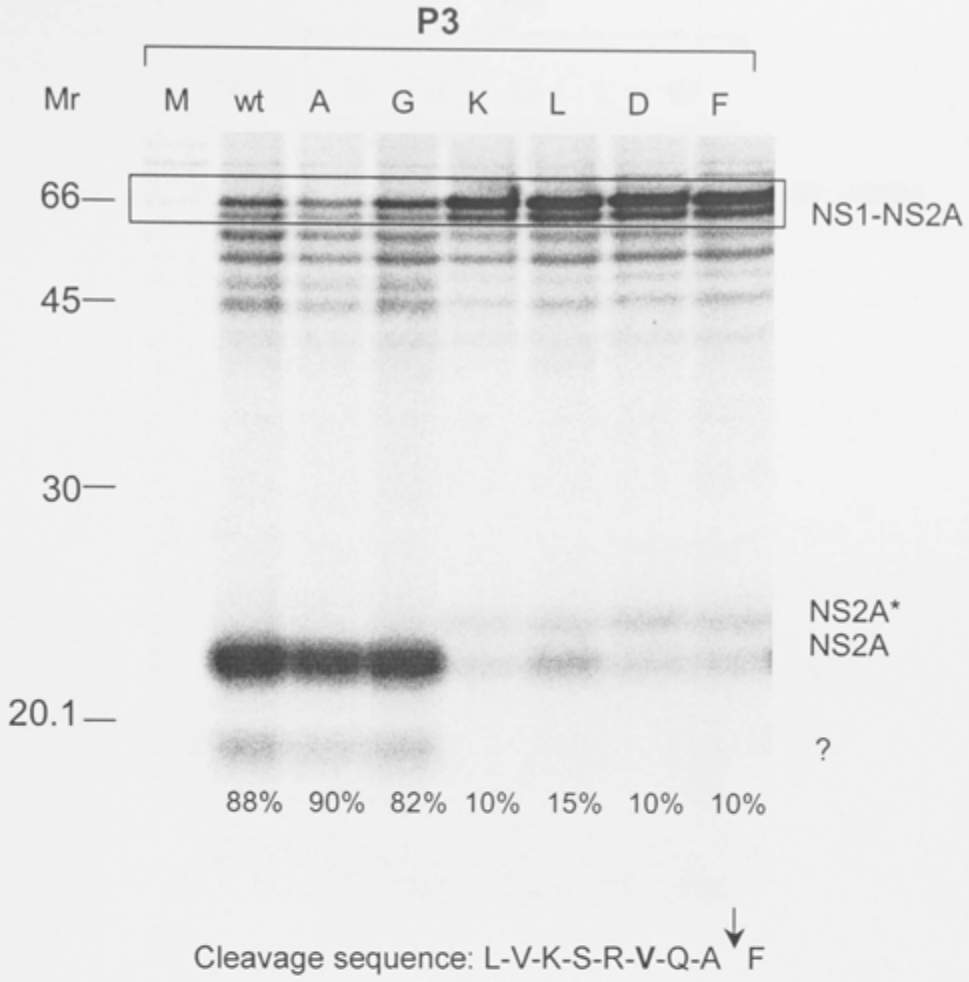

Fig. 3.5. Effect of mutations at position P3 of the octapeptide sequence motif on NS1-NS2A cleavage.

Proteins precipitated with an anti-HA Ab from cells mock transfected (M) or transfected with plasmid DNA of wt or mutants with single mutations at P3 were subjected to SDS-PAGE (12.5 % acrylamide). Nomenclature for each construct is given by the amino acid at that position that is shown at the top of each lane. Bands correspond to uncleaved NS1-NS2A precursors (shown in box), cleaved NS2A protein, NS2A* and an unknown band (?) are indicated on the right, and the positions of the ^{14}C-labeled marker proteins (in kDa) are given on the left. Cleavage percentage is shown at the bottom of each lane. Cleavage sequence at the NS1-NS2A junction is shown at the bottom with amino acid in bold letter indicating the position for substitution.

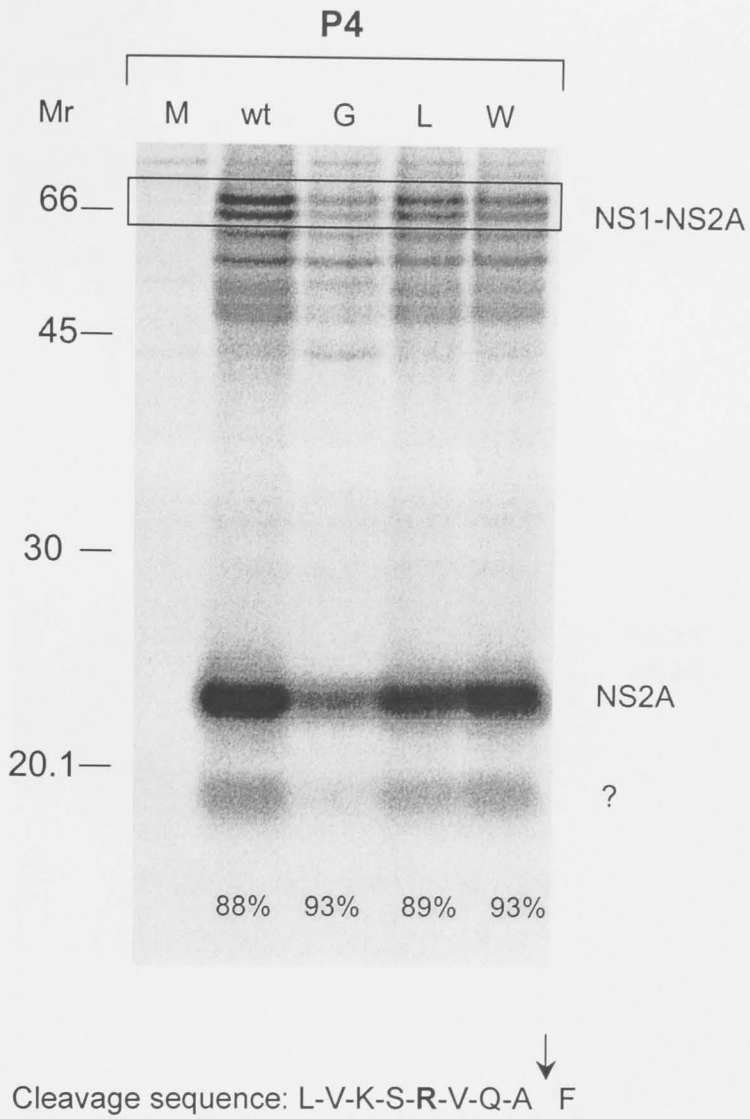

Fig. 3.6. Effect of mutations at position P4 of the octapeptide sequence motif on NS1-NS2A cleavage.

Proteins precipitated with an anti-HA Ab from cells mock transfected (M) or transfected with plasmid DNA of wt or mutants with single mutations at P4 were subjected to SDS-PAGE (12.5 % acrylamide). Nomenclature for each construct is given by the amino acid at that position that is shown at the top of each lane. Bands correspond to uncleaved NS1-NS2A precursors (shown in box), cleaved NS2A protein and an unknown band (?) are indicated on the right, and the positions of the ^{14}C-labeled marker proteins (in kDa) are given on the left. Cleavage percentage is shown at the bottom of each lane. Cleavage sequence at the NS1-NS2A junction is shown at the bottom with amino acid in bold letter indicating the position for substitution.

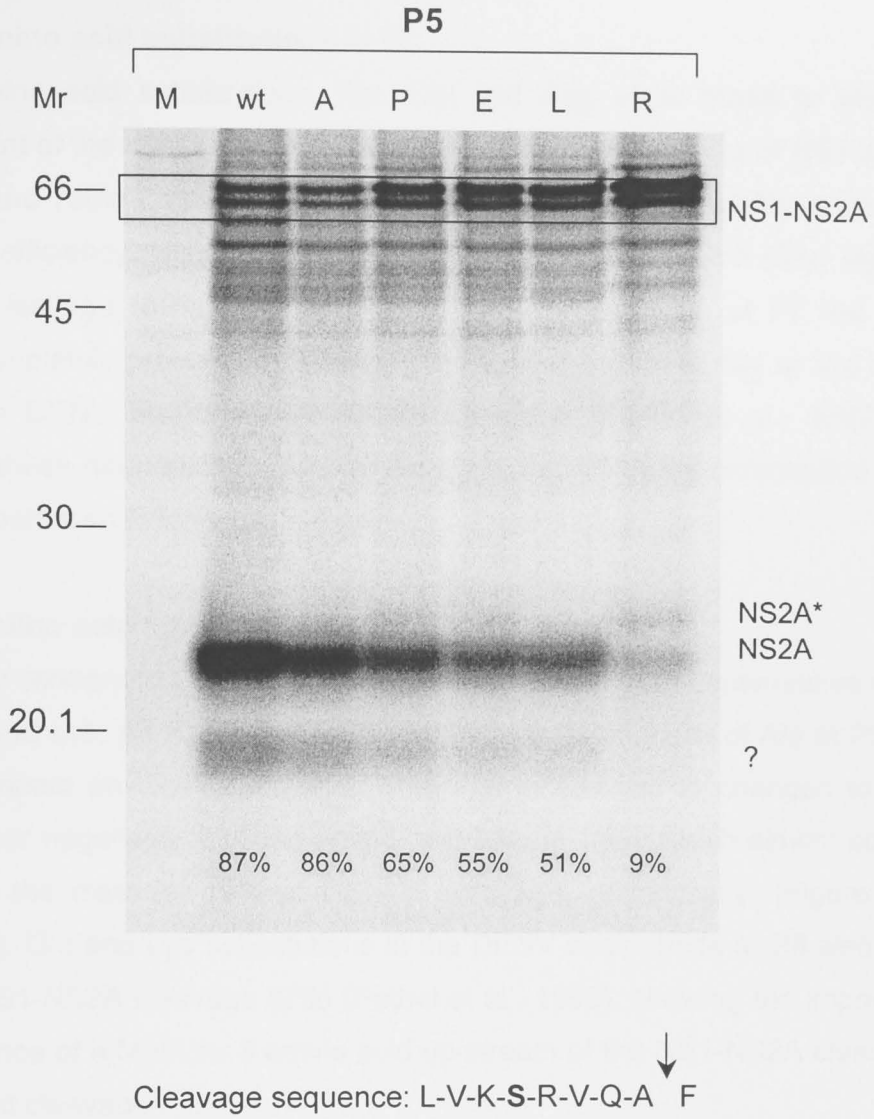

Fig. 3.7 Effect of mutations at position P5 of the octapeptide sequence motif on NS1-NS2A cleavage.

Proteins precipitated with an anti-HA Ab from cells mock transfected (M) or transfected with plasmid DNA of wt or mutants with single mutations at P5 were subjected to SDS-PAGE (12.5 % acrylamide). Nomenclature for each construct is given by the amino acid at that position that is shown at the top of each lane. Bands correspond to uncleaved NS1-NS2A precursors (shown in box), cleaved NS2A protein, NS2A* and an unknown band (?) are indicated on the right, and the positions of the ^{14}C-labeled marker proteins (in kDa) are given on the left. Cleavage percentage is shown at the bottom of each lane. Cleavage sequence at the NS1-NS2A junction is shown at the bottom with amino acid in bold letter indicating the position for substitution.

3.2.2.7 Amino acid substitutions at P7

Three amino acid substitutions, Ala, Gly and Arg, were made to test for the requirement of the conserved Val at the P7 position for cleavage of NS1 and NS2A (Fig. 3.8 and Table 3.2). The introduction of Ala at P7 had no detrimental effect on cleavage efficiency, while a second small, aliphatic, amino acid (Gly) significantly reduced cleavage (60%). The non-conservative substitution of P7 Val with Arg almost completely prevented cleavage (11%). Introduction of Gly or Val at the P7 residue in DENV abolished NS1-NS2A cleavage (Pethel et al., 1992). Taken together, these data confirm a critical role of Val at P7 in the octapeptide although an Ala substitution is tolerated in MVEV.

3.2.2.8 Amino acid substitutions at P8

The highly conserved Leu at P8 was subjected to three non-conservative changes: Ala, Gln and Lys. As note for P3, P5 and P7, the introduction of Ala at P8 had no marked impact on cleavage (80%). This was in contrast to changes to either a positively or negatively charged amino acid (Glu or Lys), which almost completely abolished the cleavage (9% and 8% of cleavage, respectively) (Figure 3.9 and Table 3.2). Glu and Lys substitutions in the DENV octapeptide at P8 also resulted in poor NS1-NS2A cleavage (2%) (Pethel et al., 1992), showing the importance of the presence of a Met/Leu 8 amino acid up-stream of the NS1-NS2A cleavage site for efficient cleavage.

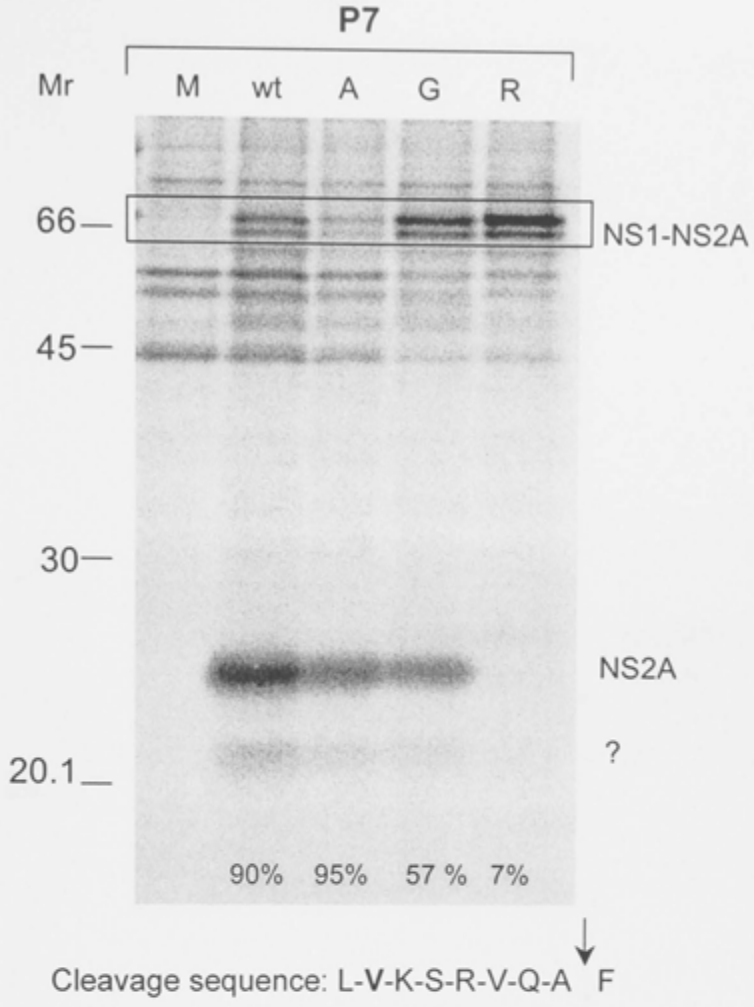

Fig. 3.8. Effect of mutations at position P7 of the octapeptide sequence motif on NS1-NS2A cleavage.

Proteins precipitated with an anti-HA Ab from cells mock transfected (M) or transfected with plasmid DNA of wt or mutants with single mutations at P7 were subjected to SDS-PAGE (12.5 % acrylamide). Nomenclature for each construct is given by the amino acid at that position that is shown at the top of each lane. Bands correspond to uncleaved NS1-NS2A precursors (shown in box), cleaved NS2A protein and an unknown band (?) are indicated on the right, and the positions of the ^{14}C-labeled marker proteins (in kDa) are given on the left. Cleavage percentage is shown at the bottom of each lane. Cleavage sequence at the NS1-NS2A junction is shown at the bottom with amino acid in bold letter indicating the position for substitution.

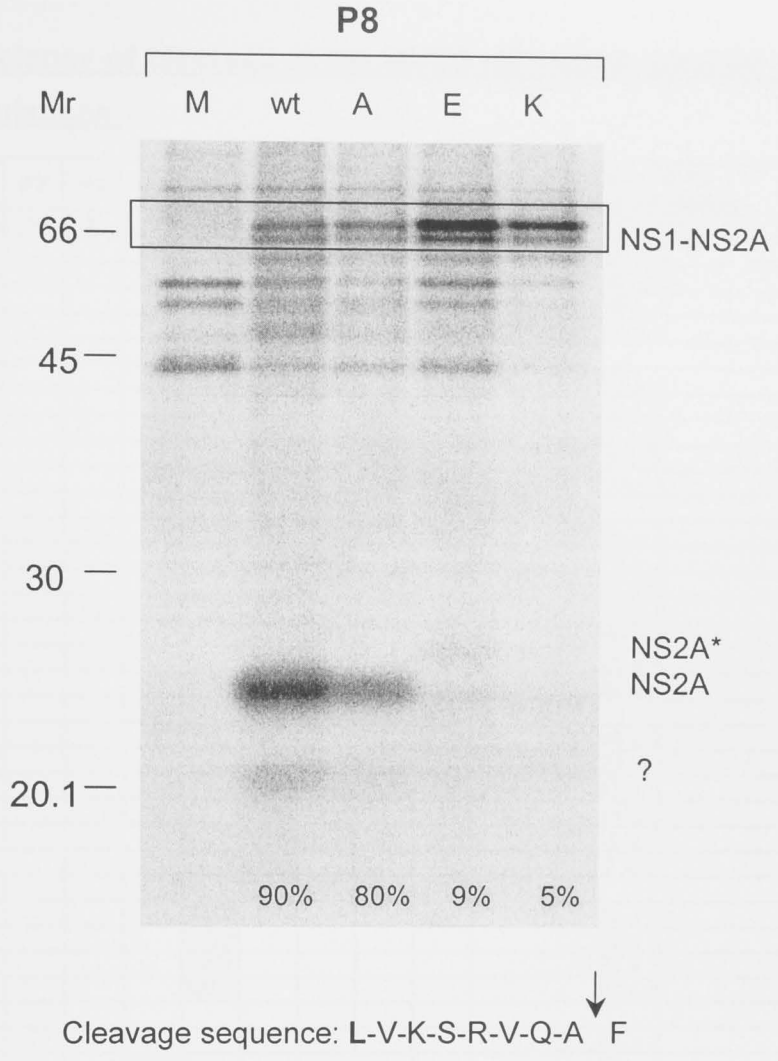

Fig. 3.9. Effect of mutations at position P8 of the octapeptide sequence motif on NS1-NS2A cleavage.

Proteins precipitated with an anti-HA Ab from cells mock transfected (M) or transfected with plasmid DNA of wt or mutants with single mutations at P8 were subjected to SDS-PAGE (12.5 % acrylamide). Nomenclature for each construct is given by the amino acid at that position that is shown at the top of each lane. Bands correspond to uncleaved NS1-NS2A precursors (shown in box), cleaved NS2A protein, NS2A* and an unknown band (?) are indicated on the right, and the positions of the ^{14}C-labeled marker proteins (in kDa) are given on the left. Cleavage percentage is shown at the bottom of each lane. Cleavage sequence at the NS1-NS2A junction is shown at the bottom with amino acid in bold letter indicating the position for substitution.

Table 3.2. Efficiency of cleavage at the MVEV NS1-NS2A junction containing amino acid mutations.

P8	P7	P6	P5	P4	P3	P2	P1	P1'	Mean ± SE % cleavage efficiency
L	V	K	S	R	V	Q	A	F	88 ± 1
								Y	84 ± 0
								V	80 ± 5
								G	86 ± 3
I								G	90 ± 6
							S		53 ± 2
							L		6 ± 1
							F		7 ± 0
							R		7 ± 0
							D		10 ± 1
						A			88 ± 2
						Y			79 ± 3
						G			37 ± 4
						D			89 ± 4
						L			89 ± 2
						P			11 ± 4
						R			87 ± 1
					A				88 ± 2
					L				23 ± 3
					G				83 ± 1
					K				14 ± 2
					D				10 ± 0
					F				7 ± 3
				E					91 ± 4
				G					91 ± 3
				L					83 ± 5
				W					92 ± 1
			A						83 ± 2
			R						13 ± 4
			L						53 ± 2
			E						57 ± 2
			P						67 ± 2
	A								94 ± 2
	G								60 ± 3
	R								11 ± 4
A									80 ± 3
E									9 ± 0
K									8 ± 3

Calculation for the determination of cleavage efficiency is described in detail in the section 3.2.1. The wt amino acid sequence at the NS1-NS2A cleavage site is shown in bold (at the top) and the amino acid substitutions at each position are given below. Mean values of at least three independent experiments are given and the standard error (S.E) is indicated. Amino acid highlighted in grey indicates non-conservative substitution.

3.2.2.9 Effect of multiple Ala substitutions in the octapeptide

Mutagenesis of single residues in the MVEV octapeptide showed that the introduction of Ala at the position of (almost) complete conservation of critical amino acids among the flaviviruses did not markedly affect cleavage efficiency at the NS1-NS2A junction. This raised the question of whether multiple Ala substitutions would also be permitted without impacting on cleavage efficiency (and thereby questioning the role of the octapeptide motif in NS1-NS2A cleavage, *per se*), or whether an additive effect of Ala substitutions on the conformation of the cleavage site would be reflected in reduced polyprotein processing.

Thus, double Ala substitutions at P2 and P3 (P2,3-Ala), P3 and P8 (P3,8-Ala) and P7 and P8 (P7,8-Ala), as well as quadruple Ala mutations from P5 through to P8 (P5-8 Ala) were engineered. Simultaneous replacement of Ala at the non-conserved P2 and the conserved P3 positions did not significantly alter cleavage efficiency (91% cleavage) relative to wt. In contrast, Ala mutations at two conserved positions (P3 and P8) caused a noticeable reduction in cleavage efficiency to 69%. A similar reduction in cleavage was found for the construct that had Ala substitution at the conserved positions, P7 and P8 (60% cleavage). The mutant construct with Ala substitutions at P5 through to P8 showed poor NS1-NS2A cleavage (28%) (Fig. 3.10). These data show that while single Ala substitutions at conserved positions in the MVEV octapeptide are well tolerated, this flexibility does not extend to the introduction of two or more Ala at these key positions.

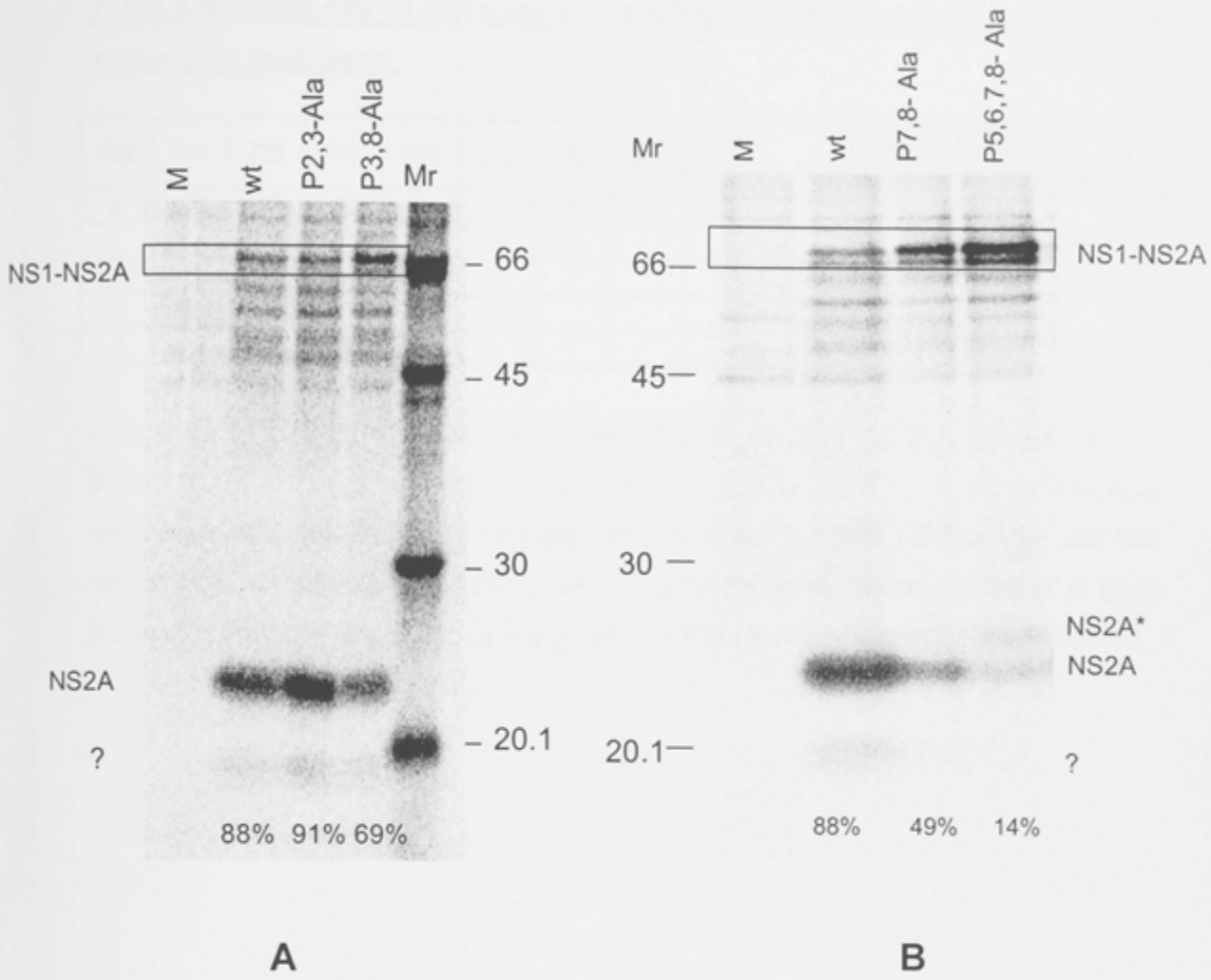

Fig. 3.10. Effect of multiple Ala mutations in the octapeptide motif on NS1-NS2A cleavage.

COS-7 cells were transfected with plasmid DNA of wt NS1-NS2A or mutants with Ala substitutions at (A) P2 and P3 or P3 and P8, (B) P7 and P8 or P5 through P8 or mock transfected (M). At 48 h post transfection, the cells were metabolically labelled for 30 min and subsequently chased for 30 min. Immunoprecipitation was with an anti-HA Ab and proteins were subjected to SDS-PAGE (12.5% acrylamide). Bands corresponding to uncleaved NS1-NS2A precursors (shown in box), cleaved NS2A protein, NS2A* and an unknown band (?) are indicated on the right, and the positions of the ^{14}C-labeled marker proteins (in kDa) are given on the left. Percentage of NS1-NS2A cleavage is shown under each lane. Nomenclature for each construct is given by the amino acid at that position that is shown at the top of each lane.

Table 3.3. Efficiency of cleavage at the MVEV NS1-NS2A junction containing amino acid mutations.

P8	P7	P6	P5	P4	P3	P2	P1	P1'	Mean ± SE % cleavage efficiency
L	**V**	**K**	**S**	**R**	**V**	**Q**	**A**	**F**	88 ± 1
					A	A			91 ± 2
A					A				69 ± 5
A	A								60 ± 5
A	A	A	A						28 ± 4

Efficiency of cleavage at the MVEV NS1-NS2A junction containing multiple Ala substitutions at various positions at the octapeptide motif. The wt amino acid sequence at the NS1-NS2A cleavage site is shown in bold (at the top) and the amino acid substitutions at each position are given below. Mean values of at least three independent experiments are given and the standard error (S.E) is indicated.

3.2.3 Requirement for NS2A protein for an efficient NS1-NS2A cleavage

It has been noted by others that the presence of ~2/3 of the NS2A protein was essential for efficient cleavage at the DENV NS1-NS2A junction (Falgout, 1990; Falgout et al., 1989; Falgout and Markoff, 1995). To test the reproducibility of this observation for a second flavivirus, COOH-terminal truncations were introduced into the MVEV NS1-NS2A construct, leaving 60% (deletion of 90 amino acids) or 86% (31 deletion of amino acid) of NS2A intact (constructs NS1-NS2A[60%] and NS1-NS2A[86%], respectively).

The COOH-terminal truncation of NS2A was reflected in the faster electrophoretic mobilities of both NS2A and NS1-NS2A precursor products in SDS-PAGE gels in line with the size of the truncations. Analysis of processing at the NS1-NS2A junction showed 6% and 76% cleavage for NS1-NS2A(60%) and NS1-NS2A(86%) constructs, respectively. This finding corroborates with that of the DENV studies showing a precipitous decrease in cleavage of NS1 and NS2A following COOH-terminal deletion of 15%, 49% and 69% of NS2A, which corresponds to the penultimate predicted transmembrane domain in NS2A (Fig. 3.16) (Falgout et al., 1989; Falgout and Markoff, 1995).

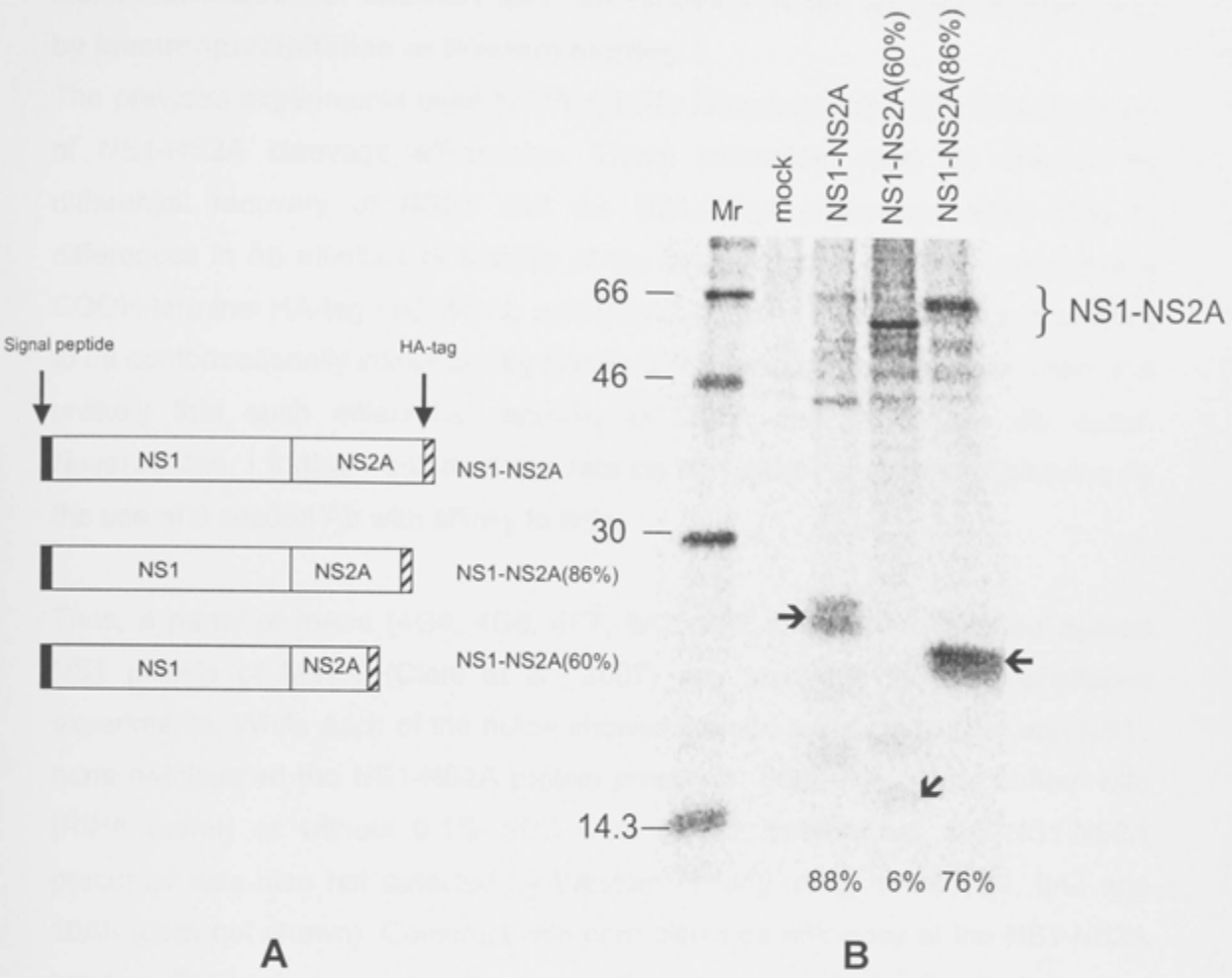

Fig. 3.11. Effect of C-terminal truncation of NS2A on NS1-NS2A cleavage.

(A) Schematic drawing of MVEV NS1-NS2A expression constructs with various NS2A truncations. The white bars show the NS1 and NS2A region, the black bars indicate the NS1 signal peptide and bars with diagonal stripes indicate the HA epitope tag. Nomenclature for each construct is given on the right. (B) Proteins precipitated with an anti-HA Ab from cells mock transfected (M) or transfected with construct containing plasmid DNA of wt or mutants with C-terminal truncations at NS2A were subjected to SDS-PAGE (12.5 % acrylamide). The bands corresponding to uncleaved NS1-NS2A precursor, wt NS2A (→), 60% of NS2A (↙) and 86% of NS2A (←) are indicated. The positions of the ^{14}C-labeled marker proteins (in kDa) are given on the left and the percentage of NS1-NS2A cleavage is shown under each lane.

3.2.4 Validation of estimates of NS1-NS2A cleavage

3.2.4.1 Evaluation of anti-NS1 mAb for recovery of the NS1-NS2A precursor by immunoprecipitation or Western blotting

The previous experiments used NS2A-specific immunoprecipitation for calculation of NS1-NS2A cleavage efficiencies. These estimates could be affected by differential recovery of NS2A and the NS1-NS2A precursors either due to differences in Ab affinities or stability of the two products. However, given that a COOH-terminal HA-tag specific Ab was employed, the epitope of which is unlikely to be conformationally influenced by folding of the preceding polypeptide chain, it is unlikely that such differential recovery of NS2A and NS1-NS2A did occur. Nevertheless, I further confirmed my data on NS1-NS2A cleavage efficiencies by the use of a second Ab with affinity to NS1.

Thus, a panel of mAbs (4G4, 4G6, 4F7, 9A2, 9B2 and 10A8) produced against NS1 protein of MVEV (Clark et al., 2007) was tested in immunoprecipitation experiments. While each of the mAbs showed specific reactivity to NS1 and NS1', none precipitated the NS1-NS2A protein precursor. Both, NP40 lysis buffers with (RIPA buffer) or without 0.1% SDS were tested; furthermore, the NS1-NS2A precursor was also not detected by Western blotting using mAbs 4G4, 9A2 and 10A8 (data not shown). Construct with poor cleavage efficiency at the NS1-NS2A junction (P3-Lys) were used to ensure the presence of significant amount of precursor in cell lysates. The inability of the NS1-specific mAb to efficiently recognize the NS1-NS2A precursor could be due to significant change in the NS1 antigenic structure when tethered to NS2A in the uncleaved NS1-NS2A precursor. This observation was further confirmed in Chapter 4 and 5 whereby the presence of NS1 protein is undetectable in rP2-Gly and rP7,8-Ala virus infected cells when analyzed with FACS, indirect IF and immunoprecipitation analysis, despite of significant amount of virus titers detected in growth assay.

3.2.4.2 Validation of estimates of NS1-NS2A cleavage based from immunoprecipitation with anti-HA and anti-NS1 Abs

Theoretically, estimates of NS1 and NS2A cleavage efficiency are determined by quantitation of the amount of NS1 or NS2A protein in relation to the total accumulation of NS1 or NS2A protein plus polyprotein precursors based from the following formula:

$$\left[\frac{NS1}{NS1+\left(NS1-NS2A_{precursor}\right)}\right]\times 100 \quad \text{or} \quad \left[\frac{NS2A}{NS2A+\left(NS1-NS2A_{precursor}\right)}\right]\times 100$$

A comparison of NS1-NS2A cleavage by parallel immunoprecipitations using two different antibodies is shown in Fig. 3.12. Lysates from radiolabelled cells transfected with plasmid DNA, wt or mutant constructs (P2-Asp, P3-Leu, P3-Gly and P5-8 Ala) were divided into two where half of each lysate was treated with anti-NS1 4G4 or anti-HA mAb and subjected to SDS PAGE. Immunoprecipitation with anti-HA mAb exhibited a doublet band consistent in size with the uncleaved NS1-NS2A precursor (shown in box). As discussed above, there was no evidence of NS1-NS2A precursor from immunoprecipitation with 4G4 mAb.

When NS1 and NS2A expressions were compared between immunoprecipitation with anti-NS1 and anti-HA Ab, is it evident that comparable amount of NS1 and NS2A proteins were expressed for wt, P2-Asp and P3-Gly (lane 2, 3 and 5), consistent with efficient NS1-NS2A cleavage (94 %, 93 % and 83 % respectively). In contrast, poor NS1-NS2A cleavage for P3-Leu and P5-8 Ala (36% and 34%, respectively) was depicted in very low NS1 and NS2A expressions (lane 4 and 6) with intense uncleaved NS1-NS2A bands (lane 4 and 6 in Fig. 3.12B). Taken together, although the immunoprecipitation with anti-NS1 (4G4) Ab was unable to recover NS1-NS2A precursor and thus does not allow expression of cleavage efficiencies, results obtained from parallel immunoprecipitation with 4G4 and anti-HA Ab clearly showed a correlation between estimates of cleavage based on anti-HA immunoprecipitation and recovery of NS1 products with 4G4.

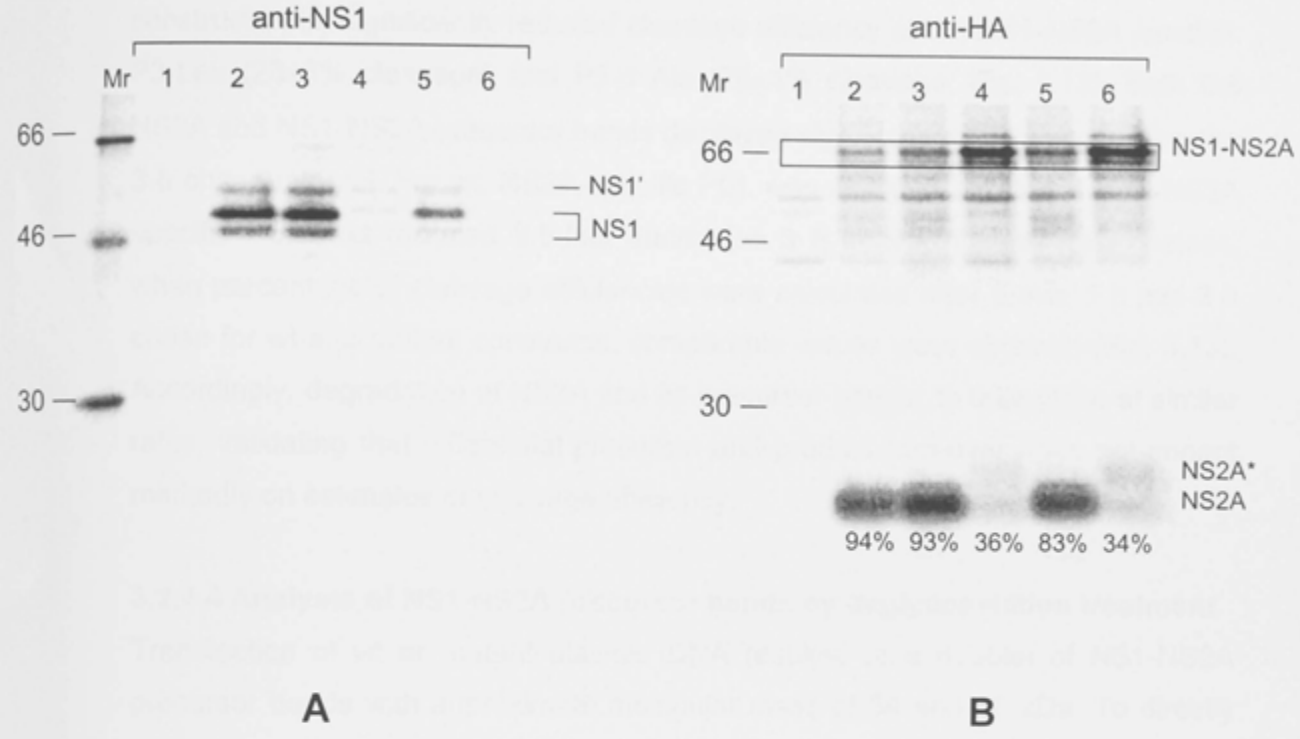

Fig. 3.12. Analysis of NS1 and NS2A proteins recovered with anti-NS1 or anti-HA Ab from cells transfected with wt or mutant NS1-NS2A constructs.

COS-7 cells were mock transfected (1) or transfected with plasmid DNA of: (2) wt, (3) P2-Asp, (4) P3-Leu, (5) P3-Gly, or (6) P5-8 Ala. At 48 h post transfection, the cells were metabolically labelled for 30 min and subsequently chased for 30 min. Immunoprecipitation was with (A) anti-NS1 (4G4) or (B) anti-HA mAb and proteins were subjected to SDS-PAGE (12.5% acrylamide). In both figures, the numbers on the left indicates the size of the ^{14}C-labelled marker proteins in kDa. The location of NS1', NS1, NS1-NS2A precursor protein, NS2A and NS2A* are shown on the right. Percentage of NS1-NS2A cleavage is shown under each lane in (B).

3.2.4.3 Stability of NS2A and NS1-NS2A precursor products

To address whether NS2A and NS1-NS2A products display differential stability, a pulse-chase experiment was performed using the wt construct and two mutant constructs with significantly reduced cleavage efficiency at the NS1-NS2A junction: P3-Leu (23±3% cleavage) and P5-8 Ala (28±4% cleavage; Fig. 3.13). Both the NS2A and NS1-NS2A precursor bands displayed significant degradation during the 3 h chase interval. For wt, NS2A-specific PSL was reduced 3-fold and NS1-NS2A specific PSL was reduced 3.5-fold during the 3 h chase interval. Nevertheless, when percentage of cleavage efficiencies were calculated after 5 min, 1 h and 3 h chase for wt and mutant constructs, comparable values were obtained (Fig. 3.13). Accordingly, degradation of NS2A and its precursor appear to take place at similar rates, validating that differential precursor and product turn-over does not impact markedly on estimates of cleavage efficiency.

3.2.4.4 Analysis of NS1-NS2A precursor bands by deglycosylation treatment

Transfection of wt or mutant plasmid DNA resulted in a doublet of NS1-NS2A precursor bands with approximate molecular mass of 64 and 66 kDa. To directly demonstrate that these two bands exist due to differential glycosylation, lysates from cells transfected with wt or P3-Phe mutant were immune precipitated with anti-HA Ab. Half of these products were digested with endo H to assay for N-linked glycans. Susceptibility of the NS1-NS2A precursors to endo H was anticipated, since the MVEV NS1 protein is N-linked glycosylated (Blitvich et al., 1999).

As shown in Fig. 3.14, both bands corresponding to the NS1-NS2A precursor were sensitive to endo H treatment and were modified to a single band with faster electrophoretic mobility. In contrast, endo H treatment did not alter the electrophoretic mobility of the NS2A protein band, consistent with the absence of a glycosylation motif in NS2A protein. Taken together, these data validate that the 64 and 66 kDa proteins represent glycosylated and partial glycosylated forms of the NS1-NS2A precursor.

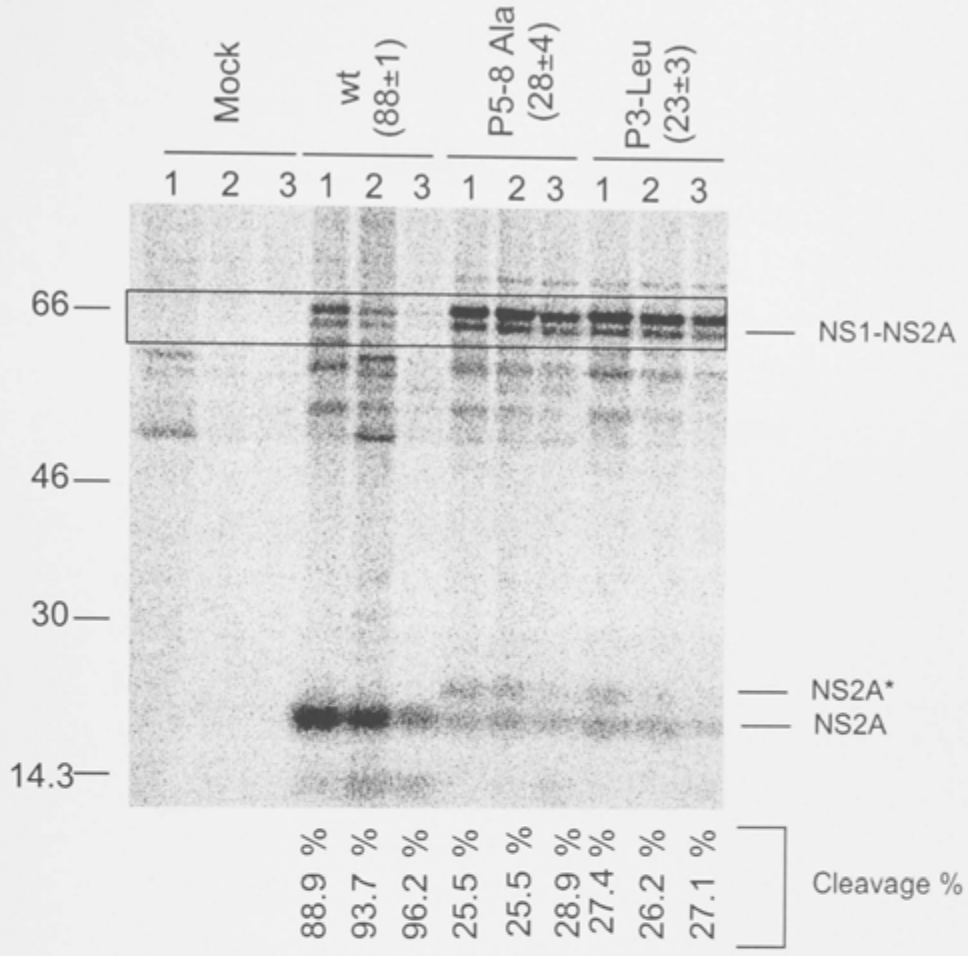

Fig. 3.13. Effect of pulse-chase labelling on NS1-NS2A cleavage efficiency. COS-7 cells were transfected with the following plasmid DNA: wt, P5-8 Ala, P3-Leu or mock. At 48 h post transfection, the cells were metabolically labelled for 30 min and were chased for 5 min (1), 1 h (2) or 3 h (3). The cell lysates were immunoprecipitated with an anti-HA Ab and subjected to SDS-PAGE (12.5% acrylamide). The position of cleaved NS2A, NS2A* and uncleaved NS1-NS2A precursors are indicated on the right. The sizes of ^{14}C-labelled marker proteins (in kDa) are shown on the left and the percentage of NS1-NS2A cleavage is shown at the bottom of each lane.

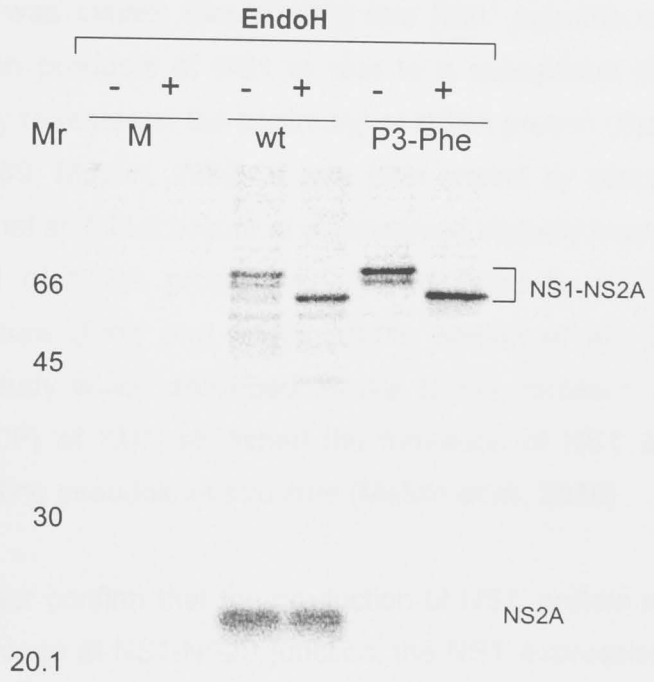

Fig. 3.14. Analysis of N- linked glycosylation of NS1-NS2A precursor and NS2A by endo H enzyme treatment.

Lysates of ^{35}S labelled COS-7 cells transfected with wt or mutant construct (P3-Phe) were immune precipitated with an anti-HA Ab and were treated with endo H (+) or mock treated (-) and the proteins were subjected to SDS-PAGE (12.5 % acrylamide). The ^{14}C-protein marker standard is shown on the left. The bands correspond to cleaved NS2A protein and uncleaved NS1-NS2A precursors are indicated on the right. A similar result was observed when the experiment was conducted in parallel with PNGase F treatment. The data are representative of three independent experiments.

3.2.5 Evaluation of NS1' expression in NS1-NS2A cleavage defective mutants

It has been shown in this chapter and by others that the NS1 protein is often detected in infected cells as heterogenous clusters of proteins of different molecular masses (NS1 and NS1') (Blitvich et al., 1995; Blitvich et al., 1999; Mason, 1989). It was initially thought that this NS1' proteins was derived from either glycosylation products of NS1 or due to a suboptimal cleavage with the cleavage site likely to reside at the beginning of NS2A protein (Blitvich et al., 1999; Falgout et al., 1989; Mason, 1989). It was later shown by others that NS1' is a product of ribosomal shift that occurs at a conserved slippery heptanucleotide motif at the N-terminal of NS2A protein and is stimulated by a downstream RNA pseudoknot structure (Firth and Atkins, 2009; Melian et al., 2010). This was confirmed by a study which described an Ala to Pro mutation at residue 30 of NS2A (NS2A A30P) of KUN abolished the formation of NS1' by disrupting the frameshift-stimulating pseudoknot structure (Melian et al., 2010).

Therefore, to further confirm that the production of NS1' protein is independent of the authentic cleavage at NS1-NS2A junction, the NS1' expression was compared to that of the production of NS1 and NS2A proteins in mutants with defective NS1-NS2A cleavage. COS-7 cells were transfected with plasmid DNA encoding wt NS1-NS2A, NS2A A30P, P1-Leu or P3-Phe. Transfected cells were labelled with ^{35}S-methionine at 48 h post transfection, followed by parallel immunoprecipitation using two different antibodies, anti-NS1 and anti-HA. Immunoprecipitation with anti-NS1 Ab showed NS1 and NS1' production for cells transfected with wt plasmid DNA and as expected, only NS1 and no NS1' was detected for NS2A A30P (Fig. 3.15A). Parallel analysis by immunoprecipitation with anti-HA further confirms this observation, whereby the expression of NS2A was comparable for wt and NS2A A30P. On the other hand, very poor NS1 was detected in immunoprecipitates from cells transfected with P1-Leu and P3-Phe and interestingly, descent amount of NS1' being expressed in these mutants (Fig. 3.15A). Complete absence of NS2A protein was observed for lysates from cells transfected with P1-Leu and P3-Phe, indicating abolishment of NS1-NS2A cleavage for these mutants (Fig. 3.15B). Taken together, it was evident from this analysis that the abolishment of NS1-

NS2A cleavage did not impact on NS1' production which confirms that NS1' production is independent of NS1-NS2A cleavage.

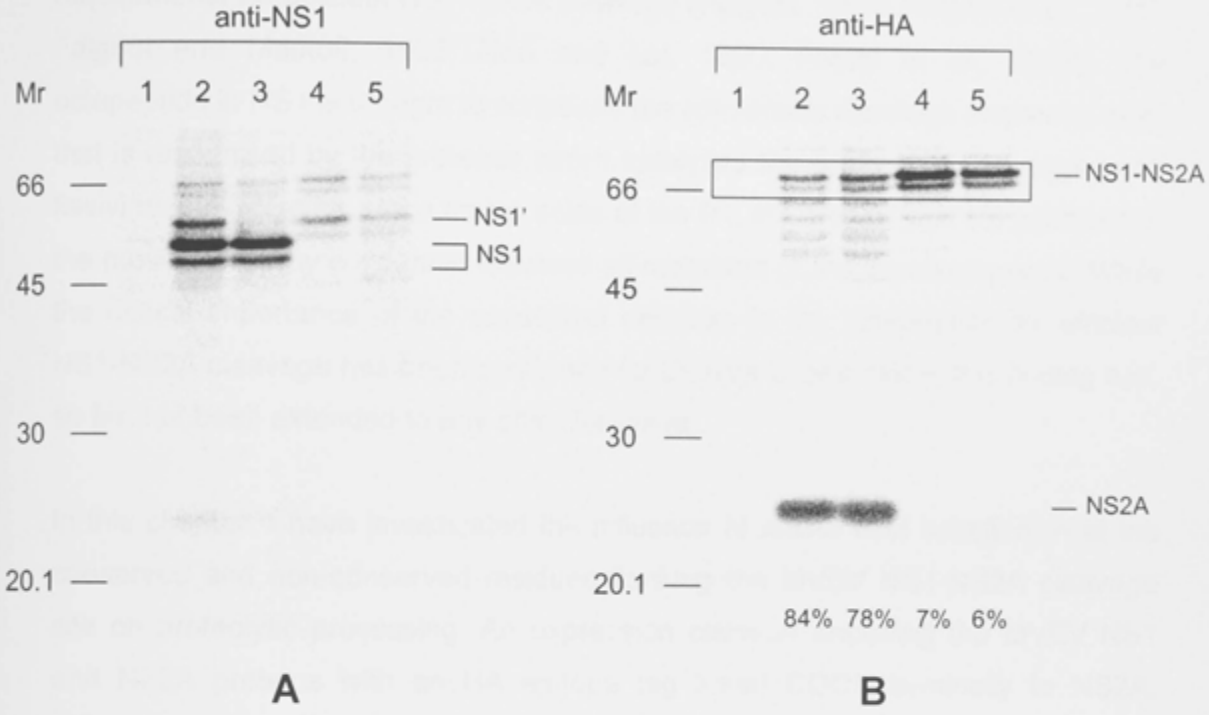

Fig. 3.15. Analysis of NS1' production in NS1-NS2A cleavage defective mutants.

Detection of NS1, NS1' and NS2A in lysates of Vero cells mock transfected (1) or transfected with plasmid DNA of wt (2), NS2A A30P (3), P1-Leu (4) and P3-Phe (5). Transfected cells were labelled with ^{35}S-methionine at 48 h post transfection, immune precipitated with anti-NS1 (A) or anti-HA (B) Ab and subjected to 12.5% SDS-PAGE. In both figures, the numbers on the left indicates the size of the ^{14}C-labelled marker proteins in kDa. The location of NS1', NS1, NS1-NS2A precursor and NS2A are shown on the right. Percentage of NS1-NS2A cleavage is shown under each lane in (B).

3.3 Discussion

The eight COOH-terminal amino acids of NS1 protein plus approximately 70% of down-stream NS2A protein have been defined for DENV as the minimal requirements for efficient NS1-NS2A cleavage (Falgout, 1990; Falgout et al., 1989; Falgout and Markoff, 1995; Hori and Lai, 1990; Pethel et al., 1992). The octapeptide in NS1 is thought to constitute the consensus cleavage sequence motif that is recognised by the protease which catalyses the NS1-NS2A cleavage in all flavivirus polyproteins, since amino acids at the P1, P3, P5, P7 and P8 positions in the motif are strictly conserved between all members of the flavivirus genus. While the critical importance of the conserved residues in the octapeptide for efficient NS1-NS2A cleavage has been confirmed for DENV4 in one study, this finding has, so far, not been extended to any other flavivirus.

In this chapter, I have investigated the influence of amino acid substitution at the conserved and non-conserved residues flanking the MVEV NS1-NS2A cleavage site on proteolytic processing. An expression cassette encoding the MVEV NS1 and NS2A proteins with an HA epitope tag fused COOH-terminally to NS2A, pRc/CMV.NS1-NS2A.HA, was generated for analysis of cleavage efficiency of wt and mutant constructs with single and multiple amino acid substitutions in the octapeptide and P1' position. Insights into structural properties that impinge on NS1-NS2A cleavage of the MVEV polyprotein will be discussed in comparison to conclusions drawn from the corresponding investigation on DENV4. I have also tested the contribution of NS2A for upstream NS1-NS2A cleavage and will discuss my results in the context of the predicted domain structure and membrane topology of this highly hydrophobic and enigmatic flavivirus protein. I will conclude by addressing the implications from my investigation on NS1-NS2A cleavage on the identity of the protease, the 'holy grail' in this research field.

The consensus cleavage motif at the MVEV NS1-NS2A junction

My investigation on MVEV NS1-NS2A proteolytic processing showed the dominant role of the strictly conserved residues in the octapeptide for efficient NS1-NS2A cleavage, judged by the observation that non-conservative substitutions at these

positions almost always greatly reduced cleavage. In contrast, non-conservative substitutions were often tolerated at the P1', P2 and P4 sites, which are occupied by amino acids that differ in hydrophobicity and molecular bulk in the octapeptides of different flaviviruses. Accordingly, sequence conservation in the octapeptide is predictive on the impact of substitutions on cleavage efficiency, supporting the view that conservation of physical and chemical properties of residues at P1, P3, P5, P7 and P8 is required to accommodate the cleavage site in the substrate-binding pocket of the protease.

Despite overall agreement with the 'octapeptide rule', several deviations were noted for the MVEV NS1-NS2A cleavage. Surprisingly, a non-conservative change of the aliphatic Val at P3 to Gly, which is a small hydrophilic amino acid, did not markedly reduce efficiency of proteolytic processing at the NS1-NS2A junction. In contrast, the conservative substitution of P3 Val with a second but slightly larger aliphatic amino acid, Leu, was not tolerated. This suggests that small size of the side chain is the overriding property required for the P3 residue in the cleavage sequence motif of MVEV, a proposition supported by a second substitution at P3, the Val→Ala change, which showed wt cleavage efficiency.

Of all other 22 changes at conserved octapeptide residues tested, only Ala substitutions at P5, P7 and P8, and a Leu→Ile change at P8 did not impact on NS1-NS2A cleavage efficiency. Whilst replacement of Leu with Ile is a conservative change where both residues have a branched, aliphatic side chain of identical size, the P5 Ser→Ala change results in loss of polarity of the side chain and introduction of Ala for Val or Leu at P7 and P8, respectively, reduces side chain hydrophobicity and size. However, although eliminating the side chain beyond the β carbon, Ala substitutions do not alter the main-chain conformation nor do they impose extreme electrostatic or steric effects (Cunningham and Wells, 1989), which is the likely explanation why these changes had minimal impact on cleavage efficiency. On the other hand, the combination of two Ala substitutions at conserved residues in the octapeptide, at P7 and P8 or at P3 and P8, showed a reduction in cleavage efficiency to 60% and 68%, respectively. A further increase

in the number of substitutions with Ala in the cleavage consensus sequence from P5 to P8 (4 mutations, 3 of which are at conserved positions) gave rise to very poor cleavage efficiency. This additive inhibitory effect on cleavage of two or more changes to Ala of conserved residues in the octapeptide illustrates yet again the important contribution of each of these conserved residues in ascertaining efficient cleavage by a process, which most likely involves their role in proper alignment of the NS1-NS2A cleavage region with key residues inside the substrate-binding pocket of the protease.

The effect of mutations at two non-conserved positions (P2 and P4) in the MVEV octapeptide on NS1-NS2A cleavage was also investigated. It appeared that P4 exhibited a greater tolerance to non-conservative amino acid changes than P2. Of a total of 11 mutations at P2 and P4, only the replacement of P2 Gln with either Gly or Pro, two strong helix-breaking residues, markedly reduced cleavage. This suggests that alteration of the main-chain conformation proximal to the cleavage site, but not changes in electrostatic and steric properties of the side chain at P2 are detrimental to cleavage site recognition by the protease.

Finally, I have also investigated the contribution of the P1' residue at the MVEV NS1-NS2A junction to cleavage of NS1 and NS2A. I found no stringent requirement for conservation of the physical and chemical property of the aromatic side chain of Phe, which occupies this position in MVEV, given that substitutions to Val (which like Phe is highly hydrophobic but less bulky) or Gly (a small, hydrophilic and helix-breaking residue) did not impact markedly on cleavage efficiency. A more detailed mutational analysis of the P1' residue at the NS1-NS2A cleavage site is needed to determine whether this position exerts any impact at all on cleavage. Nevertheless, my current results suggest that the P1' residue does not play an integral part in substrate interaction with the protease.

Comparison of the MVEV and DENV4 octapeptides

Table 3.4 shows a comparison of the effect of amino acid changes at the conserved positions in the octapeptides of MVEV and DENV4 on efficiency of NS1-NS2A cleavage. The most striking difference between the two viruses was the

differential impact of a Val→Gly substitution at P3, which almost completely prevented cleavage in the DENV polyprotein but had no marked effect on the production of MVEV NS1 and NS2A. Other differences between the two viruses were seen for P1 Ala→Ser and P7 Val→Gly substitutions, which resulted in a partial inhibition of NS1-NS2A cleavage for MVEV but were not tolerated in the DENV cleavage sequence, and for a P5 Ser→Pro change, which enhanced DENV NS1-NS2A proteolytic processing but was partially inhibitory in the case of MVEV. An additional notable difference between MVEV and DENV in the sequence requirement for cleavage at the NS1-NS2A junction is found at the P1' position: while substitutions leading to major changes in hydrophobicity and molecular bulk of the amino acid side chain at this site was tolerated in MVEV without significant effect on cleavage efficiency, this was not the case for DENV4. For instance, the introduction of Val at P1' only marginally reduced cleavage efficiency at the MVEV NS1-NS2A junction (80% cleavage) but was not tolerated at the P1' position in DENV4 (7% cleavage).

A comparative analysis between MVEV and DENV4 suggests that the octapeptide functions as a module, albeit with virus-specific differences imposed by one or more of several factors: (i) sequence variation at the non-conserved residues, P2 and P4, in the octapeptide (note that the P6 residue in MVEV and DENV4 is Lys and for most other flaviviruses either Lys or Arg; Fig. 3.1); (ii) the P8 residue, which differs between MVEV (Leu) and DENV4 (Met); the P1' residue, as discussed above; (iv) NS2A 'cofactor-like' activity, given the significant amino acid sequence variation (22%) in this protein between the two viruses. This conclusion is, however, not entirely consistent with the current view that the flavivirus NS1-NS2A cleavage is catalysed by the one protease, since the apparently exquisite substrate specificity of the protease, which is defined by 5 strictly conserved amino acids in the octapeptide, should have precluded virus-specific differences in tolerance of the cleavage consensus sequences to substitutions at the conserved octapeptide residues. If, on the other hand, the NS1-NS2A cleavage consensus sequence were a module that can accommodate virus-specific differences at the conserved positions in the octapeptide, the expectation would follow that natural variants to

the 'octapeptide rule' would have evolved among the many different members of the flaviviruses – which does not appear to be the case. The critical next step in resolving this apparent discrepancy will be to examine if variants of MVEV that contravene the 'octapeptide rule', but display a wt NS1 and NS2A cleavage phenotype in the subgenomic recombinant expression assay, can be distinguished from wt virus in growth properties in the mammalian or mosquito host (see Chapter 4). Finally, I should point out that in my discussion on virus-specific differences in the flavivirus octapeptide I make the assumption that the difference in experimental approach between my investigation on MVEV and that on DENV (Pethel et al., 1992) used recombinant vaccinia virus expression of DENV4 NS1-NS2A and a polyclonal antiserum for semi-quantitative recovery of NS1 and NS1-NS2A precursor) is not the reason for the small number but striking discrepancies.

Table 3.4. Comparison of impact of changes at conserved residues in the octapeptide of MVEV and DENV4.

Octapeptide residue	Substitution	Cleavage efficiency	
		MVEV	DENV4
P1 Ala	Ser	53 ± 2	10 ± 3
	Leu	6 ± 1	4 ± 4
	Phe	7 ± 0	0
	Arg	7 ± 0	5 ± 5
	Asp	10 ± 1	3 ± 2
P3 Val	Leu	23 ± 3	4 ± 3
	Gly	83 ± 1	10 ± 4
	Lys	14 ± 2	1 ± 2
P5 Ser	Ala	83 ± 2	100 ± 11
	Arg	13 ± 4	8 ± 3
	Pro	67 ± 2	132 ± 4
P7 Val	Gly	60 ±3	1 ± 1
	Arg	11 ± 4	1 ± 1
P8 Leu or Met	Glu	9 ± 0	2 ± 1
	Lys	8 ± 3	2 ± 3

Role of NS2A protein in NS1-NS2A cleavage

The findings for DENV4 that (i) ~70% of the NS2A protein (which is 216 amino acids in length) is essential for up-stream NS1-NS2A cleavage and (ii) NS2A is most likely not an autocatalytic protease are remarkable, because it is difficult to envisage why such a large polypeptide region should be required for providing accessibility of the NS1-NS2A cleavage site to a host-encoded protease. Furthermore, replacement of DENV NS2A with a polypeptide of similar size and hydrophobicity did not preserve cleavage competence at the COOH-terminus of NS1. Given that this intriguing 'cofactor-like' property of NS2A has, to my knowledge, not been tested in a second flavivirus model, it was important to verify this result and demonstrate that the NH_2-terminal ~two-third of the MVEV NS2A protein was also indispensable for NS1-NS2A cleavage (Fig. 3.11).

The membrane topology of the flavivirus NS2A protein has not yet been experimentally defined, other than that its NH_2-terminus must reside in the ER lumen and COOH-terminus in the cytoplasm in order for proteolytic processing by a putative ER-resident host protease and the viral NS2B-3 protease, respectively, to occur. Computational modelling of MVEV NS2A predicts 5 membrane-spanning α-helical domains, giving rise to a predicted topology as shown in Figure 3.16. Based on this model, I designed two truncations in NS2A to precisely remove the COOH-terminal one or two membrane-spanning domains. Given the relatively efficient NS1-NS2A cleavage in construct, pNS1-NS2A(86%), it appears that the last putative transmembrane domain does not contribute markedly to cleavage. In contrast, cleavage was ablated following truncation of the COOH-terminal two transmembrane domains, indicating that the region of NS2A encompassing the first four predicted membrane-spanning domains determine accessibility of the NS1-NS2A cleavage site to the protease. The mechanistic explanation for this intricate prerequisite for a down-stream polypeptide for cleavage at the NS1-NS2A junction by the unknown protease remains unclear. However, the results of this study and that of Falgout et al., (1992) on DENV4 imply that a distinct conformational characteristic of the flavivirus NS2A protein safeguards upstream cleavage and potentially other biological functions of NS2A in virus replication. One hypothesis could be that the unusually hydrophobic nature of NS2A induces a rearrangement

of the ER membranes, as observed experimentally in flavivirus infected cells and that this rearrangement of the ER membranes is central for the NS1-NS2A cleavage site to be accepted as a substrate by the enzyme.

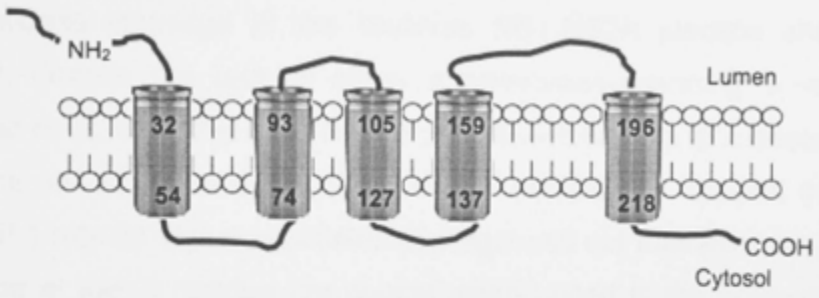

Fig. 3.16. Computational modelling prediction of MVEV NS2A protein topology.

Shaded cylinders represent transmembrane domains as predicted by the software program TMHMM Server v2.0. Positions of the first and last amino acids of each transmembrane domain are denoted.

The protease that catalyses cleavage of NS1 and NS2A

Signal peptidase is the only candidate host protease for catalysing the cleavage between flavivirus NS1 and NS2A proteins. It is a ubiquitous protease associated with the luminal side of the ER membrane, which functions in removing an NH_2-terminal signal peptide from ER-targeted and secreted proteins. The rules for recognition of signal peptidase cleavage sites demand a central hydrophobic region (h-region) followed by a more hydrophilic part (c-region) containing the cleavage site with small and uncharged residues at the -3 and -1 positions (von Heijne, 1983, 1984, 1985). While the sequence of the flavivirus NS1-NS2A junction conforms well with a typical c-region of a signal peptidase cleavage site, an obvious discrepancy is the absence of an up-stream membrane-spanning hydrophobic region thought to be essential for signal peptidase cleavage. However, during the course of my PhD studies, an intriguing "new type of signal peptidase cleavage site" was identified in the polyprotein of a pestivirus, which also lacked a hydrophobic 'h-region' but contained a canonical 'c-region' (Bintintan and

Meyers, 2010). The authors of this report suggested that an amphipathic helix upstream of the cleavage site, which functions in membrane-anchorage of the pestivirus protein, was essential and sufficient in generating the new type of signal peptidase cleavage site. Their model was supported by experiments making use of a specific signal peptidase inhibitor. Based on this recent finding, the scenario of signal peptidase cleavage at the flavivirus NS1-NS2A junction should not be discounted, despite the lack of either a membrane-spanning 'h-region' or an amphipathic helix, as is the case for the pestivirus cleavage site described above. Notably, the mutational analysis of the MVEV octapeptide showed that deviation from the -3/-1 rule for signal peptidase cleavage was not tolerated: thus, Gly or Ala substitutions at the -3 residue are neutral when tested in the context of a typical signal peptidase cleavage site and the Val→Gly or Ala changes at the P3 residue in the MVEV octapeptide were the only mutations at this position that did not markedly impact on cleavage efficiency; furthermore, a Ser at the -1 position of a typical signal peptidase cleavage site allows efficient cleavage by the enzyme, while in the MVEV octapeptide a Ala→Ser mutation reduced but did not ablate cleavage of NS1 and NS2A.

Given that cell-free signal peptidase cleavage assays are currently not available and that 'knock-down' of signal peptidase expression is lethal to the cell, the application of protease inhibitor studies using the specific inhibitor for signal peptidase, MeOSuc-Ala-Ala-Pro-Val chloromethyl ketone (Casanova et al., 2006; van Geest et al., 1999), in cleavage assays as described here, could provide a major step forward to identification of the enzyme that catalyses the flavivirus NS1-NS2A cleavage.

CHAPTER 4

MVEV variants with mutation in the octapeptide at the NS1-NS2A junction

4.1 Introduction

Previous research on proteolytic processing at the flavivirus NS1-NS2A junction has been restricted exclusively to recombinant expression models of the corresponding polyprotein region of DENV (Falgout and Markoff, 1995; Hori and Lai, 1990; Pethel et al., 1992). While the generality to other flaviviruses of the findings for DENV has, so far, not been confirmed, it is also unclear whether insights gained from subgenomic expression experiments apply to viral infections in cell culture and animal hosts. For instance, the effect of substitutions that alter NS1-NS2A cleavage efficiency on virus replication, and the stage in the viral replication cycle potentially affected by cleavage inhibition, have not been investigated. It is also intriguing if the pattern of absolute amino acid sequence conservation in the octapeptide is required exclusively for recognition of the NS1-NS2A cleavage site by the protease or serves an additional function in viral replication.

Here, I have addressed these questions by mutational analysis of the NS1-NS2A cleavage site in mutant virus infections using MVEV as a model. In Chapter 3, I have identified a large number of mutations in the 'octapeptide motif' of MVEV, which impact on cleavage of NS1 and NS2A over a wide range in a recombinant expression assay of the NS1-NS2A polyprotein region, from no apparent reduction to ablation of cleavage. These mutations included both the completely conserved as well as non-conserved positions in the octapeptide. Based on this information, I selected four changes at octapeptide residues P2, P3, P8 and P7/8, which covered a spectrum of NS1-NS2A cleavage efficiencies of 37-83%, and introduced these individually into a full-length, infectious, cDNA clone of MVEV (Lee and Lobigs, 2000; Lobigs et al., 2010). Using this reverse-genetics approach, I was able to isolate, for the first time, recombinant viruses with mutations at the flavivirus NS1-NS2A cleavage site, and to evaluate their phenotypes in cell culture and mouse infections (in Chapter 4), as well as investigate by forward-genetics structural parameters that modulate NS1-NS2A cleavage in virus replication, which will be described in Chapter 5.

4.2 Results

4.2.1 Nomenclature of NS1-NS2A cleavage site mutant constructs and viruses

To distinguish between the MVEV full-length infectious clone plasmid and recombinant virus derived thereof, the infectious clones are annotated with a '"p" for plasmid and the recombinant viruses with a "r". For example pMVEV refers to the wt MVEV full-length infectious clone plasmid and rMVEV to infectious clone-derived wt virus. The rP2-Gly virus is contains a substitution at P2 in the octapeptide from Gln to Gly, rP3-Gly, a substitution from Val to Gly at P3, rP8-Ala, a substitution from Leu to Ala at P8 and rP7,8-A, a double mutation from Val to Ala at P7 and Leu to Ala at P8.

4.2.2 Construction of NS1-NS2A cleavage site mutant viruses

To generate full-length cDNA clones of MVEV with specific mutation in the octapeptide motif, 776-bp *Nae*I-*Nhe*I fragments encompassing P2-Gly, P3-Gly, P8-Ala or P8,7-Ala mutations were excised from the mutant pRc.NS1-NS2A.HA plasmids (Chapter 3) and ligated into pMVEV, replacing the corresponding wt NS1 and NS2A region (Fig. 4.1).

To ascertain the presence of the mutations in the full-length cDNA clones, PCR fragments covering the NS1 and NS2A regions were first generated and subsequently used as templates for cycle sequencing. The PCR amplification and sequencing was performed as described in sections 2.3.1 and 2.3.2, using the oligonucleotides NS1 #2 and NS2A #3 for the PCR and NS1 #3 for cycle sequencing (Table 2.4).

Wild-type and mutant full-length RNA transcripts were generated *in vitro* as described in section 2.9. Subsequently, the transcription products were introduced into BHK cells by electroporation (section 2.10). Samples of culture supernatant from transfected BHK cells were collected on day 3 (for rMVEV, rP3-Gly and rP8-Ala) or on day 5 (for rP2-Gly and rP7,8-Ala) post-transfection.

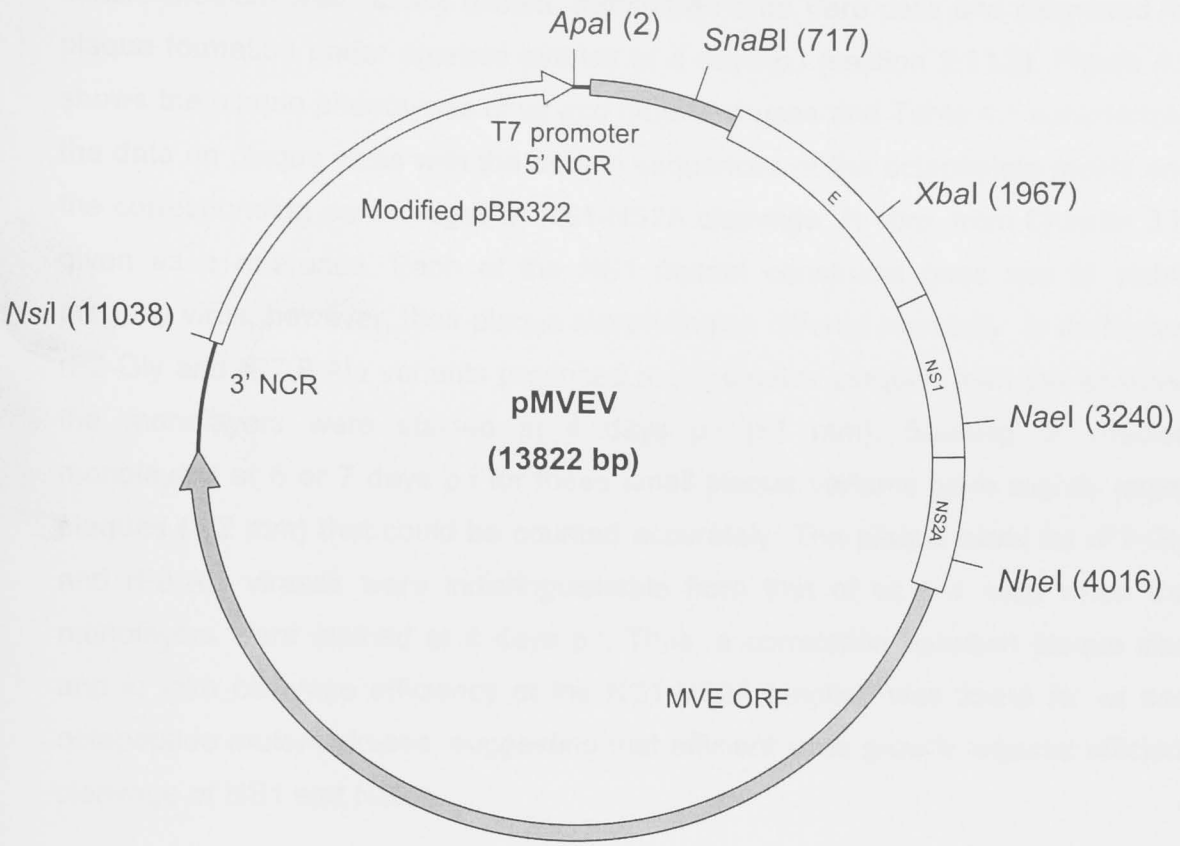

Fig. 4.1. Full-length infectious cDNA clone of MVEV (pMVEV).

Schematic drawing of the genome-length MVEV infectious cDNA clone of MVE 1-51 (Lee and Lobigs, 2000; Lobigs et al., 2010). The infectious cDNA clone contains modified pBR322 as the vector backbone and the full-length sequence of MVE 1-51 (11,013 nucleotides) encompassing an open reading frame (ORF) encoding a polyprotein of C, prM, E, NS1, NS2A, NS2B, NS3, NS4A, NS4B and NS5 (solid grey line). Restriction enzyme sites in the E-NS2A region used for subcloning and the unique *Nsi*I site used to produce linearized cDNA for *in vitro* RNA transcription are shown. The 5' non-coding region (NCR) follows the T7 promoter sequence. The position of the 3' NCR is shown, where the MVEV genome sequence ends at the engineered *Nsi*I site. All numbering shown is from the 5' terminal nucleotide in MVE 1-51.

4.2.3 Recovery of NS1-NS2A cleavage site mutant viruses

Samples of medium from cultures of BHK cells transfected with full-length recombinant MVEV RNA were collected at 3 to 5 days post electroporation. The culture medium was serially diluted, transferred onto Vero cells and examined for plaque formation under agarose overlay at 4 days p.i (section 2.11.2). Figure 4.2 shows the plaque phenotypes of wt and mutant viruses and Table 4.1 summarizes the data on plaque sizes with the protein sequences of the octapeptide motifs and the corresponding percentages of NS1-NS2A cleavage, *in vitro*, from Chapter 3 is given as a reference. Each of the NS1 mutant constructs gave rise to viable progeny virus; however, their plaque morphologies differed markedly. In particular, rP2-Gly and rP7,8-Ala variants produced much smaller plaques than the wt when the monolayers were stained at 4 days p.i (≤1 mm). Staining of infected monolayers at 6 or 7 days p.i for these small plaque variants gave slightly larger plaques (1-2 mm) that could be counted accurately. The plaque sizes for rP3-Gly and rP8-Ala viruses were indistinguishable from that of wt (~4 mm) when the monolayers were stained at 4 days p.i. Thus, a correlation between plaque size and *in vitro* cleavage efficiency at the NS1-NS2A junction was found for wt and octapeptide mutant viruses, suggesting that efficient virus growth requires efficient cleavage of NS1 and NS2A.

4.2.4 Sequence confirmation of NS1-NS2A cleavage site mutant viruses

Having recovered infectious virus from BHK cells transfected with NS1 mutant RNA genomes, it was important to confirm that the progeny viruses contained the introduced NS1 mutations. Unamplified virus resulting from electroporation of BHK cells with mutant RNA was used to infect Vero cell monolayers. Total cellular RNA was extracted from the infected cells (section 2.3.3.1), cDNA was synthesized from each RNA extract (section 2.3.3.2) before being amplified by PCR (section 2.3.2) and subjected to sequence analysis. Total RNA from Vero cells infected with wt rMVEV was also included as positive control for the cDNA synthesis, amplification and sequencing steps. A region of the MVEV genome covering the E, NS1 and NS2A genes was amplified and sequenced. Sequence analysis of RNA from mutant viruses found the presence of the input mutation in the octapeptide and absence of other sequence alteration in this region relative to wt virus.

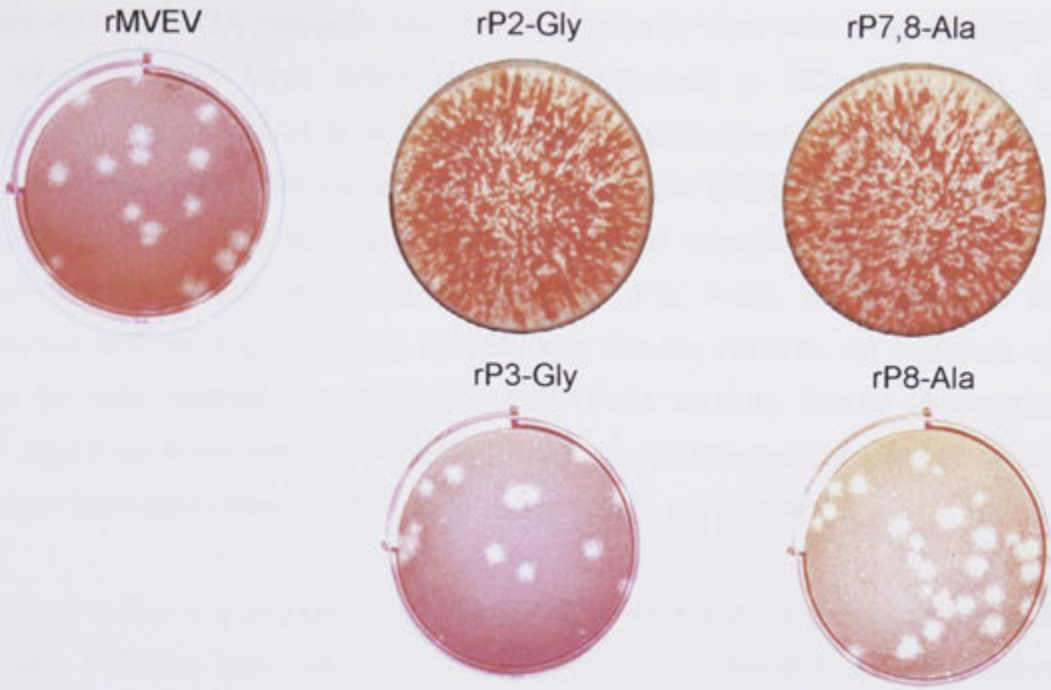

Fig. 4.2. Plaque morphology of rMVEV and NS1-NS2A cleavage site mutant viruses.

Samples of culture supernatant from BHK cells transfected with rMVEV, rP2-Gly, rP3-Gly, rP8-Ala or rP7,8-Ala were subjected to plaque assay on Vero cells. The corresponding plaque morphology on Vero cell monolayers stained with 0.02% neutral red on day 4 p.i and recorded the following day are given.

Table 4.1. Sequence analysis and plaque size of rMVEV and NS1-NS2A cleavage site mutant viruses

Construct	Octapeptide sequence[1]	Plaque size[2]	NS1-NS2A cleavage[3]
rMVEV	LVKSRVQA	4 mm	88%
rP2-Gly	LVKSRVGA	≤ 1 mm	37%
rP3-Gly	LVKSRGQA	4 mm	83%
rP8-Ala	AVKSRVQA	4 mm	80%
rP7,8-Ala	AAKSRVQA	≤ 1 mm	60%

[1]Sequence analysis of the NS1 and NS2A genes revealed that each mutant virus contained the input mutation without any additional changes in the NS1-NS2A region.

[2]Plaque morphology on Vero cell monolayers stained with 0.02% neutral red on day 4 p.i and recorded the following day are given.

[3]data from *in vitro* cleavage (Chapter 3)

4.2.5 Viral growth analysis in mammalian cells

Growth of NS1-NS2A cleavage site mutant viruses in Vero cells was compared to that of wt rMVEV. Virus infections were performed at MOI of 0.1-0.2, and extracellular virus titers of growth samples were determined by plaque assay on Vero cell monolayers. The percentage of infected cells at the end of the first round of infection (16 h p.i) was determined in parallel infections by flow-cytometry following staining with anti- NS1-specific mAb (Fig. 4.4A). While infection was consistent with virus input for wt, rP3-Gly and rP8-Ala variants, no evidence was found for cells infected with rP2-Gly and rP7,8-Ala variants. Similar observations were also seen even when the rP2-Gly and rP7,8-Ala infected cells were analyzed at longer incubation time of 48, 72 and 96 h p.i (data not shown).

As shown in Fig. 4.3, the growth of rP3-Gly and rP8-Ala in Vero cells did not differ markedly (<2-fold) from that of wt rMVEV during the 16-64 h p.i time interval, except for a ~6-fold lower titer for rP8-Ala at 16 h p.i. In contrast, rP2-Gly and rP7,8-Ala variants showed a significant defect in virus growth, consistent with their small plaque phenotype. They produced titer that were ~180-fold lower than that for rMVEV at 24 h p.i. The difference in growth became less pronounced at later time points, but was still ~9-fold and ~25-fold at 64 h p.i for rP7,8-Ala and rP2-Gly, respectively, relative to wt. It was noticeable that the growth in Vero cells of rP2-Gly was the poorest of the four NS1-NS2A cleavage site mutant viruses and this correlated with the poorest NS1-NS2A cleavage efficiency of this mutant observed in the *in vitro* assay. Finally, it should also be noted that the small plaque phenotype of variants rP2-Gly and rP7,8-Ala did not revert to a larger size during the course of the growth assay.

4.2.6 Viral growth analysis in mosquito cells

To access the growth properties of MVEV variants with mutation in the NS1-NS2A cleavage site in mosquito cells, C6/36 cells were infected at MOI of ~0.2 and virus yield in culture fluids were titrated by plaque formation on Vero cells. To evaluate the infectivity of wt and variant viruses, dishes infected in parallel were fixed at 24 h p.i, stained with a NS1-specific mAb and subjected to flow-cytometry analysis (Fig. 4.4B). While wt MVEV, rP3-Gly and rP8-Ala showed infectivity on C6/36 cells that

was in the expected range, two mutant viruses, rP2-Gly and rP7,8-Ala, yet again failed to produce sufficient antigen for detection by FACS at 24 h p.i.

Wild-type MVEV grew to a high titer in C6/36 cells, reaching a plateau of ~10^8 PFU/ml at 72 h p.i (Fig. 4.3B). The two NS1-NS2A cleavage site variants, rP3-Gly and rP8-Ala, showed similar growth efficiency in terms of kinetics and maximum titers reached, where the latter was only slightly lower (<2-fold) than that of the wt virus. The two variants which were deficient in NS1 and NS2A production in the *in vitro* assay, rP2-Gly and rP7,8-Ala, were severely affected in their growth phenotype in the insect cell line (Fig. 4.3B). While the 24 h p.i growth samples produced uniformly small plaques in Vero cells with titers close to the detection threshold of the assay (10^2 PFU/ml), which could have been the result of residual input virus, growth samples harvested at and after 48 h p.i contained a mixture of virus that produced small and larger plaques. Given that an increase in plaque size is indicative of the selection and amplification of viruses with genetic changes that revert or compensate for the defect in NS1-NS2A cleavage, the growth properties of the two mutant viruses could not be accurately measured. Moreover, it can be concluded that efficient proteolytic processing at the NS1-NS2A junction plays a more important role for virus growth in the mosquito cell line than in mammalian Vero cells.

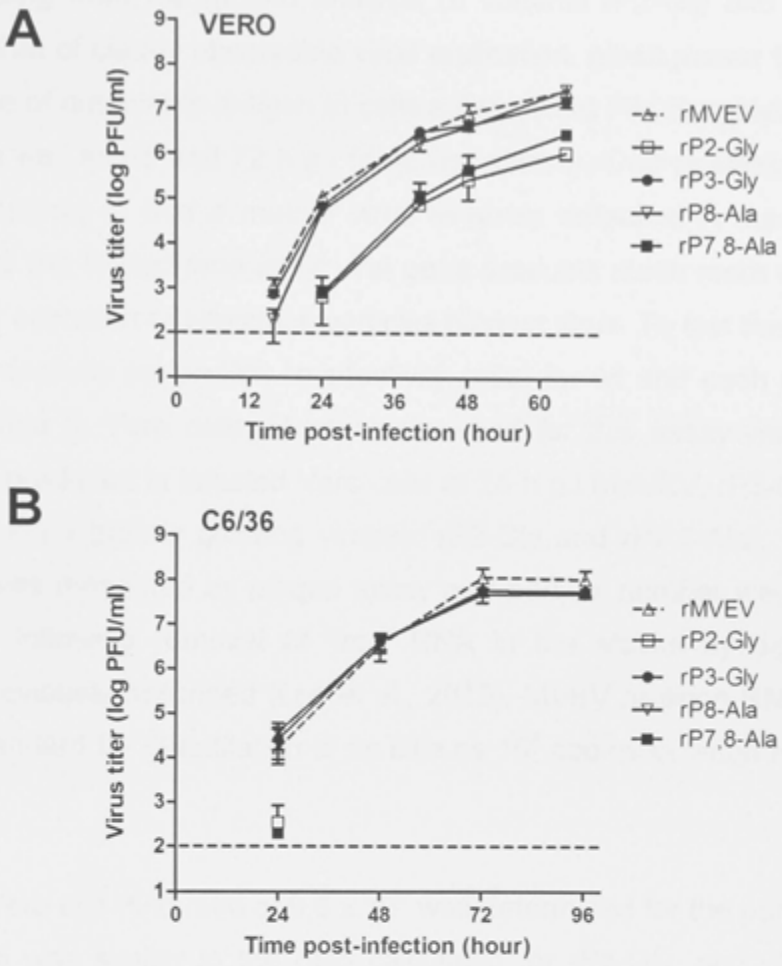

Fig. 4.3. Growth of rMVEV and NS1-NS2A cleavage site mutant viruses in mammalian and insect cells.

Vero and C6/36 monolayers were infected with rMVEV, rP2-Gly, rP2-Gly, rP8-Ala or rP7,8-Ala viruses at MOI of 0.1-0.2. Unbound virus was removed after 1 h of adsorption, and growth medium was added. (A) At 0, 16, 24, 40, 48 and 64 h p.i, culture medium was collected from Vero cells for titration of virus content. (B) For C6/36 cells, culture medium was collected at 0, 24, 48, 72 and 96 p.i. Virus titers were determined by the plaque assay on Vero cells. Interrupted lines indicate plaque assay detection limit. Growth curves for rP2-Gly and rP7,8-Ala viruses in C6/36 cells were not included due to emergence of heterogenous plaque populations in samples collected after 24 h p.i. Error bars indicate standard error of mean (SEM) for two plaque assay determinations for each sample shown.

4.2.7 Specific infectivity for mammalian cells

A striking finding from the growth analysis of variants rP2-Gly and rP7,8-Ala in Vero cells is that of clearly observable virus replication, albeit poorer than wt virus, in the absence of detectable antigen in cells subjected to FACS analysis at 24 h p.i (Fig. 4.4A) as well as 48 and 72 h p.i (data not shown). One possible explanation for this discrepancy is that a mutant virus severely defective in macromolecular synthesis uses the limited amount of viral gene products much more efficiently for assembly and secretion of infectious particles than wt virus. To test this hypothesis, the specific infectivity (or particle-to-infectivity ratio) for wt and each mutant virus were determined in Vero cells. Virus stocks used for this assay were 2-h virus release stock produced in infected Vero cells at 24 h p.i (rMVEV, rP3-Gly and rP8-Ala) or at 48 h p.i (poorly growing viruses: rP2-Gly and rP7,8-Ala). Infectivity of virus stocks was measured by plaque assay and particle number were measured by qRT-PCR following removal of 'free' RNA in the stocks by digestion with RNAse, as previously described (Lee et al., 2010). MVEV replicon RNA was used as internal standard for quantitation of as little as 10^4 copies of virion RNA (Lobigs et al., 2010).

A particle to Vero cell PFU ratio of 9.6×10^2 was determined for the parental strain, rMVEV, which was similar to the ratio calculated for rP3-Gly, and ~2-fold lower than that for rP8-Ala (2.3×10^3) (Fig. 4.5 and Table 4.2). In contrast, the particle-to-PFU ratios for rP2-Gly (1) and rP7,8-Ala (9) were almost 1000-fold and ~100-fold lower than those for rMVEV, suggesting that the mutations that reduced NS1-NS2A cleavage lead to assembly and release of particles with markedly greater infectivity for mammalian cells than wt virus. Specific infectivity values for wt flavivirus could vary between 5×10^2 to 3×10^3 as previously reported from our laboratory (Leang, 2008; Lee et al., 2010).

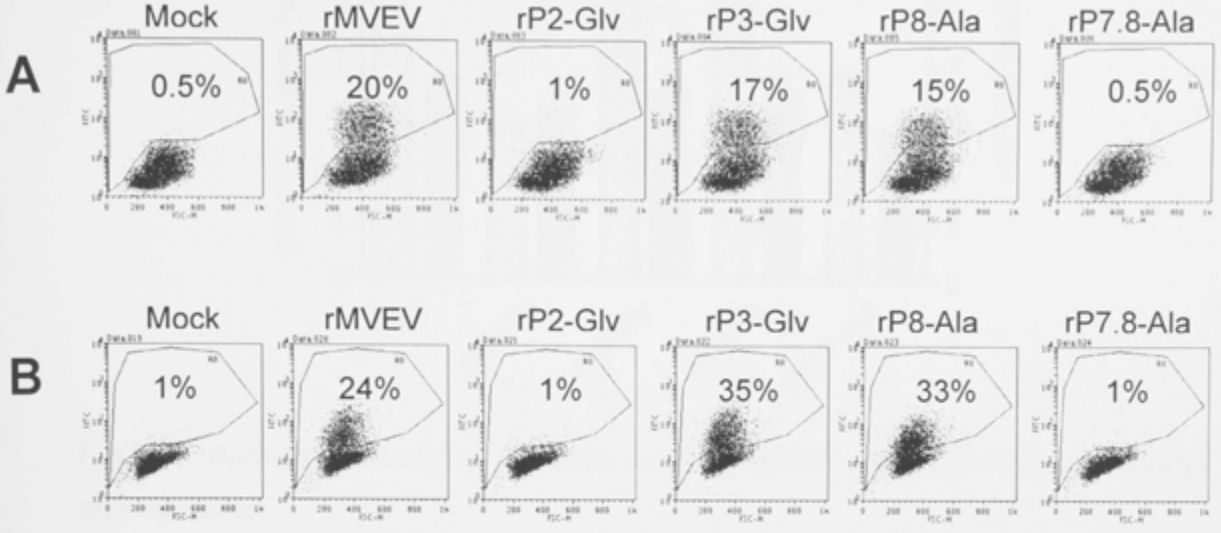

Fig. 4.4 FACS analysis for determination of the percentage of Vero and C6/36 cells infected with rMVEV, rP2-Gly, rP3-Gly, rP8-Ala and rP7,8-Ala for growth phenotype comparisons.

Vero (A) or mosquito C6/36 (B) cell monolayers were infected at a multiplicity of ~0.2 or left untreated. The Vero and C6/36 cells were harvested at 16 h or 24 h p.i, respectively, and stained with an anti-NS1 mAb and FITC-conjugated anti-mouse IgG. Cells gated within region R0 represent the percentages of NS1-positive cells

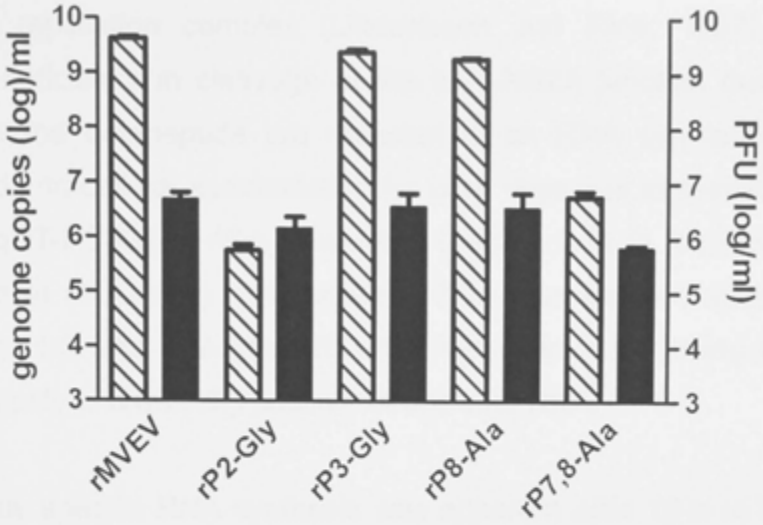

Fig. 4.5. Specific infectivity for Vero cells of rMVEV and NS1-NS2A cleavage site variants.

Vero cell monolayers were infected at MOI of 0.1. Culture supernatants were removed at 48 (rMVEV, rP3-Gly and rP8-Ala) or 72 h p.i (rP2-Gly or rP7,8-Ala), cell monolayers were washed 2 times with prewarmed PBS and medium was replaced. The monolayers were incubated for a further 2 h and culture supernatants were collected. Virus content in culture supernatant was titrated by plaque assay on Vero cells (black bars) and the number of viral RNA copies was determined by real-time qRT-PCR (diagonal bars). Error bars indicate SEM for two real-time qRT-PCR and plaque assay determinations for each sample shown.

Table 4.2. Specific infectivity for Vero cells of rMVEV and NS1 mutant viruses

Virus	Specific infectivity[1] (genome equivalent/ PFU)
rMVEV	9.6×10^2
rP2-Gly	1
rP3-Gly	9.6×10^2
rP8-Ala	2.3×10^3
rP7,8-Ala	9

[1]data calculated from Fig. 4.5.

4.2.8 Analysis of RNA synthesis and intracellular accumulation

The NS1 protein is thought to function in early RNA synthesis as an integral part of the flaviviral replication complex (Lindenbach and Rice, 1997). To evaluate whether the deficiency in cleavage at the NS1-NS2A junction due to mutations introduced in the octapeptide are reflected in an RNA synthesis defect, RNA synthesis and intracellular accumulation for each virus was assessed quantitatively by real-time qRT-PCR over 48 h of infection (section 2.12.3). Vero cell monolayers were infected at MOI of ~1.0, intracellular RNA was isolated at time interval as shown in Fig. 4.6 and real-time qRT-PCR was performed using MVEV-specific primers to amplify and quantify positive-strand viral RNA.

Wild-type virus specific RNA synthesis was apparent after 12 h of infection when the level of intracellular viral RNA had increased ~13 fold relative to cell-associate residual input. Over the following 12 h, viral RNA continued to accumulate exponentially and by 48 h p.i, a ~3 log increase in intracellular viral RNA relative to input was found. Two NS1-NS2A cleavage site variants, rP3-Gly and rP8-Ala, differed from wt in a slower kinetics of intracellular viral RNA accumulation but reached similar levels relative to wt at 48 h p.i. Small-plaque variants, rP2-Gly and rP7,8-Ala, displayed a severe RNA synthesis deficiency. The input RNA for both variants was <17-fold lower than that for wt, which was expected, given the difference in specific infection for Vero cells between the mutants and wt. A low level of virus-specific RNA synthesis was first detectable in the 12-18 h p.i time interval and intracellular viral accumulated to ~250-fold and ~11-fold at 48 h p.i relative to input for variants rP7,8-Ala and rP2-Gly, respectively.

The result from this experiment illustrates an excellent correlation between viral RNA synthesis and *in vitro* cleavage efficiency of NS1 and NS2A proteins. It should be noted that intracellular viral RNA accumulation at time points after the latent period of infection (~12 h p.i) reflects the differential of viral RNA synthesis and RNA release in the form of secreted viral particles. Therefore, the ~1500-fold difference between wt and rP2-Gly in intracellular viral RNA at 48 h p.i would give rise to a much smaller difference in infectious viral particle release, if the viral genomes of the mutant were packaged into virions and released more efficiently than those of wt as a consequence of their limited availability in the infected cell.

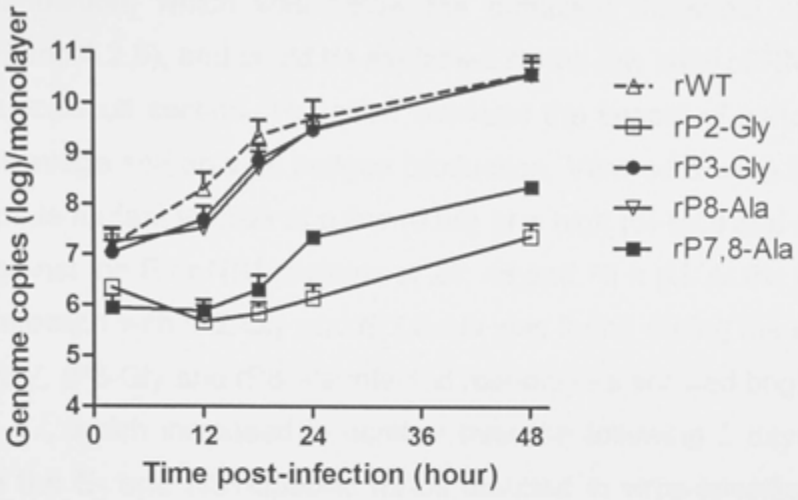

Fig. 4.6. Analysis of virus-specific RNA synthesis in Vero cells.

Vero cells were infected with rMVEV and NS1-NS2A cleavage site variants at a multiplicity of 1. Unbound virus was removed after 1 h of adsorption and growth medium was added. At 2, 12, 18, 24 and 48 h p.i, infected cell monolayers were harvested for total RNA extraction. Virus-specific RNA was measured by real-time qRT-PCR. Error bars indicate the SEM for two real-time qRT-PCR determinations for each sample.

4.2.9 Analysis of MVEV-specific E and NS1 protein synthesis by immunofluorescence staining

Analysis by flow-cytometry of rP2-Gly and rP7,8-Ala infected cells indicated poor antigen accumulation, which was below the detection threshold of the assay (section 4.2.5 and 4.2.6), and could be explained by the low level of RNA synthesis shown in the previous section. To further evaluate the impact of mutations at the NS1-NS2A cleavage site on viral antigen production, Vero cells were infected with wt or octapeptide mutant viruses at a low (0.05) or a high (5) MOI and subjected to IF staining against the E or NS1 proteins at 24, 48 and 72 h p.i. At the low MOI, no evidence of infection with rP2-Gly and rP7,8-Ala was found during the time course, while wt rMVEV, rP3-Gly and rP8-Ala infected monolayers showed brightly staining cells at 24 h p.i, which increased in number over the following 2 days (Fig. 4.7). Staining with the E- and NS1-specific mAbs resulted in virus-specific staining of similar intensity and of similar cell numbers. As expected, the monolayers infected at the high MOI revealed a large number of foci of infection (Fig. 4.8) than the monolayers infected at the low MOI. However, even at the high MOI, no immunofluorescent cells were detected for variant rP2-Gly between 24 and 72 h p.i. Interestingly, a small number of fluorescent foci were seen in Vero cells infected with rP7,8-Ala, which increased in number during the time course (Fig. 4.8). The likely explanation for the appearance of detectable MVEV antigen in cells infected with this variant at the high MOI only is the occurrence of reversions or compensatory mutations, which overcome, at least in part, the deficiency in RNA synthesis and, in turn, protein synthesis of the mutant. Notably, a similar scenario was not found for variant, rP2-Gly, which may reflect the poorer NS1-NS2A cleavage efficiency and RNA synthesis of the latter, reducing the probability of selection of reversions/compensatory mutations during the course of the experiments.

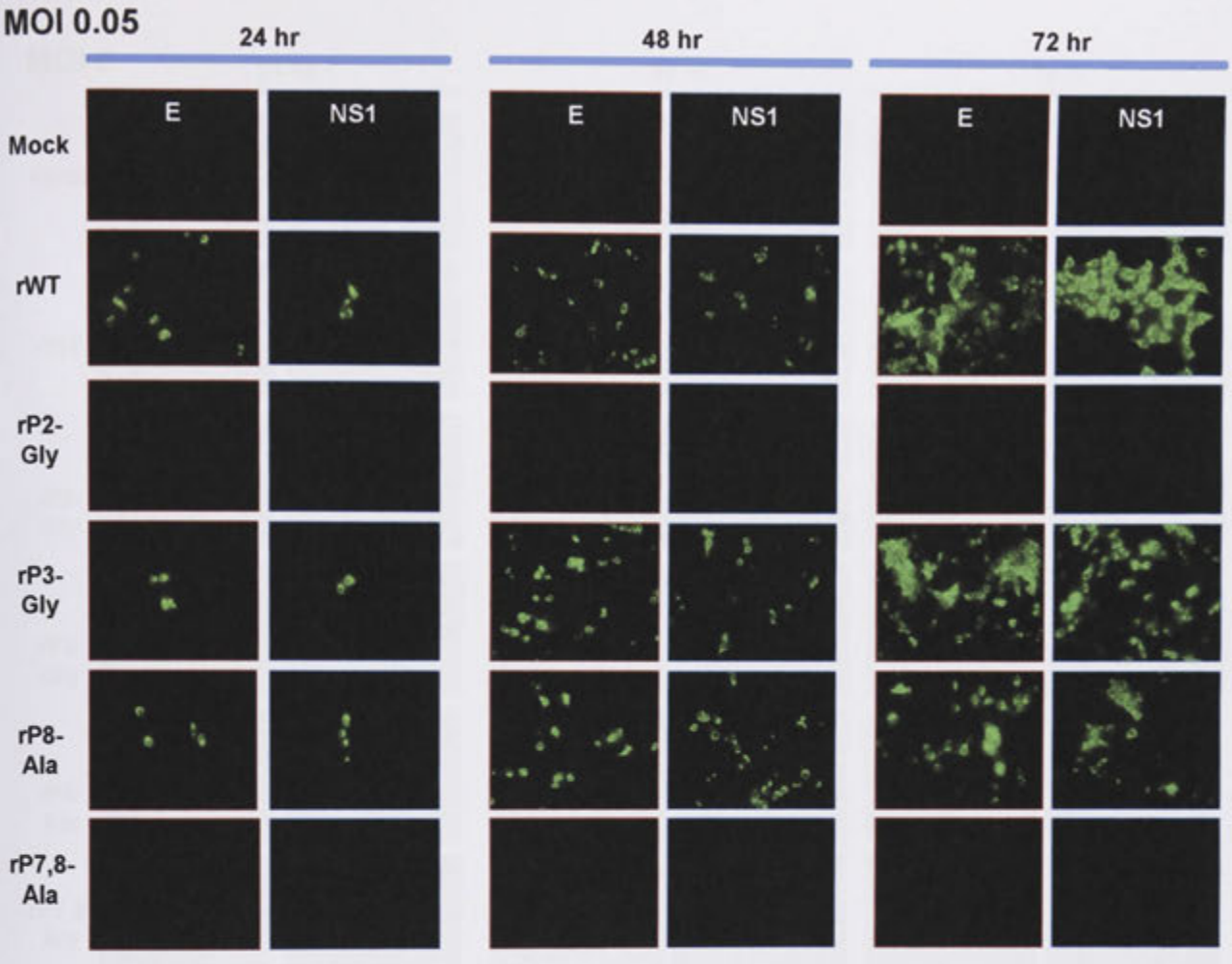

Fig. 4.7. Immunofluorescence analysis of E and NS1 protein expressions in Vero cells following a low multiplicity infection.

Vero cells were infected at multiplicity of 0.05 with wt or NS1-NS2A cleavage site variants or were mock infected, as indicated on the left. Viral protein expression was detected after cell permeabilization and indirect IF staining with mAb 8E7 or 4G4 specific for MVEV E and NS1 proteins, respectively, at 24, 48 and 72 h p.i. The cells were magnified x400.

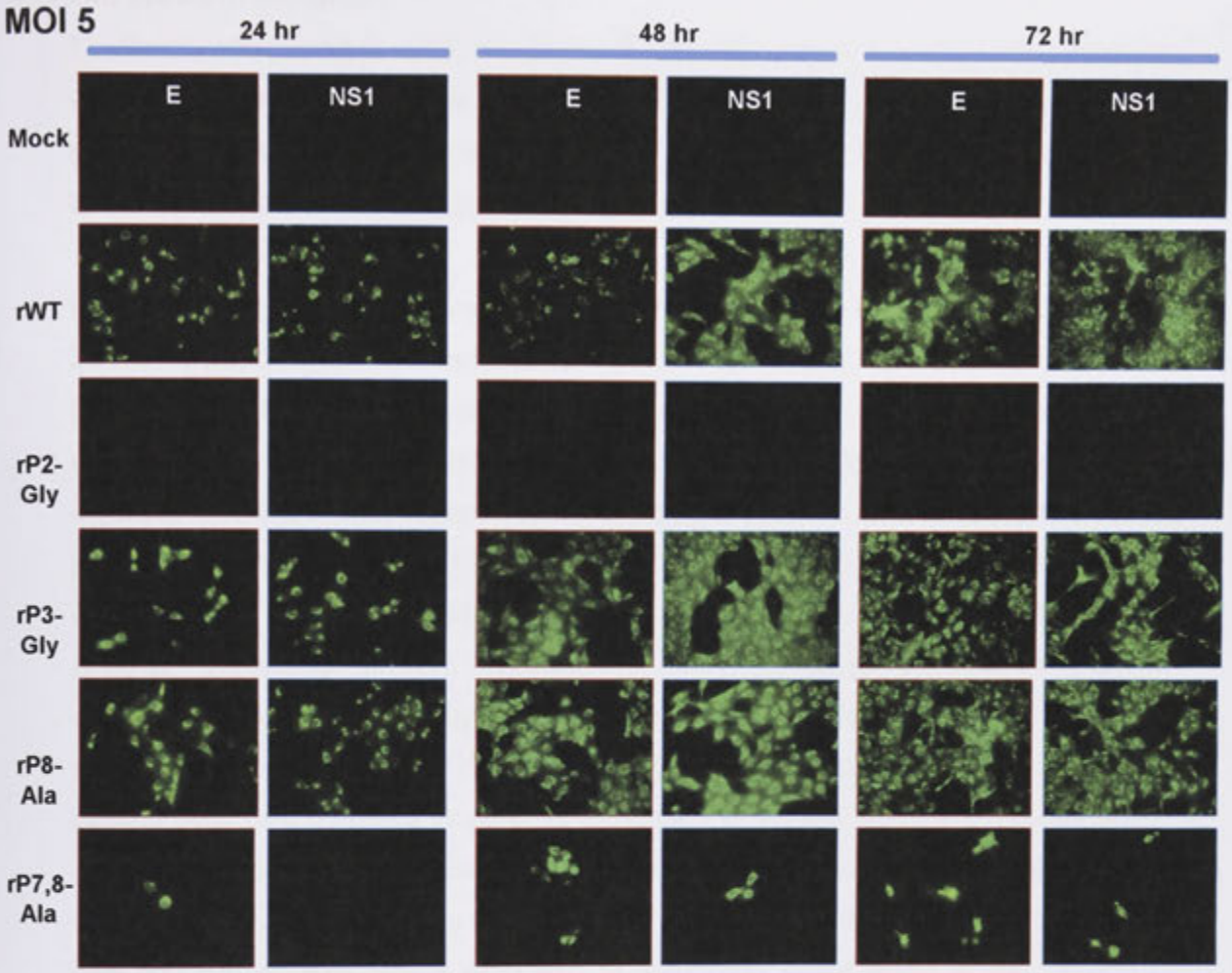

Fig. 4.8. Immunofluorescence analysis of E and NS1 protein expressions in Vero cells following a high multiplicity infection.

Vero cells were infected at multiplicity of 5 with wt or NS1-NS2A cleavage site variants or were mock infected, as indicated on the left. Viral protein expression was detected after cell permeabilization and indirect IF staining with mAb 8E7 or 4G4 specific for MVEV E and NS1 proteins, respectively, at 24 to 72 h p.i. The cells were magnified x400.

4.2.10 Analysis of E and NS1 protein synthesis by radio-immunoprecipitation and Western blotting

To directly visualize the synthesis of the E and NS1 proteins in Vero cells infected with the NS1-NS2A cleavage site mutant viruses relative to wt rMVEV and in an attempt to assess proteolytic processing at the NS1-NS2A junction, radio-immuneprecipitation and Western blotting experiments were performed.

For analysis by radio-immunoprecipitation, Vero cells were infected at MOI of 5 for 24 h, pulsed with ^{35}S-methionine for 30 min, and chased for 5 min. Immunoprecipitation with an anti-NS1 mAb yielded three bands, which corresponded to NS1 (48 kDa), a NS1 glycosylation variation product (lower band; 46 kDa) and NS1' with higher molecular weight (Blitvich et al., 1999; Firth and Atkins, 2009; Mason, 1989; Melian et al., 2010) from wt virus infected cell lysates (Fig. 4.9). An equivalent NS1 expression pattern was recovered for rP3-Gly and rP8-Ala, indicating efficient synthesis of NS1, although the overall protein expression level was slightly lower than that for wt. Notably, no NS1 protein expression was detected for rP2-Gly and rP7,8-Ala, confirming the extremely poor protein synthesis by these viruses, as previously observed with the IF (at low MOI) and FACS assays. Immunoprecipitation with an anti-E mAb resulted in recovery of the E-prM dimer from lysates of wt, rP3-Gly and rP8-Ala infected cells (Fig. 4.9). E and prM protein expression were also at marginally lower levels in cells infected with the variants in comparison to rMVEV wt infected cells, consistent with the observation for NS1. Variants rP2-Gly and P7,8-Ala did not produce sufficient E protein at 24 h p.i for detection by radio-immunoprecipitation. Due to this low level of protein synthesis, it was not possible to analyse processing at the NS1-NS2A junction for the two small-plaque variants by either recovery of an NS1-NS2A precursor product or indirectly by comparison of E and NS1 band intensities.

Viral protein expression was also analyzed after a longer incubation time by Western blotting. Staining with an anti-E or anti-NS1 mAb showed an equivalent E and NS1 protein expression for cells infected with rP3-Gly and rP8-Ala, which was comparable to that of wt (Fig. 4.10). While immunoprecipitation and IF assay (at low MOI) were unable to detect E and NS1 protein expression for rP2-Gly and

rP7,8-Ala, traces amount of E and NS1 proteins were detected at 72 h p.i by Western blotting. However, the overall protein expression level was relatively poorer than that for wt, coherent with the poor RNA synthesis for these small-plaque variants.

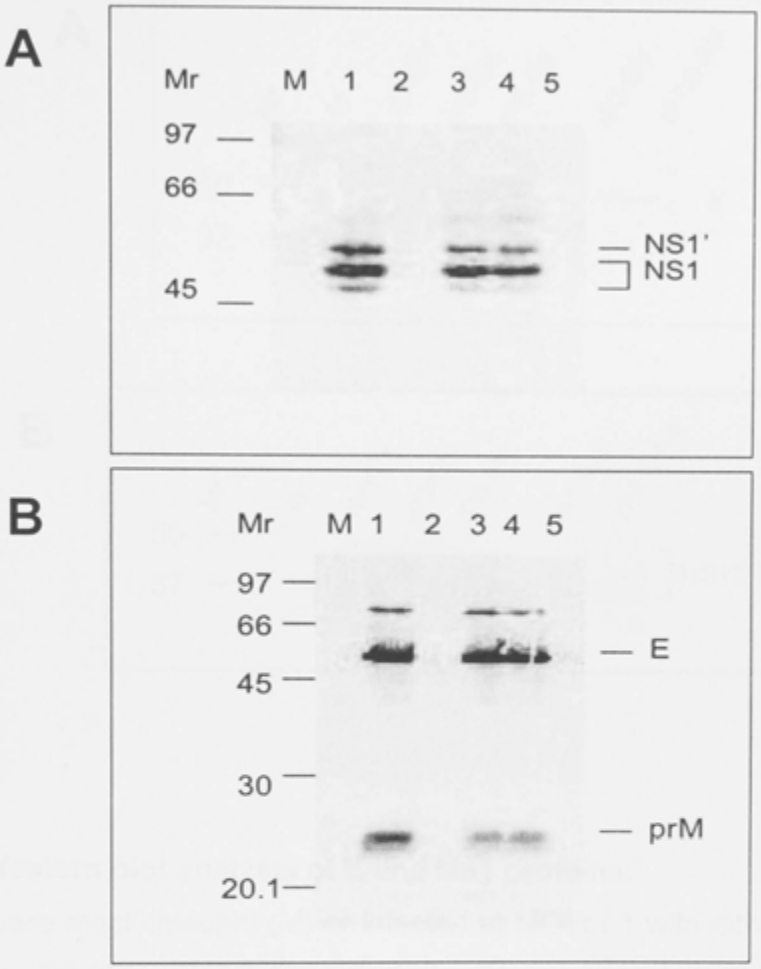

Fig. 4.9. Immunoprecipitation of metabolically labelled viral proteins.

Vero cells were mock-infected (M) or infected with either wt virus (1), rP2-Gly (2), rP3-Gly (3), rP8-Ala (4) or rP7,8-Ala (5) at MOI of 5. At 24 h p.i, cells were labelled with ^{35}S-methionine for 45 min and chased for 5 min and then lysed with RIPA buffer. Lysates were immunoprecipitated with MVEV-specific anti-NS1 (A) or -E protein mAb (B), and analysed by 15% (A) or 10% (B) SDS-PAGE as described in Materials and Methods. The positions of molecular weight marker proteins are indicated on the left (in kDa) and MVEV-specific proteins on the right.

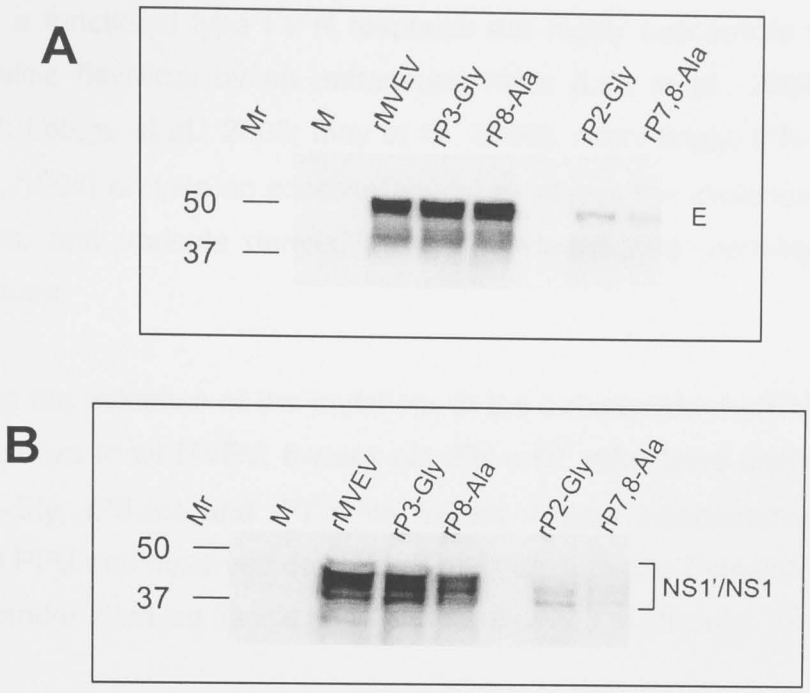

Fig. 4.10. Western blot analysis of E and NS1 proteins.

Vero cells were mock-infected (M) or infected at MOI of 1 with either rMVEV, rP2-Gly, rP3-Gly, rP8-Ala or rP7,8-Ala. Infected cells were lysed at 72 h p.i, subjected to Western blot analysis and viral proteins were detected using specific anti-E (A) or anti-NS1 (B) mAbs. The positions of E and NS1 are marked on the right. The positions of molecular weigh marker proteins are indicated on the left (in kDa).

4.2.11 Effect of mutations at the NS1-NS2A cleavage site on virus growth and virulence in mice

Mice lacking a functional type I IFN response are highly susceptible to infection with encephalitic flavivirus by an extraneural route (Lee et al., 2004; Lee and Lobigs, 2002; Lobigs et al., 2003; May et al., 2006). Accordingly, IFN-α-$R^{-/-}$ mice (Muller et al., 1994) provide an excellent model to assess the virulence properties of flaviviruses, and variants derived thereof, by measuring mortality and viral burden in tissues.

To investigate the influence of the mutations in the octapeptide motif on virulence of variants relative to wt MVEV, 6-week-old IFN-α-$R^{-/-}$ mice were challenged with rP2-Gly, rP3-Gly, rP8-Ala and rP7,8-Ala mutant viruses intraperitoneally with a dose of 1000 PFU and observed daily for signs of encephalitis (hunching, lethargy, eye closure, and/or hind leg flaccid paralysis) for a period of 28 days.

The dose of 1000 PFU of wt MVEV was previously shown to produce 100% mortality in these mice, with an average survival time of 6 days (Hurrelbrink et al., 1999; Lee et al., 2004; Lobigs et al., 2010; Lobigs et al., 2003). Analysis of the mortality profile for rP3-Gly and rP8-Ala demonstrated virulence that was comparable to that of the parental rMVEV with 100% mortality and an average survival time of 5.5 days (rP3-Gly) or 6 days (rMVEV and rP8-Ala) (Fig. 4.11). In contrast, the rP2-Gly and rP7,8-Ala variants were highly attenuated in IFN-α-$R^{-/-}$ mice relative to rMVEV, with 10% and 33% mortality, respectively ($P = 0.0001$ and $P = 0.001$, respectively). While the majority of IFN-α-$R^{-/-}$ mice infected with rP2-Gly and rP7,8-Ala did not succumb to infection, those mice which developed signs of encephalitis exhibited a substantial delay in the onset of mortality, ranging from day 10 for rP2-Gly and 13.5 for rP7,8-Ala. In view of the small number of late death observed for the two variants, it was of interest to test whether reversion or compensatory mutations accounted for the mortality. Brain from dead mice infected with rP7,8-Ala were collected and analyzed by plaque assay. When the plaque morphology for rP7,8-Ala exhibited much smaller plaques than wt (≤1 mm), larger

plaques (1-2 mm) were observed from the brain samples, suggesting the occurrence of variants that contributes to an increased in virulence.

Day 2 viremia in IFN-α-$R^{-/-}$ mice infected with rMVEV wt or NS1-NS2A cleavage site mutant viruses was also measured (Fig. 4.4B). While the parental virus elicited a high viremia (mean titer = 2.4 x 10^5 PFU/ml), there was no detectable virus in blood of mice infected with rP2-Gly and rP7,8-Ala. This suggested that the inability of these variants to efficiently replicate in mouse tissue accounts for the lost of virulence. Interestingly, viremia levels detected in mice infected with rP3-Gly and rP8-Ala (mean titer = 3.5 x 10^4 PFU/ml), were reduced by ~7-fold relative to titers in wt rMVEV infected mice (P = 0.0005). The latter indicates a significant impact on virus growth, *in vivo*, of the two mutations at the conservative P3 and P8 positions in the octapeptide, which was not clearly apparent in plaque morphology, or growth in cell culture, nor in cleavage efficiency at the NS1-NS2A junction using transient expression of NS1 and NS2A (Chapter 3).

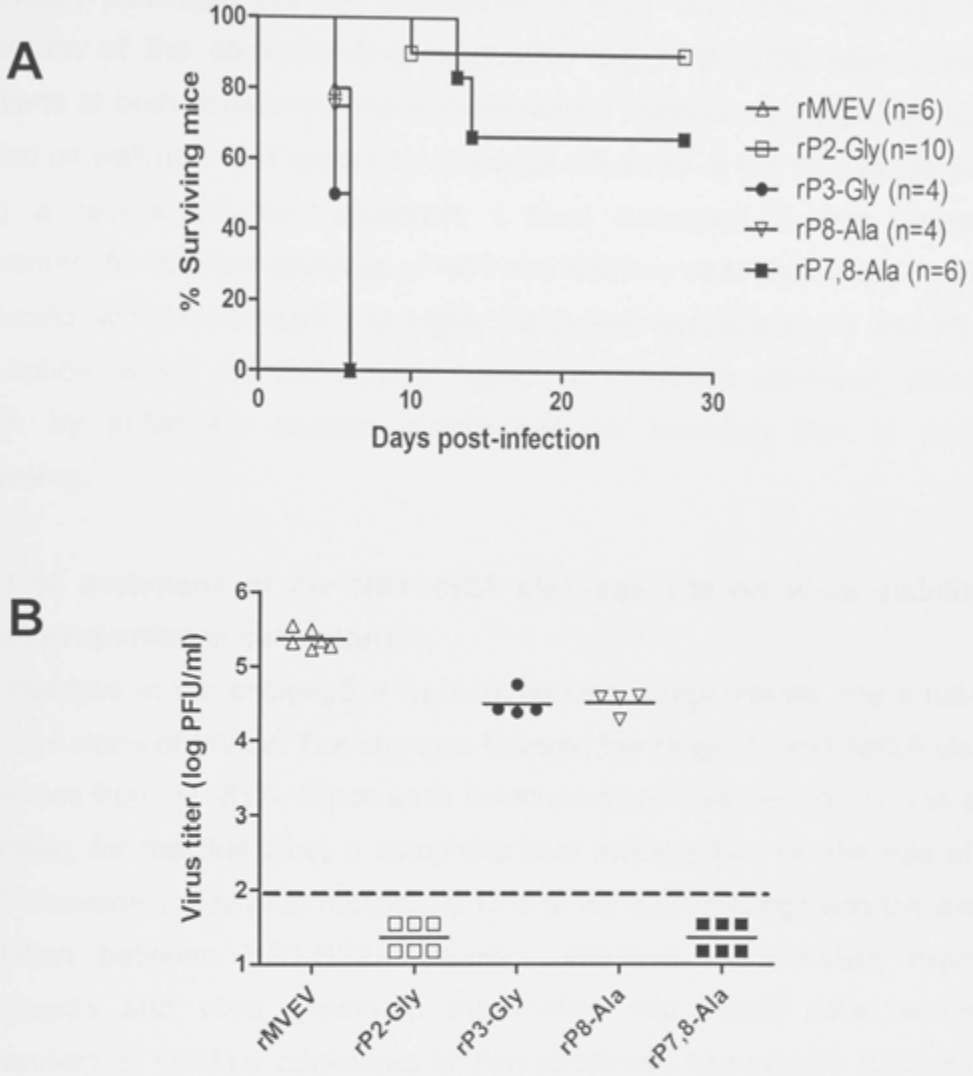

Fig. 4.11. Virulence in six–week-old IFN-α-receptor knockout mice.

(A) Groups of six-week-old IFN-α-R $^{-/-}$ mice were infected intraperitoneally with 1000 PFU of rMVEV (n=6), rP2-Gly (n=10), rP3-Gly (n=4), rP8-Ala (n=4) or rP7,8-Ala (n=6). Morbidity and mortality were recorded daily for a period of 28 days. (B) Sera were collected on day 2 p.i and frozen at -70 °C. Viremia titers were determined by plaque assay on Vero cells. Each symbol represents an individual mouse and the mean titers are indicated by a horizontal line. The interrupted line indicates the plaque assay detection limit.

4.3 Discussion

In the previous chapter, I characterized the effect of amino acid substitutions at the NS1-NS2A cleavage site on production of NS1 and NS2A using transient expression of the corresponding polyprotein region in COS cells. I identified mutations at both conserved and non-conserved residues in the octapeptide with minimal as well as major impact on cleavage efficiency at the NS1-NS2A junction. Using a reverse-genetics approach, I have examined in this chapter the requirement for efficient cleavage of NS1 and NS2A in virus replication. I have also addressed, whether mutations at highly conserved residues at P3 and P8 in the octapeptide, which did not notably impact on cleavage efficiency, affect virus growth by potentially another mechanism not involving that of proteolytic processing.

Effect of mutations at the NS1-NS2A cleavage site on virus viability and growth properties in cell culture

Four changes in the octapeptide were introduced independently into a full-length infectious clone of MVEV. The changes covered the range of NS1-NS2A cleavage efficiencies from 37–83%. Since each construct gave a viable virus, I was able to undertake, for the first time, a comprehensive investigation on the role of NS1-NS2A cleavage in flavivirus replication. One of my main findings was the excellent correlation between NS1-NS2A cleavage efficiency in transient expression experiments and virus growth in mammalian and insect cells, which was independent of whether conserved or non-conserved octapeptide residues were substituted. Thus, variants rP3-Gly and rP8-Ala, which had mutations that only slightly reduced NS1-NS2A cleavage efficiency relative to wt, produced plaques on Vero cell monolayers of similar size to wt and grew in Vero and C6/36 cells with a kinetics that differed <2-fold from that of rMVEV. On the other hand, the moderate (60%) and poor (37%) cleavage efficiencies associated with P7,8-Ala and P2-Gly substitutions, respectively, greatly reduced plaque size and lowered virus yield from infected Vero cells by between 1 and 2 logs during the course of the growth assay in comparison to wt virus. Of the two small-plaque variants, rP2-Gly grew to ~5-fold lower titers than rP7,8-Ala, consistent with the poorer cleavage of NS1 and

NS2A as a result of the mutation incorporated in the variant. Growth of MVEV in mosquito cells was more sensitive to the effect of substitutions, which substantially reduced proteolytic processing at the NS1-NS2A junction, than that in Vero cells. This was illustrated by the rapid appearance of plaque size heterogeneity, suggesting increased selective pressure for reversions or compensatory changes to occur in the rP2-Gly and rP7,8-Ala variant genomes when replicating in the insect than in the mammalian cell. This could be a consequence of the lower temperature (28°C) used for maintenance of C6/36 cells than that for Vero cells (37°C) and possibly associated further reduction in proteolytic processing at the NS1-NS2A junction in the small-plaque variants, as has been described for a mutation altering cleavage at the flavivirus C-prM junction (Lobigs et al., 2010).

A second major finding from this investigation was the tolerance of growth in cell culture of MVEV to the non-conservative Val→Gly change at P3 in the octapeptide, despite absolute conservation of Val at this position in the octapeptide among all flaviviruses. Similarly, an Ala substitution at the highly conserved P8 position in the octapeptide (either Leu or Met among all flaviviruses) did not markedly impact on virus macromolecular synthesis or growth in cell culture. This result shows that octapeptide mutations, which did not reduce cleavage at the NS1-NS2A junction in recombinant expression of the NS1-NS2A polyprotein region, also did not markedly impinge on RNA and virus replication in cell culture, regardless of amino acid conservation. From this I can conclude that the dominant role of the amino acid sequence conservation at the flavivirus NS1-NS2A cleavage site is in substrate recognition by the protease, which cleaves NS1 and NS2A. However, the question arises of why natural flavivirus isolates with comparable changes at the conserved positions in the octapeptide as described here cannot be found. The likely explanation for this apparent contradiction is that Vero and C6/36 cells are relatively insensitive to mutations in the MVEV genome that are only marginally deleterious for virus replication, given that these cell culture systems are used because of a high virus yield, which may allow a significant level of wastage of viral gene products. This may not be the case in hosts and vectors essential for natural transmission of flaviviruses. In support of this proposition, I found that viremia in mice infected with variants rP3-Gly and rP8-Ala was significantly lower than in mice

infected with wt rMVEV. A greater sensitivity of the mouse relative to cell culture models has also been noted for a MVEV variant with a mutation in the signal peptide that coordinated the two cleavages at the C-prM junction in the flavivirus polyprotein (Lobigs et al., 2010).

Effect of changes at the NS1-NS2A cleavage site on viral macromolecular synthesis

The work by Lindenbach and Rice on YFV first identified a physiological role of the flavivirus NS1 protein as an essential component of the viral replication complex in early RNA synthesis (Lindenbach and Rice, 1997). Additional to its role in replication, it is likely that NS1 has other important functions in the flavivirus life cycle, given that the protein is not only found intracellularly, but is also secreted to high levels (Crooks et al., 1994; Flamand et al., 1999; Winkler et al., 1989; Winkler et al., 1988), associated with the plasma membrane of infected and uninfected cells (Avirutnan et al., 2007; Jacobs et al., 2000; Noisakran et al., 2008; Noisakran et al., 2007) and undergoes an alternative processing pathway involving ribosomal slippage and a translational frame-shift at the NS1-NS2A junction to yield the larger NS1' product (Firth and Atkins, 2009; Melian et al., 2010). Like NS1, the flavivirus NS2A protein is probably also multifunctional and plays an essential role in replication as part of the replication complex (Mackenzie et al., 1998), but also in virus assembly by an unknown mechanism (Khromykh et al., 2001; Kummerer and Rice, 2002; Leung et al., 2008; Liu et al., 2003). Based on this information, it was anticipated that mutations in the flaviviral genome, which decreased cleavage at the NS1-NS2A junction, would be detrimental for RNA and protein synthesis and, in turn, virus growth. This detrimental effect could be due to (i) the straightforward reduction in the quantitative availability of the two non-structural proteins essential for replication and/or (ii) an inhibitory effect of the NS1-NS2A precursor, which may associate with other non-structural proteins to produce a non-functional replication complex or defective intermediate assembly complexes thereof. Indeed, synthesis and intracellular accumulation of viral RNA were closely linked to NS1-NS2A cleavage efficiency in transient expression experiments and accurately discriminated between wt virus, variants with cleavage site mutations leading to a marginal reduction of cleavage efficiency (rP3-Gly and rP8-Ala), the variant with a

mutation leading to an intermediate reduction of cleavage efficiency (rP7,8-Ala) and the variant with a mutation resulting in poor cleavage efficiency (rP2-Gly). This result does not only validate the measures of cleavage efficiency obtained in the transient transfection assays in Chapter 3, but also supports the interpretation that, at least for virus growth in cell culture, the main (and possibly sole) impact of modulation of proteolytic processing at the NS1-NS2A junction is on viral RNA replication.

The pronounced deficiency in RNA synthesis of variants, rP2-Gly and rP7,8-Ala, was reflected in a remarkably low level of protein synthesis and viral antigen accumulation in infected cells, which remained below the detection threshold of the flow-cytometry, indirect IF and radio-immunoprecipitation assays. On the other hand, variants rP3-Gly and rP8-Ala could not be discriminated from wt rMVEV in terms of antigen accumulation in infected cells measured by FACS or IF analysis; however, there was an indication of a marginal reduction in viral protein synthesis in rP3-Gly and rP8-Ala infected cells when pulse-labelling at 24 h p.i and radio-immunoprecipitation of E and NS1 proteins was used. The latter is in accord with the data on RNA synthesis and accumulation between 12 and 24 h p.i (Fig. 4.6).

Further to measuring the effect of substitutions in the octapeptide on viral macromolecular synthesis, protein synthesis experiments were also performed to analyse cleavage of NS1 and NS2A in rMVEV wt and variant infected cells. Given that the NS1-specific mAb (4G4) did not efficiently recognize the NS1-NS2A precursor (perhaps due to significant change in NS1 antigenic structure when tethered to NS2A), I attempted to gain an insight into the relative cleavage efficiencies at the NS1-NS2A junction in virus infection by comparison of the amount of NS1 relative to E protein detected in infected cell lysates. Thus, it was anticipated that in rP2-Gly and rP7,8-Ala infected cell lysates a higher ratio of E/NS1 proteins would be found than in those of cells infected with wt or rP3-Gly and rP8-Ala, given the severe NS1-NS2A cleavage defect in the small-plaque variants, which should lead to a reduced production of mature NS1 relative to E protein. However, this analysis was not informative, because pulse-chase and radio-immunoprecipitation failed to detect the viral proteins for the two growth-

deficient variants. Nonetheless, the use of another viral protein, for example anti-NS5 mAb would gave been a useful control to determine the actual protein synthesis in these mutants.

Effect of changes at the NS1-NS2A cleavage site on specific infectivity

NS1-NS2A cleavage site variants, rP2-Gly and rP7,8-Ala, showed a remarkable increase in infectivity for Vero cells per virion particle released into the culture supernatant of infected cells, in comparison to wt and variants, rP3-Gly and rP8-Ala. Accordingly, specific infectivity appeared to be directly linked to cleavage efficiency at the NS1-NS2A junction and the down-stream impact on viral macromolecular synthesis and virus growth. While providing an explanation for the ability of the two small-plaque variants to grow to moderate titers in Vero cells despite the very poor RNA and protein synthesis efficiencies, the mechanism for release of viral particles with 100- to 1000-fold higher infectivity than those of wt remains unclear. There are a number of potential, and not exclusive, explanations for the phenomenon: (i) aggregation of virions and associated loss of infectivity is proportional to the concentration of viral antigen in the culture supernatant; (ii) secreted NS1 reduces virus infectivity; (iii) defective interfering (DI) particles are a dominant by-product of wt virus replication, but are not produced to a significant level during replication of the small-plaque variants. Since DI particle production requires a highly active RNA replication machinery (Debnath et al., 1991; Poidinger et al., 1991), the latter proposition could account, at least in part, for the difference in specific infectivity between the poorly replicating variants, rP2-Gly and rP7,8-Ala, and wt MVEV.

Effect of changes at the NS1-NS2A junction on virulence in mice

The virulence phenotypes of the NS1-NS2A cleavage site mutant viruses in type I IFN response-defective mice followed their growth properties in cell culture and their growth in mouse tissues measured by viremia. Variants rP2-Gly and rP7,8-Ala were attenuated and failed to produce detectable viremia, while variants rP3-Gly and rP8-Ala generated a high viremia and killed all infected mice with the same average survival time as was found for wt rMVEV. This supports the view that the efficiency of growth and dissemination in extraneural tissues are critical

determinants for central nervous system (CNS) invasion by encephalitic flaviviruses in the mammalian host, where the latter is often associated with lethality; the deficiency in the IFN response in the IFN-α-$R^{-/-}$ mouse model for flaviviral encephalitis eliminates one of the key innate immune pathways that restricts virus growth in extraneural tissues, and thereby allows measurement of the viscerotropism of wt and mutant virus strains (Lee et al., 2004; Lobigs et al., 2003). Notably, the mouse model discriminated between the viscerotropism of wt rMVEV and variants rP3-Gly and rP8-Ala and demonstrated a significant (~10-fold) difference in viremia at day 2 p.i, although this was not reflected in a difference in mortality.

CHAPTER 5

Selection and characterization of the MVEV NS1-NS2A cleavage site variants with enhanced virus growth

5.1 Introduction

During the course of my investigations on the two NS1-NS2A cleavage site mutants, rP2-Gly and rP7,8-Ala, I observed heterogenous plaque sizes that emerged following virus amplification on Vero and C6/36 cells. This was indicative of reversions or compensatory changes taking place in the mutant viral genomes. While the identification of reversions would not contribute to a better understanding of the phenotypes of the original mutant viruses other than highlighting their growth deficiency relative to wt virus, the discovery of compensatory mutations elsewhere in the genome can lead to new insights into the biology of the virus. This "forward-genetics" approach has been instrumental in uncovering viral protein-protein interactions and has provided clues to the often multiple functions of viral proteins in the replication cycle. For instance, in terms of understanding the role of the flavivirus non-structural proteins in virus replication, forwards-genetics first identified an interaction of NS2A with NS3, which is important in virus assembly or release (Kummerer and Rice, 2002; Liu et al., 2003), as well as an interaction of NS1 and NS4A as putative components of the replication complex (Lindenbach and Rice, 1999), a putative role of NS2A in assembly (Leung et al., 2008), specific function of non-structural protein in inhibition of IFN-β promoter-driven transcription (Liu et al., 2004) and role of HCV NS3 in increasing virus yield in cell culture (Murray et al., 2007; Yi et al., 2007) have also been identified using this approach.

The power of forward genetics as a tool for the discovery of novel and unanticipated events in flavivirus replication was yet again laid bare in the research carried out for this chapter. Thus, analysis of 5 plaque isolates from rP2-Gly and 7 plaque isolates from rP7,8-Ala showed revertant phenotype with increased growth, RNA synthesis and protein expression. Intriguingly, the growth deficiencies of the NS1-NS2A cleavage site mutants were substantially repaired by compensatory mutations in E protein.

5.2 Results

5.2.1 Isolation of rP2-Gly and rP7,8-Ala variants that produce plaques of increased size relative to the original mutants

The NS1-NS2A cleavage site variants, rP2-Gly and rP7,8-Ala showed marked plaque size heterogeneity following more than 2 cycles of virus propagation on Vero cells or a single passage on C6/36 cells. Larger-sized plaques were isolated, amplified twice on Vero cells, and sequenced in the entire C to NS5 gene region with results shown in Table 5.1.

Analysis of 5 plaque isolates derived from rP2-Gly showed a uniform morphology with marked increased size (3-4 mm) relative to the original rP2-Gly mutant (≤1 mm) (Fig. 5.1 and Table 5.1). Remarkably, sequence analysis of the plaque isolates did not identify a single reversion or alternative change in the octapeptide at the NS1-NS2A junction but uncovered two mutations in E protein: a nonconservative change at codon 59 (Tyr-to-His) and a substitution at residue 65 (Val-to-Ala).

Similarly, 7 plaque isolates derived from rP7,8-Ala originating from infected Vero or C6/36 cells or infected mouse brain showed a homogenously larger size (1-2 mm) than the original rP7,8-Ala mutant (≤1 mm) (Fig. 5.1 and Table 5.1). Yet again, 5 of the 6 variants only showed a single amino acid change at different positions in E protein (L91S, I176N, F242L, P339S, I340M). A sixth variant isolated from rP7,8-Ala infected mouse brain displayed two mutations: a reversion at the P7 residue in the octapeptide (A346V) and a Y61C substitution in E protein. Two variants derived from the original two mutants, rP2-Gly/V1 and V2 and rP7,8-Ala/V1 and V2 were selected to undertake a more detailed investigation of their phenotypic properties in comparison to wt and original mutant viruses.

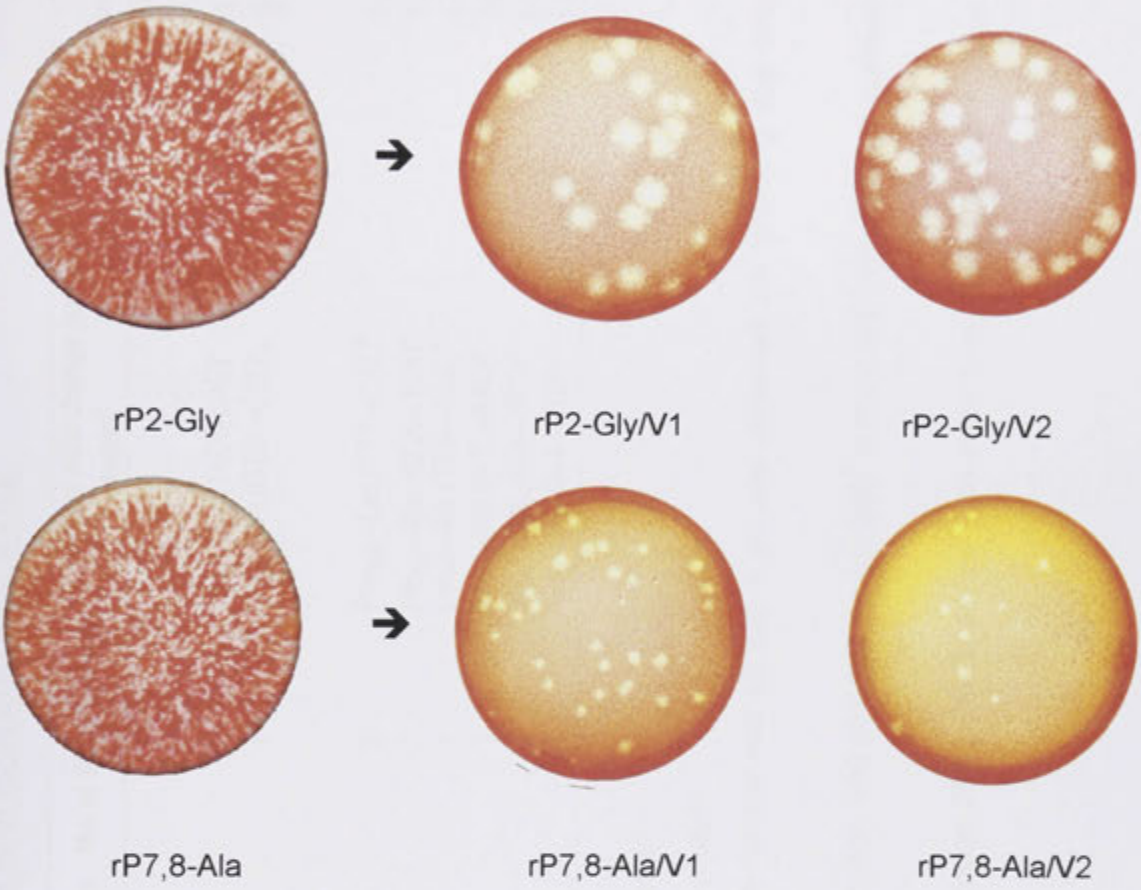

Fig. 5.1. Plaque morphology of NS1-NS2A cleavage site mutants and variants with increased plaque size.

Plaque assay on Vero cells of samples of culture supernatant from BHK cells transfected with rP2-Gly and rP7,8-Ala predominantly showed small plaque phenotype. Heterogenous plaque populations were observed following stocks amplification on Vero or C6/36 cells. Two plaques were isolated from rP2-Gly or rP7,8-Ala, namely rP2-Gly/V1 and V2 or P7,8-Ala/V1 and V2, respectively.

Table 5.1. Recovery of rP2-Gly and rP7,8-Ala variants with increased plaque size.

Original mutant (bold) and variants derived thereof	Cell/tissue origin	No. of times isolated	Amino acid change (nucleotide change) E protein[a]	NS1 protein[b]	Plaque size[c]
rP2-Gly					
rP2-Gly/V1	Vero	1	Tyr_{59}→His (TAC→CAC)[e]		3-4 mm
rP2-Gly/V2	Vero	4	Val_{65}→Ala (GTG→GCG)[d]		3-4 mm
rP7,8-Ala					
rP7,8-Ala/V1	Vero	2	Phe_{242}→Leu (TTT→CTT)[d]		1-2 mm
rP7,8-Ala/V2	C6/36	1	Pro_{339}→Ser (CCA→TCA)[e]		1-2 mm
rP7,8-Ala/V3	Vero	1	Leu_{91}→Ser (TTG→TCG)[e]		1-2 mm
rP7,8-Ala/V4	Vero	1	Ile_{176}→Asn (ATC→AAC)[e]		1-2 mm
rP7,8-Ala/V5	Vero	1	Ile_{340}→Met (ATA→ATG)[e]		1-2 mm
rP7,8-Ala/V6	Mouse brain	1	Tyr_{61}→Cys (TAT→TGT)[e]	Ala_{346}→Val (GCT→GTT)	1-2 mm

[a] Amino acid numbering from the first residue in the E protein.

[b] Amino acid numbering from the first residue in the NS1 protein.

[c] Plaque morphology on Vero cells stained with 0.02% neutral red on day 4 p.i and recorded the following day are given. Plaque size for wt rMVEV was 3-4 mm.

[d] Based from sequencing result from codon 1 in C to codon 900 in NS5. Amino acid numbering from the first residue in the indicated protein.

[e] Based from sequencing result from codon 1 in C to codon 286 in NS3. Amino acid numbering from the first residue in the indicated protein.

5.2.2 Growth in mammalian cells

The growth kinetics of rP2-Gly- and rP7,8-Ala-derived variants in Vero cells was compared to that of wt rMVEV in parallel with that of the original small-plaque mutants. Cells were infected at MOI ~0.1 and extracellular virus yield was determined by plaque assay on Vero cell monolayers. Variants, rP2-Gly/V1 and V2 showed similarly enhanced (~10- to 25-fold) virus yield during the course of the growth experiment in comparison to mutant rP2-Gly, although their growth remained slightly poorer than that of wt virus (Fig. 5.2A). In contrast, growth of variants, rP7,8-Ala/V1 and V2, was only marginally enhanced (~2- to 5-fold) in the 24 h to 64 h p.i time interval relative the rP7,8-Ala mutant and remained >10-fold less efficient than that of wt rMVEV (Fig. 5.2A). The outcome of the comparison is consistent with the plaque sizes on Vero cells for the different viruses (Table 5.1).

The growth efficiency of the mutants, variants and wt rMVEV was also compared by flow-cytometry to measure antigen production in infected Vero cells during the first round of replication (Fig. 5.3). In stark contrast to mutants, rP2-Gly and rP7,8-Ala which, as previously shown, did not produce detectable levels of intracellular NS1 protein after 18 h of infection, infection consistent with virus input (MOI = 0.1 - 0.3) was observed for each of the variants and wt virus.

5.2.3 Specific infectivity for mammalian cells

Greater specific infectivity for mammalian cells was previously observed for rP2-Gly and rP7,8-Ala relative to wt rMVEV and was proposed to account for the discrepancy between the observed growth of these mutants in the absence of detectable amount of antigen in flow-cytometry analysis and extremely poor protein expression (section 4.2.7). To test whether this finding is also true for the variants derived from these mutants, their specific infectivity was assessed by determining the particle-to-PFU ratio using 2-h virus released stocks produced in Vero cells at 48 or 72 h p.i. Infectivity of virus stocks was determined by plaque assay on Vero cells and virus-specific RNA genome copy numbers were determined by real-time qRT-PCR, as previously described (Lee et al., 2010).

As expected from the determinations in Chapter 4 (see Table 4.2), the particle-to-PFU ratio for rMVEV was ~1000-fold greater than those for rP2-Gly and rP7,8-Ala (Table 5.2). This difference was not found for the variant pairs derived from the two mutants: each variant displayed a specific infectivity, which was ~3 log greater than that of the respective mutants and similar to wt virus (Table 5.2 and Fig. 5.4).

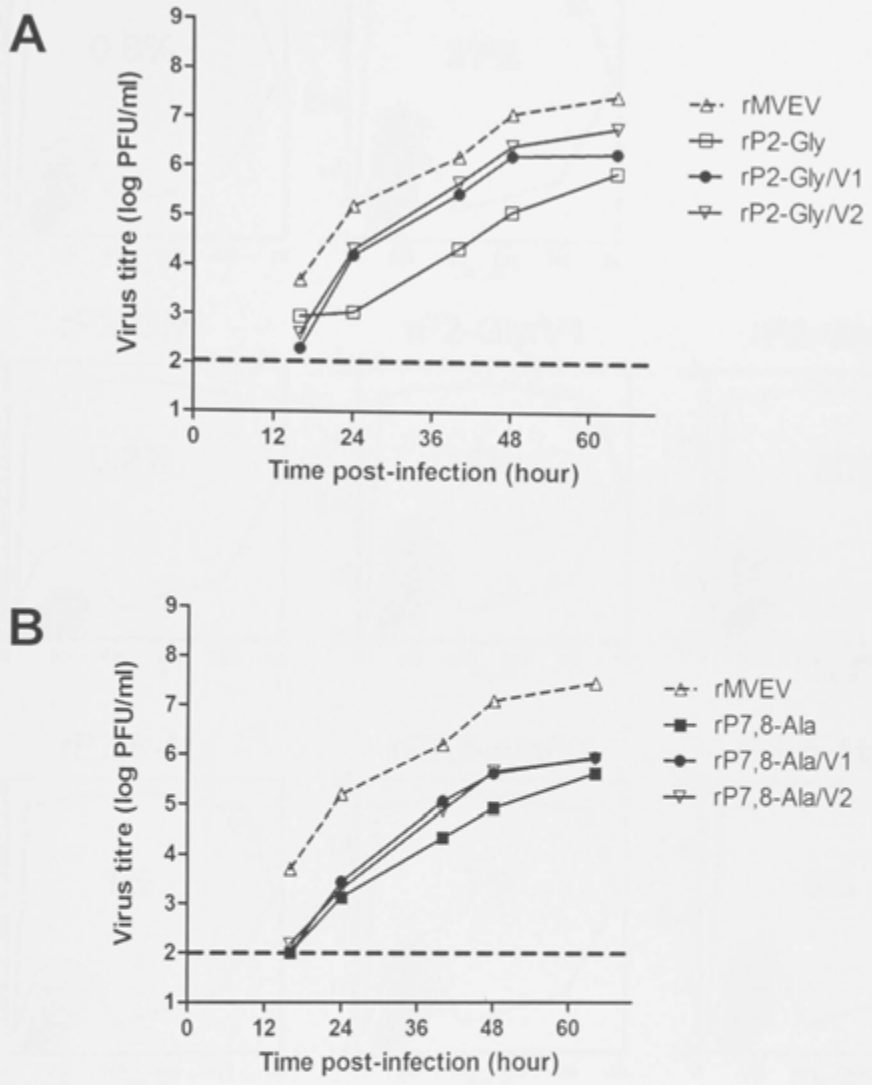

Fig 5.2. Growth kinetics of wt rMVEV, NS1-NS2A cleavage site mutants and variants on Vero cells.

Vero cell monolayers were infected with (A) rMVEV, rP2-Gly, rP2-Gly/V1 or rP2-Gly/V2 and (B) rMVEV, rP7,8-Ala or rP7,8-Ala/V1 or rP7,8-Ala/V2 at a multiplicity of ~0.1. Culture medium was collected at the indicated times and virus titers were determined by plaque assay on Vero cells. Interrupted line indicated the plaque assay detection limit.

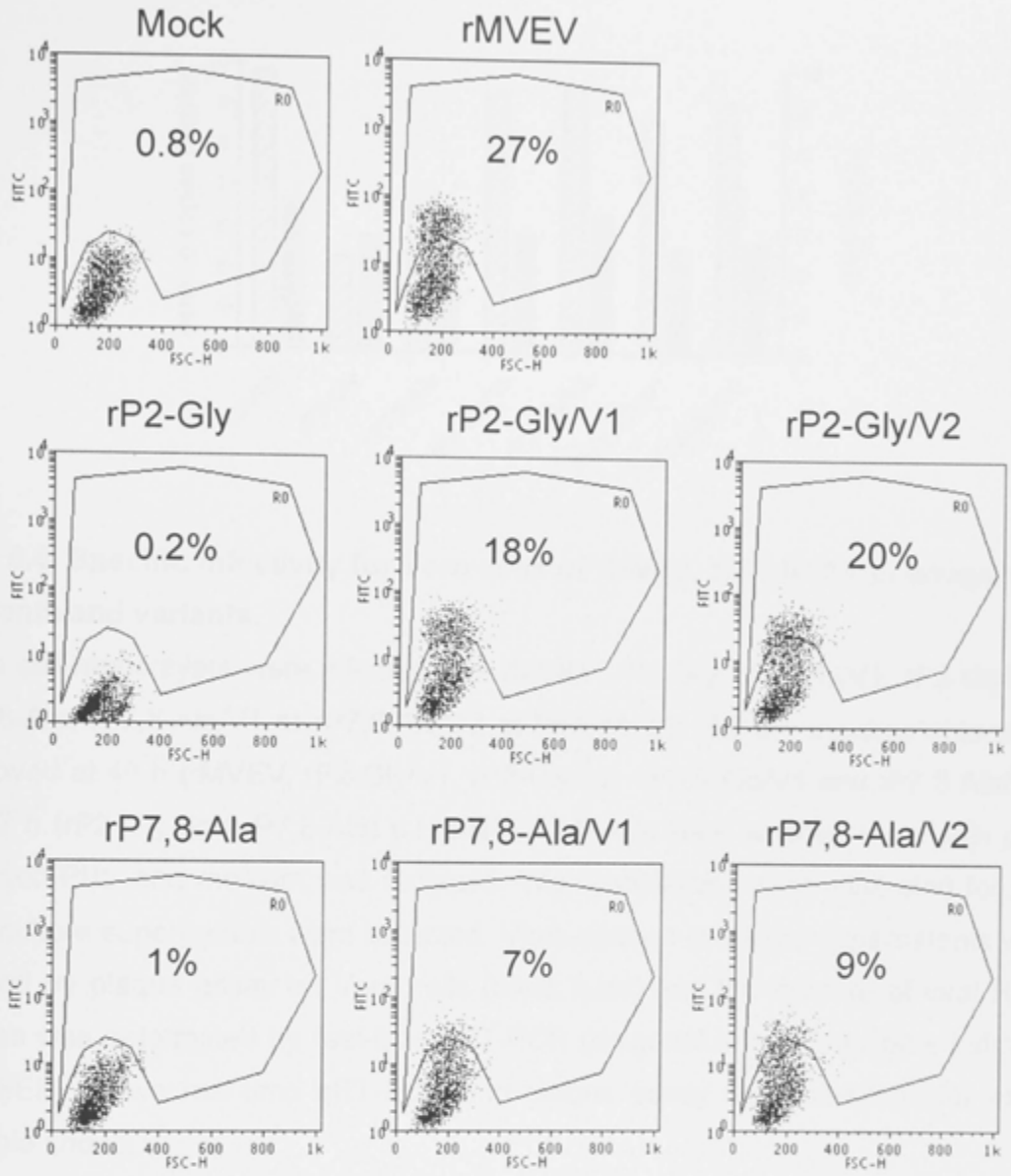

Fig. 5.3. FACS analysis for determination of the percentage of Vero cells infected with rMVEV, rP2-Gly, rP2-Gly/V1, rP2-Gly/V2, rP7,8-Ala, rP7,8-Ala/V1 or rP7,8-Ala/V2 for growth phenotype comparisons.

Vero cell monolayers were infected at a multiplicity of 0.1 - 0.3 or left untreated. The cells were harvested at 18 h p.i, and stained with an anti-NS1 mAb and FITC-conjugated anti-mouse IgG. Cells gated within region R0 represent the percentages of NS1-positive cells.

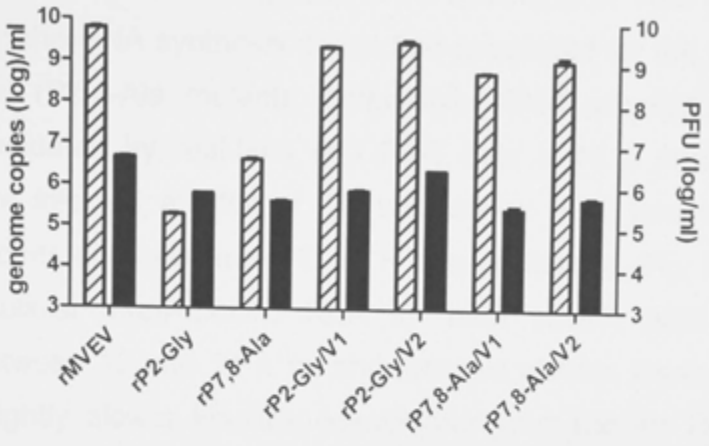

Fig. 5.4. Specific infectivity for Vero cells of rMVEV, NS1-NS2A cleavage site mutants and variants.

Vero cell monolayers were infected with rMVEV, rP2-Gly, rP2-Gly/V1, rP2-Gly/V2, rP7,8-Ala, rP7,8-Ala/V1 or rP7,8-Ala/V2 at MOI of 0.1. Culture supernatants were removed at 48 h (rMVEV, rP2-Gly/V1, rP2-Gly/V2, rP7,8-Ala/V1 and rP7,8-Ala/V2) or 72 h (rP2-Gly and rP7,8-Ala) p.i, cell monolayers were washed twice with pre-warmed PBS and medium was replaced. The monolayers were incubated for 2 h and culture supernatants were collected. Virus content in culture supernatants was titrated by plaque assay on Vero cells (black bars) and the number of viral RNA copies was determined by real-time qRT-PCR (diagonal bars). Error bars indicate the SEM of two real-time qRT-PCR and plaque assay determinations for each sample shown.

Table 5.2. Specific infectivity for Vero cells of rMVEV, NS1-NS2A cleavage site mutants and variants.

Virus	Specific infectivity[1] (genome equivalent/ PFU)
rMVEV	1.3×10^3
rP2-Gly	0.3
rP2-Gly/V1	3×10^3
rP2-Gly/V2	1.3×10^3
rP7,8-Ala	1×10^1
rP7,8-Ala/V1	2.1×10^3
rP7,8-Ala/V2	2.2×10^3

[1] data calculated from Fig. 5.4

5.2.4 Analysis of RNA synthesis of rP2-Gly and rP7,8-Ala variants

To analyze whether the increased growth of the revertants in Vero cells correlated with the repair of the RNA synthesis defect that accounted for the poor growth of the rP2-Gly and rP7,8-Ala mutants, intracellular RNA accumulation for each variants was evaluated by real-time qRT-PCR over a 48 h interval. Vero cell monolayers were infected at MOI of ~1, intracellular RNA was isolated at the indicated time points and real-time qRT-PCR was performed (Fig. 5.5). Similar to wt virus, intracellular virus-specific RNA for both variant pairs accumulated exponentially between 12 and 24 h p.i and reached plateau levels by ~48 h p.i. Albeit with a slightly slower kinetics, intracellular virus-specific RNA in variant infected cells accumulated to levels that were similar in magnitude to that in wt virus infected cells and ~4 log and ~2 log higher than those for rP2-Gly and rP7,8-Ala, respectively. Thus, the result from this experiment clearly illustrates that the growth enhancement observed for the variants is due to an increase in the efficiency of RNA synthesis.

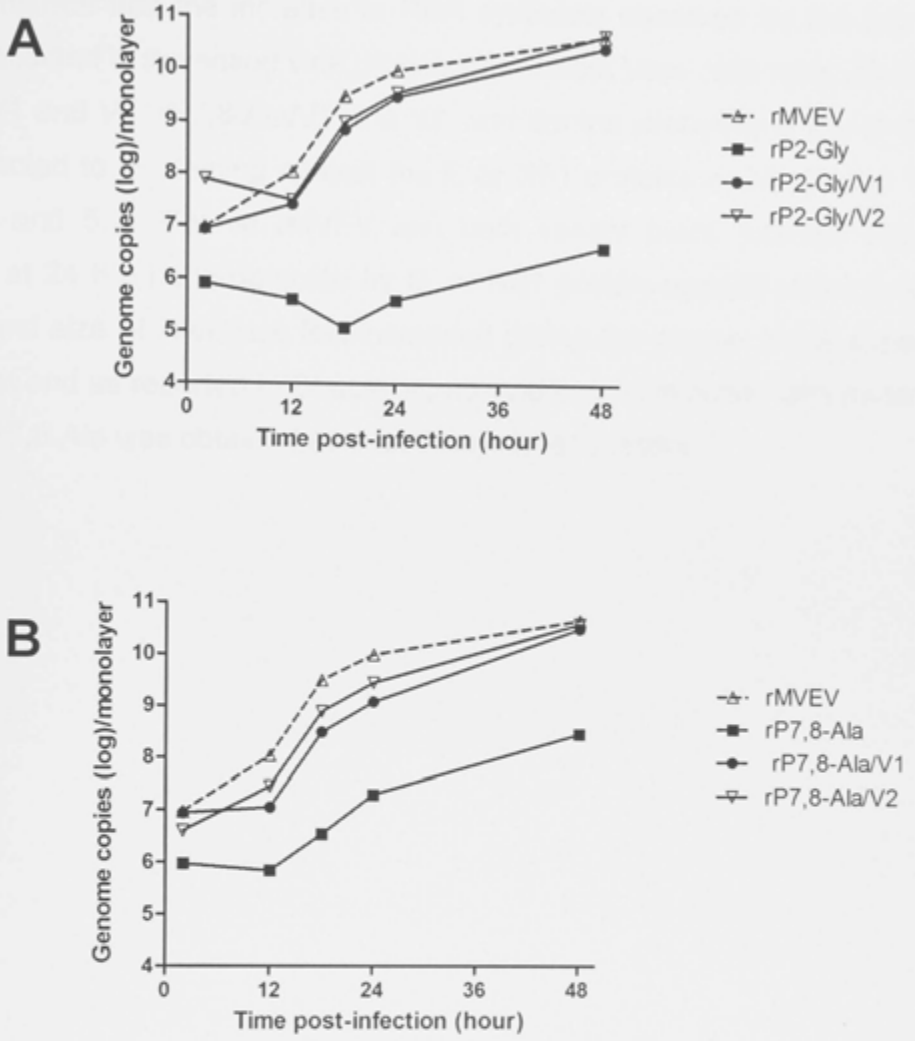

Fig. 5.5. Analysis of virus-specific RNA synthesis in Vero cells.

Vero cells were infected with (A) rMVEV, rP2-Gly, rP2-Gly/V1 or rP2-Gly/V2 or (B) rMVEV, rP7,8-Ala or rP7,8-Ala/V1 or rP7,8-Ala/V2 at a multiplicity of 1. Unbound virus was removed after 1 h of adsorption and growth medium was added. At 2, 12, 18, 24 and 48 h p.i, infected cell monolayers were harvested for total RNA extraction. Virus-specific RNA synthesis was measured by real-time qRT-PCR.

5.2.5 Analysis of MVEV-specific E and NS1 protein synthesis by immunofluorescence staining

To demonstrate that the increase in RNA synthesis observed for the two variant pairs is reflected in increased viral protein expression, Vero cells were infected with rP2-Gly/V1 and V2, rP7,8-Ala/V1 and V2, and control viruses at a low (0.05) MOI and subjected to IF staining against the E or NS1 proteins at 24, 48 and 72 h p.i (Fig. 5.6 and 5.7). For wt rMVEV and both variant pairs, infected cells were apparent at 24 h p.i and detected by E- or NS1 protein-specific staining, and the number and size of infectious foci increased during the course of the experiment. In contrast and as reported in Chapter 4, no evidence of infection with mutants P2-Gly and P7,8-Ala was obtained even at 3 days after infection.

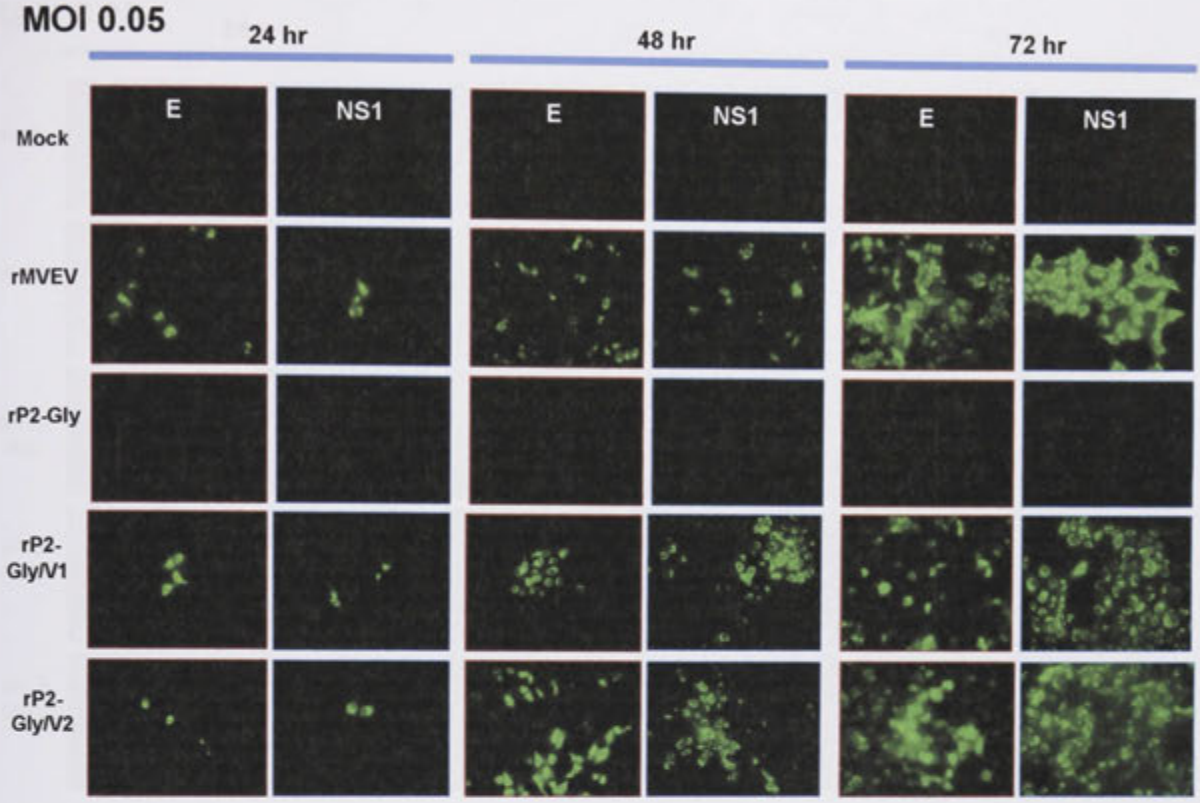

Fig. 5.6. Immunofluorescence analysis of viral E and NS1 protein expressions in Vero cells following low multiplicity of infection.

Vero cells were infected at a multiplicity of 0.05 with rMVEV, rP2-Gly, rP2-Gly/V1, rP2-Gly/V2 or were mock infected as indicated on the left. Viral protein expression was detected after cell permeabilization and indirect IF staining with mAb (8E7 or 4G4) specific for MVEV E and NS1 protein, respectively at 24 to 72 h p.i. The cells were magnified x400.

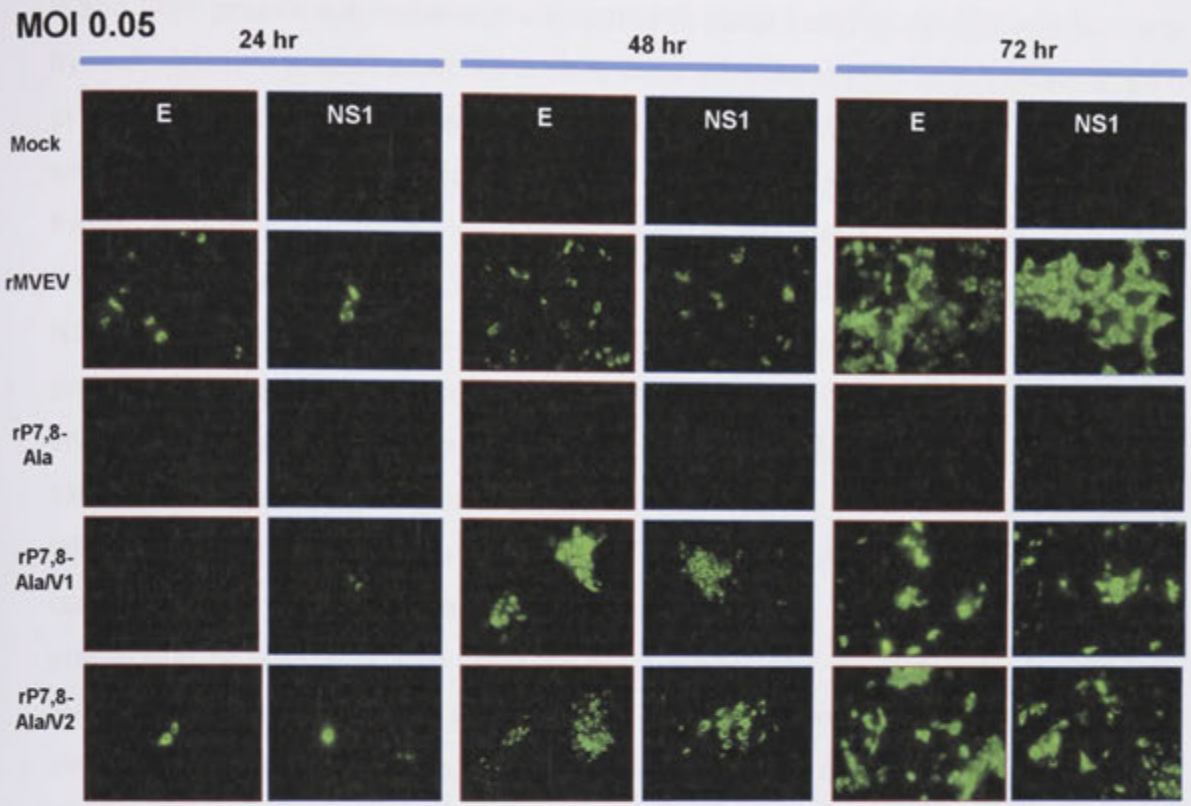

Fig. 5.7. Immunofluorescence analysis of viral E and NS1 protein expressions in Vero cells following low multiplicity of infection.

Vero cells were infected at a multiplicity of 0.05 with rMVEV, rP7,8-Ala, rP7,8-Ala/V1, rP7,8-Ala/V2 or were mock infected as indicated on the left. Viral protein expression was detected after cell permeabilization and indirect IF staining with mAb (8E7 or 4G4) specific for MVEV E and NS1 protein, respectively at 24 to 72 h p.i. The cells were magnified x400.

5.2.6 Investigation of polyprotein processing by radio-immunoprecipitation and Western blotting

E and NS1 protein synthesis was compared in variant and wt rMVEV infected cells by radio-immunoprecipitation. Vero cells were infected at MOI of 5, labeled at 24 h pi with ^{35}S-methione/cysteine for 45 min and chase for 5 min or 3 h. Cell lysates were treated with anti-NS1 or anti-E mAb, and heated and reduced prior to SDS-PAGE. E protein synthesis in rP2-Gly/V1 and V2 infected cells was detected at an equivalent level to that in wt virus infected cells (Fig. 5.8). However, processing of NS1 occurred with a delayed kinetics: thus while for wt rMVEV the amount of NS1 protein recovered by immunoprecipitation was similar after the 5 min and 3 h chase intervals (suggesting rapid polyprotein processing at the corresponding cleavage sites), the amount of mature NS1 protein precipitated from rP2-Gly/V1 and V2 infected cells following the 3 h chase interval was markedly increased in comparison to that after the short chase period (Fig. 5.9). A similar delay in processing of NS1 was also seen for rP7,8-Ala/V1 and V2 (Fig. 5.9). In addition, there was an indication of a somewhat poorer protein synthesis for the latter variants in comparison to the other viruses, reflected in an ~2-fold lower yield of E protein (Fig. 5.8). This observation is consistent with the poorer growth of the rP7,8-Ala-derived variants relative to rP2-Gly/V1 and V2 and wt rMVEV.

Interestingly, I consistently observed additional, higher molecular weight bands in E and NS1 protein-specific immunoprecipitates from rP2-Gly/V1 and V2 infected cell lysates, which were not found in lysates from wt or rP7,8-Ala/V1 and V2 infected Vero cells (Fig. 5.8 and 5.9). Of particular interest is a band of ~100 kDa, which in view of its reactivity with both E and NS1-specific mAbs and size could represent uncleaved E/NS1; the molecular weights of E and NS1 are ~50 and ~48 kDa, respectively.

Western blot analysis on infected cell lysates harvested at 48 h pi detected a difference in the amount of virus-specific protein synthesis between wt and variant viruses, with the following order: wt > rP2-Gly/V1 and V2 >> rP7,8-Ala/V1 and V2 (Fig. 5.10). These differences in protein synthesis efficiencies are consistent with plaque size and growth properties of the different viruses. Furthermore, additional

bands of higher molecular weight than E and NS1/NS1' were also detected by this method in lysates of rP2-Gly/V1 and V2 infected Vero cells using both the E and NS1-specific mAbs. The intensities of these bands of unknown origin differed depending on the antibodies used for blotting but also between the Western blotting and radio-immunoprecipitation procedures. The latter could reflect the increased detection of partial degradation products by Western blotting in comparison to pulse-labelling and radio-immunoprecipitation. Nevertheless, evidence of a putative E/NS1 precursor band was observed in each instance. Analysis with PNGase F treatment showed sensitivity of the ~100 kDa bands towards the treatment, which could be observed by both anti-NS1 and anti-E mAbs staining (data not shown).

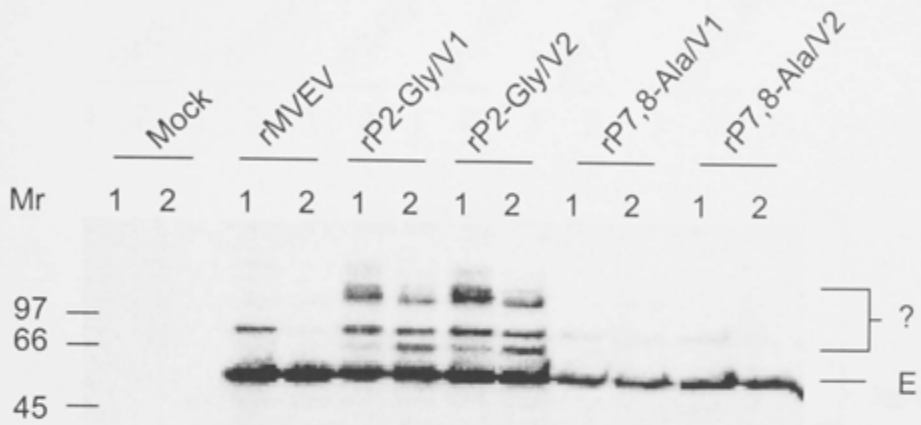

Fig. 5.8. Immunoprecipitation with anti-E mAb of metabolically labelled viral proteins.

Vero cells were mock-infected or infected at MOI of 5 PFU with either rMVEV, rP2-Gly variants or rP7,8-Ala variants. At 24 h p.i, cells were labelled with ^{35}S-methionine for 45 min and chased for (1) 5 min or (2) 3 h and then lysed with RIPA lysis buffer. Lysates were immunoprecipitated with MVEV-specific anti-E protein mAb and analysed with 15% SDS-PAGE as described in Materials and Methods. The positions of molecular weigh marker are indicated on the left (in kDa) and MVEV-specific proteins on the right.

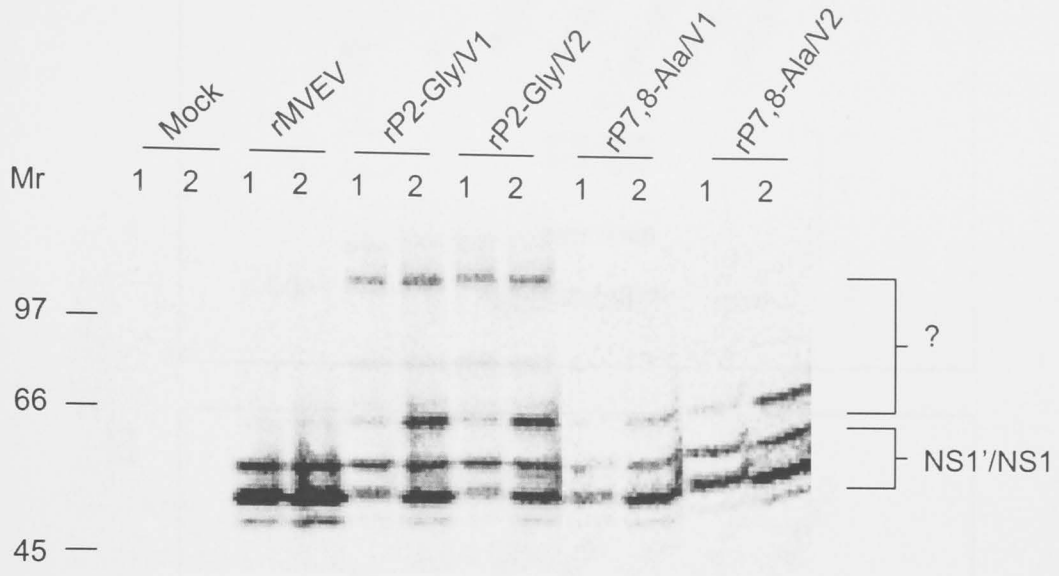

Fig. 5.9. Immunoprecipitation with anti-NS1 mAb of metabolically labelled viral proteins.

Vero cells were mock-infected or infected at MOI of 5 PFU with either rMVEV, rP2-Gly variants or rP7,8-Ala variants. At 24 h p.i, cells were labelled with ^{35}S-methionine for 45 min and chased for (1) 5 min or (2) 3 h and then lysed with RIPA lysis buffer. Lysates were immunoprecipitated with MVEV-specific anti-NS1 protein mAb and analysed with 10% SDS-PAGE as described in Materials and Methods. The positions of molecular weigh marker are indicated on the left (in kDa) and MVEV-specific proteins on the right.

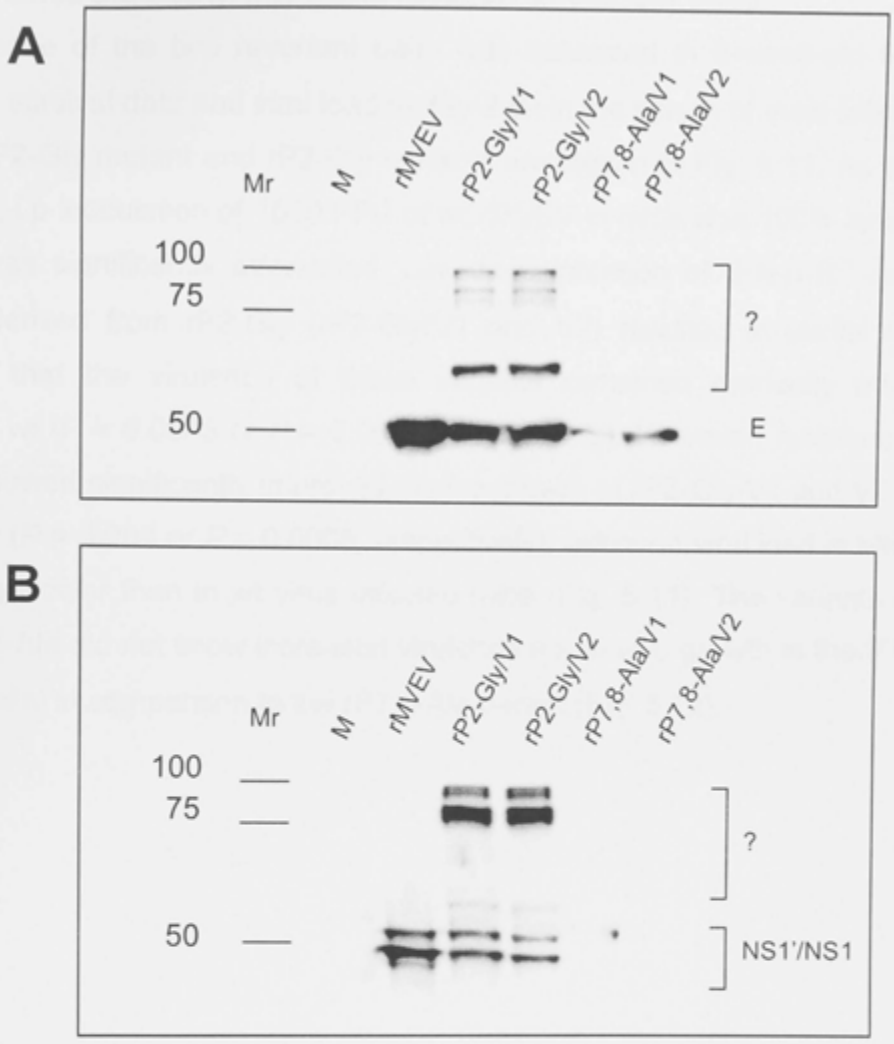

Fig. 5.10. Western blot analysis of rP2-Gly and rP7,8-Ala variants-infected cells lysates.

Vero cells were infected at multiplicity of 5 and analyzed at 48 h p.i. Lysates were heated in reducing sample buffer and proteins were separated on 12% SDS-PAGE. Samples were stained with specific anti-E (A) or NS1 (B) mAbs. The position of E, NS1 and NS1' are marked on the right. The positions of molecular weight marker proteins are indicated on the left (in kDa).

5.2.7 Virulence studies in IFN-alpha receptor knock-out mice

The virulence of the two revertant pairs was assessed in 6-week-old IFN-α-$R^{-/-}$ mice. The survival data and viral load at day 2 p.i in the serum of mice infected with rMVEV, rP2-Gly mutant and rP2-Gly variants are shown in Fig. 5.11. As shown in Chapter 4, i.p inoculation of 1000 PFU of wt rMVEV in mice was 100% lethal, while rP2-Gly was significantly attenuated. Low-dose infection of IFN-α-$R^{-/-}$ mice with variants derived from rP2-Gly (rP2-Gly/V1 and V2) resulted in partial mortality indicating that the virulence of these variants remained markedly attenuated relative to wt (P = 0.0005 or P = 0.0004, respectively). However, measurement of viremia showed significantly improved *in vivo* growth of rP2-Gly/V1 and V2 relative to rP2-Gly (P = 0.003 or P = 0.0005, respectively), although viral load in blood was still ~2 logs lower than in wt virus infected mice (Fig. 5.11). The variants derived from rP7,8-Ala did not show increased virulence nor *in vivo* growth in the IFN-α-$R^{-/-}$ mouse model in comparison to the rP7,8-Ala parent (Fig. 5.12).

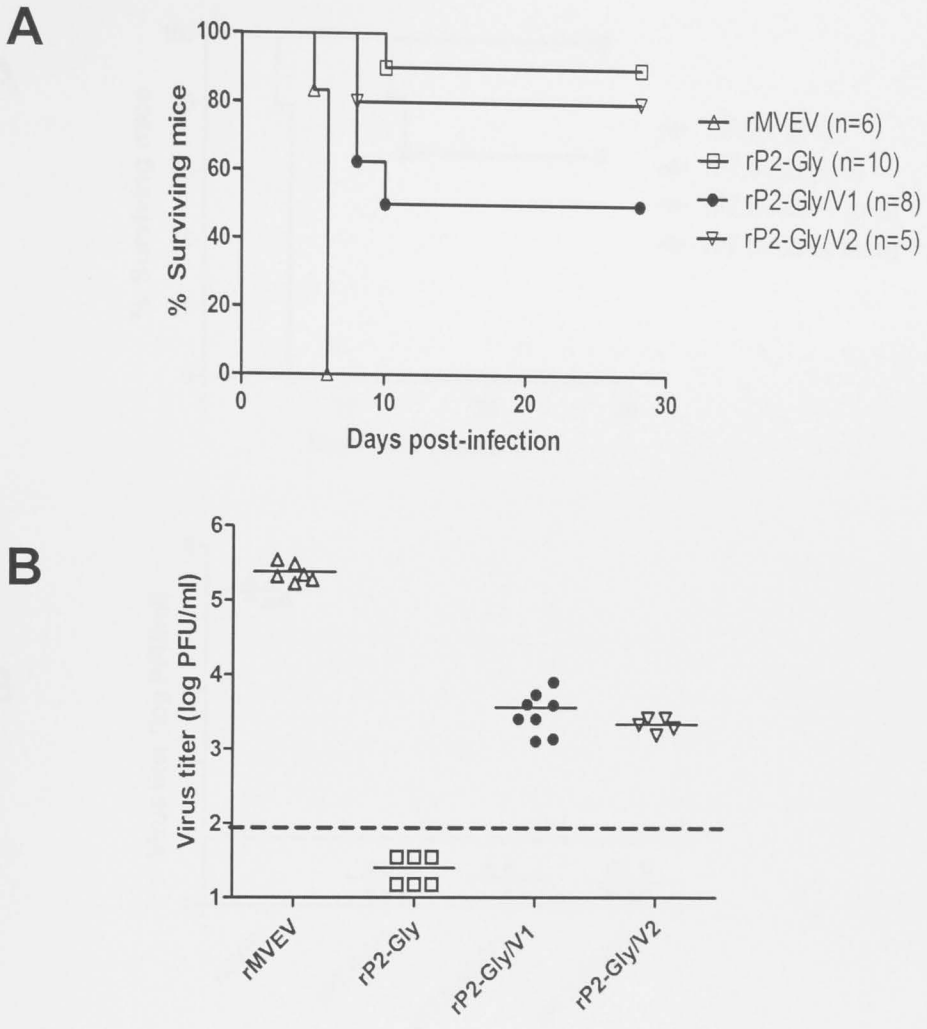

Fig. 5.11. Virulence of rP2-Gly variants in six–week old IFN-α-receptor knockout mice.

(A) Groups of six-week old of IFN-α-R $^{-/-}$ mice were infected intraperitoneally with 1000 PFU of rMVEV, rP2-Gly, rP2-Gly/V1 or rP2-Gly/V2 and morbidity and mortality were recorded daily for a period of 28 days. (B) Sera were collected on day 2 p.i, and frozen at -70 °C. Viremia titers were determined by plaque assay on Vero cells. Each symbol represents an individual mouse and mean titers are indicated by a horizontal line. Interrupted line indicates the plaque assay detection limit. Data for rMVEV and rP2-Gly was accumulated from animal experiments in Chapter 4 and 5.

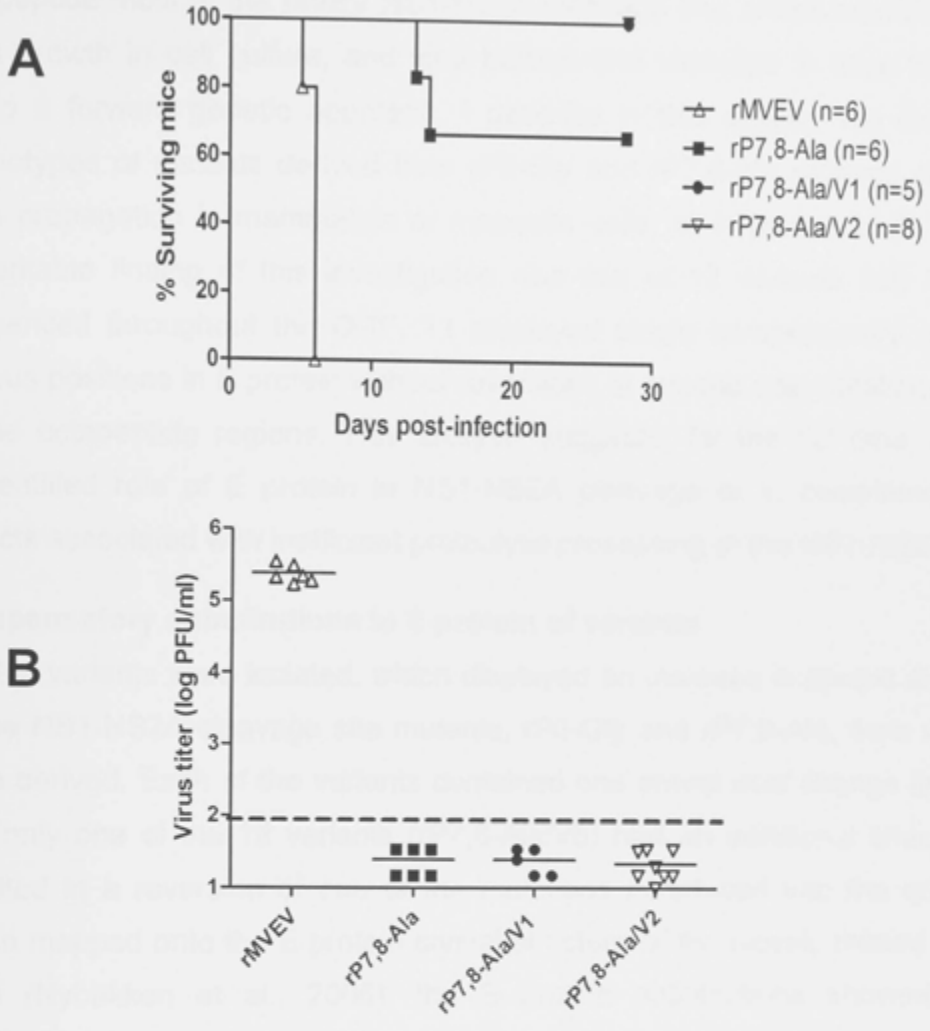

Fig. 5.12. Virulence of rP7,8-Ala variants in six–week old IFN-α-receptor knockout mice

(A) Groups of six-week old of IFN-α-R $^{-/-}$ mice were infected intraperitoneally with 1000 PFU of rMVEV, rP7,8-Ala, rP7,8-Ala/V1 or rP7,8-Ala/V2 and morbidity and mortality were recorded daily for a period of 28 days. (B) Sera were collected on day 2 p.i and frozen at -70 °C. Viremia titers were determined by plaque assay on Vero cells. Each symbol represents an individual mouse and mean titers are indicated by a horizontal line. Interrupted line indicates the plaque assay detection limit. Data for rMVEV and rP7,8-Ala was accumulated from animal experiments in Chapter 4 and 5.

5.3 Discussion

I have previously identified amino acid substitutions at P2 and P7/8 in the octapeptide motif at the MVEV NS1-NS2A cleavage site, which markedly reduced virus growth in cell culture, and viral burden and virulence in mice (Chapter 4). Using a forward genetic approach, I describe in this chapter the isolation and phenotypes of variants derived from rP2-Gly and rP7,8-Ala mutants obtained by virus propagation in mammalian or mosquito cells, or in mouse brain. The most remarkable finding of this investigation was that of 12 variants fully or partially sequenced throughout the ORF, 11 displayed single compensatory changes at various positions in E protein without reversions or second-site-mutations identified in the octapeptide regions. This analysis suggests, for the fist time, an as-yet-unidentified role of E protein in NS1-NS2A cleavage or in complementation of defects associated with inefficient proteolytic processing at the NS1-NS2A junction.

Compensatory substitutions in E protein of variants

Twelve variants were isolated, which displayed an increase in plaque size relative to the NS1-NS2A cleavage site mutants, rP2-Gly and rP7,8-Ala, from which they were derived. Each of the variants contained one amino acid change in E protein and only one of the 12 variants (rP7,8-Ala/V6) had an additional change, which resulted in a reversion of one of the mutations introduced into the octapeptide. When mapped onto the E protein crystal structure of the closely related West Nile virus (Nybakken et al., 2006), the E protein substitutions showed a broad distribution on domain I (residue 176), domain II (residues 59, 61, 65, 91 and 242) and domain III (residues 339 and 340) (Fig. 5.13). However, the two substitutions identified for the variants derived from the rP2-Gly mutant (Y59H and V65A) are located in relatively close proximity on either side of a disulfide bond, encompassed by the so-called surface exposed "a and b strands" of domain II (Nybakken et al., 2006). Given that these two changes elicited the strongest phenotypes in terms of enhancement of virus growth, this E protein region is of particular interest. Notably, three other changes identified for variants derived from the rP7,8-Ala mutant also mapped to the "a strand" (Y61C) or to neighboring strands (L91S and F242I), thus collectively forming a cluster of changes on domain II. While residue 242 is highly conserved, residues 59, 61, 65 and 91 show

similarity among flaviviruses (Fig. 5.14). Each of the changes found at these 5 domain II residues resulted in alteration of size or electrostatic properties of the amino acid side chains. A single nonconservative change (Ile to Asn) was identified at domain I residue, 176, which is variable among the flaviviruses and known to play a role in virulence attenuation of Japanese encephalitis virus vaccine strain, 14-14-2 (Arroyo et al., 2001). The two domain III substitutions (P339S and I340M) identified in the E proteins of variants rP7,8-Ala/V2 and V5 mapped to neighboring residues on the surface-exposed "C strand" (Nybakken et al., 2006). Pro_{339} is highly conserved, while Ile_{340} shows similarity among flaviviruses. These structural data identify candidate regions and residues in the E protein involved in complementation of the defect(s) in virus replication caused by mutations introduced at the NS1-NS2A cleavage site; nevertheless, it remains unclear by what mechanism the altered E protein of the variants accomplish this partial repair of the defect(s) that account for the poor growth of the cleavage site mutants.

Fig. 5.13. Summary of compensatory mutations in the MVEV E protein on a plane view, three-dimensional representation of the WNV E protein.

Location of amino acid changes occurred on rP2-Gly and rP7,8-Ala variants are mapped on the WNV E protein structure (Nybakken et al., 2006). Mutations with rP2-Gly background are labeled in blue and for rP7,8-Ala background are labeled in green. Dots indicate the locations of amino acids which were altered in the rP2-Gly and rP7,8-Ala variants. Numbers in the bottom of the structure indicate the domains of monomeric E protein.

```
                59 61  65
MVEV        LALVRNYCYAATVSDVSTV
JEV         LAEVRSYCYHASVTDISTV
KUNV        LAEVRSYCYLATVSELSTK
WNV         LADVRSYCYLASVSDLSTR
DENV-1      PAVLRKLCIEAKISNTTTD
DENV-2      PATLRKYCIEAKLTNTTTE
DENV-3      LATLRKLCIEGKITNITTD
DENV-4      VALLRTYCIEASISNITTA
YFV         PAEARKVCYNAVLTHVKIN
TBEV        PAKTREYCLHAKLSDTKVA

                91                      176
MVEV        RADHNYLCKRGVT           SPNAPAITAKMGDY
JEV         RADSSYVCKQGFT           TPNAPSITLKLGDY
KUNV        RADPSFVCKQGVV           TPAAPSYTLKLGEY
WNV         RADPAFVCKQGVV           TPSAPSYTLKLGEY
DENV-1      EQDTNFVCRRTFV           TPQAPTSEIQLTDY
DENV-2      EQDKRFVCKHSMV           TPQASTTEAILPEY
DENV-3      EQDQNYVCKHTYV           TPQSSITEAELTGY
DENV-4      EQDQQYICRRDVV           TPRSPSVEVKLPDY
YFV         ENEGDNACKRTYS           DALSGSQEAEFTGY
TBEV        EHQGGTVCKRDQS           TISSEKTILTMGEY

                242                     339/340
MVE         REILVEFEEPHAT           DGPCKIPISSVASLN
JEV         RELLMEFEEAHAT           DGPCKIPIVSVASLN
KUNV        RETLMEFEEPHAT           DGPCKIPISSVASLN
WNV         RETLMEFEEPHAT           DGPCKVPISSVASLN
DENV-1      QDLLVTFKTAHAK           DAPCKIPFSSQ-DEK
DENV-2      KETLVTFKNPHAK           GSPCKIPFEIM-DLE
DENV-3      KELLVTFKNAHAK           DAPCKIPFSTE-DGQ
DENV-4      KERMVTFKVPHAK           GAPCKVPIEIR-DVN
YFV         MHHLVEFEPPHAA           GAPCKIPVIVADDLT
TBEV        AERLVEFGAPHAV           -KPCRIPVRAVAHGS
```

Fig. 5.14. E protein sequence alignments of 10 flaviviruses. E protein sequences are aligned to MVEV sequence surrounding residues 59, 61, 65, 91, 176, 242, 339 and 340. Deletions in the sequence are represented by a dash (-). Sequence information is obtained from GenBank with accession number of NC_000943 (MVEV), NC_001437 (JEV), D00246 (KUNV), NC_001563 (WNV), NC_001477 (DENV-1), NC_001474 (DENV-2), NC_001475 (DENV-3), NC_002640 (DENV-4), NC_ 002031 (YFV) and NC_001672 (TBEV).

Effect of compensatory mutation in E on virus growth of NS1-NS2A cleavage site variants

In the previous chapter, I have shown that the deficiency in NS1-NS2A cleavage strongly correlated with inefficient virus growth and small plaque size. Therefore, variants were selected by the criterion of an increase in plaque size in comparison to the corresponding rP2-Gly and rP7,8-Ala mutants, with the assumption that this would select for viruses with improved growth properties. This was found to be the case: each of four variants characterized demonstrated markedly enhanced growth in Vero cells relative to the respective mutants. Interestingly, there appeared to be an inverse correlation of growth efficiency (and cleavage efficiency of NS1 and NS2A) of the mutant viruses and that of the variants derived thereof: propagation in Vero cells of the mutant (rP2-Gly), which showed poorest growth, resulted in appearance of plaque size variants producing larger plaques and better growth than that of the less defective mutant (rP7,8-Ala). This finding was surprising, given the expectation that compensatory mutations should be more effective in repairing the phenotype of the less defective than that of the more defective mutant. It remains unclear, if the number of mutations introduced at the NS1-NS2A cleavage site (one and two changes in case of rP2-Gly and rP7,8-Ala) impacts on the level by which single compensatory changes in E protein can complement the defective phenotypes of the mutants.

It could be envisioned that the substitutions in E proteins selected for in the variants derived from the NS1-NS2A cleavage site mutants complement the growth-defective phenotype of the mutants by a mechanism that involves enhancement of a process in virus replication unrelated to that which is affected by the introduction of the mutations at the NS1-NS2A cleavage site. For instance, it has been observed in the case of influenza virus that antibody escape variants arise by selection of mutations, which involve an unrelated stage of the virus life cycle, viz. receptor-binding avidity (Hensley et al., 2009). Thus, the compensatory changes in E protein could increase the efficiency of various events critical in virus replication, such as assembly, fusion and host cell receptor-binding, which are known to be influenced by mutations in E protein (Arroyo et al., 2001; Chambers et al., 1998; Chen et al., 2003; Lee et al., 2004; Lee et al., 2010; Lee and Lobigs,

2002; Lobigs et al., 2010; Yi et al., 2007), without impacting on NS1-NS2A cleavage. However, this does not seem to be the case: a defect in viral RNA synthesis, which accounts for the poor growth of the mutant viruses, was substantially repaired in the variants, most likely as a result of mutations at single residues in E protein. This is convincingly illustrated by comparison of intracellular accumulation of viral RNA in cells infected with wt, rP2-Gly mutant and variants derived thereof, which showed that a 3 to 4 log difference in intracellular accumulation of viral RNA found between mutant and wt was largely complemented by the altered structure of E protein of the variant viruses. This resulted, in turn, in markedly enhanced viral protein synthesis in variant relative to mutant virus infected cells.

Intriguingly, an investigation of protein synthesis for the variants, rP2-Gly/V1 and V2 by radio-immunoprecipitation and Western blotting revealed additional protein bands, which were not detected in wt or rP2-Gly mutant virus infected cells. These bands showed reactivity to both anti-E and anti-NS1 mAbs and included an ~100 kDa polypeptide, which was consistent in size with that predicted for an uncleaved E-NS1 precursor product. Blitvich et al. (1995) have reported that the MVEV E and NS1 proteins can interact to form a heterodimer, which dissociates when exposed to reduction and heat-treatment, while the ~100 kDa polypeptide described here did not dissociate when boiled and treated with reducing agent. It remains unclear, whether E/NS1 heterodimerisation has a physiological function in flavivirus replication; it is well established that most of nascent E protein heterodimerizes with the prM protein to initiate assembly of the virus particle (Li et al., 2008; Lin and Wu, 2005; Lorenz et al., 2002; Lorenz et al., 2003; Markoff et al., 1994; Op De Beeck et al., 2004; Yu et al., 2008), and that most of nascent NS1 protein forms homodimers and hexamers, which are retained intracellularly or secreted, respectively (Crooks et al., 1994; Flamand et al., 1999; Macdonald et al., 2005; Mason, 1989; Parrish et al., 1991; Winkler et al., 1989; Winkler et al., 1988). Nevertheless, the observation that protein-protein interaction can occur between E and NS1 supports the possibility that the E protein may have some modulating influence on NS1-NS2A cleavage, which could be enhanced by the compensatory changes in E protein that were identified for the variants derived from the NS1-

NS2A cleavage site mutants. The question remains why the putative E-NS1 precursor found in rP2-Gly/V1 and V2 infected cells failed to be cleaved by signal peptidase, and whether this also impinges on down-stream processing at the NS1-NS2A junction encompassing a mutated octapeptide motif. Given that the E-NS1 and NS1-NS2A cleavages may be catalyzed by the same enzyme, viz. signal peptidase, it is tempting to speculate that the compensatory mutations in the variant E proteins reduce accessibility of the E-NS1 site, thereby increasing preference of the enzyme to catalyze the down-stream cleavage.

It should be noted that partial processing at the NS1-NS2A junction is most likely sufficient to generate the required amounts of non-structural proteins in order to effectively restore virus growth in cell culture and that a significant level of wastage of viral gene products is tolerated without markedly reducing virus growth (Lobigs et al., 2010). This seems to be the case for the variants derived from the NS1-NS2A cleavage site mutant viruses, which showed for instance a delay in production of NS1 protein in comparison to wt rMVEV. Thus, the compensatory changes in E protein clearly did not restore the fitness level of the variants to that of wt virus. This was convincingly illustrated in a mouse model for flaviviral encephalitis, where growth of the variants remained substantially poorer than that of wt, or even undetectable.

CHAPTER 6

Confirmation of complementation of a deleterious mutation at the NS1-NS2A cleavage site by a single amino acid change in E protein

6.1 Introduction

The genotypic and phenotypic analysis of variants derived from NS1-NS2A cleavage site mutants, rP2-Gly and rP7,8-Ala, undertaken in the previous chapter strongly suggested that single amino acid changes in E protein repaired, at least in part, the growth defect associated with a deficiency in proteolytic processing at the NS1-NS2A junction. While the nucleotide sequence of the entire ORF of several variants was determined and revealed in 11 out of 12 variants only single amino acid substitutions in E protein in addition the originally introduced octapeptide mutations, it was important to directly confirm the exclusive compensatory effect of E protein substitutions when introduced into the genome of a growth-defective octapeptide mutant virus. This constitutes the aim of the work described in this chapter: thus, the E protein V65A mutation identified in 4 large-plaque isolates derived from the rP2-Gly mutant was introduced into an infectious cDNA clone of MVEV in the presence or absence of the P2-Gly mutation at the NS1-NS2A cleavage site. This combination of changes was selected in view of the strong phenotypes associated with the P2-Gly mutation and the compensatory V65A change in E protein of the variants.

6.2 Results

6.2.1 Construction of full-length MVEV cDNA clones encompassing an E protein V65A mutation on wt and P2-Gly background

To determine whether the V65A mutation in E protein compensates for the deleterious impact on virus growth of the P2-Gly mutation at NS1-NS2A cleavage site and to evaluate the impact of the V65A change on growth phenotype of wt virus, the V65A mutation was introduced into MVEV full-length cDNA clones either individually (rV65A^{Env}) or combined with the P2-Gly mutation at the NS1-NS2A cleavage site (rP2-Gly.V65A^{Env}). To generate these constructs, a 1950 bp PCR fragment encompassing the V65A mutation was amplified from rP2-Gly/V2 cDNA using the primer pair, C #1 and E #6 (Table. 2.4). A 1250 bp *SnaB*I–*Xba*I fragment was excised from the PCR product and ligated into plasmids, pMVEV or pP2-Gly, replacing the corresponding E region (Fig. 4.1).

6.2.2 Recovery of infectious clone-derived viruses

When the E and NS1-NS2A cleavage site mutations were introduced simultaneously into an MVEV full-length infectious clone and electroporation of *in vitro* synthesised RNA was performed, rP2-Gly.V65A^{Env} exhibited a plaque size of 3-4 mm, which was similar to that of variant, rP2-Gly/V2, and wt rMVEV (Table 6.1), suggesting rescue of the growth defect caused by the P2-Gly mutation. Intriguingly, rV65A^{Env} consistently displayed a plaque phenotype, which was slightly larger than that of wt (4 – 5 mm). RNA from the recovered viruses was sequenced in the E and NS1-NS2A gene regions and the presence of the introduced mutations was confirmed.

6.2.3 A mutation in E protein rescues the defect in virus growth caused by the P2-Gly mutation at the NS1-NS2A cleavage site

Growth in Vero cells of rP2-Gly.V65A^{Env} was compared to that of the wt rMVEV, NS1-NS2A cleavage site mutant, rP2-Gly, variant rP2-Gly/V2 and E protein mutant, rV65A^{Env}. Cells were infected at a multiplicity of ~0.1 and extracellular virus titers of growth samples were determined by plaque assay on Vero cells. As shown in Fig. 6.1, growth of rP2-Gly.V65A^{Env} was comparable to that of rP2-Gly/V2 during the 60 h time interval, while growth of rV65A^{Env} was similar to that of the wt, except for a ~8-fold lower titer for rV65A^{Env} at 16 h p.i. As expected, growth of rP2-Gly was markedly poorer that that of the other viruses. Accordingly, it can be concluded that the V65A change in E protein complements, at least in part, the growth defect caused by the P2-Gly mutation at the NS1-NS2A cleavage site.

Table 6.1. Plaque size of rMVEV, rP2-Gly/V2, rP2-Gly.E65V^{Env} and rV65A viruses

Virus	Plaque size[1]
rMVEV	3-4 mm
rP2-Gly	≤ 1 mm
rP2-Gly/V2	3-4 mm
rP2-Gly.V65^{Env}	3-4 mm
rV65A^{Env}	4-5 mm

[1]Plaque morphology on Vero cells stained with 0.02% neutral red on day 4 p.i and recorded the following day are given.

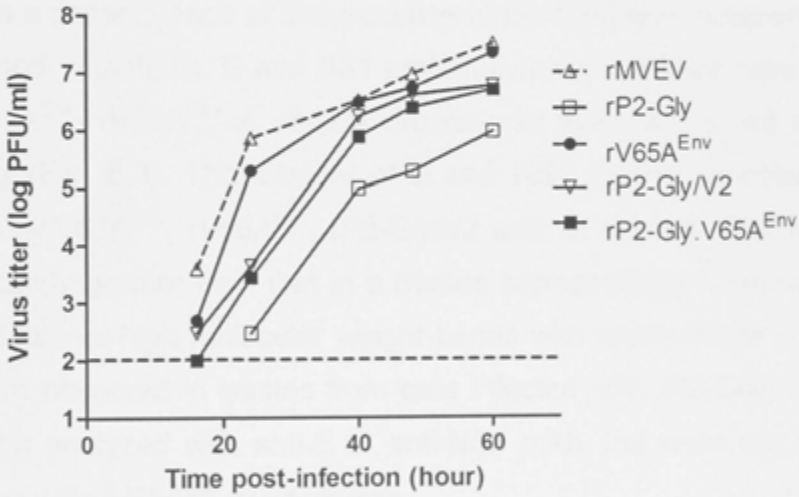

Fig. 6.1. Growth kinetics of wt rMVEV, rP2-Gly, rV65A^{Env}, rP2-Gly/V2 and rP2-Gly.V65A^{Env} on Vero cells.

Vero cell monolayers were infected with rMVEV, rP2-Gly, rV65A^{Env}, rP2-Gly/V2 and infectious clone derived rP2-Gly.V65A^{Env} at multiplicity of ~0.1. Culture medium was collected at the indicated time points and virus titers in growth samples were measured by plaque assay on Vero cells. Interrupted line indicated detection limit of virus yield by plaque assay.

6.2.4 Analysis of rP2-Gly.V65A^{Env} protein synthesis

To provide evidence that the comparable growth of infectious clone-derived rP2-Gly.V65A^{Env} and variant rP2-Gly/V2 is a consequence of partial restoration of virus macromolecular synthesis, the presence of virus antigen in infected Vero cells was analysed by flow-cytometry. Vero cells were infected at MOI ~0.5 and the percentage of infected cells was determined at 18 h p.i, based on the presence of NS1 antigen measured by flow-cytometry (Fig. 6.2). While, as previously shown, infection with rP2-Gly did not result in accumulation of detectable levels of NS1 protein in infected cells, infection with rP2-Gly.V65A^{Env} and control viruses showed efficient production of NS1.

In the previous chapter I presented evidence suggesting that the combination of the P2-Gly mutation and compensatory changes in E protein domain II yielded a polyprotein cleavage intermediate consistent with that of uncleaved E-NS1. To test whether this was a consequence of the presence of the E protein mutations, or the combination of both mutations, E and NS1 protein synthesis in Vero cells infected with rP2-Gly.V65A^{Env}, rV65A^{Env} or control viruses was evaluated at 48 h p.i by Western blotting (Fig. 6.3). The amount of E and NS1 protein detected in cell lysates for rP2-Gly.V65A^{Env}, rV65A^{Env}, rP2-Gly/V2 and wt did not differ markedly and was significantly greater than that in a lysates corresponding to mutant, rP2-Gly. Notably, additional high molecular weight bands with approximate size of 63 and 100kDa were observed in lysates from cells infected with rP2-Gly/V2 or rP2-Gly.V65A^{Env} when analyzed with anti-E or anti-NS1 mAb, but were not detected following infection with rV65A^{Env} or wt viruses.

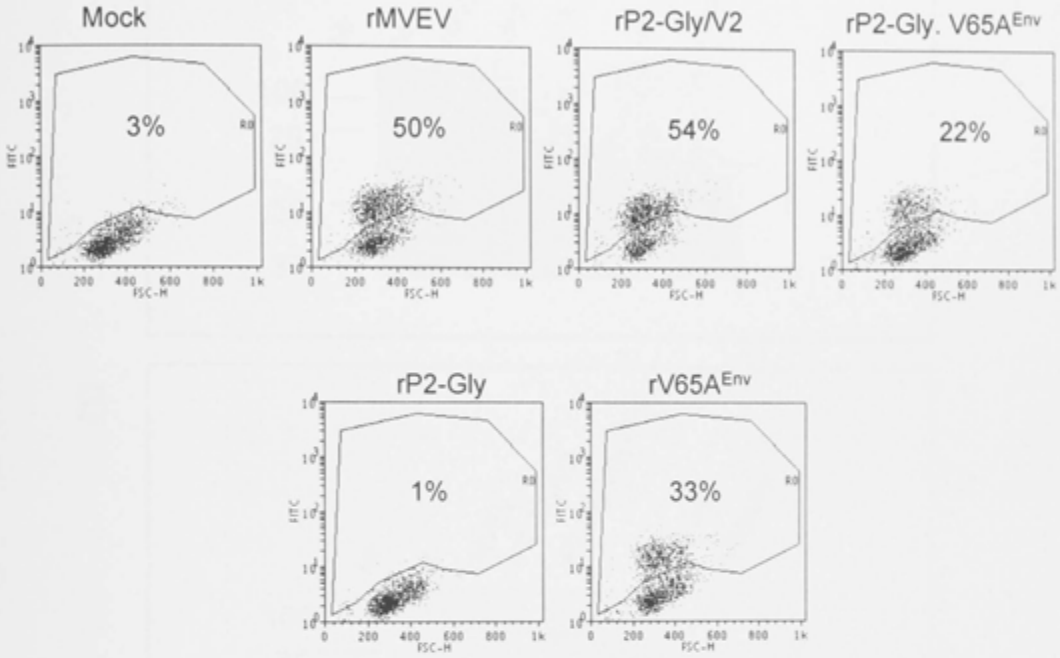

Fig. 6.2. FACS analysis for determination of the percentage of Vero cells infected with rMVEV, rP2-Gly/V2, rP2-Gly. V65A^{Env}, rP2-Gly and rV65A^{Env} for growth phenotype comparison.

Vero cell monolayers were infected at a multiplicity of 0.2 to 0.5 or left untreated. The cells were harvested at 18 h p.i, and stained with an anti-NS1 mAb and FITC-conjugated anti-mouse IgG. Cells gated within region R0 represent the percentages of NS1-positive cells.

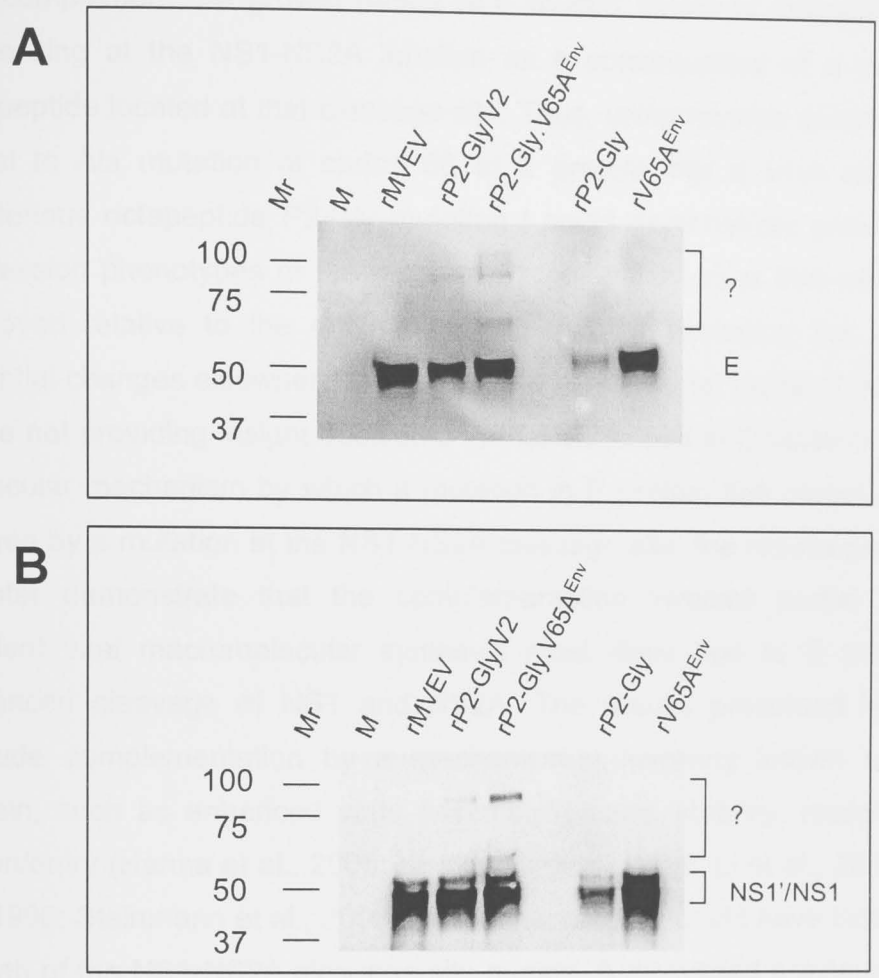

Fig. 6.3. Western blot analysis of E and NS1 protein.

Vero cells were mock-infected (M) or infected at MOI of 5 with either wt rMVEV, rP2-Gly/V2, rP2-Gly or rV65A^{Env}. Cells were lysed at 48 h p.i, subjected to Western blot analysis and viral proteins were detected using specific anti-E (A) or anti-NS1 (B) mAbs. The positions of E and NS1 are indicated on the right. The positions of molecular weigh marker proteins (in kDa) are indicated on the left.

6.3 Discussion

In this chapter, I provide conclusive evidence that a defined change in the E protein can complement the growth defect of a mutant flavivirus deficient in proteolytic processing at the NS1-NS2A junction as a consequence of a mutation in the octapeptide located at that cleavage site. Thus, using reverse genetics to engineer a Val to Ala mutation at codon 65 of E protein into a virus also encoding a deleterious octapeptide P2-Gly mutation I could demonstrate growth and protein expression phenotypes of the recovered recombinant virus that were significantly improved relative to the original mutant, thereby excluding the contribution of potential changes elsewhere in the genome in the partial repair of the phenotypes. While not providing insight additional to that discussed in Chapter 5 relating to the molecular mechanism by which a mutation in E protein can complement a defect caused by a mutation at the NS1-NS2A cleavage site, the results presented in this chapter demonstrate that the complementation involves partial restoration of efficient viral macromolecular synthesis most likely due to E protein-mediated enhanced cleavage of NS1 and NS2A. The results presented in this chapter exclude complementation by a mechanism(s) involving known functions of E protein, such as enhanced virus assembly/release, stability, receptor-binding, or fusion/entry (Hanna et al., 2005; Khromykh et al., 1998; Li et al., 2006; Schalich et al., 1996; Steinmann et al., 2008), which theoretically could have indirectly rescued growth of the NS1-NS2A cleavage site mutant. A discussed previously, the impact of the V65A substitution in E protein on processing at the NS1-NS2A junction most likely occurs via a heterodimeric interaction of E with NS1, which has been observed by others (Blitvich et al., 1995), but for which my results of Chapters 5 and 6 of this thesis, for the first time, show a putative physiological role with significant effect on virus replication.

A second critical finding from the work presented in this chapter was the demonstration that the V65A substitution in E protein did not alter the kinetics and/or efficiency of proteolytic processing at the E-NS1 junction when present in the absence of the P2-Gly mutation in the octapeptide. Thus it appears that

detectable production of the putative E-NS1 precursor protein requires inefficient processing of NS1 and NS2A in addition to the mutation in domain II of E.

CHAPTER 7

Concluding remarks

7.1 Key observations from this PhD study

Studies on the flavivirus life cycle in the past two decades have shown that viral gene expression involves RNA translation into a single polyprotein, which is cleaved into the mature viral proteins by host proteases and the virally encoded NS2B-NS3 protease (Cahour et al., 1992; Chambers et al., 1989; Falgout et al., 1991; Markoff, 1989; Speight et al., 1988). However, despite the advances in the knowledge of flavivirus proteolytic processing, the cleavage events that lead to the generation of the two non-structural proteins, NS1 and NS2A remain elusive.

Thus, this study was set out to understand the requirements for efficient NS1-NS2A proteolytic cleavage in MVEV. In this thesis, I have focussed my investigations on the role of the octapeptide motif at the C-terminus of NS1 in the processing of NS1-NS2A protein. The studies presented in this thesis provide compelling evidence that the efficiency of NS1-NS2A cleavage tightly controls viral replication, growth in mammalian/insect cells and virulence in mice.

The study was initiated by investigating the significance of single and multiple amino acid residues in the octapeptide motif by a site-directed mutagenesis approach and transient protein expression (Chapter 3). From the overall analysis of 42 mutants, I have described the relationship between amino acid substitutions at the octapeptide motif and the efficiency of NS1-NS2A cleavage. The size and the electrostatic properties of each residue relative to its position in the cleavage site significantly impacted on the processing of NS1-NS2A. It was also observed that the NS1' production is independent of the authentic NS1-NS2A cleavage, and irrespective of the mutation at the octapeptide region NS1' protein was always expressed. This study also revalidated the requirement of ~2/3 of NS2A for efficient NS1-NS2A processing, although the mechanistic explanation for this intricate prerequisite remains unclear. To my best knowledge, this is the first study to reinvestigate the NS1-NS2A proteolytic processing in an encephalitic flavivirus model. In general, the present studies on MVEV NS1-NS2A cleavage is in overall agreement with the proposed 'octapeptide rules' in DENV although several virus-specific differences were noted. Mutations at the conserved residues in the

octapeptide generally resulted in reduced cleavage, although some exceptions were observed. On the contrary, significant NS1-NS2A cleavage inhibition was observed for mutants with substitution in the non-conserved residue (P2), regardless of variability of amino acids that could occupy this position. Collectively, comparative analysis between MVEV and DENV suggests that the octapeptide motif functions as a module rather than a specific determinant for NS1-NS2A cleavage that can accommodate virus-specific differences in the octapeptide region.

The previous NS1-NS2A cleavage studies by Falgout et al., (1989), Falgout and Markoff (1995), Hori and Lai (1990) and Pethel et al., (1992) are only limited to transient protein expression. These studies demonstrated the requirements of three major prerequisites for NS1-NS2A cleavage: (i) the NH_2-terminal NS1 signal sequence (ii) the octapeptide motif and (iii) ~70% of NS2A. However these studies did not further define whether the observation gained from subgenomic expression experiments could be directly translated to viral infections in cell culture and animal hosts. Thus, to investigate the physiological role of the octapeptide motif in virus replication, MVEV containing four different mutations in the octapeptide motif (P2-Gly, P3-Gly, P8-Ala and P7,8-Ala) were engineered by making use of a reverse genetics approach (Chapter 4). Using this methodology a direct relationship can be established between the introduced mutation in the octapeptide motif and the observed phenotype. Demonstrated in these investigations is the relationship between NS1-NS2A cleavage and viral replication. An excellent correlation was observed between the NS1-NS2A cleavage efficiency in transient protein expression experiments and growth of mutant viruses in mammalian and insect cells. Intriguingly, despite the high conservation of the positions P3 and P8 in the octapeptide, MVEV having mutations in these positions (Val to Gly at P3 and Leu to Ala at P8) did not show significant alteration in growth properties. Although these substitutions did not affect the virus growth in the cell culture, significantly lower viremia was observed in mice infected with these mutants relative to the mice infected with wt virus. This may suggest an insensitivity of the cell culture system, which may allow a significant level of wastage of viral gene products that may not

be the case during natural transmission of flaviviruses. Additionally, I also observed that the MVEV specific infectivity (infectious virus particle to PFU ratio) is directly linked to cleavage efficiency at the NS1-NS2A junction, and the downstream impact on viral macromolecular synthesis and virus growth.

The structural proteins of flaviviruses have been shown to facilitate virus entry via receptor-mediated endocytosis, fusion/release of viral RNA into the cytoplasm, assembly of virion components and virulence in mice (Chambers et al., 1998; Halevy et al., 1994; Hanna et al., 2005; Kawano et al., 1993; Lee et al., 2004; Lee et al., 2010; Lee and Lobigs, 2000, 2002, 2008; Nybakken et al., 2006; Tassaneetrithep et al., 2003; Zhang et al., 2004). However, direct protein-protein interaction between structural-non-structural proteins during NS1-NS2A polyprotein cleavage, so far, has never been experimentally identified. Using the forward genetic approach, 12 variants with revertant phenotypes were isolated from the NS1-NS2A cleavage defective mutants with rP2-Gly or rP7,8-Ala background (Chapter 5). The most remarkable finding of this investigation was that out of 12 variants, 11 displayed single compensatory changes at various positions in E protein without reversions or second-site-mutations in the octapeptide regions. Intriguingly, the growth deficiencies of the NS1-NS2A cleavage site mutants were substantially repaired by second-site compensatory mutations in E protein. This study proposes for the first time an as-yet-unidentified role of E protein in NS1-NS2A cleavage or in complementation of defects associated with inefficient proteolytic processing at the NS1-NS2A junction. In support of this proposition, a putative E-NS1 precursor was observed in rP2-Gly variant infected cells. This observation clearly demonstrates a protein-protein interaction between E and NS1, supporting the possibility that the E protein may have some modulating influence on NS1-NS2A cleavage although this interaction did not directly restore the fitness level of the variants to that of the wt. The E substitution (V65A) alone did not result in the production of E-NS1 precursor when present in the absence of P2-Gly mutation, which illustrates that the putative E-NS1 precursor protein formation is a consequence of inefficient processing of NS1 and NS2A in addition to the mutation in domain II of E protein. Finally, the analysis in Chapter 6 provides conclusive

experimental evidence that a specific change in E protein (V65A) can complement the growth defect of a flavivirus deficient in proteolytic processing at the NS1-NS2A junction as a result of a mutation in the octapeptide motif, using our infectious clone technology.

While the mechanism of cleavage at NS1-NS2A junction and topology of NS2A is currently unclear (Falgout and Markoff, 1995), it could be postulated that the E-NS1 and NS1-NS2A cleavages are catalysed by the same host protease. In the cleavage scenario of the variant viruses with mutations in E and the octapeptide, the mutations could result in suboptimal cleavage at E-NS1 region in order to allow improved accessibility of the protease to cleave at NS1-NS2A junction. However, such a model awaits rigorous examination to show direct or indirect physical interaction among the proteins. Motifs responsible for the complementation of the defect in NS1-NS2A cleavage have been localized to the E protein and further studies with E protein *trans* complementation in conjunction with mutations at the octapeptide motif may define a protein-protein interaction, which might also rescue the defect in the NS1-NS2A cleavage site mutants without covalent interaction of E and NS1.

The data obtained during the course of this project have led to new insights into the process of flavivirus NS1-NS2A polyprotein processing by means of forward and reverse genetic approaches. Future studies will utilize the information acquired from this project to further define the mechanism of NS1-NS2A cleavage and the role of E protein in NS1-NS2A polyprotein processing. This information could potentially lead to the identification of the protease responsible for this cleavage and fill an important gap in the fundamental knowledge on the biology of flavivirus.

CHAPTER 8

Bibliography

Allison, S. L., Schalich, J., Stiasny, K., Mandl, C. W., and Heinz, F. X. (2001). Mutational evidence for an internal fusion peptide in flavivirus envelope protein E. *J Virol* **75**, 4268-75.

Allison, S. L., Schalich, J., Stiasny, K., Mandl, C. W., Kunz, C., and Heinz, F. X. (1995). Oligomeric rearrangement of tick-borne encephalitis virus envelope proteins induced by an acidic pH. *J Virol* **69**, 695-700.

Alvarez, D. E., De Lella Ezcurra, A. L., Fucito, S., and Gamarnik, A. V. (2005). Role of RNA structures present at the 3'UTR of dengue virus on translation, RNA synthesis, and viral replication. *Virology* **339**, 200-12.

Alvarez, D. E., Filomatori, C. V., and Gamarnik, A. V. (2008). Functional analysis of dengue virus cyclization sequences located at the 5' and 3'UTRs. *Virology* **375**, 223-35.

Amberg, S. M., Nestorowicz, A., McCourt, D. W., and Rice, C. M. (1994). NS2B-3 proteinase-mediated processing in the yellow fever virus structural region: in vitro and in vivo studies. *J Virol* **68**, 3794-802.

Ambrose, R. L., and Mackenzie, J. M. (2011). West Nile virus differentially modulates the unfolded protein response to facilitate replication and immune evasion. *J Virol* **85**, 2723-32.

Arias, C. F., Preugschat, F., and Strauss, J. H. (1993). Dengue 2 virus NS2B and NS3 form a stable complex that can cleave NS3 within the helicase domain. *Virology* **193**, 888-99.

Arroyo, J., Guirakhoo, F., Fenner, S., Zhang, Z. X., Monath, T. P., and Chambers, T. J. (2001). Molecular basis for attenuation of neurovirulence of a yellow fever Virus/Japanese encephalitis virus chimera vaccine (ChimeriVax-JE). *J Virol* **75**, 934-42.

Avirutnan, P., Hauhart, R. E., Somnuke, P., Blom, A. M., Diamond, M. S., and Atkinson, J. P. (2011). Binding of Flavivirus Nonstructural Protein NS1 to C4b Binding Protein Modulates Complement Activation. *J Immunol.*

Avirutnan, P., Zhang, L., Punyadee, N., Manuyakorn, A., Puttikhunt, C., Kasinrerk, W., Malasit, P., Atkinson, J. P., and Diamond, M. S. (2007). Secreted NS1 of dengue virus attaches to the surface of cells via interactions with heparan sulfate and chondroitin sulfate E. *PLoS Pathog* **3**, e183.

Bartelma, G., and Padmanabhan, R. (2002). Expression, purification, and characterization of the RNA 5'-triphosphatase activity of dengue virus type 2 nonstructural protein 3. *Virology* **299**, 122-32.

Bazan, J. F., and Fletterick, R. J. (1989). Detection of a trypsin-like serine protease domain in flaviviruses and pestiviruses. *Virology* **171**, 637-9.

Beasley, D. W., Whiteman, M. C., Zhang, S., Huang, C. Y., Schneider, B. S., Smith, D. R., Gromowski, G. D., Higgs, S., Kinney, R. M., and Barrett, A. D. (2005). Envelope protein glycosylation status influences mouse neuroinvasion phenotype of genetic lineage 1 West Nile virus strains. *J Virol* **79**, 8339-47.

Best, S. M., Morris, K. L., Shannon, J. G., Robertson, S. J., Mitzel, D. N., Park, G. S., Boer, E., Wolfinbarger, J. B., and Bloom, M. E. (2005). Inhibition of interferon-stimulated JAK-STAT signaling by a tick-borne flavivirus and identification of NS5 as an interferon antagonist. *J Virol* **79**, 12828-39.

Bhardwaj, S., Holbrook, M., Shope, R. E., Barrett, A. D., and Watowich, S. J. (2001). Biophysical characterization and vector-specific antagonist activity of domain III of the tick-borne flavivirus envelope protein. *J Virol* **75**, 4002-7.

Bintintan, I., and Meyers, G. (2010). A new type of signal peptidase cleavage site identified in an RNA virus polyprotein. *J Biol Chem* **285**, 8572-84.

Blackwell, J. L., and Brinton, M. A. (1995). BHK cell proteins that bind to the 3' stem-loop structure of the West Nile virus genome RNA. *J Virol* **69**, 5650-8.

Blitvich, B. J., Mackenzie, J. S., Coelen, R. J., Howard, M. J., and Hall, R. A. (1995). A novel complex formed between the flavivirus E and NS1 proteins: analysis of its structure and function. *Arch Virol* **140**, 145-56.

Blitvich, B. J., Scanlon, D., Shiell, B. J., Mackenzie, J. S., and Hall, R. A. (1999). Identification and analysis of truncated and elongated species of the flavivirus NS1 protein. *Virus Res* **60**, 67-79.

Bollati, M., Alvarez, K., Assenberg, R., Baronti, C., Canard, B., Cook, S., Coutard, B., Decroly, E., de Lamballerie, X., Gould, E. A., Grard, G., Grimes, J. M., Hilgenfeld, R., Jansson, A. M., Malet, H., Mancini, E. J., Mastrangelo, E., Mattevi, A., Milani, M., Moureau, G., Neyts, J., Owens, R. J., Ren, J., Selisko, B., Speroni, S., Steuber, H., Stuart, D. I., Unge, T., and Bolognesi, M. (2010). Structure and functionality in flavivirus NS-proteins: perspectives for drug design. *Antiviral Res* **87**, 125-48.

Borowski, P., Niebuhr, A., Mueller, O., Bretner, M., Felczak, K., Kulikowski, T., and Schmitz, H. (2001). Purification and characterization of West Nile virus nucleoside triphosphatase (NTPase)/helicase: evidence for dissociation of the NTPase and helicase activities of the enzyme. *J Virol* **75**, 3220-9.

Borowski, P., Schalinski, S., and Schmitz, H. (2002). Nucleotide triphosphatase/helicase of hepatitis C virus as a target for antiviral therapy. *Antiviral Res* **55**, 397-412.

Bredenbeek, P. J., Kooi, E. A., Lindenbach, B., Huijkman, N., Rice, C. M., and Spaan, W. J. (2003). A stable full-length yellow fever virus cDNA clone and the role of conserved RNA elements in flavivirus replication. *J Gen Virol* **84**, 1261-8.

Brierley, I., Jenner, A. J., and Inglis, S. C. (1992). Mutational analysis of the "slippery-sequence" component of a coronavirus ribosomal frameshifting signal. *J Mol Biol* **227**, 463-79.

Brinkworth, R. I., Fairlie, D. P., Leung, D., and Young, P. R. (1999). Homology model of the dengue 2 virus NS3 protease: putative interactions with both substrate and NS2B cofactor. *J Gen Virol* **80 (Pt 5)**, 1167-77.

Brinton, M. A. (2002). The molecular biology of West Nile Virus: a new invader of the western hemisphere. *Annu Rev Microbiol* **56**, 371-402.

Brinton, M. A., Fernandez, A. V., and Dispoto, J. H. (1986). The 3'-nucleotides of flavivirus genomic RNA form a conserved secondary structure. *Virology* **153**, 113-21.

Brooks, A. J., Johansson, M., John, A. V., Xu, Y., Jans, D. A., and Vasudevan, S. G. (2002). The interdomain region of dengue NS5 protein that binds to the viral helicase NS3 contains independently functional importin beta 1 and importin alpha/beta-recognized nuclear localization signals. *J Biol Chem* **277**, 36399-407.

Bruenn, J. A. (2003). A structural and primary sequence comparison of the viral RNA-dependent RNA polymerases. *Nucleic Acids Res* **31**, 1821-9.

Buckley, A., Gaidamovich, S., Turchinskaya, A., and Gould, E. A. (1992). Monoclonal antibodies identify the NS5 yellow fever virus non-structural protein in the nuclei of infected cells. *J Gen Virol* **73 (Pt 5)**, 1125-30.

Bulich, R., and Aaskov, J. G. (1992). Nuclear localization of dengue 2 virus core protein detected with monoclonal antibodies. *J Gen Virol* **73 (Pt 11)**, 2999-3003.

Cabrera-Hernandez, A., Thepparit, C., Suksanpaisan, L., and Smith, D. R. (2007). Dengue virus entry into liver (HepG2) cells is independent of hsp90 and hsp70. *J Med Virol* **79**, 386-92.

Cahour, A., Falgout, B., and Lai, C. J. (1992). Cleavage of the dengue virus polyprotein at the NS3/NS4A and NS4B/NS5 junctions is mediated by viral protease NS2B-NS3, whereas NS4A/NS4B may be processed by a cellular protease. *J Virol* **66**, 1535-42.

Cahour, A., Pletnev, A., Vazielle-Falcoz, M., Rosen, L., and Lai, C. J. (1995). Growth-restricted dengue virus mutants containing deletions in the 5' noncoding region of the RNA genome. *Virology* **207**, 68-76.

Casanova, C. L., Xue, G., Taracha, E. L., and Dobbelaere, D. A. (2006). Post-translational signal peptide cleavage controls differential epitope recognition in the QP-rich domain of recombinant Theileria parva PIM. *Mol Biochem Parasitol* **149**, 144-54.

Castle, E., Leidner, U., Nowak, T., and Wengler, G. (1986). Primary structure of the West Nile flavivirus genome region coding for all nonstructural proteins. *Virology* **149**, 10-26.

Castle, E., Nowak, T., Leidner, U., and Wengler, G. (1985). Sequence analysis of the viral core protein and the membrane-associated proteins V1 and NV2 of the flavivirus West Nile virus and of the genome sequence for these proteins. *Virology* **145**, 227-36.

Cecilia, D., and Gould, E. A. (1991). Nucleotide changes responsible for loss of neuroinvasiveness in Japanese encephalitis virus neutralization-resistant mutants. *Virology* **181**, 70-7.

Chambers, T. J., Droll, D. A., Tang, Y., Liang, Y., Ganesh, V. K., Murthy, K. H., and Nickells, M. (2005). Yellow fever virus NS2B-NS3 protease: characterization of charged-to-alanine mutant and revertant viruses and analysis of polyprotein-cleavage activities. *J Gen Virol* **86**, 1403-13.

Chambers, T. J., Grakoui, A., and Rice, C. M. (1991). Processing of the yellow fever virus nonstructural polyprotein: a catalytically active NS3 proteinase domain and NS2B are required for cleavages at dibasic sites. *J Virol* **65**, 6042-50.

Chambers, T. J., Hahn, C. S., Galler, R., and Rice, C. M. (1990). Flavivirus genome organization, expression, and replication. *Annu Rev Microbiol* **44**, 649-88.

Chambers, T. J., Halevy, M., Nestorowicz, A., Rice, C. M., and Lustig, S. (1998). West Nile virus envelope proteins: nucleotide sequence analysis of strains differing in mouse neuroinvasiveness. *J Gen Virol* **79 (Pt 10)**, 2375-80.

Chambers, T. J., McCourt, D. W., and Rice, C. M. (1989). Yellow fever virus proteins NS2A, NS2B, and NS4B: identification and partial N-terminal amino acid sequence analysis. *Virology* **169**, 100-9.

Chambers, T. J., Nestorowicz, A., Amberg, S. M., and Rice, C. M. (1993). Mutagenesis of the yellow fever virus NS2B protein: effects on proteolytic processing, NS2B-NS3 complex formation, and viral replication. *J Virol* **67**, 6797-807.

Chappell, K. J., Stoermer, M. J., Fairlie, D. P., and Young, P. R. (2008). West Nile Virus NS2B/NS3 protease as an antiviral target. *Curr Med Chem* **15**, 2771-84.

Chen, W. J., Wu, H. R., and Chiou, S. S. (2003). E/NS1 modifications of dengue 2 virus after serial passages in mammalian and/or mosquito cells. *Intervirology* **46**, 289-95.

Chen, Y. C., Wang, S. Y., and King, C. C. (1999). Bacterial lipopolysaccharide inhibits dengue virus infection of primary human monocytes/macrophages by blockade of virus entry via a CD14-dependent mechanism. *J Virol* **73**, 2650-7.

Chu, J. J., and Ng, M. L. (2004). Interaction of West Nile virus with alpha v beta 3 integrin mediates virus entry into cells. *J Biol Chem* **279**, 54533-41.

Chu, P. W., and Westaway, E. G. (1985). Replication strategy of Kunjin virus: evidence for recycling role of replicative form RNA as template in semiconservative and asymmetric replication. *Virology* **140**, 68-79.

Chu, P. W., and Westaway, E. G. (1992). Molecular and ultrastructural analysis of heavy membrane fractions associated with the replication of Kunjin virus RNA. *Arch Virol* **125**, 177-91.

Chung, K. M., Nybakken, G. E., Thompson, B. S., Engle, M. J., Marri, A., Fremont, D. H., and Diamond, M. S. (2006). Antibodies against West Nile Virus nonstructural protein NS1 prevent lethal infection through Fc gamma receptor-dependent and -independent mechanisms. *J Virol* **80**, 1340-51.

Clark, D. C., Lobigs, M., Lee, E., Howard, M. J., Clark, K., Blitvich, B. J., and Hall, R. A. (2007). In situ reactions of monoclonal antibodies with a viable mutant of Murray Valley encephalitis virus reveal an absence of dimeric NS1 protein. *J Gen Virol* **88**, 1175-83.

Cleaves, G. R., and Dubin, D. T. (1979). Methylation status of intracellular dengue type 2 40 S RNA. *Virology* **96**, 159-65.

Cleaves, G. R., Ryan, T. E., and Schlesinger, R. W. (1981). Identification and characterization of type 2 dengue virus replicative intermediate and replicative form RNAs. *Virology* **111**, 73-83.

Clum, S., Ebner, K. E., and Padmanabhan, R. (1997). Cotranslational membrane insertion of the serine proteinase precursor NS2B-NS3(Pro) of dengue virus type 2 is required for efficient in vitro processing and is mediated through the hydrophobic regions of NS2B. *J Biol Chem* **272**, 30715-23.

Coia, G., Parker, M. D., Speight, G., Byrne, M. E., and Westaway, E. G. (1988). Nucleotide and complete amino acid sequences of Kunjin virus: definitive gene order and characteristics of the virus-specified proteins. *J Gen Virol* **69 (Pt 1)**, 1-21.

Corver, J., Lenches, E., Smith, K., Robison, R. A., Sando, T., Strauss, E. G., and Strauss, J. H. (2003). Fine mapping of a cis-acting sequence element in yellow fever virus RNA that is required for RNA replication and cyclization. *J Virol* **77**, 2265-70.

Crooks, A. J., Lee, J. M., Easterbrook, L. M., Timofeev, A. V., and Stephenson, J. R. (1994). The NS1 protein of tick-borne encephalitis virus forms multimeric species upon secretion from the host cell. *J Gen Virol* **75 (Pt 12)**, 3453-60.

Cui, T., Sugrue, R. J., Xu, Q., Lee, A. K., Chan, Y. C., and Fu, J. (1998). Recombinant dengue virus type 1 NS3 protein exhibits specific viral RNA binding and NTPase activity regulated by the NS5 protein. *Virology* **246**, 409-17.

Cunningham, B. C., and Wells, J. A. (1989). High-resolution epitope mapping of hGH-receptor interactions by alanine-scanning mutagenesis. *Science* **244**, 1081-5.

Dalgarno, L., Trent, D. W., Strauss, J. H., and Rice, C. M. (1986). Partial nucleotide sequence of the Murray Valley encephalitis virus genome. Comparison of the encoded polypeptides with yellow fever virus structural and non-structural proteins. *J Mol Biol* **187**, 309-23.

Danecek, P., and Schein, C. H. (2010). Flavitrack analysis of the structure and function of West Nile non-structural proteins. *Int J Bioinform Res Appl* **6**, 134-46.

Davis, C. W., Nguyen, H. Y., Hanna, S. L., Sanchez, M. D., Doms, R. W., and Pierson, T. C. (2006). West Nile virus discriminates between DC-SIGN and DC-SIGNR for cellular attachment and infection. *J Virol* **80**, 1290-301.

De Nova-Ocampo, M., Villegas-Sepulveda, N., and del Angel, R. M. (2002). Translation elongation factor-1alpha, La, and PTB interact with the 3' untranslated region of dengue 4 virus RNA. *Virology* **295**, 337-47.

Debnath, N. C., Tiernery, R., Sil, B. K., Wills, M. R., and Barrett, A. D. (1991). In vitro homotypic and heterotypic interference by defective interfering particles of West Nile virus. *J Gen Virol* **72 (Pt 11)**, 2705-11.

Dokland, T., Walsh, M., Mackenzie, J. M., Khromykh, A. A., Ee, K. H., and Wang, S. (2004). West Nile virus core protein; tetramer structure and ribbon formation. *Structure* **12**, 1157-63.

Edward, Z., and Takegami, T. (1993). Localization and functions of Japanese encephalitis virus nonstructural proteins NS3 and NS5 for viral RNA synthesis in the infected cells. *Microbiol Immunol* **37**, 239-43.

Elghonemy, S., Davis, W. G., and Brinton, M. A. (2005). The majority of the nucleotides in the top loop of the genomic 3' terminal stem loop structure are cis-acting in a West Nile virus infectious clone. *Virology* **331**, 238-46.

Falgout, B., and C.-J. Lai (1990). "Synthesis of dengue virus nonstructural protein NS1 requires the N-terminal signal sequence and the downstream nonstructural protein NS2A," American Society for Microbiology, Washington, D.C.

Falgout, B., Chanock, R., and Lai, C. J. (1989). Proper processing of dengue virus nonstructural glycoprotein NS1 requires the N-terminal hydrophobic signal sequence and the downstream nonstructural protein NS2a. *J Virol* **63**, 1852-60.

Falgout, B., and Markoff, L. (1995). Evidence that flavivirus NS1-NS2A cleavage is mediated by a membrane-bound host protease in the endoplasmic reticulum. *J Virol* **69**, 7232-43.

Falgout, B., Miller, R. H., and Lai, C. J. (1993). Deletion analysis of dengue virus type 4 nonstructural protein NS2B: identification of a domain required for NS2B-NS3 protease activity. *J Virol* **67**, 2034-42.

Falgout, B., Pethel, M., Zhang, Y. M., and Lai, C. J. (1991). Both nonstructural proteins NS2B and NS3 are required for the proteolytic processing of dengue virus nonstructural proteins. *J Virol* **65**, 2467-75.

Filomatori, C. V., Lodeiro, M. F., Alvarez, D. E., Samsa, M. M., Pietrasanta, L., and Gamarnik, A. V. (2006). A 5' RNA element promotes dengue virus RNA synthesis on a circular genome. *Genes Dev* **20**, 2238-49.

Firth, A. E., and Atkins, J. F. (2009). A conserved predicted pseudoknot in the NS2A-encoding sequence of West Nile and Japanese encephalitis flaviviruses suggests NS1' may derive from ribosomal frameshifting. *Virol J* **6**, 14.

Flamand, M., Megret, F., Mathieu, M., Lepault, J., Rey, F. A., and Deubel, V. (1999). Dengue virus type 1 nonstructural glycoprotein NS1 is secreted from mammalian cells as a soluble hexamer in a glycosylation-dependent fashion. *J Virol* **73**, 6104-10.

French, E. L. (1952). Murray Valley encephalitis isolation and characterization of the aetiological agent. *Med J Aust* **1**, 100-3.

Funk, A., Truong, K., Nagasaki, T., Torres, S., Floden, N., Balmori Melian, E., Edmonds, J., Dong, H., Shi, P. Y., and Khromykh, A. A. (2010). RNA structures required for production of subgenomic flavivirus RNA. *J Virol* **84**, 11407-17.

Gardner, C. L., and Ryman, K. D. (2010). Yellow fever: a reemerging threat. *Clin Lab Med* **30**, 237-60.

Gaunt, M. W., Sall, A. A., de Lamballerie, X., Falconar, A. K., Dzhivanian, T. I., and Gould, E. A. (2001). Phylogenetic relationships of flaviviruses correlate with their epidemiology, disease association and biogeography. *J Gen Virol* **82**, 1867-76.

Gollins, S. W., and Porterfield, J. S. (1985). Flavivirus infection enhancement in macrophages: an electron microscopic study of viral cellular entry. *J Gen Virol* **66 (Pt 9)**, 1969-82.

Gorbalenya, A. E., Donchenko, A. P., Koonin, E. V., and Blinov, V. M. (1989a). N-terminal domains of putative helicases of flavi- and pestiviruses may be serine proteases. *Nucleic Acids Res* **17**, 3889-97.

Gorbalenya, A. E., Koonin, E. V., Donchenko, A. P., and Blinov, V. M. (1989b). Two related superfamilies of putative helicases involved in replication, recombination, repair and expression of DNA and RNA genomes. *Nucleic Acids Res* **17**, 4713-30.

Grun, J. B., and Brinton, M. A. (1986). Characterization of West Nile virus RNA-dependent RNA polymerase and cellular terminal adenylyl and uridylyl transferases in cell-free extracts. *J Virol* **60**, 1113-24.

Gubler, D. J. (2007). The continuing spread of West Nile virus in the western hemisphere. *Clin Infect Dis* **45**, 1039-46.

Guirakhoo, F., Bolin, R. A., and Roehrig, J. T. (1992). The Murray Valley encephalitis virus prM protein confers acid resistance to virus particles and alters the expression of epitopes within the R2 domain of E glycoprotein. *Virology* **191**, 921-31.

Hahn, C. S., Hahn, Y. S., Rice, C. M., Lee, E., Dalgarno, L., Strauss, E. G., and Strauss, J. H. (1987). Conserved elements in the 3' untranslated region of flavivirus RNAs and potential cyclization sequences. *J Mol Biol* **198**, 33-41.

Halevy, M., Akov, Y., Ben-Nathan, D., Kobiler, D., Lachmi, B., and Lustig, S. (1994). Loss of active neuroinvasiveness in attenuated strains of West Nile virus: pathogenicity in immunocompetent and SCID mice. *Arch Virol* **137**, 355-70.

Hall, R. A., Kay, B. H., Burgess, G. W., Clancy, P., and Fanning, I. D. (1990). Epitope analysis of the envelope and non-structural glycoproteins of Murray Valley encephalitis virus. *J Gen Virol* **71 (Pt 12)**, 2923-30.

Hall, R. A., Khromykh, A. A., Mackenzie, J. M., Scherret, J. H., Khromykh, T. I., and Mackenzie, J. S. (1999). Loss of dimerisation of the nonstructural protein NS1 of Kunjin virus delays viral replication and reduces virulence in mice, but still allows secretion of NS1. *Virology* **264**, 66-75.

Hanna, S. L., Pierson, T. C., Sanchez, M. D., Ahmed, A. A., Murtadha, M. M., and Doms, R. W. (2005). N-linked glycosylation of west nile virus envelope proteins influences particle assembly and infectivity. *J Virol* **79**, 13262-74.

Heinz, F. X., M. S. Collett, R. H. Purcell, E. A. Gould, C. R. Howard, M. Houghton, R. J. M. Moormann, C. M. Rice, and Theil., a. H.-J. (2000). Family Flaviviridae *In* "Seventh report of the International Committee for the Taxonomy of Viruses. " (C. F. MHV Regenmortel, DHL Bishop, EB Carsten, MK Estes, ed.), pp. 860-78. Academic Press, San Diego, CA.

Heinz, F. X., Stiasny, K., Puschner-Auer, G., Holzmann, H., Allison, S. L., Mandl, C. W., and Kunz, C. (1994). Structural changes and functional control of the tick-borne encephalitis virus glycoprotein E by the heterodimeric association with protein prM. *Virology* **198**, 109-17.

Hensley, S. E., Das, S. R., Bailey, A. L., Schmidt, L. M., Hickman, H. D., Jayaraman, A., Viswanathan, K., Raman, R., Sasisekharan, R., Bennink, J. R., and Yewdell, J. W. (2009). Hemagglutinin receptor binding avidity drives influenza A virus antigenic drift. *Science* **326**, 734-6.

Hilgard, P., and Stockert, R. (2000). Heparan sulfate proteoglycans initiate dengue virus infection of hepatocytes. *Hepatology* **32**, 1069-77.

Hirsch, A. J., Medigeshi, G. R., Meyers, H. L., DeFilippis, V., Fruh, K., Briese, T., Lipkin, W. I., and Nelson, J. A. (2005). The Src family kinase c-Yes is required for maturation of West Nile virus particles. *J Virol* **79**, 11943-51.

Ho, S. N., Hunt, H. D., Horton, R. M., Pullen, J. K., and Pease, L. R. (1989). Site-directed mutagenesis by overlap extension using the polymerase chain reaction. *Gene* **77**, 51-9.

Hoenen, A., Liu, W., Kochs, G., Khromykh, A. A., and Mackenzie, J. M. (2007). West Nile virus-induced cytoplasmic membrane structures provide partial protection against the interferon-induced antiviral MxA protein. *J Gen Virol* **88**, 3013-7.

Holden, K. L., and Harris, E. (2004). Enhancement of dengue virus translation: role of the 3' untranslated region and the terminal 3' stem-loop domain. *Virology* **329**, 119-33.

Hollidge, B. S., Gonzalez-Scarano, F., and Soldan, S. S. (2010). Arboviral encephalitides: transmission, emergence, and pathogenesis. *J Neuroimmune Pharmacol* **5**, 428-42.

Hong, S. S., and Ng, M. L. (1987). Involvement of microtubules in Kunjin virus replication. Brief report. *Arch Virol* **97**, 115-21.

Hori, H., and Lai, C. J. (1990). Cleavage of dengue virus NS1-NS2A requires an octapeptide sequence at the C terminus of NS1. *J Virol* **64**, 4573-7.

Hung, J. J., Hsieh, M. T., Young, M. J., Kao, C. L., King, C. C., and Chang, W. (2004). An external loop region of domain III of dengue virus type 2 envelope protein is involved in serotype-specific binding to mosquito but not mammalian cells. *J Virol* **78**, 378-88.

Hurrelbrink, R. J., Nestorowicz, A., and McMinn, P. C. (1999). Characterization of infectious Murray Valley encephalitis virus derived from a stably cloned genome-length cDNA. *J Gen Virol* **80 (Pt 12)**, 3115-25.

Ingrosso, D., Fowler, A. V., Bleibaum, J., and Clarke, S. (1989). Sequence of the D-aspartyl/L-isoaspartyl protein methyltransferase from human erythrocytes. Common sequence motifs for protein, DNA, RNA, and small molecule S-adenosylmethionine-dependent methyltransferases. *J Biol Chem* **264**, 20131-9.

Issur, M., Geiss, B. J., Bougie, I., Picard-Jean, F., Despins, S., Mayette, J., Hobdey, S. E., and Bisaillon, M. (2009). The flavivirus NS5 protein is a true RNA guanylyltransferase that catalyzes a two-step reaction to form the RNA cap structure. *Rna* **15**, 2340-50.

Jacobs, M. G., Robinson, P. J., Bletchly, C., Mackenzie, J. M., and Young, P. R. (2000). Dengue virus nonstructural protein 1 is expressed in a glycosyl-phosphatidylinositol-linked form that is capable of signal transduction. *Faseb J* **14**, 1603-10.

Jan, L. R., Yang, C. S., Trent, D. W., Falgout, B., and Lai, C. J. (1995). Processing of Japanese encephalitis virus non-structural proteins: NS2B-NS3 complex and heterologous proteases. *J Gen Virol* **76 (Pt 3)**, 573-80.

Jiang, L., Yao, H., Duan, X., Lu, X., and Liu, Y. (2009). Polypyrimidine tract-binding protein influences negative strand RNA synthesis of dengue virus. *Biochem Biophys Res Commun* **385**, 187-92.

Jindadamrongwech, S., Thepparit, C., and Smith, D. R. (2004). Identification of GRP 78 (BiP) as a liver cell expressed receptor element for dengue virus serotype 2. *Arch Virol* **149**, 915-27.

Johansson, M., Brooks, A. J., Jans, D. A., and Vasudevan, S. G. (2001). A small region of the dengue virus-encoded RNA-dependent RNA polymerase, NS5, confers interaction with both the nuclear transport receptor importin-beta and the viral helicase, NS3. *J Gen Virol* **82**, 735-45.

Jones, C. T., Ma, L., Burgner, J. W., Groesch, T. D., Post, C. B., and Kuhn, R. J. (2003). Flavivirus capsid is a dimeric alpha-helical protein. *J Virol* **77**, 7143-9.

Kamer, G., and Argos, P. (1984). Primary structural comparison of RNA-dependent polymerases from plant, animal and bacterial viruses. *Nucleic Acids Res* **12**, 7269-82.

Kapoor, M., Zhang, L., Ramachandra, M., Kusukawa, J., Ebner, K. E., and Padmanabhan, R. (1995). Association between NS3 and NS5 proteins of dengue virus type 2 in the putative RNA replicase is linked to differential phosphorylation of NS5. *J Biol Chem* **270**, 19100-6.

Kawano, H., Rostapshov, V., Rosen, L., and Lai, C. J. (1993). Genetic determinants of dengue type 4 virus neurovirulence for mice. *J Virol* **67**, 6567-75.

Khromykh, A. A., Kenney, M. T., and Westaway, E. G. (1998a). trans-Complementation of flavivirus RNA polymerase gene NS5 by using Kunjin virus replicon-expressing BHK cells. *J Virol* **72**, 7270-9.

Khromykh, A. A., Meka, H., Guyatt, K. J., and Westaway, E. G. (2001a). Essential role of cyclization sequences in flavivirus RNA replication. *J Virol* **75**, 6719-28.

Khromykh, A. A., Sedlak, P. L., and Westaway, E. G. (2000). cis- and trans-acting elements in flavivirus RNA replication. *J Virol* **74**, 3253-63.

Khromykh, A. A., Varnavski, A. N., Sedlak, P. L., and Westaway, E. G. (2001b). Coupling between replication and packaging of flavivirus RNA: evidence derived from the use of DNA-based full-length cDNA clones of Kunjin virus. *J Virol* **75**, 4633-40.

Khromykh, A. A., Varnavski, A. N., and Westaway, E. G. (1998b). Encapsidation of the flavivirus kunjin replicon RNA by using a complementation system providing Kunjin virus structural proteins in trans. *J Virol* **72**, 5967-77.

Khromykh, A. A., and Westaway, E. G. (1996). RNA binding properties of core protein of the flavivirus Kunjin. *Arch Virol* **141**, 685-99.

Kiermayr, S., Kofler, R. M., Mandl, C. W., Messner, P., and Heinz, F. X. (2004). Isolation of capsid protein dimers from the tick-borne encephalitis flavivirus and in vitro assembly of capsid-like particles. *J Virol* **78**, 8078-84.

Kitano, T., Suzuki, K., and Yamaguchi, T. (1974). Morphological, chemical, and biological characterization of Japanese encephalitis virus virion and its hemagglutinin. *J Virol* **14**, 631-9.

Knipe, D. M., and Howley, P.M. (2001). "Fields Virology," 4th/Ed. Lippincott, William & Wilkins, Philadelphia.

Kofler, R. M., Heinz, F. X., and Mandl, C. W. (2002). Capsid protein C of tick-borne encephalitis virus tolerates large internal deletions and is a favorable target for attenuation of virulence. *J Virol* **76**, 3534-43.

Kontny, U., Kurane, I., and Ennis, F. A. (1988). Gamma interferon augments Fc gamma receptor-mediated dengue virus infection of human monocytic cells. *J Virol* **62**, 3928-33.

Koonin, E. V. (1991). The phylogeny of RNA-dependent RNA polymerases of positive-strand RNA viruses. *J Gen Virol* **72 (Pt 9)**, 2197-206.

Koonin, E. V. (1993). Computer-assisted identification of a putative methyltransferase domain in NS5 protein of flaviviruses and lambda 2 protein of reovirus. *J Gen Virol* **74 (Pt 4)**, 733-40.

Krishna, V. D., Rangappa, M., and Satchidanandam, V. (2009). Virus-specific cytolytic antibodies to nonstructural protein 1 of Japanese encephalitis virus effect reduction of virus output from infected cells. *J Virol* **83**, 4766-77.

Kuhn, R. J., Zhang, W., Rossmann, M. G., Pletnev, S. V., Corver, J., Lenches, E., Jones, C. T., Mukhopadhyay, S., Chipman, P. R., Strauss, E. G., Baker, T. S., and Strauss, J. H. (2002). Structure of dengue virus: implications for flavivirus organization, maturation, and fusion. *Cell* **108**, 717-25.

Kummerer, B. M., and Rice, C. M. (2002). Mutations in the yellow fever virus nonstructural protein NS2A selectively block production of infectious particles. *J Virol* **76**, 4773-84.

Kuo, M. D., Chin, C., Hsu, S. L., Shiao, J. Y., Wang, T. M., and Lin, J. H. (1996). Characterization of the NTPase activity of Japanese encephalitis virus NS3 protein. *J Gen Virol* **77 (Pt 9)**, 2077-84.

Laemmli, U. K. (1970). Cleavage of structural proteins during the assembly of the head of bacteriophage T4. *Nature* **227**, 680-5.

Leang, S. K. (2008). The biological roles of Asn-linked glycosylations in the E protein of DENV-2. Master thesis, The Australian National University, Canberra, Australia.

Leblois, H., and Young, P. R. (1995). Maturation of the dengue-2 virus NS1 protein in insect cells: effects of downstream NS2A sequences on baculovirus-expressed gene constructs. *J Gen Virol* **76 (Pt 4)**, 979-84.

Lee, E., Hall, R. A., and Lobigs, M. (2004). Common E protein determinants for attenuation of glycosaminoglycan-binding variants of Japanese encephalitis and West Nile viruses. *J Virol* **78**, 8271-80.

Lee, E., Leang, S. K., Davidson, A., and Lobigs, M. (2010). Both E protein glycans adversely affect dengue virus infectivity but are beneficial for virion release. *J Virol* **84**, 5171-80.

Lee, E., and Lobigs, M. (2000). Substitutions at the putative receptor-binding site of an encephalitic flavivirus alter virulence and host cell tropism and reveal a role for glycosaminoglycans in entry. *J Virol* **74**, 8867-75.

Lee, E., and Lobigs, M. (2002). Mechanism of virulence attenuation of glycosaminoglycan-binding variants of Japanese encephalitis virus and Murray Valley encephalitis virus. *J Virol* **76**, 4901-11.

Lee, E., and Lobigs, M. (2008). E protein domain III determinants of yellow fever virus 17D vaccine strain enhance binding to glycosaminoglycans, impede virus spread, and attenuate virulence. *J Virol* **82**, 6024-33.

Lee, E., Stocks, C. E., Amberg, S. M., Rice, C. M., and Lobigs, M. (2000). Mutagenesis of the signal sequence of yellow fever virus prM protein: enhancement of signalase cleavage In vitro is lethal for virus production. *J Virol* **74**, 24-32.

Lee, E., Wright, P. J., Davidson, A., and Lobigs, M. (2006). Virulence attenuation of Dengue virus due to augmented glycosaminoglycan-binding affinity and restriction in extraneural dissemination. *J Gen Virol* **87**, 2791-801.

Leung, D., Schroder, K., White, H., Fang, N. X., Stoermer, M. J., Abbenante, G., Martin, J. L., Young, P. R., and Fairlie, D. P. (2001). Activity of recombinant dengue 2 virus NS3 protease in the presence of a truncated NS2B co-factor, small peptide substrates, and inhibitors. *J Biol Chem* **276**, 45762-71.

Leung, J. Y., Pijlman, G. P., Kondratieva, N., Hyde, J., Mackenzie, J. M., and Khromykh, A. A. (2008). Role of nonstructural protein NS2A in flavivirus assembly. *J Virol* **82**, 4731-41.

Leyssen, P., De Clercq, E., and Neyts, J. (2000). Perspectives for the treatment of infections with Flaviviridae. *Clin Microbiol Rev* **13**, 67-82, table of contents.

Li, H., Clum, S., You, S., Ebner, K. E., and Padmanabhan, R. (1999). The serine protease and RNA-stimulated nucleoside triphosphatase and RNA helicase functional domains of dengue virus type 2 NS3 converge within a region of 20 amino acids. *J Virol* **73**, 3108-16.

Li, J., Bhuvanakantham, R., Howe, J., and Ng, M. L. (2006). The glycosylation site in the envelope protein of West Nile virus (Sarafend) plays an important role in replication and maturation processes. *J Gen Virol* **87**, 613-22.

Li, L., Lok, S. M., Yu, I. M., Zhang, Y., Kuhn, R. J., Chen, J., and Rossmann, M. G. (2008). The flavivirus precursor membrane-envelope protein complex: structure and maturation. *Science* **319**, 1830-4.

Lin, C., Amberg, S. M., Chambers, T. J., and Rice, C. M. (1993). Cleavage at a novel site in the NS4A region by the yellow fever virus NS2B-3 proteinase is a prerequisite for processing at the downstream 4A/4B signalase site. *J Virol* **67**, 2327-35.

Lin, R. J., Chang, B. L., Yu, H. P., Liao, C. L., and Lin, Y. L. (2006). Blocking of interferon-induced Jak-Stat signaling by Japanese encephalitis virus NS5 through a protein tyrosine phosphatase-mediated mechanism. *J Virol* **80**, 5908-18.

Lin, Y. J., and Wu, S. C. (2005). Histidine at residue 99 and the transmembrane region of the precursor membrane prM protein are important for the prM-E heterodimeric complex formation of Japanese encephalitis virus. *J Virol* **79**, 8535-44.

Lindenbach, B. D., and Rice, C. M. (1997). trans-Complementation of yellow fever virus NS1 reveals a role in early RNA replication. *J Virol* **71**, 9608-17.

Lindenbach, B. D., and Rice, C. M. (1999). Genetic interaction of flavivirus nonstructural proteins NS1 and NS4A as a determinant of replicase function. *J Virol* **73**, 4611-21.

Lindenbach, B. D., Thiel, H.-J., and Rice, C.M. (2007). "Flaviviridae: The viruses and Their Replication," Lippincott-Raven, Philadelphia.

Lindenbach, B. D. a. R., C.M (2001). "Flaviviridae: The viruses and Their Replication," Fourth/Ed. Lippincott Williams & Wilkins, Philadelphia.

Liu, H., Chiou, S. S., and Chen, W. J. (2004a). Differential binding efficiency between the envelope protein of Japanese encephalitis virus variants and heparan sulfate on the cell surface. *J Med Virol* **72**, 618-24.

Liu, W. J., Chen, H. B., and Khromykh, A. A. (2003). Molecular and functional analyses of Kunjin virus infectious cDNA clones demonstrate the essential roles for NS2A in virus assembly and for a nonconservative residue in NS3 in RNA replication. *J Virol* **77**, 7804-13.

Liu, W. J., Chen, H. B., Wang, X. J., Huang, H., and Khromykh, A. A. (2004b). Analysis of adaptive mutations in Kunjin virus replicon RNA reveals a novel role for the flavivirus nonstructural protein NS2A in inhibition of beta interferon promoter-driven transcription. *J Virol* **78**, 12225-35.

Liu, W. J., Sedlak, P. L., Kondratieva, N., and Khromykh, A. A. (2002). Complementation analysis of the flavivirus Kunjin NS3 and NS5 proteins defines the minimal regions essential for formation of a replication complex and shows a requirement of NS3 in cis for virus assembly. *J Virol* **76**, 10766-75.

Liu, W. J., Wang, X. J., Clark, D. C., Lobigs, M., Hall, R. A., and Khromykh, A. A. (2006). A single amino acid substitution in the West Nile virus nonstructural protein NS2A disables its ability to inhibit alpha/beta interferon induction and attenuates virus virulence in mice. *J Virol* **80**, 2396-404.

Liu, W. J., Wang, X. J., Mokhonov, V. V., Shi, P. Y., Randall, R., and Khromykh, A. A. (2005). Inhibition of interferon signaling by the New York 99 strain and Kunjin subtype of West Nile virus involves blockage of STAT1 and STAT2 activation by nonstructural proteins. *J Virol* **79**, 1934-42.

Lo, M. K., Tilgner, M., Bernard, K. A., and Shi, P. Y. (2003). Functional analysis of mosquito-borne flavivirus conserved sequence elements within 3' untranslated region of West Nile virus by use of a reporting replicon that differentiates between viral translation and RNA replication. *J Virol* **77**, 10004-14.

Lobigs, M. (1993). Flavivirus premembrane protein cleavage and spike heterodimer secretion require the function of the viral proteinase NS3. *Proc Natl Acad Sci U S A* **90**, 6218-22.

Lobigs, M., Lee, E., Ng, M. L., Pavy, M., and Lobigs, P. (2010). A flavivirus signal peptide balances the catalytic activity of two proteases and thereby facilitates virus morphogenesis. *Virology* **401**, 80-9.

Lobigs, M., Mullbacher, A., Wang, Y., Pavy, M., and Lee, E. (2003). Role of type I and type II interferon responses in recovery from infection with an encephalitic flavivirus. *J Gen Virol* **84**, 567-72.

Lobigs, M., Usha, R., Nestorowicz, A., Marshall, I. D., Weir, R. C., and Dalgarno, L. (1990). Host cell selection of Murray Valley encephalitis virus variants altered at an RGD sequence in the envelope protein and in mouse virulence. *Virology* **176**, 587-95.

Lobigs, M., Weir, R. C., and Dalgarno, L. (1986). Genetic analysis of Kunjin virus isolates using HaeIII and TaqI restriction digests of single-stranded cDNA to virion RNA. *Aust J Exp Biol Med Sci* **64 (Pt 2)**, 185-96.

Lorenz, I. C., Allison, S. L., Heinz, F. X., and Helenius, A. (2002). Folding and dimerization of tick-borne encephalitis virus envelope proteins prM and E in the endoplasmic reticulum. *J Virol* **76**, 5480-91.

Lorenz, I. C., Kartenbeck, J., Mezzacasa, A., Allison, S. L., Heinz, F. X., and Helenius, A. (2003). Intracellular assembly and secretion of recombinant subviral particles from tick-borne encephalitis virus. *J Virol* **77**, 4370-82.

Ma, L., Jones, C. T., Groesch, T. D., Kuhn, R. J., and Post, C. B. (2004). Solution structure of dengue virus capsid protein reveals another fold. *Proc Natl Acad Sci U S A* **101**, 3414-9.

Macdonald, J., Tonry, J., Hall, R. A., Williams, B., Palacios, G., Ashok, M. S., Jabado, O., Clark, D., Tesh, R. B., Briese, T., and Lipkin, W. I. (2005). NS1 protein secretion during the acute phase of West Nile virus infection. *J Virol* **79**, 13924-33.

Mackenzie, J. (2005). Wrapping things up about virus RNA replication. *Traffic* **6**, 967-77.

Mackenzie, J. M., Jones, M. K., and Westaway, E. G. (1999). Markers for trans-Golgi membranes and the intermediate compartment localize to induced membranes with distinct replication functions in flavivirus-infected cells. *J Virol* **73**, 9555-67.

Mackenzie, J. M., Jones, M. K., and Young, P. R. (1996). Immunolocalization of the dengue virus nonstructural glycoprotein NS1 suggests a role in viral RNA replication. *Virology* **220**, 232-40.

Mackenzie, J. M., Kenney, M. T., and Westaway, E. G. (2007). West Nile virus strain Kunjin NS5 polymerase is a phosphoprotein localized at the cytoplasmic site of viral RNA synthesis. *J Gen Virol* **88**, 1163-8.

Mackenzie, J. M., Khromykh, A. A., Jones, M. K., and Westaway, E. G. (1998). Subcellular localization and some biochemical properties of the flavivirus Kunjin nonstructural proteins NS2A and NS4A. *Virology* **245**, 203-15.

Mackenzie, J. M., and Westaway, E. G. (2001). Assembly and maturation of the flavivirus Kunjin virus appear to occur in the rough endoplasmic reticulum and along the secretory pathway, respectively. *J Virol* **75**, 10787-99.

Mackenzie, J. S., and Broom, A. K. (1995). Australian X disease, Murray Valley encephalitis and the French connection. *Vet Microbiol* **46**, 79-90.

Mackenzie, J. S., Gubler, D. J., and Petersen, L. R. (2004). Emerging flaviviruses: the spread and resurgence of Japanese encephalitis, West Nile and dengue viruses. *Nat Med* **10**, S98-109.

Mackenzie, J. S., Lindsay, M. D., Coelen, R. J., Broom, A. K., Hall, R. A., and Smith, D. W. (1994). Arboviruses causing human disease in the Australasian zoogeographic region. *Arch Virol* **136**, 447-67.

Mackenzie, J. S., Smith, D. W., Broom, A. K., and Bucens, M. R. (1993). Australian encephalitis in Western Australia, 1978-1991. *Med J Aust* **158**, 591-5.

Malet, H., Egloff, M. P., Selisko, B., Butcher, R. E., Wright, P. J., Roberts, M., Gruez, A., Sulzenbacher, G., Vonrhein, C., Bricogne, G., Mackenzie, J. M., Khromykh, A. A., Davidson, A. D., and Canard, B. (2007). Crystal structure of the RNA polymerase domain of the West Nile virus non-structural protein 5. *J Biol Chem* **282**, 10678-89.

Mandl, C. W., Heinz, F. X., and Kunz, C. (1988). Sequence of the structural proteins of tick-borne encephalitis virus (western subtype) and comparative analysis with other flaviviruses. *Virology* **166**, 197-205.

Markoff, L. (1989). In vitro processing of dengue virus structural proteins: cleavage of the pre-membrane protein. *J Virol* **63**, 3345-52.

Markoff, L. (2003). 5'- and 3'-noncoding regions in flavivirus RNA. *Adv Virus Res* **59**, 177-228.

Markoff, L., Chang, A., and Falgout, B. (1994). Processing of flavivirus structural glycoproteins: stable membrane insertion of premembrane requires the envelope signal peptide. *Virology* **204**, 526-40.

Markoff, L., Falgout, B., and Chang, A. (1997). A conserved internal hydrophobic domain mediates the stable membrane integration of the dengue virus capsid protein. *Virology* **233**, 105-17.

Mason, P. W. (1989). Maturation of Japanese encephalitis virus glycoproteins produced by infected mammalian and mosquito cells. *Virology* **169**, 354-64.

Matusan, A. E., Pryor, M. J., Davidson, A. D., and Wright, P. J. (2001). Mutagenesis of the Dengue virus type 2 NS3 protein within and outside helicase motifs: effects on enzyme activity and virus replication. *J Virol* **75**, 9633-43.

May, F. J., Lobigs, M., Lee, E., Gendle, D. J., Mackenzie, J. S., Broom, A. K., Conlan, J. V., and Hall, R. A. (2006). Biological, antigenic and phylogenetic characterization of the flavivirus Alfuy. *J Gen Virol* **87**, 329-37.

McLean, J. E., Wudzinska, A., Datan, E., Quaglino, D., and Zakeri, Z. (2011). Flavivirus NS4A-induced autophagy protects cells against death and enhances virus replication. *J Biol Chem*.

McMeniman, C. J., Lane, R. V., Cass, B. N., Fong, A. W., Sidhu, M., Wang, Y. F., and O'Neill, S. L. (2009). Stable introduction of a life-shortening Wolbachia infection into the mosquito Aedes aegypti. *Science* **323**, 141-4.

Melian, E. B., Hinzman, E., Nagasaki, T., Firth, A. E., Wills, N. M., Nouwens, A. S., Blitvich, B. J., Leung, J., Funk, A., Atkins, J. F., Hall, R., and Khromykh, A. A. (2010). NS1' of flaviviruses in the Japanese encephalitis virus serogroup is a product of ribosomal frameshifting and plays a role in viral neuroinvasiveness. *J Virol* **84**, 1641-7.

Miller, S., Kastner, S., Krijnse-Locker, J., Buhler, S., and Bartenschlager, R. (2007). The non-structural protein 4A of dengue virus is an integral membrane protein inducing membrane alterations in a 2K-regulated manner. *J Biol Chem* **282**, 8873-82.

Misra, M., and Schein, C. H. (2007). Flavitrack: an annotated database of flavivirus sequences. *Bioinformatics* **23**, 2645-7.

Misra, U. K., and Kalita, J. (2010). Overview: Japanese encephalitis. *Prog Neurobiol* **91**, 108-20.

Modis, Y., Ogata, S., Clements, D., and Harrison, S. C. (2003). A ligand-binding pocket in the dengue virus envelope glycoprotein. *Proc Natl Acad Sci U S A* **100**, 6986-91.

Modis, Y., Ogata, S., Clements, D., and Harrison, S. C. (2004). Structure of the dengue virus envelope protein after membrane fusion. *Nature* **427**, 313-9.

Monath, T. P., Arroyo, J., Levenbook, I., Zhang, Z. X., Catalan, J., Draper, K., and Guirakhoo, F. (2002). Single mutation in the flavivirus envelope protein hinge region increases neurovirulence for mice and monkeys but decreases viscerotropism for monkeys: relevance to development and safety testing of live, attenuated vaccines. *J Virol* **76**, 1932-43.

Mondotte, J. A., Lozach, P. Y., Amara, A., and Gamarnik, A. V. (2007). Essential role of dengue virus envelope protein N glycosylation at asparagine-67 during viral propagation. *J Virol* **81**, 7136-48.

Mukhopadhyay, S., Kim, B. S., Chipman, P. R., Rossmann, M. G., and Kuhn, R. J. (2003). Structure of West Nile virus. *Science* **302**, 248.

Muller, U., Steinhoff, U., Reis, L. F., Hemmi, S., Pavlovic, J., Zinkernagel, R. M., and Aguet, M. (1994). Functional role of type I and type II interferons in antiviral defense. *Science* **264**, 1918-21.

Munoz-Jordan, J. L., Laurent-Rolle, M., Ashour, J., Martinez-Sobrido, L., Ashok, M., Lipkin, W. I., and Garcia-Sastre, A. (2005). Inhibition of alpha/beta interferon signaling by the NS4B protein of flaviviruses. *J Virol* **79**, 8004-13.

Murphy, F. A., Harrison, A. K., Gary, G. W., Jr., Whitfield, S. G., and Forrester, F. T. (1968). St. Louis encephalitis virus infection in mice. Electron microscopic studies of central nervous system. *Lab Invest* **19**, 652-62.

Murray, C. L., Jones, C. T., Tassello, J., and Rice, C. M. (2007). Alanine scanning of the hepatitis C virus core protein reveals numerous residues essential for production of infectious virus. *J Virol* **81**, 10220-31.

Muylaert, I. R., Chambers, T. J., Galler, R., and Rice, C. M. (1996). Mutagenesis of the N-linked glycosylation sites of the yellow fever virus NS1 protein: effects on virus replication and mouse neurovirulence. *Virology* **222**, 159-68.

Muylaert, I. R., Galler, R., and Rice, C. M. (1997). Genetic analysis of the yellow fever virus NS1 protein: identification of a temperature-sensitive mutation which blocks RNA accumulation. *J Virol* **71**, 291-8.

Navarro-Sanchez, E., Altmeyer, R., Amara, A., Schwartz, O., Fieschi, F., Virelizier, J. L., Arenzana-Seisdedos, F., and Despres, P. (2003). Dendritic-cell-specific ICAM3-grabbing non-integrin is essential for the productive infection of human dendritic cells by mosquito-cell-derived dengue viruses. *EMBO Rep* **4**, 723-8.

Nestorowicz, A., Chambers, T. J., and Rice, C. M. (1994). Mutagenesis of the yellow fever virus NS2A/2B cleavage site: effects on proteolytic processing, viral replication, and evidence for alternative processing of the NS2A protein. *Virology* **199**, 114-23.

Ng, M. L. (1987). Ultrastructural studies of Kunjin virus-infected Aedes albopictus cells. *J Gen Virol* **68 (Pt 2)**, 577-82.

Ng, M. L., and Lau, L. C. (1988). Possible involvement of receptors in the entry of Kunjin virus into Vero cells. *Arch Virol* **100**, 199-211.

Nishimura, C., Nomura, M., and Kitaoka, M. (1968). Comparative studies on the structure and properties of two selected strains of Japanese encephalitis virus. *Jpn J Med Sci Biol* **21**, 1-10.

Noisakran, S., Dechtawewat, T., Avirutnan, P., Kinoshita, T., Siripanyaphinyo, U., Puttikhunt, C., Kasinrerk, W., Malasit, P., and Sittisombut, N. (2008). Association of dengue virus NS1 protein with lipid rafts. *J Gen Virol* **89**, 2492-500.

Noisakran, S., Dechtawewat, T., Rinkaewkan, P., Puttikhunt, C., Kanjanahaluethai, A., Kasinrerk, W., Sittisombut, N., and Malasit, P. (2007). Characterization of dengue virus NS1 stably expressed in 293T cell lines. *J Virol Methods* **142**, 67-80.

Nowak, T., Farber, P. M., Wengler, G., and Wengler, G. (1989). Analyses of the terminal sequences of West Nile virus structural proteins and of the in vitro translation of these proteins allow the proposal of a complete scheme of the proteolytic cleavages involved in their synthesis. *Virology* **169**, 365-76.

Nowak, T., and Wengler, G. (1987). Analysis of disulfides present in the membrane proteins of the West Nile flavivirus. *Virology* **156**, 127-37.

Nybakken, G. E., Nelson, C. A., Chen, B. R., Diamond, M. S., and Fremont, D. H. (2006). Crystal structure of the West Nile virus envelope glycoprotein. *J Virol* **80**, 11467-74.

Op De Beeck, A., Rouille, Y., Caron, M., Duvet, S., and Dubuisson, J. (2004). The transmembrane domains of the prM and E proteins of yellow fever virus are endoplasmic reticulum localization signals. *J Virol* **78**, 12591-602.

Pace, C. N., and Scholtz, J. M. (1998). A helix propensity scale based on experimental studies of peptides and proteins. *Biophys J* **75**, 422-7.

Parrish, C. R., Woo, W. S., and Wright, P. J. (1991). Expression of the NS1 gene of dengue virus type 2 using vaccinia virus. Dimerisation of the NS1 glycoprotein. *Arch Virol* **117**, 279-86.

Patkar, C. G., and Kuhn, R. J. (2008). Yellow Fever virus NS3 plays an essential role in virus assembly independent of its known enzymatic functions. *J Virol* **82**, 3342-52.

Pethel, M., Falgout, B., and Lai, C. J. (1992). Mutational analysis of the octapeptide sequence motif at the NS1-NS2A cleavage junction of dengue type 4 virus. *J Virol* **66**, 7225-31.

Pijlman, G. P., Funk, A., Kondratieva, N., Leung, J., Torres, S., van der Aa, L., Liu, W. J., Palmenberg, A. C., Shi, P. Y., Hall, R. A., and Khromykh, A. A. (2008). A highly structured, nuclease-resistant, noncoding RNA produced by flaviviruses is required for pathogenicity. *Cell Host Microbe* **4**, 579-91.

Pijlman, G. P., Kondratieva, N., and Khromykh, A. A. (2006). Translation of the flavivirus kunjin NS3 gene in cis but not its RNA sequence or secondary structure is essential for efficient RNA packaging. *J Virol* **80**, 11255-64.

Poch, O., Sauvaget, I., Delarue, M., and Tordo, N. (1989). Identification of four conserved motifs among the RNA-dependent polymerase encoding elements. *Embo J* **8**, 3867-74.

Poidinger, M., Coelen, R. J., and Mackenzie, J. S. (1991). Persistent infection of Vero cells by the flavivirus Murray Valley encephalitis virus. *J Gen Virol* **72 (Pt 3)**, 573-8.

Preugschat, F., and Strauss, J. H. (1991). Processing of nonstructural proteins NS4A and NS4B of dengue 2 virus in vitro and in vivo. *Virology* **185**, 689-97.

Preugschat, F., Yao, C. W., and Strauss, J. H. (1990). In vitro processing of dengue virus type 2 nonstructural proteins NS2A, NS2B, and NS3. *J Virol* **64**, 4364-74.

Proutski, V., Gould, E. A., and Holmes, E. C. (1997). Secondary structure of the 3' untranslated region of flaviviruses: similarities and differences. *Nucleic Acids Res* **25**, 1194-202.

Pugachev, K. V., Guirakhoo, F., Trent, D. W., and Monath, T. P. (2003). Traditional and novel approaches to flavivirus vaccines. *Int J Parasitol* **33**, 567-82.

Randolph, V. B., Winkler, G., and Stollar, V. (1990). Acidotropic amines inhibit proteolytic processing of flavivirus prM protein. *Virology* **174**, 450-8.

Rauscher, S., Flamm, C., Mandl, C. W., Heinz, F. X., and Stadler, P. F. (1997). Secondary structure of the 3'-noncoding region of flavivirus genomes: comparative analysis of base pairing probabilities. *Rna* **3**, 779-91.

Ray, D., Shah, A., Tilgner, M., Guo, Y., Zhao, Y., Dong, H., Deas, T. S., Zhou, Y., Li, H., and Shi, P. Y. (2006). West Nile virus 5'-cap structure is formed by sequential guanine N-7 and ribose 2'-O methylations by nonstructural protein 5. *J Virol* **80**, 8362-70.

Rey, F. A., Heinz, F. X., Mandl, C., Kunz, C., and Harrison, S. C. (1995). The envelope glycoprotein from tick-borne encephalitis virus at 2 A resolution. *Nature* **375**, 291-8.

Rice, C. M., Lenches, E. M., Eddy, S. R., Shin, S. J., Sheets, R. L., and Strauss, J. H. (1985). Nucleotide sequence of yellow fever virus: implications for flavivirus gene expression and evolution. *Science* **229**, 726-33.

Richardson, J. S. (1981). The anatomy and taxonomy of protein structure. *Adv Protein Chem* **34**, 167-339.

Robertson, K. (2011). Toddler latest victim of deadly mosquito-borne disease. *In* "PerthNow". Sunday Times, Perth.

Roehrig, J. T., Johnson, A. J., Hunt, A. R., Bolin, R. A., and Chu, M. C. (1990). Antibodies to dengue 2 virus E-glycoprotein synthetic peptides identify antigenic conformation. *Virology* **177**, 668-75.

Roosendaal, J., Westaway, E. G., Khromykh, A., and Mackenzie, J. M. (2006). Regulated cleavages at the West Nile virus NS4A-2K-NS4B junctions play a major role in rearranging cytoplasmic membranes and Golgi trafficking of the NS4A protein. *J Virol* **80**, 4623-32.

Sato, T., Takamura, C., Yasuda, A., Miyamoto, M., Kamogawa, K., and Yasui, K. (1993). High-level expression of the Japanese encephalitis virus E protein by recombinant vaccinia virus and enhancement of its extracellular release by the NS3 gene product. *Virology* **192**, 483-90.

Schalich, J., Allison, S. L., Stiasny, K., Mandl, C. W., Kunz, C., and Heinz, F. X. (1996). Recombinant subviral particles from tick-borne encephalitis virus are fusogenic and provide a model system for studying flavivirus envelope glycoprotein functions. *J Virol* **70**, 4549-57.

Scherret, J. H., Mackenzie, J. S., Khromykh, A. A., and Hall, R. A. (2001). Biological significance of glycosylation of the envelope protein of Kunjin virus. *Ann N Y Acad Sci* **951**, 361-3.

Schlesinger, J. J., Brandriss, M. W., Cropp, C. B., and Monath, T. P. (1986). Protection against yellow fever in monkeys by immunization with yellow fever virus nonstructural protein NS1. *J Virol* **60**, 1153-5.

Schlesinger, J. J., Brandriss, M. W., and Walsh, E. E. (1985). Protection against 17D yellow fever encephalitis in mice by passive transfer of monoclonal antibodies to the nonstructural glycoprotein gp48 and by active immunization with gp48. *J Immunol* **135**, 2805-9.

Solomon, T. (2004). Flavivirus encephalitis. *N Engl J Med* **351**, 370-8.

Solomon, T., Dung, N. M., Kneen, R., Gainsborough, M., Vaughn, D. W., and Khanh, V. T. (2000). Japanese encephalitis. *J Neurol Neurosurg Psychiatry* **68**, 405-15.

Speight, G., Coia, G., Parker, M. D., and Westaway, E. G. (1988). Gene mapping and positive identification of the non-structural proteins NS2A, NS2B, NS3, NS4B and NS5 of the flavivirus Kunjin and their cleavage sites. *J Gen Virol* **69 (Pt 1)**, 23-34.

Stadler, K., Allison, S. L., Schalich, J., and Heinz, F. X. (1997). Proteolytic activation of tick-borne encephalitis virus by furin. *J Virol* **71**, 8475-81.

Steinmann, E., Brohm, C., Kallis, S., Bartenschlager, R., and Pietschmann, T. (2008). Efficient trans-encapsidation of hepatitis C virus RNAs into infectious virus-like particles. *J Virol* **82**, 7034-46.

Stocks, C. E., and Lobigs, M. (1995). Posttranslational signal peptidase cleavage at the flavivirus C-prM junction in vitro. *J Virol* **69**, 8123-6.

Stocks, C. E., and Lobigs, M. (1998). Signal peptidase cleavage at the flavivirus C-prM junction: dependence on the viral NS2B-3 protease for efficient processing requires determinants in C, the signal peptide, and prM. *J Virol* **72**, 2141-9.

Stollar, V., Schlesinger, R. W., and Stevens, T. M. (1967). Studies on the nature of dengue viruses. III. RNA synthesis in cells infected with type 2 dengue virus. *Virology* **33**, 650-8.

Sumiyoshi, H., Tignor, G. H., and Shope, R. E. (1995). Characterization of a highly attenuated Japanese encephalitis virus generated from molecularly cloned cDNA. *J Infect Dis* **171**, 1144-51.

Takegami, T., Sakamuro, D., and Furukawa, T. (1995). Japanese encephalitis virus nonstructural protein NS3 has RNA binding and ATPase activities. *Virus Genes* **9**, 105-12.

Tassaneetrithep, B., Burgess, T. H., Granelli-Piperno, A., Trumpfheller, C., Finke, J., Sun, W., Eller, M. A., Pattanapanyasat, K., Sarasombath, S., Birx, D. L., Steinman, R. M., Schlesinger, S., and Marovich, M. A. (2003). DC-SIGN (CD209) mediates dengue virus infection of human dendritic cells. *J Exp Med* **197**, 823-9.

Thepparit, C., and Smith, D. R. (2004). Serotype-specific entry of dengue virus into liver cells: identification of the 37-kilodalton/67-kilodalton high-affinity laminin receptor as a dengue virus serotype 1 receptor. *J Virol* **78**, 12647-56.

Tilgner, M., Deas, T. S., and Shi, P. Y. (2005). The flavivirus-conserved penta-nucleotide in the 3' stem-loop of the West Nile virus genome requires a specific sequence and structure for RNA synthesis, but not for viral translation. *Virology* **331**, 375-86.

Utama, A., Shimizu, H., Morikawa, S., Hasebe, F., Morita, K., Igarashi, A., Hatsu, M., Takamizawa, K., and Miyamura, T. (2000). Identification and characterization of the RNA helicase activity of Japanese encephalitis virus NS3 protein. *FEBS Lett* **465**, 74-8.

Valle, R. P., and Falgout, B. (1998). Mutagenesis of the NS3 protease of dengue virus type 2. *J Virol* **72**, 624-32.

van Geest, M., Nilsson, I., von Heijne, G., and Lolkema, J. S. (1999). Insertion of a bacterial secondary transport protein in the endoplasmic reticulum membrane. *J Biol Chem* **274**, 2816-23.

Vlaycheva, L., Nickells, M., Droll, D. A., and Chambers, T. J. (2004). Yellow fever 17D virus: pseudo-revertant suppression of defective virus penetration and spread by mutations in domains II and III of the E protein. *Virology* **327**, 41-9.

von Heijne, G. (1983). Patterns of amino acids near signal-sequence cleavage sites. *Eur J Biochem* **133**, 17-21.

von Heijne, G. (1984). How signal sequences maintain cleavage specificity. *J Mol Biol* **173**, 243-51.

von Heijne, G. (1985). Signal sequences. The limits of variation. *J Mol Biol* **184**, 99-105.

Wallner, G., Mandl, C. W., Kunz, C., and Heinz, F. X. (1995). The flavivirus 3'-noncoding region: extensive size heterogeneity independent of evolutionary relationships among strains of tick-borne encephalitis virus. *Virology* **213**, 169-78.

Wang, A. L., Yang, H. M., Shen, K. A., and Wang, C. C. (1993). Giardiavirus double-stranded RNA genome encodes a capsid polypeptide and a gag-pol-like fusion protein by a translation frameshift. *Proc Natl Acad Sci U S A* **90**, 8595-9.

Wang, S. H., Syu, W. J., Huang, K. J., Lei, H. Y., Yao, C. W., King, C. C., and Hu, S. T. (2002). Intracellular localization and determination of a nuclear localization signal of the core protein of dengue virus. *J Gen Virol* **83**, 3093-102.

Warrener, P., Tamura, J. K., and Collett, M. S. (1993). RNA-stimulated NTPase activity associated with yellow fever virus NS3 protein expressed in bacteria. *J Virol* **67**, 989-96.

Weaver, S. C., and Reisen, W. K. (2010). Present and future arboviral threats. *Antiviral Res* **85**, 328-45.

Wengler, G. (1991). The carboxy-terminal part of the NS 3 protein of the West Nile flavivirus can be isolated as a soluble protein after proteolytic cleavage and represents an RNA-stimulated NTPase. *Virology* **184**, 707-15.

Wengler, G. (1993). The NS 3 nonstructural protein of flaviviruses contains an RNA triphosphatase activity. *Virology* **197**, 265-73.

Wengler, G., Castle, E., Leidner, U., and Nowak, T. (1985). Sequence analysis of the membrane protein V3 of the flavivirus West Nile virus and of its gene. *Virology* **147**, 264-74.

Wengler, G., and Gross, H. J. (1978). Studies on virus-specific nucleic acids synthesized in vertebrate and mosquito cells infected with flaviviruses. *Virology* **89**, 423-37.

Wengler, G., and Wengler, G. (1989). Cell-associated West Nile flavivirus is covered with E+pre-M protein heterodimers which are destroyed and reorganized by proteolytic cleavage during virus release. *J Virol* **63**, 2521-6.

Westaway, E. G., Brinton, M. A., Gaidamovich, S., Horzinek, M. C., Igarashi, A., Kaariainen, L., Lvov, D. K., Porterfield, J. S., Russell, P. K., and Trent, D. W. (1985). Flaviviridae. *Intervirology* **24**, 183-92.

Westaway, E. G., Khromykh, A. A., Kenney, M. T., Mackenzie, J. M., and Jones, M. K. (1997a). Proteins C and NS4B of the flavivirus Kunjin translocate independently into the nucleus. *Virology* **234**, 31-41.

Westaway, E. G., Khromykh, A. A., and Mackenzie, J. M. (1999). Nascent flavivirus RNA colocalized in situ with double-stranded RNA in stable replication complexes. *Virology* **258**, 108-17.

Westaway, E. G., Mackenzie, J. M., Kenney, M. T., Jones, M. K., and Khromykh, A. A. (1997b). Ultrastructure of Kunjin virus-infected cells: colocalization of NS1 and NS3 with double-stranded RNA, and of NS2B with NS3, in virus-induced membrane structures. *J Virol* **71**, 6650-61.

Westaway, E. G., Mackenzie, J. M., and Khromykh, A. A. (2002). Replication and gene function in Kunjin virus. *Curr Top Microbiol Immunol* **267**, 323-51.

Wilson, I. A., Niman, H. L., Houghten, R. A., Cherenson, A. R., Connolly, M. L., and Lerner, R. A. (1984). The structure of an antigenic determinant in a protein. *Cell* **37**, 767-78.

Winkler, G., Maxwell, S. E., Ruemmler, C., and Stollar, V. (1989). Newly synthesized dengue-2 virus nonstructural protein NS1 is a soluble protein but becomes partially hydrophobic and membrane-associated after dimerization. *Virology* **171**, 302-5.

Winkler, G., Randolph, V. B., Cleaves, G. R., Ryan, T. E., and Stollar, V. (1988). Evidence that the mature form of the flavivirus nonstructural protein NS1 is a dimer. *Virology* **162**, 187-96.

Wu, C. F., Wang, S. H., Sun, C. M., Hu, S. T., and Syu, W. J. (2003). Activation of dengue protease autocleavage at the NS2B-NS3 junction by recombinant NS3 and GST-NS2B fusion proteins. *J Virol Methods* **114**, 45-54.

Yi, M., Ma, Y., Yates, J., and Lemon, S. M. (2007). Compensatory mutations in E1, p7, NS2, and NS3 enhance yields of cell culture-infectious intergenotypic chimeric hepatitis C virus. *J Virol* **81**, 629-38.

You, S., and Padmanabhan, R. (1999). A novel in vitro replication system for Dengue virus. Initiation of RNA synthesis at the 3'-end of exogenous viral RNA templates requires 5'- and 3'-terminal complementary sequence motifs of the viral RNA. *J Biol Chem* **274**, 33714-22.

Youn, S., Cho, H., Fremont, D. H., and Diamond, M. S. (2010). A short N-terminal peptide motif on flavivirus nonstructural protein NS1 modulates cellular targeting and immune recognition. *J Virol* **84**, 9516-32.

Yu, I. M., Zhang, W., Holdaway, H. A., Li, L., Kostyuchenko, V. A., Chipman, P. R., Kuhn, R. J., Rossmann, M. G., and Chen, J. (2008a). Structure of the immature dengue virus at low pH primes proteolytic maturation. *Science* **319**, 1834-7.

Yu, L., and Markoff, L. (2005). The topology of bulges in the long stem of the flavivirus 3' stem-loop is a major determinant of RNA replication competence. *J Virol* **79**, 2309-24.

Yu, L., Nomaguchi, M., Padmanabhan, R., and Markoff, L. (2008b). Specific requirements for elements of the 5' and 3' terminal regions in flavivirus RNA synthesis and viral replication. *Virology* **374**, 170-85.

Zeng, L., Falgout, B., and Markoff, L. (1998). Identification of specific nucleotide sequences within the conserved 3'-SL in the dengue type 2 virus genome required for replication. *J Virol* **72**, 7510-22.

Zhang, B., Dong, H., Stein, D. A., Iversen, P. L., and Shi, P. Y. (2008). West Nile virus genome cyclization and RNA replication require two pairs of long-distance RNA interactions. *Virology* **373**, 1-13.

Zhang, Y., Corver, J., Chipman, P. R., Zhang, W., Pletnev, S. V., Sedlak, D., Baker, T. S., Strauss, J. H., Kuhn, R. J., and Rossmann, M. G. (2003). Structures of immature flavivirus particles. *Embo J* **22**, 2604-13.

Zhang, Y., Kaufmann, B., Chipman, P. R., Kuhn, R. J., and Rossmann, M. G. (2007). Structure of immature West Nile virus. *J Virol* **81**, 6141-5.

Zhang, Y., Zhang, W., Ogata, S., Clements, D., Strauss, J. H., Baker, T. S., Kuhn, R. J., and Rossmann, M. G. (2004). Conformational changes of the flavivirus E glycoprotein. *Structure* **12**, 1607-18.

Zhao, B. T., Prince, G., Horswood, R., Eckels, K., Summers, P., Chanock, R., and Lai, C. J. (1987). Expression of dengue virus structural proteins and nonstructural protein NS1 by a recombinant vaccinia virus. *J Virol* **61**, 4019-22.

Zhou, Y., Ray, D., Zhao, Y., Dong, H., Ren, S., Li, Z., Guo, Y., Bernard, K. A., Shi, P. Y., and Li, H. (2007). Structure and function of flavivirus NS5 methyltransferase. *J Virol* **81**, 3891-903.